NASA CR-121136
PWA-4542

FINAL REPORT

DEVELOPMENT OF ADVANCED FUEL CELL SYSTEM

by

P. E. Grevstad

PRATT & WHITNEY AIRCRAFT
South Windsor Engineering Facility
Box 109, Governors Highway
South Windsor, Connecticut 06074

prepared for

NATIONAL AERONAUTICS AND SPACE ADMINISTRATION

November 1972

CONTRACT NAS3-15339

NASA Lewis Research Center
Cleveland, Ohio
Dr. L. H. Thaller, Project Manager
Power Procurement Section

NOTICE

This report was prepared as an account of Government-sponsored work. Neither the United States, nor the National Aeronautics and Space Administration (NASA), nor any person acting on behalf of NASA:

(A) Makes any warranty or representation, expressed or implied, with respect to the accuracy, completeness, or usefulness of the information contained in this report, or that the use of any information, apparatus, method, or process disclosed in this report may not infringe privately-owned rights; or

(B) Assumes any liabilities with respect to the use of, or for damages resulting from the use of, any information, apparatus, method or process disclosed in this report.

As used above, "person acting on behalf of NASA" includes any employees or contractor of NASA, or employee of such contractor, to the extent that such employee or contractor of NASA or employee of such contractor prepares, disseminates, or provides access to any information pursuant to his employment or contract with NASA, or his employment with such contractor.

NASA CR-121136
PWA-4542

DEVELOPMENT OF ADVANCED

FUEL CELL SYSTEM

by

P. E. Grevstad

PRATT & WHITNEY AIRCRAFT

prepared for

NATIONAL AERONAUTICS AND SPACE ADMINISTRATION

NASA Lewis Research Center
Contract NAS3-15339
Dr. L. H. Thaller, Project Manager
Power Procurement Section

FOREWORD

This report describes the several research and development tasks performed during Phase 1 of an advanced fuel cell technology program.

The work was performed under a NASA Contract NAS3-15339 from 7 June 1971 through 30 June 1972. The NASA Program Manager for this contract was Dr. Lawrence H. Thaller. The contributions of Dr. Thaller and other members of the Direct Energy Conversion Laboratory staff at the NASA Lewis Research Center are gratefully acknowledged.

Principal Pratt and Whitney Aircraft personnel who directed the tasks performed in this program were:

Project Manager, Paul E. Grevstad

Principal Investigator, Cell and Stack Development, Raymond L. Gelting

CONTENTS

ILLUSTRATIONS

ILLUSTRATIONS(CONT'D)

ILLUSTRATIONS(CONT'D)

ILLUSTRATIONS (CONT'D)

ILLUSTRATIONS(CONT'D)

ILLUSTRATIONS(CONT'D)

ILLUSTRATIONS(CONT'D)

ILLUSTRATIONS(CONT'D)

TABLES

TABLES (CONT'D)

Abstract

A multiple task research program was performed to improve the weight, life and performance characteristics of hydrogen-oxygen fuel cell power systems. A promising gold alloy cathode catalyst was identified and tested in a cell for 5,000 hours. The compatibility characteristics of candidate polymer structural materials were measured after exposure to electrolyte and water vapor for 8,000 hours. Lightweight cell designs were prepared and fabrication techniques to produce them were developed. Testing demonstrated that predicted performance was achieved. Lightweight components for passive product water removal and evaporative cooling of cells were demonstrated. Systems studies identified fuel cell powerplant concepts for meeting the requirements of advanced spacecraft.

I. SUMMARY

In keeping with NASA objectives, the program reported herein focused on long range research to improve the life, weight and performance characteristics of the basic cell. A key part of this work was evolutionary development of lightweight cells, and water removal and cooling subsystems specifically oriented to meet the objectives of the Engineering Model System (EMS). These tasks were an important part of the program elements for translating research findings into practical hardware. Preliminary design studies of the Engineering Model System provided information on system characteristics to guide the several technology advancement efforts.

A summary description of the work performed in each task and the results achieved follows:

A. Cell Component Research

1. Electrodes

Description - This project emphasized evaluation of gold-based cathode catalyst and Teflon-catalyst cathode structures. Gold was selected as offering the best potential for a long life cathode because of its superior stability compared to the platinum catalysts. It is also a highly active catalyst showing potential for superior performance. Investigations were also performed to improve anode long term structural stability.

Results - Gold catalyzed cathodes, with the gold alloyed with either platinum, nickel, rhodium and copper to stabilize the gold in a high surface area form, were tested and shown to have activities equivalent to platinum. A 90 percent gold, 10 percent platinum catalyzed cathode was tested for 5,000 hours at 200 amp/ft^2 (215.2 ma/cm^2), 190°F (87.8°C) in a subscale fuel cell. Post-test analysis showed the gold did not corrode. Cell performance decay due to loss of cathode activity was approximately 2 microvolts-per-hour.

A modified structure was developed for platinum-palladium anode which demonstrated improved interfacial stability.

2. Structural Materials Compatibility

Description - The long term (up to 8,000 hours) comptability characteristics of candidate polymer materials and adhesives were measured by testing in potassium hydroxide electrolyte and steam. A rapid method for determining the relative oxidation resistance of structural materials and cell components was developed and used to aid in selecting materials suitable for long life, minimum weight fuel cell systems.

Results - Exposure of candidate materials to 35 percent potassium hydroxide at 200°F (93.3°C) showed the most compatible materials to be: polypropylene, polysulfone and 50 percent asbestos - filled polyphenylene sulfide.

Exposure of candidate materials to saturated water vapor at 230°F (110°C) showed the most compatible materials to be: polyaryl, ether, polyarylsulfone, polysulfone, polypropylene, and 50 percent asbestos-filled polyphenylene sulfide.

A gas chromatograph technique was developed to assess relative resistance of materials to oxidation. The materials most resistant to oxidation at 250°F (121.1°C) were found to be: tetrafluoroethylene, fluorinated ethylene propylene, polypropylene, polyphenylene sulfide and polyaryl-sulfide.

3. Lightweight Electrolyte Reservoir Plate

Description - The heaviest single component in the EMS cell is the nickel electrolyte reservoir plate. Substituting a nonmetallic material for this porous structure would result in sizeable system weight savings. A research effort to investigate a structure with high porosity and closely controlled pore spectra made of low density materials was therefore performed.

Results - Two electrolyte reservoir plate structures were developed and characterized: sintered polysulfone powder and fibrillar carbon. The sintered polysulfone structure, made wettable by electroless nickel plating, was selected for further development. This structure has a weight potential one-sixth that of the nickel sinters presently used.

4. Matrix Materials

Description - Potassium titanate has demonstrated superior compatibility with electrolyte compared to the asbestos presently used in the cell's matrix. Availability of a new source for supplying potassium titanate fibers (Fybex ® produced by DuPont) allowed a matrix development activity to begin near the end of the program.

Results - 13 x 13 inch (33 x 33 cm) matrices made of potassium titanate were prepared. These mats had pore spectra equal to those of asbestos matrices. Bubble pressures of 30 to 40 psid (20.7 to 27.6 n/cm^2) differential pressure were achieved in 10 mil (0.25 mm) thick matrices with asbestos contents of 10 and 15 percent by weight. All matrices made with Fybex were found to be much more fragile than those made with asbestos.

B. Power Section Component Development

1. Passive Water Removal Fuel Cells

Description - Several single cell tasks provide the means for evaluating the performance and endurance characteristics of evolutionary EMS cell designs. The investigations performed in this area are: evaluation of alternate designs to accomplish passive water removal, evaluation of EMS baseline cell configurations, testing to measure the compatibility of alternate cell frame materials and construction techniques in the actual cell environment, and development of cell fabrication procedures to translate the most compatible materials available into practical cell configurations. Single cell hardware was also produced and shipped to NASA.

Results - A lightweight fuel cell design was defined . The thickness of the cell, including the reactant flow passages, is 45 percent that of current state-of-the-art fuel cells. Testing demonstrated that this design met or exceeded predicted performance.

Alternate lightweight passive water removal water transport plate assemblies were evaluated and demonstrated the effectiveness of the design in preventing electrolyte loss. The design used in the program has a thickness 35 percent that of water transport plates used in other programs.

20,000 operating hours were accumulated on 26 passive water removal fuel cells. The longest duration cell tests were 2,100 hours of operation at 100 amp/ft^2 (107.6 ma/cm^2) and 1200 hours of operation at 200 amp/ft^2 (215.2 ma/cm^2); both tests were continuing at the conclusion of Phase 1. Diagnostic test techniques were used to define the several aspects of cell performance and to provide data for improving cell performance and stability.

Non-operating cell testing techniques were developed and successfully used in accelerated compatibility testing to measure the compatibility characteristics of alternate cell frame designs.

Fabrication techniques were developed and used to produce cells using improved compatibility cell frame materials.

- An epoxy-asbestos composite frame construction proved simple to fabricate and reliable in cell operation.

- A cell frame construction technique based on the use of polymer films was shown to have compatibility superior to all other designs. Further development is required to achieve the reliability provided by epoxy-based designs.

2. Plaque

Description - Development of a lightweight method for packaging groups of cells into a planar multi-cell stack (termed a plaque) was performed under this task. The plaque integrated six EMS cells and a passive water removal water transport plate into a single assembly. Fabrication procedures were developed and performance evaluation testing was conducted.

Results - Alternate designs for unitizing six cells into a planar stack were evaluated. The plaque was shown to be particularly attractive for systems where a large total cell area must be divided into a large number of series connected cells to meet system voltage and power requirements.

Fabrication techniques were developed to produce 6-cell plaques containing 0.7 ft^2 (650 cm^2) total cell area. The plaque used the same thin cell design developed under the single cell effort. Operation of one plaque for 540 hours demonstrated predicted performance.

3. Evaporative Cooler

Description - The EMS concept includes removal of cell waste heat by evaporation of water. The evaporative cooler task developed lightweight cooler designs based on the use of a thin, porous, hydrophobic membrane to separate the steam and water. Evaluation of alternate designs for low weight reactant/water flow distribution plates and steam flow fields was also a part of this task.

Results - A lightweight method of cooling fuel cells by evaporation of water was designed and tested. Testing to twice the system peak power heat flux demonstrated the adequacy of the water and steam flow fields, the water-steam separator membranes and membrane support. A 1,000-hour endurance test showed no change in the hydrophobicity characteristics of the separator membrane.

C. System Design Analysis

Description - The system design task provided for definition of a preliminary EMS design and specified design goals for the several fuel cell power section components and ancillary components.

Results - A fuel cell power system was defined which can meet or exceed cell EMS design objectives except for specific reactant consumption. The estimated specific weight of the system is 20 percent less than the design objective.

Trade-off studies and design analyses were performed and used to specify baseline and alternate configurations for power system components.

D. Ancillary Component Design Verification Testing

1. Condenser

Description - The EMS integrates the product water and evaporative cooling vapor streams into a common loop. The condenser converts the water vapor to subcooled liquid for reuse in the evaporative cooler and to condition the product water for delivery to the spacecraft. Performance mapping testing and analysis of the plate-fin heat exchanger configuration

selected for this component was performed.

Results - A plate-fin heat exchanger demonstrated stable operation when condensing water vapor with flow orientations horizontal, vertical up, and vertical down. Pressure drop and heat transfer data were used to define a flow model. The testing indicated the sensitivity of this type of heat exchanger to small amounts of non-condensable gases present in the vapor.

2. Reactant Purifiers

Description - Testing and analysis was performed on sodium hydroxide scrubber material to determine its effectiveness in in removing the low levels of carbon dioxide contained in propulsion grade reactant gases.

Results - Testing showed that sodium hydroxide is capable of reducing the carbon dioxide level in a flowing oxygen stream to less than 1 ppm. Less than one pound of this material is sufficient to purify the oxygen consumed by a powerplant operating at 5 kw for a Space Shuttle mission. Further investigations to increase the absorption capacity of scrubbers were identified.

II. INTRODUCTION

The Lewis Research Center of the National Aeronautics and Space Administration is performing a fuel cell system technology advancement program oriented to Space Shuttle applications. The emphasis in this program is on applied fuel cell research and development to build a new technology base from which advanced fuel cell systems can be developed. The work is being guided by an advanced fuel cell system, the specifications for which require a factor of three reduction in system weight and a factor of five improvement in life.

The technology being developed has broad applicability for space and undersea power systems touching as it does on the fundamentals of fuel cell science and art (electrode catalysts and structures, matrix materials, compatibility of structural materials, lightweight cell components and fabrication techniques).

The several work areas of the program and the emphasis in each were planned to meet the objectives stated by NASA-LeRC; the key elements of these objectives are:

> "Goals - The NASA-Lewis Research Center is embarking on an advanced fuel cell program... The overall goal is to advance the technology to provide a low cost, long life fuel cell system to meet Shuttle requirements...
>
> Phasing - A multi-phase development program is anticipated. The first phase covers two aspects of the total program.
>
> 1) The initiation of an on-going technology program to achieve necessary improvements in the fuel cells and ancillary components.
>
> 2) A preliminary design for an Engineering Model System that will incorporate the best current ideas for meeting the program goals."

The program consists of contractor performed work and complementary work performed at the Lewis Research Center. Several interrelated program tasks are being performed aimed at meeting requirements of the next generation of fuel cell systems as well as providing supporting technology for on-going, mission-oriented fuel cell system programs. In programs that are specifically mission-oriented, very often scheduling constraints require that technology shortcomings be designed around rather then addressed directly. Advanced technology programs on the

other hand permit more effort to be applied for solving basic problems. The potential benefits of such a program are two-fold. First a superior system can emerge at a technology level where a potential user can compare it to an existing inventory system. Second, and of equal importance, technology generated during such a program can be utilized by on-going mission oriented programs.

This report describes the several research and development tasks performed by P&WA during Phase 1 of this advanced fuel cell program. The program tasks performed during Phase 1 were organized into four areas:

A) Cell Component Research

- Electrodes
- Structural Materials
- Lightweight Electrolyte Reservoir Plate
- Matrices

B) Power Section Component Development

- Single Cells
- Plaques
- Evaporative Cooler

C) System Design Studies

D) Ancillary Component Design Verification Testing

- Condenser
- Reactant Purifiers

A summary of the objectives and the results achieved in each of these areas is presented in Section II Summary. Detailed discussion of the work performed in the several task areas is presented in the order listed above. Readers who are primarily interested in Power Section Components (Section IV) should first read the introduction to System Design Analysis (Section V) to gain an understanding of the type and functioning of the components investigated in the program.

III. CELL COMPONENT RESEARCH

A. Electrodes

Approach

The original objective of the electrode technology advancement effort was to improve the performance and stability of the alkaline electrolyte-matrix fuel cell, principally by the development of new cathode catalysts. As the work progressed, data was generated which indicated that structural development of both electrodes would improve stability of cells operating at EMS conditions.

There were three factors which set the initial direction of the program. The first was the large body of data derived from previous programs which demonstrated that the dissolution of platinum (and palladium when present) from the cathode and its subsequent redeposition in the matrix represented a life limiting mechanism. The second factor was thermodynamic data which predicted that gold would not be oxidized at cathode potential and thus would not be dissolved and transported from the cathode. Thirdly, work at P&WA^{TM} over a period of several years had demonstrated that gold is an excellent catalyst for the reduction of oxygen, at least the equal of platinum.

Previous P&WA studies in which the catalytic activity of gold had been demonstrated had also shown that the high surface area of a gold black could not be maintained during the normal electrode fabrication procedure due to mechanical and thermal sintering which occurred when the electrode was heated to bond the structure together. When gold black electrodes were made by alternative processes, which resulted in high surface areas, the catalyst sintering process occurred during cell operation resulting in high decay rates.

The approach taken in P&WA investigations prior to this contract to solve this problem was to alloy the gold with other metals which would harden the gold black and thus reduce the rate of recrystallization. The metals selected, principally for chemical compatibility, were platinum, rhodium, nickel and copper. High surface area blacks could be made of the gold alloys of each of these materials by the chemical reduction/precipitation methods normally employed to make metallic catalysts. Since each of the catalysts is different in microstructure, the techniques of electrode fabrication have to be individually tailored to each catalyst. In addition, the fabrication techniques also affect the endurance capability of the electrodes and thus also require optimization for endurance. This is true of anodes as well as cathodes.

Early in the program, changes were observed in anode behavior which could contribute to cell performance decay. For this reason, changes in anode fabrication methods were examined which would reduce the degree to which electrolyte could penetrate the anode structure.

The methods used to fabricate the electrodes used in this study were filter/transfer and spraying. Although the specific details varied for specific requirements, the general methods are as follows.

In the filter transfer method, the catalyst powder is mixed with aqueous suspension of Teflon powder and filtered onto a porous mat. The catalyst layer is then transferred to a screen with a pressing operation to force the catalyst into the screen. In the spraying method, the catalyst powder is mixed with an aqueous suspension of Teflon and sprayed onto a screen. The two methods produce electrodes with very similar performance. However, the filter transfer method is easier to control and makes effective use of the catalyst. In the spray method, some of the catalyst solution is lost during the process because of masking and overspray.

Test Facilities

The initial testing of the catalyst/electrode structures is accomplished in floating electrode half cell rigs in which one cm^2 samples are tested. This rig compares the performance of the electrode against a hydrogen reference electrode as the current is varied giving the half-cell polarization curve. The cell resistance is measured by a pulse method and the polarization corrected to a resistance free basis. With data from half-cell measurements on an anode and cathode and an estimate of cell resistance, the performance of a full cell can be corrected to compare half-cell and full cell cathode performance.

Catalyst/electrode structures for which further testing is merited are tested in complete cells with an active electrode area of 2 x 2 inch (5.1 x 5.1 cm). The basic cell elements used in the 2 x 2 inch (5.1 x 5.1 cm) cells are similar to those of full scale cells, i.e., the electrodes are separated by a 10 mil (0.25 mm) thick reconstituted asbestos matrix with a nickel sinter electrolyte reservoir plate in contact with the anode. Facilities are available to operate these small scale cells in the laboratory (generally short term performance tests) and in automated endurance test stands. In either case, the performance of the cells is monitored as they are run at fixed conditions (generally 200 amp/ft^2 (215.2 ma/cm^2), a temperature of 190°F (87.8°C) and reactant pressure of one atmosphere). An excess of humidified hydrogen flows

through the cell to set electrolyte concentration. Oxygen flow is essentially dead-ended. Diagnostic data is taken at regular intervals (0, 500, 1000, 2000, etc., hours). The diagnostics generally include a measurement of the IR loss in the cell by pulse interrupter techniques, the anode and cathode limiting current taken on 4 percent oxygen and hydrogen (necessary to keep the current within measurable bounds and also to prevent excess electrode temperatures), and performance over the current region from 0.1 (.093) to several hundred ASF (ma/cm^2) from which Tafel plots may be made.

At the conclusion of an endurance test, final diagnostics are done and the cell removed to the lab where post-test examination of the cell is made. These steps taken depend on the cell type and the purpose of the test but would include some of the following tests:

- Carbonate analysis - This analysis is performed by filling the cell with triply distilled water, allowing time for equilibration with the electrolyte, draining the analytical sample from the cell and titrating by standard procedures for KOH and $K_2 CO_3$.

- Half-Cell Test - Portions of the electrodes are tested in the half cell rig after teardown so that comparisons can be made between initial and final electrode performance in the absence of cell related problems.

- Portions of the cell may be analyzed for metals content to determine the degree to which catalyst dissolution and transport has occurred. The principal analytical method used has been atomic absorption. However, a non-destructive method employing X-ray fluorscence has also been developed for platinum content.

- Samples of catalyst and/or electrodes may be examined by X-ray diffraction to determine the catalyst crystallite dimensions and the degree of alloying present. The crystallite size measured permits an independent check to be made on the catalyst surface area which is also measured by the BET-nitrogen adsorption method.

Cathode Catalysts

The catalysts evaluated in this program have been gold-oxide, gold-copper, gold-platinum, gold-nickel and gold-rhodium with variations on the composition and methods of fabrication of the last three. Since the catalyst is gold in each case and since the methods of fabrication result in approximately equivalent catalyst areas, the initial half cell measurements show equivalent performance for each of these catalysts

(Figure 1). Thus, additional information is required to select the most likely candidates.

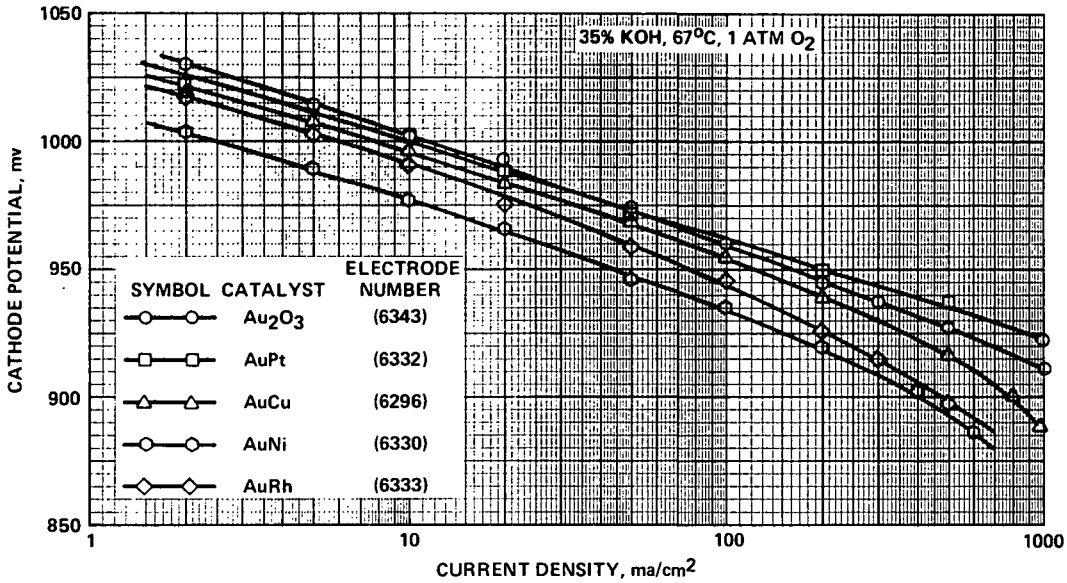

Figure 1 - Performance of Gold Based Catalysts

Gold-oxide was eliminated by a short endurance test followed by half-cell measurements on the electrode, which (see Figure 2) demonstrated that severe recrystallization had occurred, reducing the area by a factor of ten in 200 hours.

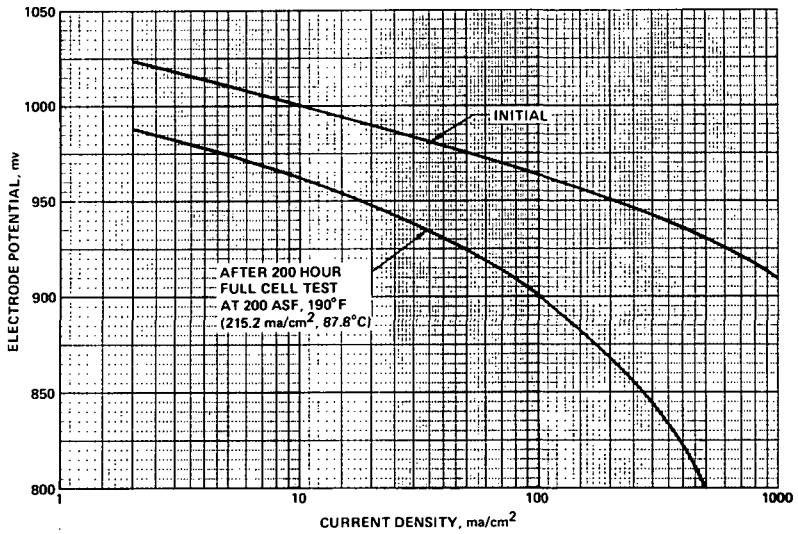

Figure 2 - $Au_2 O_3$ Cathode Half-Cell Performance Data

The endurance results with gold-nickel and gold-copper demonstrated an entirely different problem. In both cases, the electrodes pumped electrolyte into the cathode gas space at a rate such that the cells failed after a few hours of operation. These cells could run only by transferring the expelled electrolyte back to the anode side continuously. This problem is not a property of the activity of the catalyst but rather a problem in the electrode structure.

The gold-rhodium cathode was not run on the endurance bench because it was found in half-cell tests that the electrode resistance increased at oxygen potential because of oxidation of the rhodium present, perhaps external to the gold-rhodium alloy crystallites. This represents a fundamental problem and the catalyst was therefore eliminated from consideration.

The first endurance test with a gold-platinum cathode demonstrated excellent endurance characteristics and excellent cell performance.

As a result of these early tests a decision was made to limit the major portion of electrode studies to the gold-platinum catalyst, optimizing for performance and life, and deferring further work on gold-nickel. The gold-nickel catalyst remains of particular interest since it should be more stable at cathode potential reducing the recrystallization rate.

The gold-platinum catalyst made at the inception of this program had a predicted platinum content of 10 percent based on the quantity of platinum used in the catalyst manufacturing procedure. The actual platinum was lower than predicted and varied considerably as is indicated in Table 1. The reason for this lack of reproducibility was traced to a step in the catalyst manufacturing procedure. The control of this step was tightened and the resulting improvement in reproducibility is shown in Table 2. The procedure still resulted in lower platinum contents than predicted but since the product could be controlled it was not considered desirable to change the procedure at that time.

The initial half-cell performance of the gold-platinum catalyst was determined as a function of platinum content from zero to 10 percent platinum; equivalent platinum loadings expressed in mg of platinum per cm^2 of electrode area ranged from zero to 2.5. The results of this study are shown in Figure 3. The performance does not depend significantly on platinum content or platinum loading. X-ray diffraction analysis demostrated that the catalysts are essentially alloys of gold and platinum. Since the amount of platinum is low and may be present as very small crystallites, it is not possible to prove that all of the platinum is alloyed. For this reason, the loss of a relatively large percentage of the platinum from the cathode may not affect either performance or recrystallization.

TABLE 1

Predicted Platinum Content vs. Measured Platinum Content - Original Fabrication Procedure

Catalyst #	Predicted Platinum %	Measured Platinum %	Measured Predicted %
362-50	2.5	2.09	84
362-57	3.0	0.80	37
362-59	5.0	3.6	72
431-15	5.0	3.9	78
362-48	10	5.6	56
362-49	10	7.6	76
431-8	10	10.1	101

TABLE 2

Predicted Platinum Content vs. Measured Platinum Content - Modified Fabrication Procedure

Catalyst #	Predicted Platinum %	Measured Platinum %	Measured Predicted %
362-106	10	6.6	66
362-109	10	5.5	55
362-110	10	6.6	66
362-114	10	7.5	75
362-116	10	7.1	71

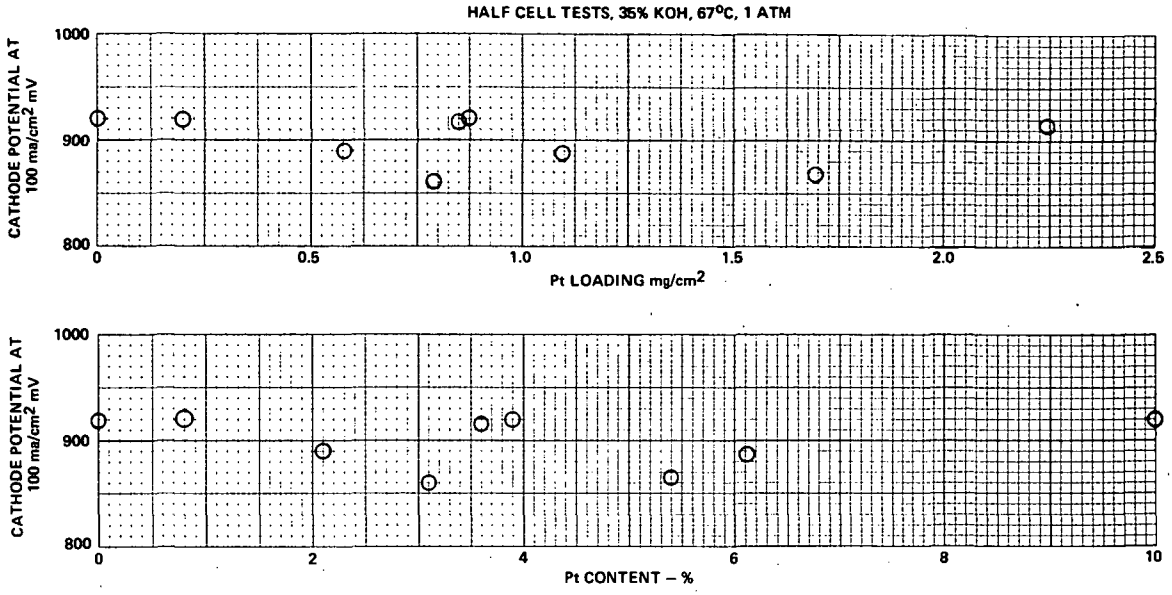

Figure 3 - Effect of Platinum Loading and Content on Performance of Au-Pt Catalyst

Since the catalysts contain a range of particle sizes, with the smaller fractions of these particles undergoing sintering at a much higher rate than the average fraction, samples were heat treated (350°F (176.7°C) for 4 hours in air) to produce a pre-recrystallization material. The results of X-ray defraction measurements indicated that the crystallite size has about doubled (120 Å to 260 Å) and the surface and (BET) decreased from 8 to 4.5 m^2/gm. Full cell endurance tests, however, have not shown any significant difference between treated and untreated catalysts. This is in part because of the relatively small contribution of cathode recrystallization to the overall cell decay and in part due to the performance scatter between different cell builds.

The endurance potential of gold-platinum cathodes was first demonstrated by Cell No. 2097, which was placed on test in June 1971 and operated continuously for 5,000 hours at 190°F (87.8°C), one atmosphere hydrogen and oxygen and a current density of 200 ASF (215.2 ma/cm^2). The performance history of this cell is shown in Figure 4. After 5,000 hours of operation at 200 ASF (215.2 ma/cm^2), approximately 25 percent of the electrolyte was converted to carbonate. This amount of carbonation would cause an estimated performance loss of 20 mV. Correcting for this loss, the carbonate free decay rate would be approximately 10 μV/hr. At the time that this cell was run the diagnostic testing techniques now used were not available, therefore it was not possible to separate the decay modes present during the run.

Post-test half-cell measurements made after the cathode has been washed and dried showed that recrystallization could account for only 8 mV of the total performance loss indicating good stability of the gold-platinum catalyst. The pre- and post- test half cell data is shown in Figure 5. Based on these data, it appears that the majority of performance decay is caused by increased diffusion losses of the cathode. The amount of such performance loss is a function of the reactant pressure at which the cells operate. Hence, the one atmosphere pressure at which the endurance cells operate show a higher loss than if the cells were run at higher reactant pressures.

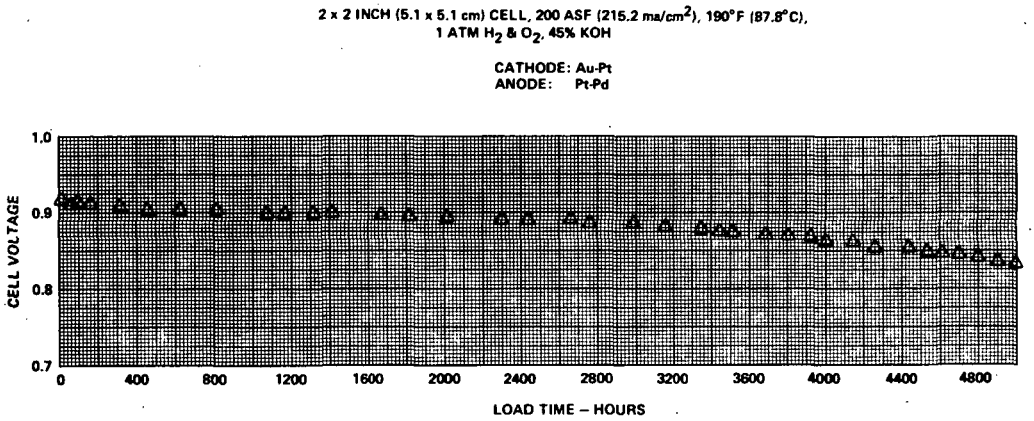

Figure 4 - Endurance Evaluation of Au-Pt Cathode (Cell No. 2097)

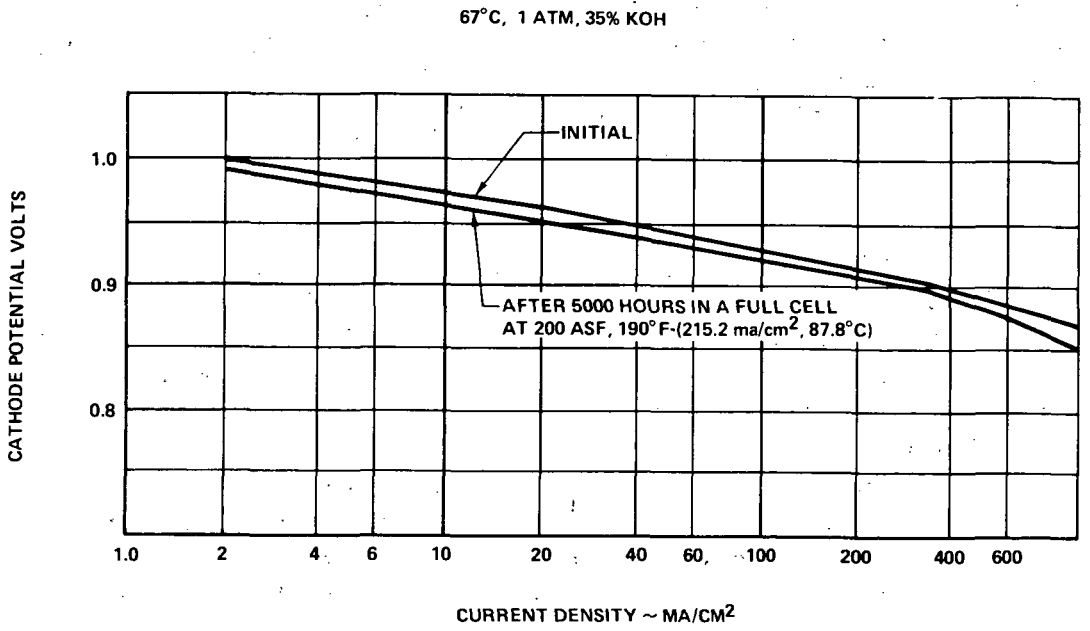

Figure 5 - Cathode Pre-and Post-Test Half Cell Data (Cell No. 2097)

Analysis of the cathode for platinum and the anode and matrix for gold demonstrated the validity of selection of gold as a long term catalyst candidate. The results of this analysis is shown below and confirms that gold is stable at the cathode potential.

Pre- and Post-test Metals Analysis of Cell 2097

5,000 Hours of Operation at 200 ASF (215.2 ma/cm^2),190°F (87.8°C)

Pre-test Cathode Loading

Gold	25 mg/cm^2
Platinum	0.79 mg/cm^2

Post-Test Results

Platinum at Cathode	0.30 mg/cm^2
Gold in Matrix	0.039 mg/cm^2
Gold at Anode	0.044 mg/cm^2

Electrode Structures

During the early life of Cell No. 2097, other cells with gold-platinum cathodes were placed on endurance tests. These cells showed poor endurance characteristics compared to Cell No. 2097, as shown by the data in Figure 6. The performance decay was believed to be due primarily to increased diffusional losses. This is an electrode structural problem resulting in an increased thickness of electrolyte film covering the catalyst. This prompted two developments: 1) the development of additional diagnostic measurements and the implementation of these on the endurance test stands to allow separation of activities vs. diffusion losses; 2) the initiation of an effort to develop electrodes having structures which would be more stable in maintaining the reactant-electrolyte interface.

Several structural variations were tested as follows:

1) Electrodes were made by the usual filter transfer techniques except that the sintering temperature was increased from 590°F (310°C) to 635°F (335°C) which is above the Teflon phase transition temperature (623°F 328°C). This results in a slight structural change but the hydrophobicity of the electrode is increased.

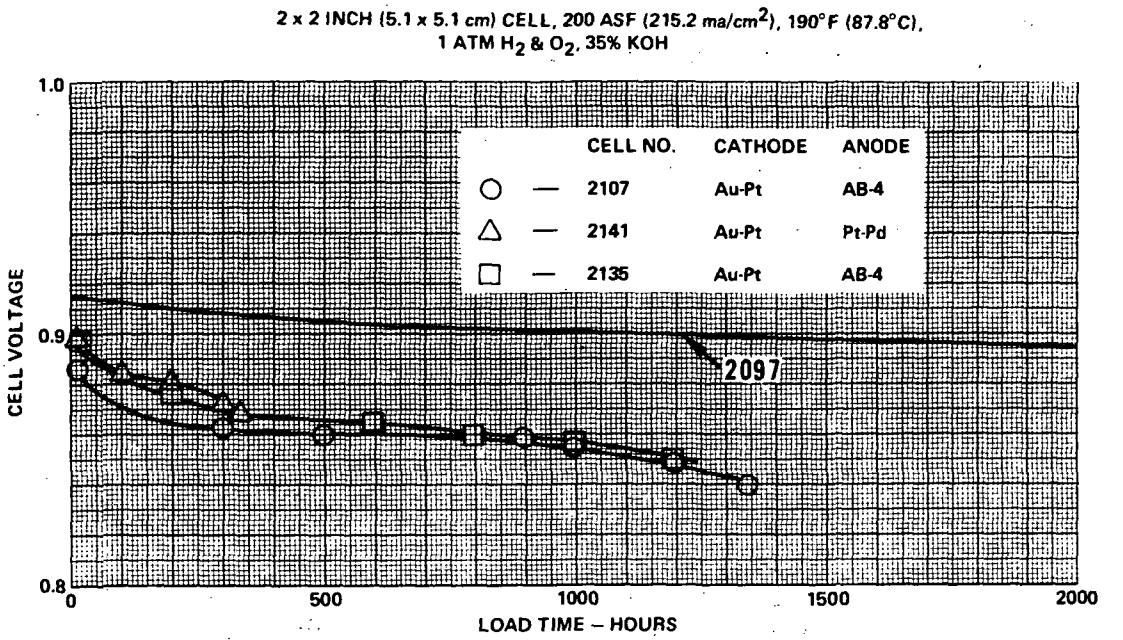

Figure 6 - *Comparison of Early Au-Pt Cathode Cells Endurance with Cell 2097*

2) To achieve the desired suspension of Teflon and catalyst requires the addition of surface active materials beyond that contained in the Teflon slurry as manufactured. This slurry contains about 7 percent of Triton X-100, a non-ionic surface active material. Triton X-100 is difficult to remove from the electrode prior to sintering, but removal is necessary since the presence of organic materials can cause overheating of the electrode during the sintering step. Therefore, other surface active materials have been used, such as gelatin and gum tragacanth, which can be washed from the structure with water, making it possible to change the quantity of surfactant without adversely affecting the structure during sintering.

3) The ideal electrode structure would have very specifically *defined gas (Teflon) and liquid (catalyst) channels of the* appropriate size and distribution (each catalyst channel surrounded by a gas space). Mixing Teflon and catalyst slurries tends to produce a poorly defined geometry which results in some catalyst being isolated in the Teflon spaces and other catalyst being lost in large flooded spaces. One method of preventing these problems, at least in part, would be to form the Teflon agglomerates prior to mixing with the

catalyst, preventing penetration of catalyst into the gas space and imparting more order to the structure. This changes the methods of fabrication which may be used requiring development of new technqiues.

4) The use of higher Teflon content electrodes should tend to stabilize the electrode structure, although there is a trade-off between initial performance and endurance capability unless the structural order can be improved. Electrodes containing up to 50 percent Teflon by weight were fabricated by the filter transfer method and tested.

5) The mechanical working of the Teflon-catalyst suspension can be used to change the structure. One method of making electrodes, which incorporates stressing the slurry mechanically, is to spray the slurry onto the screen support. Whether this results in significantly different structures than the filter transfer method depends on the number of properties and can not at this time be predicted. Therefore, sprayed electrodes were fabricated and tested.

Half-cell evaluation of the electrodes made by these modified techniques indicated that the high temperature sinter, the sprayed electrodes and the Triton X-100 substitute (gum tragacanth leached) electrodes had equivalent performance and were suitable for endurance tests. The results of endurance testing shown in Figure 7 indicate that the high sinter temperature cathode (Cell No. 2221) displayed the most stable performance of several modified structure cathodes tested in full cells.

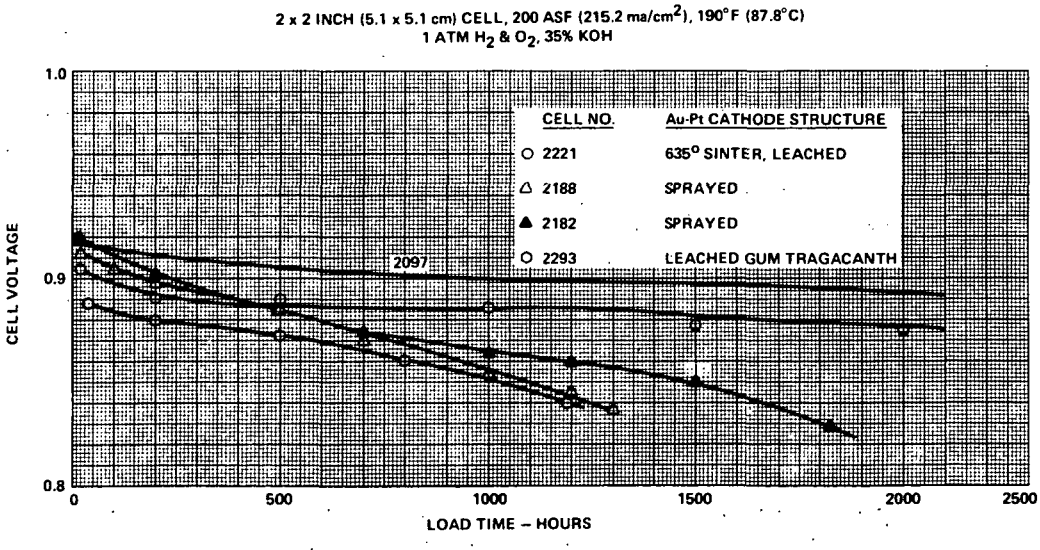

Figure 7 - Decay of Cells with Modified Structure Electrodes

The most effective gold-platinum catalyst cathode structure tested to date has been the 635°F (335°C) sinter temperature, isopropanol leached cathode. A cell incorporating this type of cathode was tested for 5,000 hours. This cell also incorporated on improved structure anode. A description of test results is presented immediately after the anode structure discussion which follows.

As additional diagnostic techniques were developed and used on endurance test cells, it became apparent that the anode structure was less stable than the cathode, with the film thickness increasing with time (as determined by decreasing hydrogen limiting current). Therefore a series of electrodes with different structures were made and half cell tested to determine candidates for endurance testing. The modifications in structure made are as follows:

1) Anodes made by the filter transfer technique were leached with isopropanol prior to sintering to remove all Triton X-100 wetting agent and the sintering temperature raised to 635°F (335°C) as in the cathode modifications.

   The results of half-cell tests are shown in Table 3 and show good performance characteristics. This type of electrode was tested on endurance and demonstrated a considerable improvement in limiting current stability (see discussion of Cell No. 2221 which follows).

2) Anodes with high Teflon content proved very difficult to wet and the half-cell test indicated that the electrodes were poorer than standard, thus no endurance tests were planned.

3) Anodes were made by a procedure in which the Teflon suspension and catalyst are mixed to give a slurry which can be applied directly to the electrode substrate by a technique similar to screen printing, followed by sintering at both 590°F (310°C) and 635°F (335°C). These electrodes gave lower anode performance than the standard electrodes and pumped at a higher rate as cathodes, however this technique is a very inexpensive method of fabrication and should be of interest for further development. No endurance tests were made on these electrodes.

4) As discussed under cathode structure modifications, pre-agglomerated Teflon is a means of stability control. This is a difficult method to control and the electrodes made had

low performance as shown in Table 3. No endurance tests were made on these electrodes. This method should have further development since it offers the best structural control at reasonable cost levels of any of the modified structures.

5) In one set of electrodes, the catalyst - Teflon slurry was mixed by ultrasonic blending as a means of applying a high mechanical stress to the system. As the data shows (Table 3), this does not offer any advantage and no endurance tests were performed.

6) As in the case of the cathode, electrodes have been made using dispersion agents in addition to the Triton X-100 contained in the Teflon suspension. The agents used were the water soluble fraction of gum tragacanth and gelatin. Both structures gave electrodes having good performance although the gelatin seemed to give a somewhat better dispersion. Endurance tests of these electrodes would be desirable but have not yet been made.

7) In addition to changing the structure of platinum-palladium electrode, one new structure was made using standard fabrication techniques, but with a new anode catalyst. The catalyst is a gold-rhodium alloy, made by the same technique as with the gold-platinum cathode catalyst. The performance of this anode was very good, although, since it contains a relatively low amount of rhodium which is the active catalytic agent, it has a low level of tolerance for catalytic poisons in the electroylte. One endurance test has been made with this anode with a gold-platinum cathode. The anode limiting current in this cell decayed rapidly after 500 hours. Thus the structure is not a useful one; however, the catalyst may be advantageous in a different structure.

The result of the anode structure modification to date is that the high temperature sinter - isopropanol leached electrode gives a reasonable solution to the problem for time periods of several thousand hours. Further work in this area should be aimed at structures with more defined organization, as the preagglomerated Teflon type, which have the best ultimate potential.

TABLE 3

Anode Structural Modification Platinum/Palladium Filtered Electrodes

Variable	Loading mg/cm²	Sinter Temper. °C	Performance, mv, on H_2 1,000 mA	O_2 100mA	O_2 1,000mA	Air 100 mA	Air 1,000 mA
Standard	8.27	310	55	960	908	926	-
		335	70	958	902	924	838
Ultrasonic Blend	9.54	310	40	956	905	923	850
		335	115	937	872	903	802
Flocculated Teflon	11.82	310	26	955	907	920	-
		335	46	961	900	922	-
Soluble Gum Tragacanth	9.44	310	30	950	895	912	-
		335	95	906	844	875	-
Gelatin	10.82	310	65	965	905	935	-
		335	40	930	862	909	807
10% Rh-Au	12.74	335	22	945	900	No Data	No Data
33% Teflon	13.0	310	81	930	865	902	-

(-) Limited before 1,000 mA

The most promising cathode and anode structures available at a point approximately mid-way through the program were selected for endurance testing. A 2 x 2 inch cell(5.1 x 5.1 cm), No. 2221, was assembled using the following electrodes:

Cathode

Catalyst	22 mg/cm² gold-platinum
Structure	635°F(335°C) sinter temperature isopropanol leached

Anode

Catalyst	10 mg/cm² platinum-palladium
Structure	635°F(335°C) sinter temperature isopropanol leached

The cell was tested at standard endurance test conditions: 200 amp/ft² (215.2 ma/cm²), 190°F(87.8°C), 1 atmosphere hydrogen and oxygen reactants, 35 percent electrolyte concentration. Tafel performance sweeps, IR and limiting current diagnostic tests were performed at 1000 hour intervals. A plot of cell performance vs. time is shown in Figure 8. The cell was operated for 5,000 hours at which time it was shutdown for electrolyte refurbishment which, at the time of writing, is in process. The overall decay rate at 200 ASF(215.2 ma/cm²) was

10.6μV/hr. Correcting for the performance loss due to electrolyte carbonation(23 percent conversion or an estimated 17 mV loss) results in a carbonate free decay rate of 7.2μV/hour.

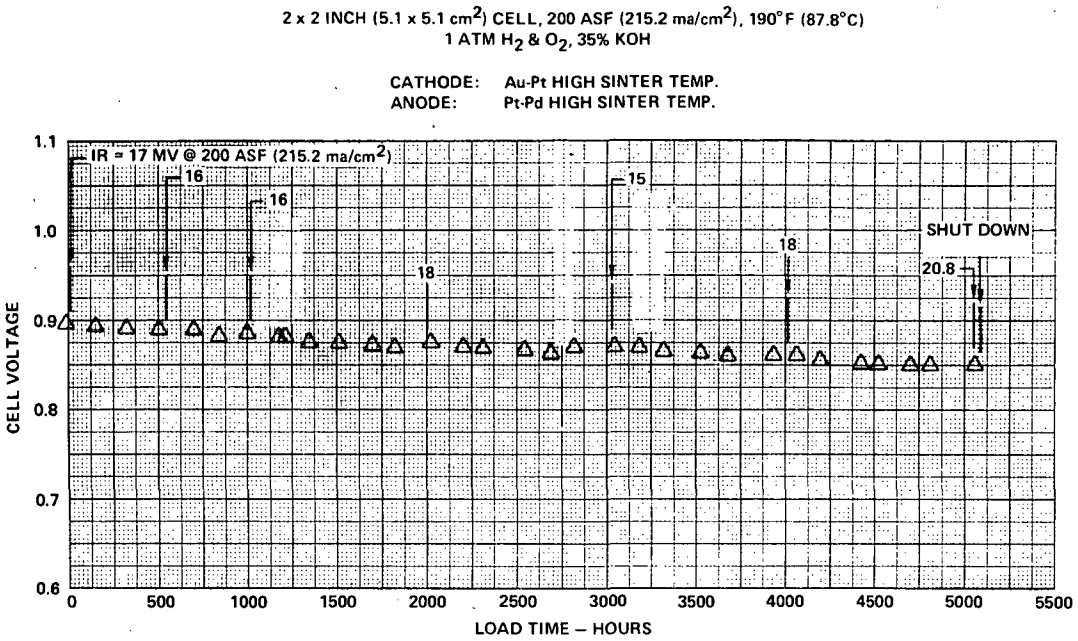

Figure 8 - Cell No. 2221 Performance

The periodic diagnostic data taken during the test indicates that the majority of the performance loss was due to a decrease in cathode activity. Tafel region data indicates that the cathode performance loss was approximately 30 mV or a decay rate of 6 μ V/hr. This result does not correspond to the results from Cell No. 2097 discussed above. That cell showed a cathode activity loss of 8 mV over a 5,000-hour test duration. Possible causes for the lower stability of the catalyst used in Cell No. 2221 are under investigation.

Limiting current diagnostic tests provided data on the stability of the electrode structure. These tests measure the maximum current carrying capacity of an electrode when the electrode operates on very dilute reactants - 4 percent reactants, 96 percent inerts. The importance of these tests is not in determining the absolute value of an electrode's current carrying capability, but rather to detect electrode structural changes or increasing electrolyte film thicknesses which may occur with operating time. Because very dilute reactants are used, these tests can detect small changes in an electrode diffusional behavior which would be unmeasurable when operating on pure reactants.

Figure 9 shows the relative limiting current change with time for the anode of Cell No. 2221 and anodes made using the low temperature sinter/no isopropanol leach method. It is seen that the modified fabrication procedure used for the anode of Cell No. 2221 resulted in superior stability.

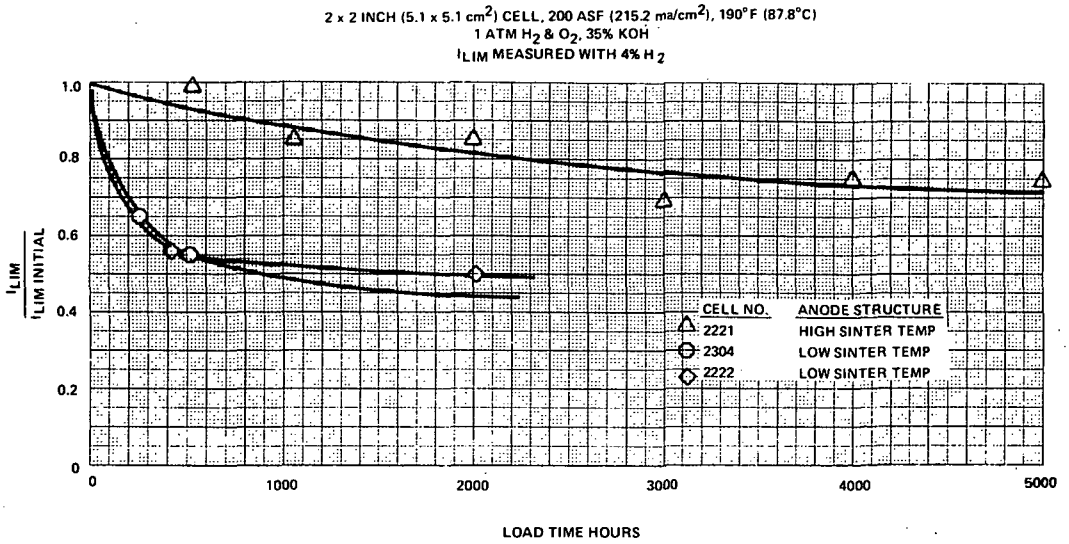

Figure 9 - Cell No. 2221 Anode Relative Limiting Current Change with Time

Figure 10 shows the relative limiting current stability for the gold-platinum cathode used in Cell No. 2221 compared to laboratory platinum-palladium cathodes. The gold-platinum cathode is seen to be less stable than the platinum-palladium cathode. In 2,200 hours of operation, the platinum-palladium cathode limiting current decreased at a lower rate than that of the gold-platinum cathode. In addition, the platinum-palladium initial level was approximately 50 percent higher than the initial level of the gold-platinum cathode. Thus, further structural development is required to optimize the performance and stability of gold-platinum cathodes.

Conclusions

Gold is an electrochemically stable and active catalyst for high performance, hydrogen oxygen alkaline electrolyte fuel cell cathodes.

The use of gold cathode catalysts eliminates metals migration as a source of performance degradation and possible cell shorting failure modes.

Alloys of gold using platinum, nickel and copper display performance levels equivalent to or greater than platinum.

Several gold alloy systems show potential for reducing recrystallization of the gold at fuel cell operating conditions to acceptable levels. Additional cell endurance testing is required to select and optimize the best alloy system.

Cathode and anode structures made by sintering the catalyst-Teflon mixture at temperature above the Teflon phase transition temperature demonstrated improved diffusion region operating stability. Further research into the properties of electrode structures, including evaluation by cell endurance testing, is required to define optimum catalyst-structure combinations.

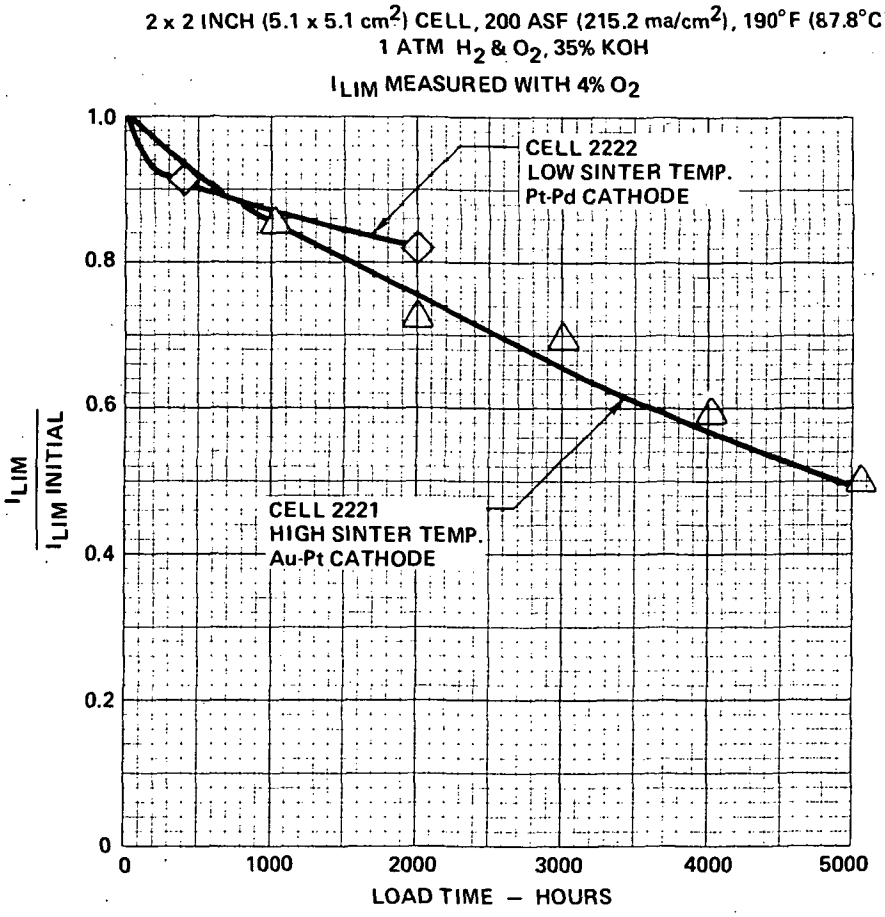

Figure 10 - Cell No. 2221 Gold Platinum Cathode Relative Limiting Current Stability

B. Structural Materials

Materials Selection

The effects of fuel cell environments on candidate cell structural materials were determined for up to 8000 hours of exposure. The materials selected for testing were candidates for use in the electrolyte reservoir plates (ERP), water transport plates (WTP), cooler and reactant flow plates and unitizing frames. They were evaluated in laboratory tests which simulated cell operating conditions to determine their resistance to the potassium hydroxide electrolyte and steam-water environments typical of the Engineering Model System (EMS) Power Section. Measurements were made periodically to determine changes in mechanical properties and to determine tendencies to contaminate the electrolyte and form potassium carbonate.

The candidate materials were selected on the basis of previous test results in which the materials exhibited less than 1.0 percent loss in weight after 1000 hours of exposure to electrolyte. The selected materials are listed in Table 4. Additional materials were added during the program when it became apparent that several of the original candidates were unacceptable and when cell stack component testing indicated the need for materials not originally selected. The materials added are listed in Table 5.

TABLE 4

Initial Candidate Structural Materials

Material		
Polyaryl Ether	Arylon	Uni-Royal Inc.
Polyaryl Sulfone	Astrel 360	Minnesota Mining and Mfg. Co.
Polysulfone	Bakelite Polysulfone	Union Carbide Corp.
Polypropylene	D-100	Enjay Chemical Co.
30 weight % Glass Filled Modified Polyphenylene Oxide	Noryl - 3	General Electric Co.
50 weight % Asbestos Filled Polybutadiene	FCR 1261-IV	Firestone Tire and Rubber Co.
50 weight % Asbestos Filled Polyphenylene Sulfide	Ryton	Phillips Petroleum Co.
Ethylene Propylene		
Butyl		
Hypon Adhesive		
EPR Adhesive		

TABLE 5

Additional Candidate Structural Materials

30 weight % Fybex Filled TFE	-	Liquid Nitrogen Products
30 weight % Fybex Filled Polypropylene	E-0834-77-2	DuPont
30 weight % Fybex Filled Polysulfone	PXMD-5540	Union Carbide Corporation
Hypon Impregnated Asbestos, Cured at 165°F (73.9°C), 1 Hour		
Hypon Impregnated Asbestos, Cured at 220°F (104.4°C), 3.5 Hours		

Test Apparatus

The relative resistance of candidate materials to electrolyte was determined by immersing specimens of the materials in 30 weight percent/ KOH at 200°F(93.3°C). The electrolyte was contained in a Teflon beaker in a sealed glass reaction kettle, Figure 11. At 1000 hour intervals of testing, duplicate specimens were removed, rinsed for 48 hours in cold running water, dried for 24 hours at 150°F(65.6°C) and changes in appearance, weight, compressive strength and compressive modulus determined.

Specimens of materials being considered for the evaporative cooler were exposed to a steam-water environment at 220°F (104.4°C) and 18 psig (22.56 n/cm^2) in an autoclave, see Figure 12. Duplicate samples were removed at 2000-hour test intervals, rinsed for 48 hours in cold running water, dried for 24 hours at 150°F (65.6°C) and changes in appearance, weight, compressive strength and compressive modulus determined.

Specimen size and shape for both tests were dictated by mechanical testing requirements and conformed to ASTM specification D695-63, for polymer samples and ASTM specification D575-67, for elastomer samples. A modified polymer sample was used to evaluate adhesives.

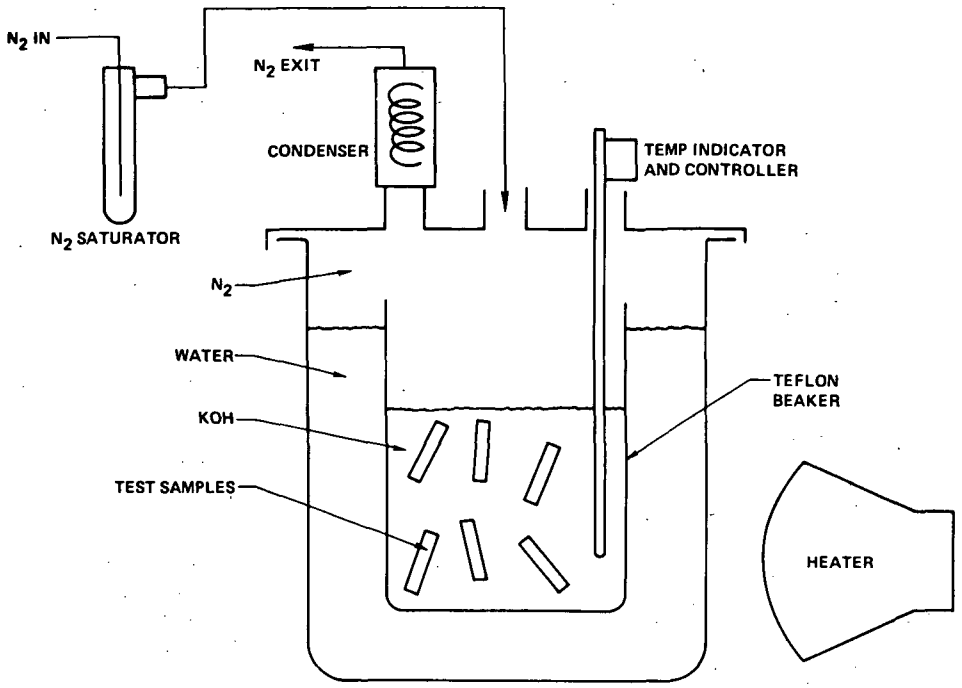

Figure 11 - Electrolyte Compatibility Test Apparatus

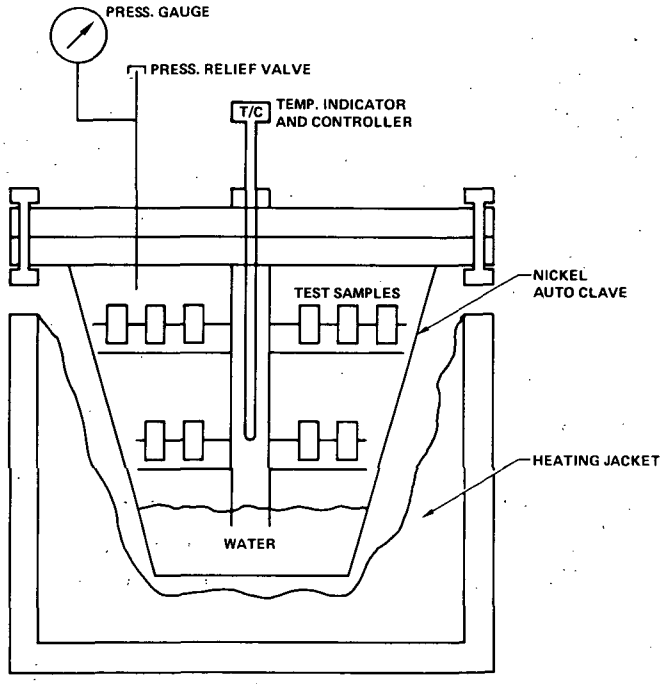

Figure 12 - Steam Compatibility Test Apparatus

The relative tendancies of materials to carbonate the electrolyte were determined by immersing specimens similar to those used in the compatibility tests in 30 weight percent KOH at 200°F (93.3°C) in a sealed Teflon bottle which was contained in a sealed glass reaction kettle (see Figure 13). A sample of electrode was placed in the sealed bottle with the test specimens and an oxygen blanket covered the electrolyte to simulate cell conditions conducive to electrolyte carbonation. The test specimen surface area to electrolyte volume was standarized and remained constant throughout the test. All tests were prepared at room temperature in a glove box containing pressurized oxygen to preclude air contamination. A test set-up not containing material specimens was also prepared so that a carbonate background level for the test procedure could be established. The test procedure provided a positive oxygen pressure within the sealed bottle at the testing temperature to minimize the possibility of air contamination. The sealed glass reaction kettles also contained a carbon dioxide scrubbed nitrogen environment to further preclude contamination. Samples of electrolyte were taken at 1000-hour intervals from each test and the carbonate content determined using a double end point titration technique. The results were reported as grams of carbonate per cm^2 of specimen surface per cm^3 of electrolyte. All sampling was conducted in an oxygen atmosphere glove box.

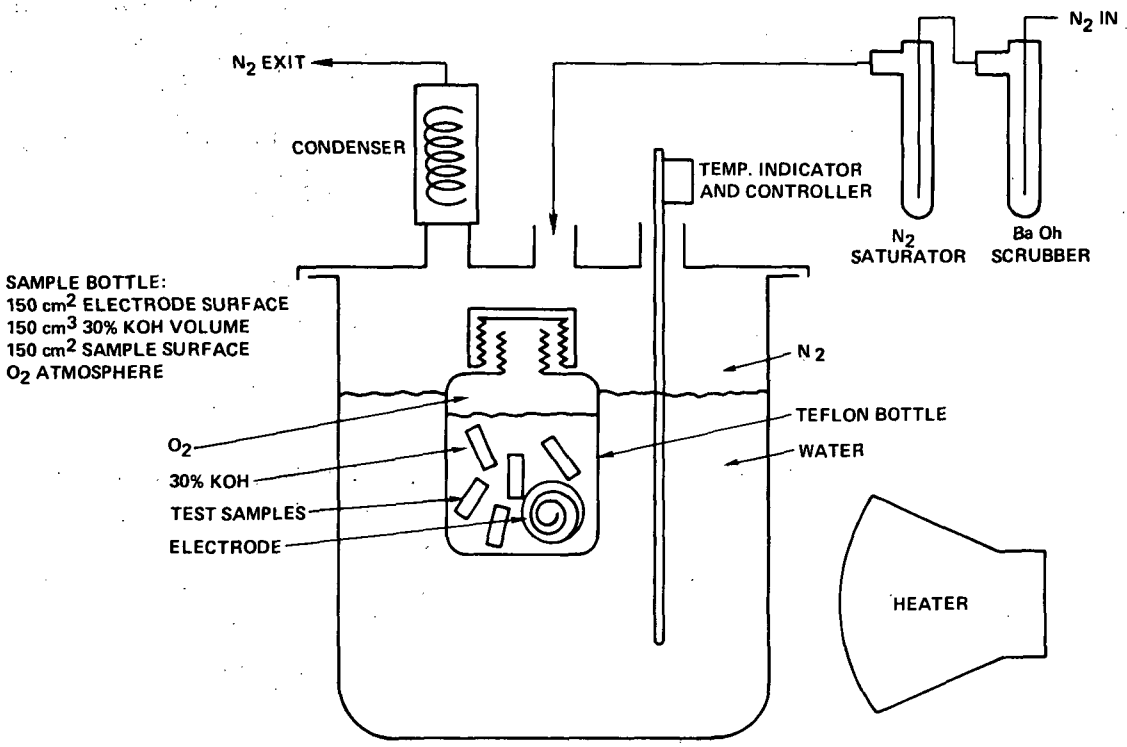

Figure 13 - Electrolyte Carbonation Test Apparatus

In addition to the electrolyte carbonation tests, a series of tests were conducted to determine the types and amounts of gaseous reaction products that resulted from the exposure of candidate materials to an oxygen containing environment. This was accomplished by inserting material specimens having a surface area of 150 cm^2 into a 500 cm^3 stainless steel sample bottle. The bottle was charged to 50 psi (34.5 n/cm^2) with a 30 percent oxygen/70 percent helium (by volume) gas mixture. The sample bottles were then held for 100 hours at a temperature of 250°F (121.1°C) and the resulting gases passed through a gas chromatograph. The chromatograph indicated the relative amounts of carbon monoxide, carbon dioxide and methane which were evolved.

Electrolyte Compatibility Test Results

The changes in weight, compressive yield and compressive modulus of the candidate materials when exposed to the electrolyte are shown in Figures 14 through 19. Three materials; polypropylene, polysulfone, and 50 percent asbestos filled polyphenylene sulfide showed less than a 0.5 percent variation in weight and displayed relatively stable compressive strengths and moduli after 8000 hours of testing. The remaining materials; polyaryl ether, ethylene propylene, butyl, 30 percent glass-filled Noryl, 50 percent asbestos-filled polybutadiene and polyaryl sulfone exhibited what was considered excessive changes in weight, compressive strength and compressive yield after 8000 hours of testing. The two candidate adhesives, Hypon joining polyaryl ether and ethylene propylene joining polysulfone were considered unacceptable because of their tendancy to fracture through the bond while exposed to the electrolyte or during compressive strength measurements.

Steam Compatibility Test Results

The changes in weight, compressive yield and compressive modulus of the candidate materials upon exposure to a steam environment are shown in Figures 20 through 25. On the basis of these results, five materials; polyaryl ether, polyaryl sulfone, polysulfone, polypropylene and 50 percent asbestos-filled polyphenylene sulfide were considered acceptable after 8000 hours of testing. The remaining materials and adhesives were considered unacceptable for structural components exposed to a steam environment.

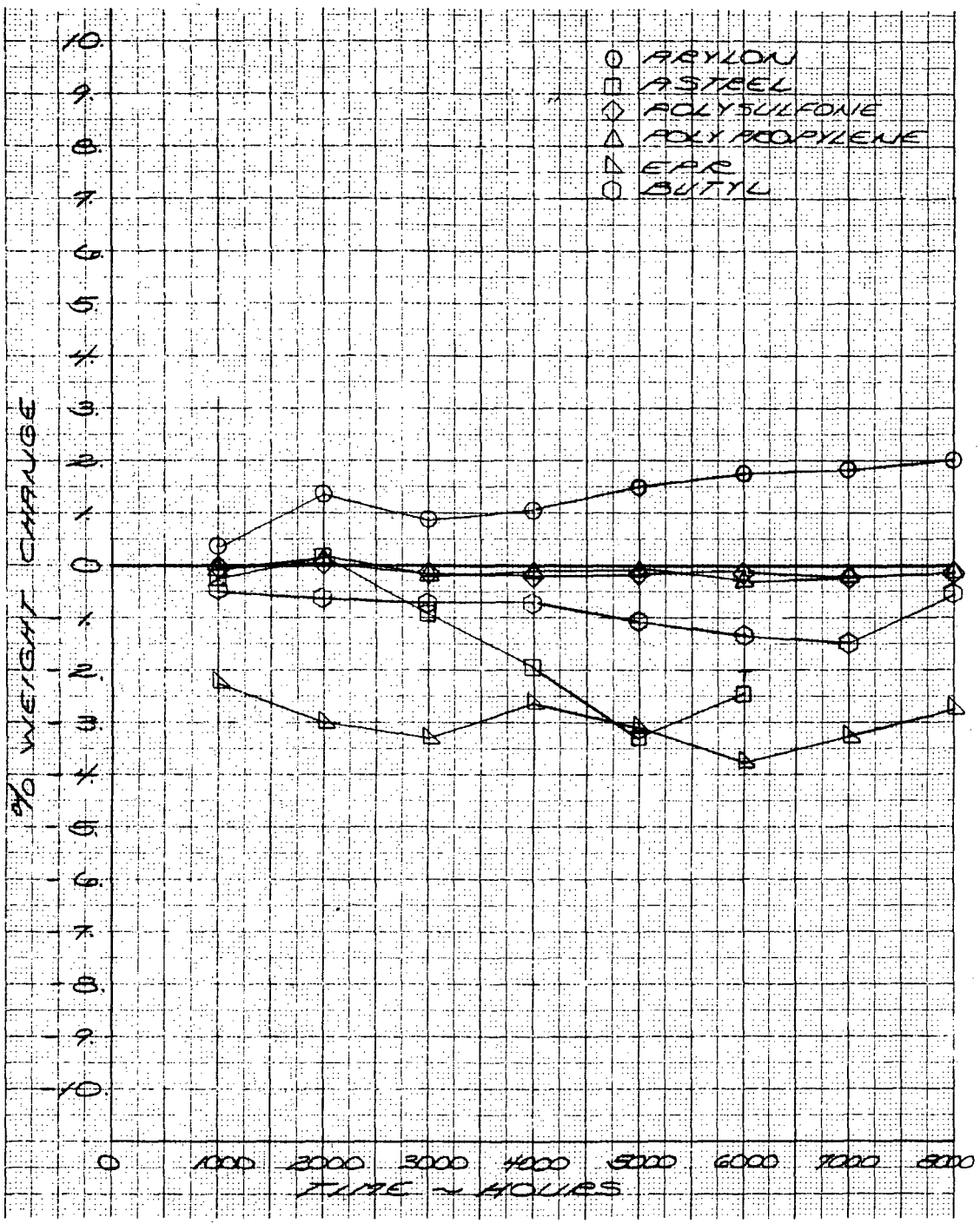

Figure 14 - KOH Immersion Test Results

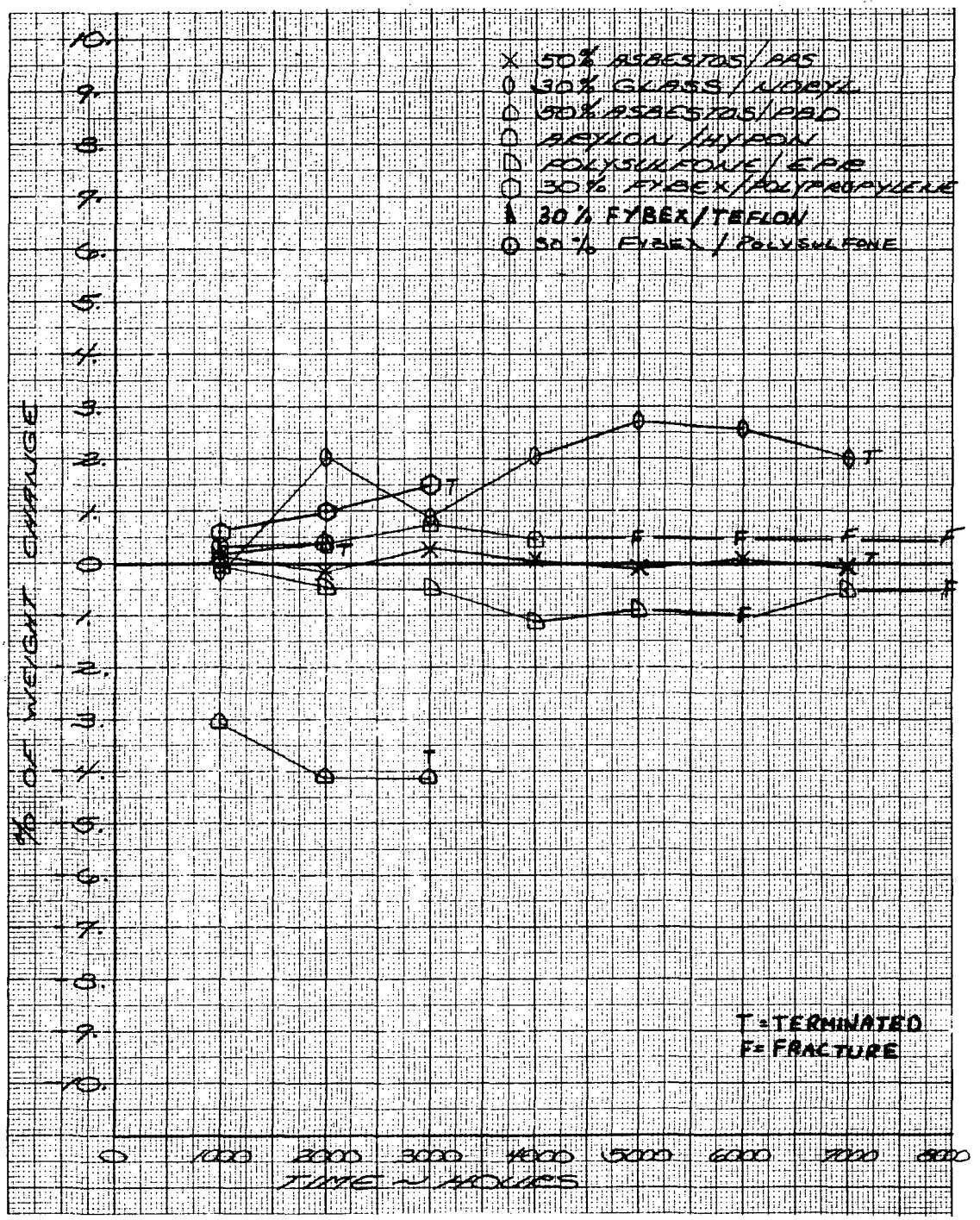

Figure 15 - KOH Immersion Test Results

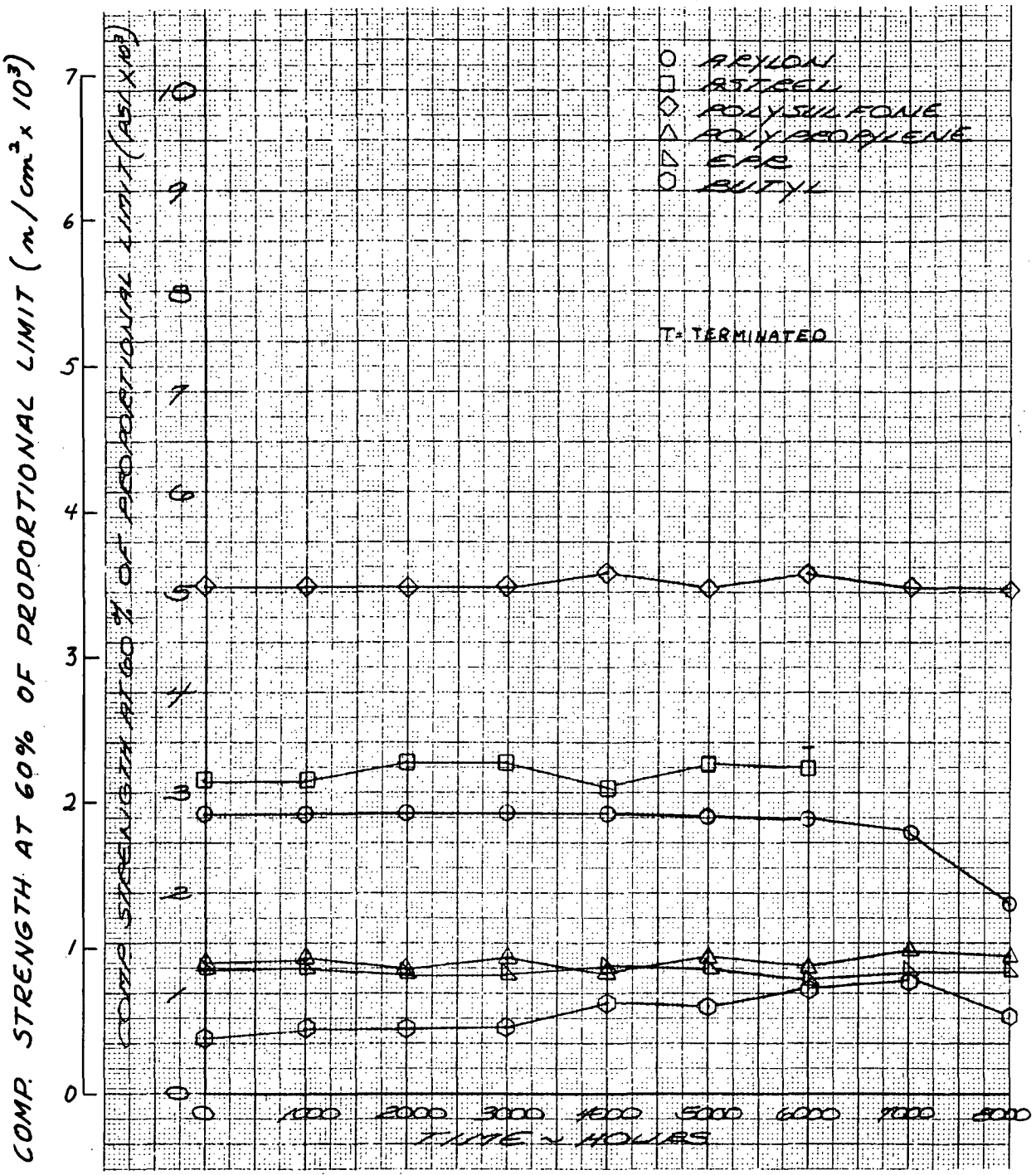

Figure 16 - KOH Immersion Test Results

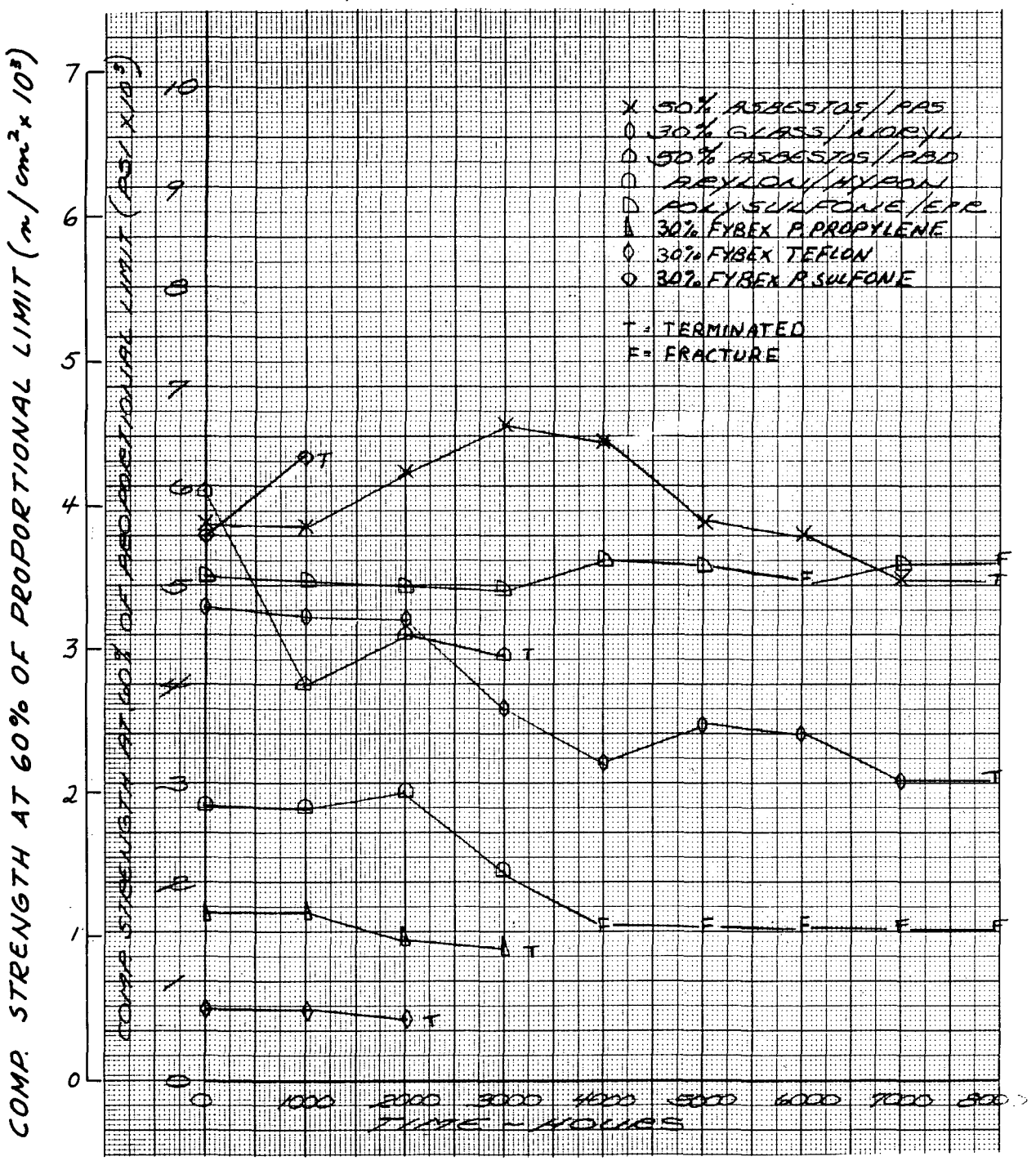

Figure 17 - KOH Immersion Test Results

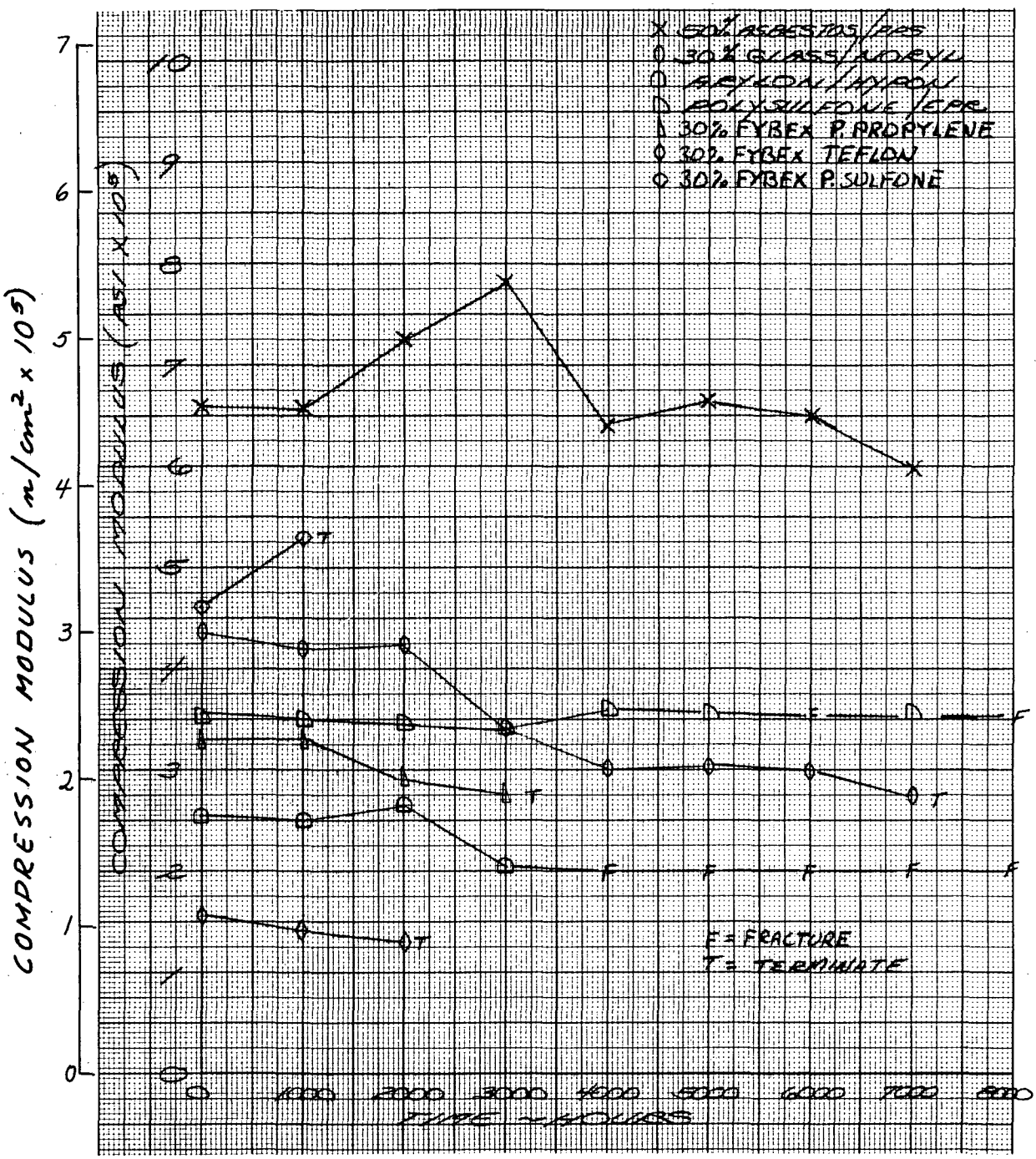

Figure 18 - KOH Immersion Test Results

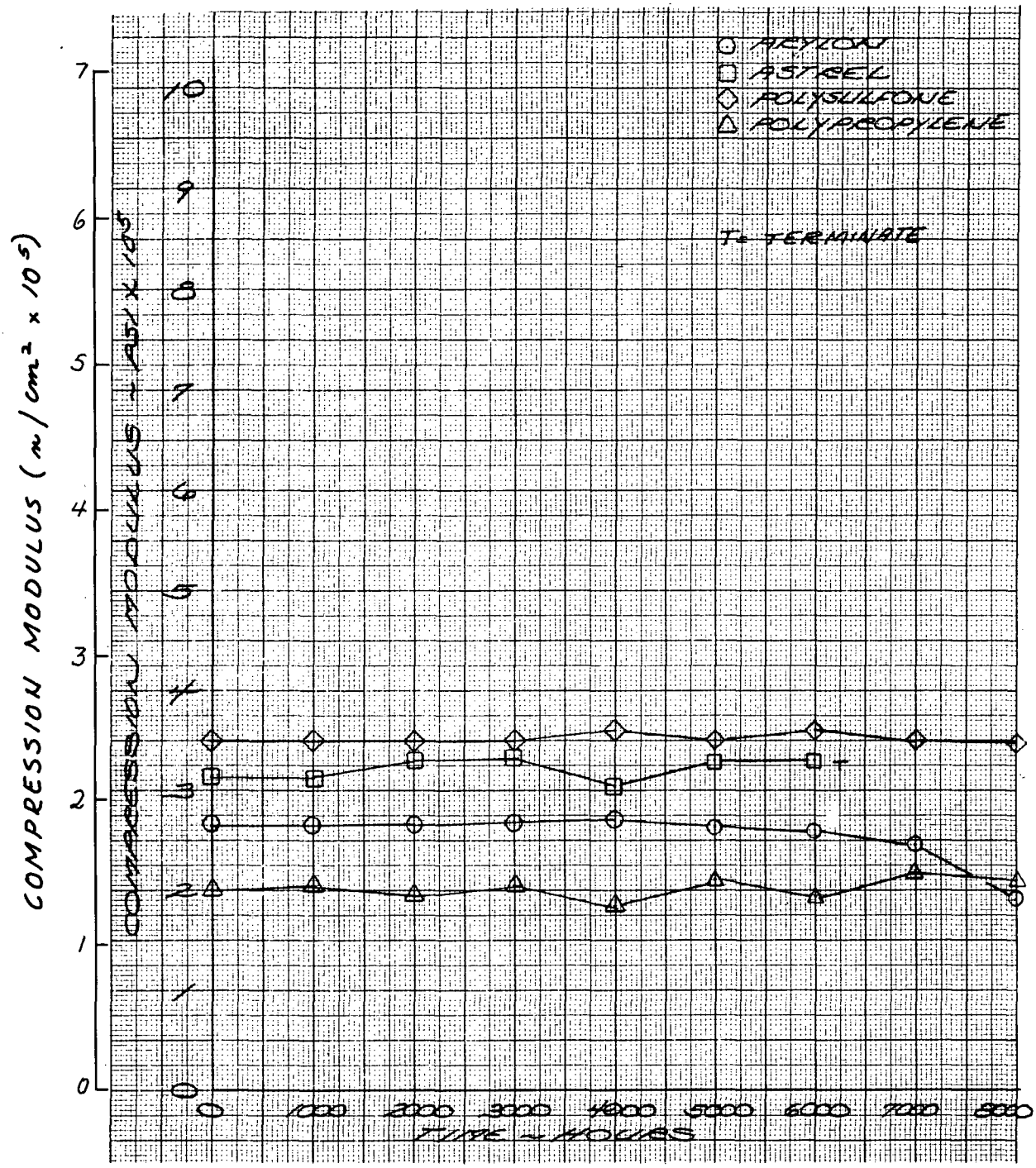

Figure 19 - KOH Immersion Test Results

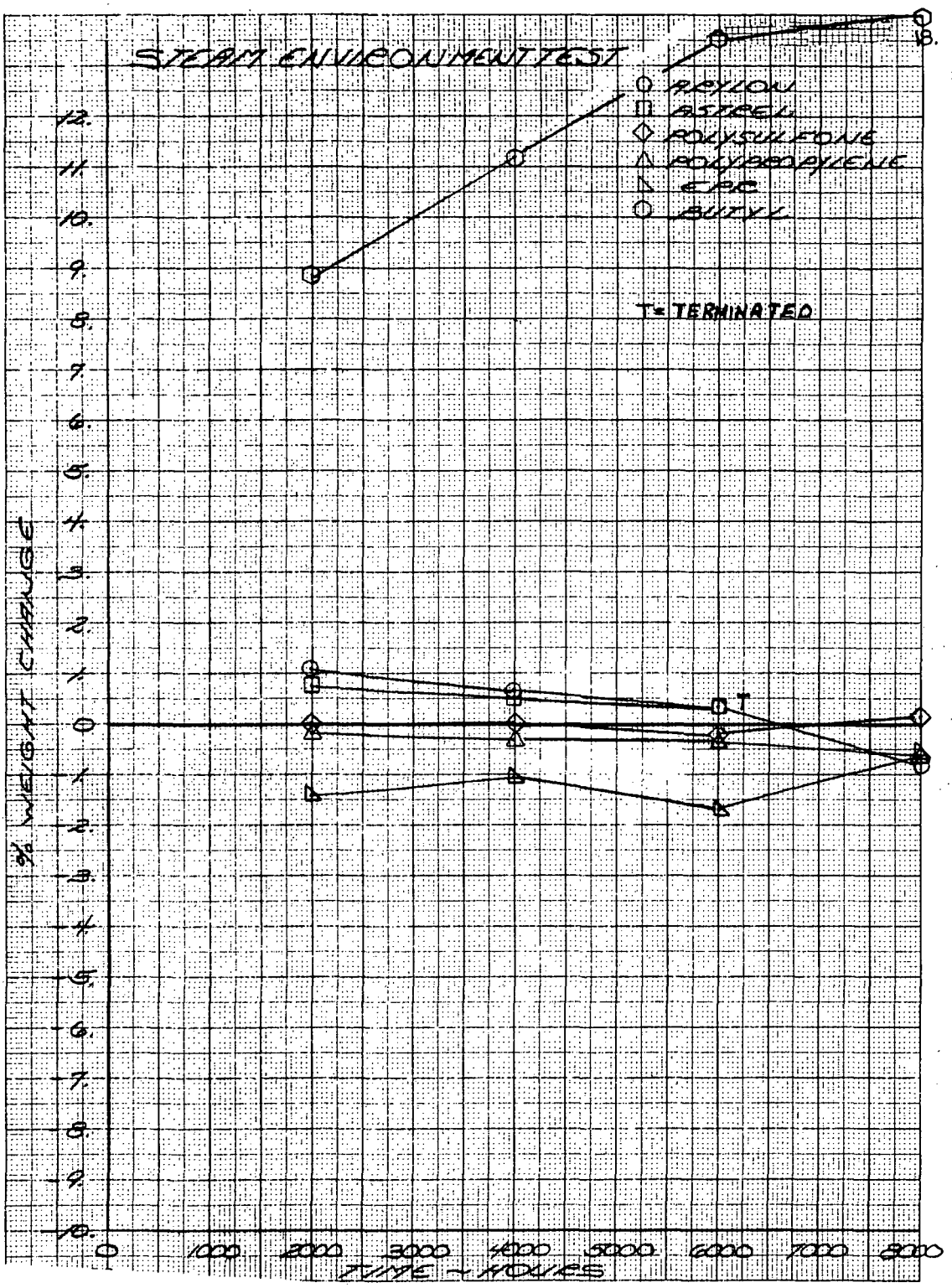

Figure 20 - Steam Environment Test Results

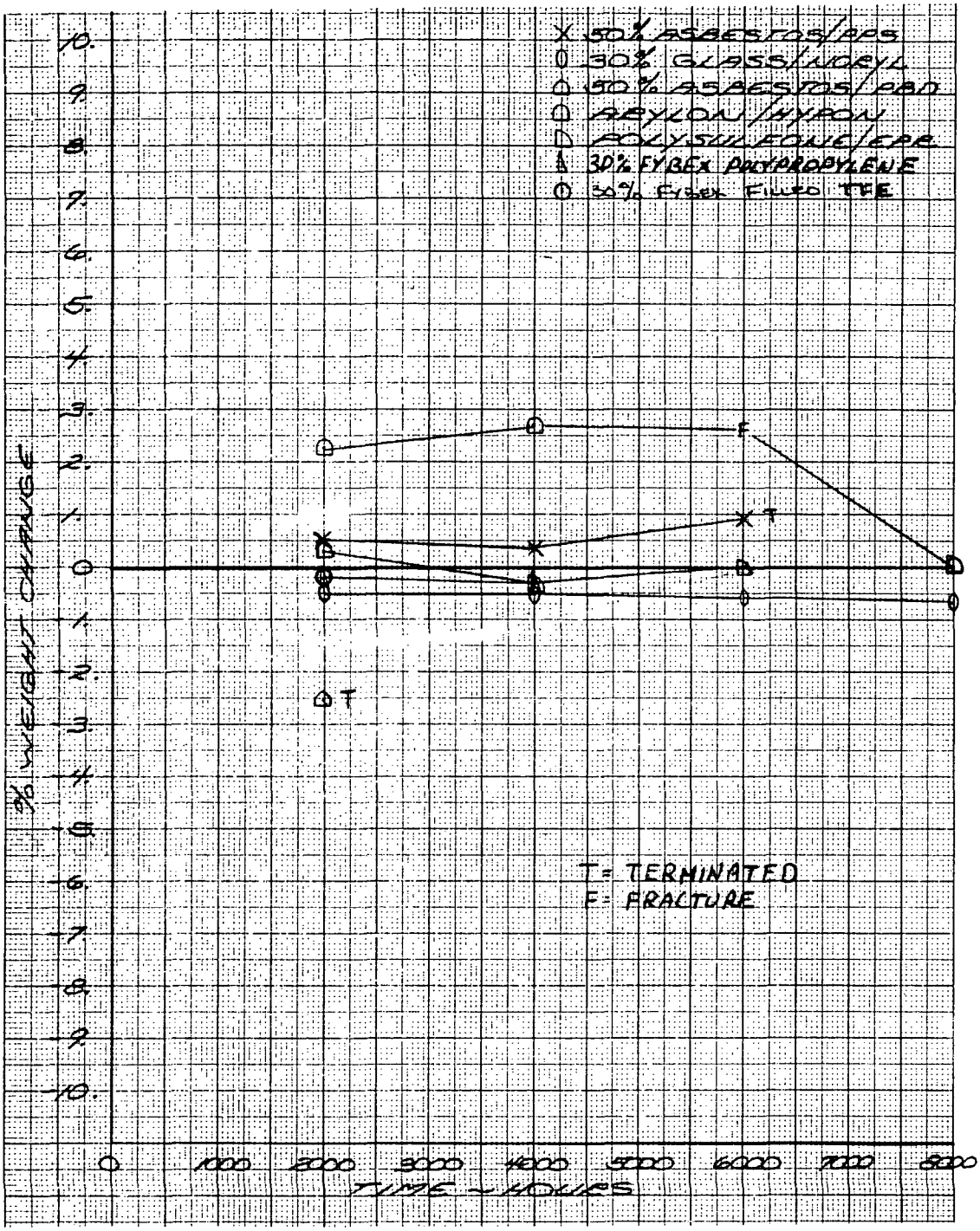

Figure 21 - Steam Environment Test Results

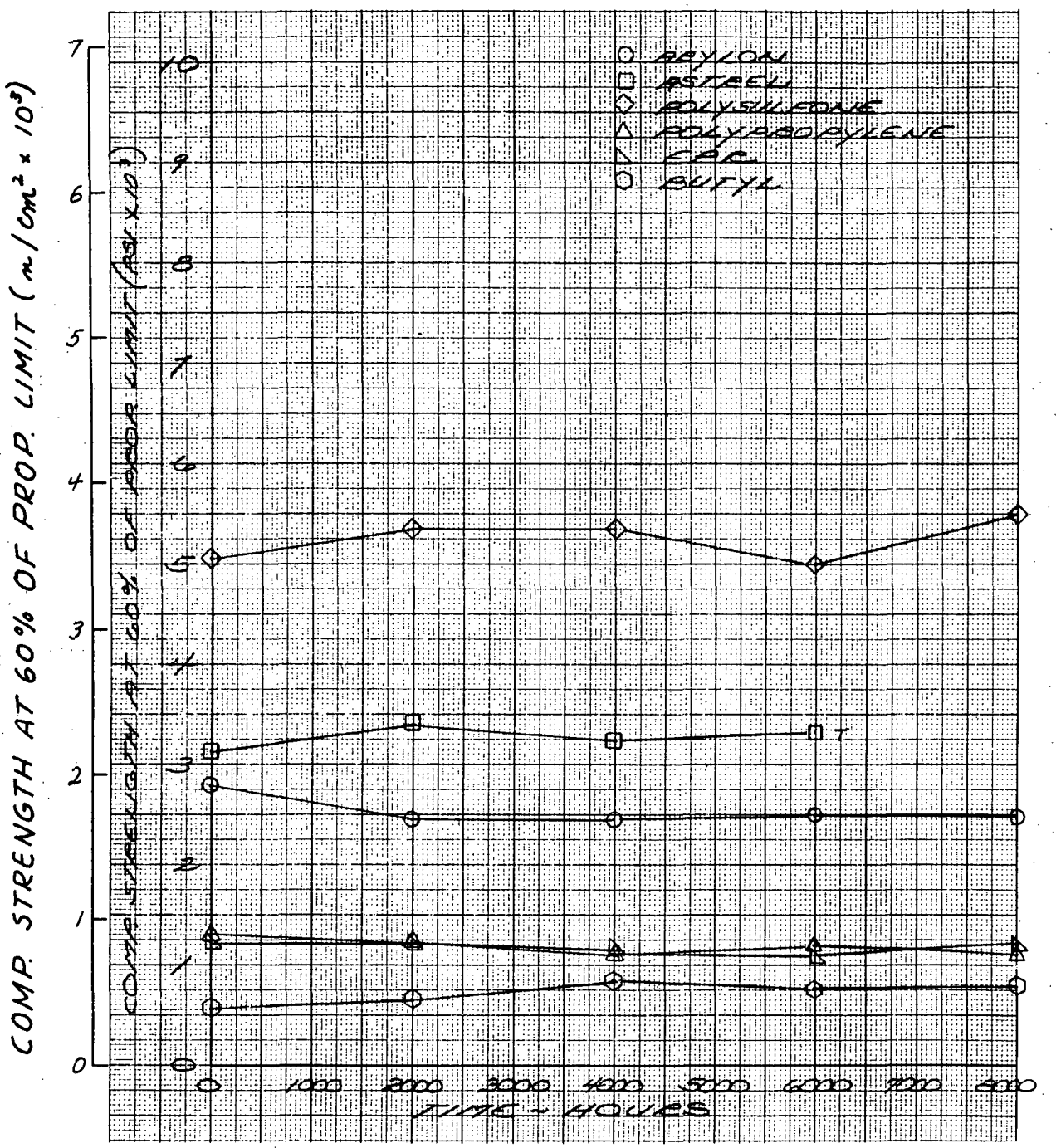

Figure 22 - Steam Environment Test Results

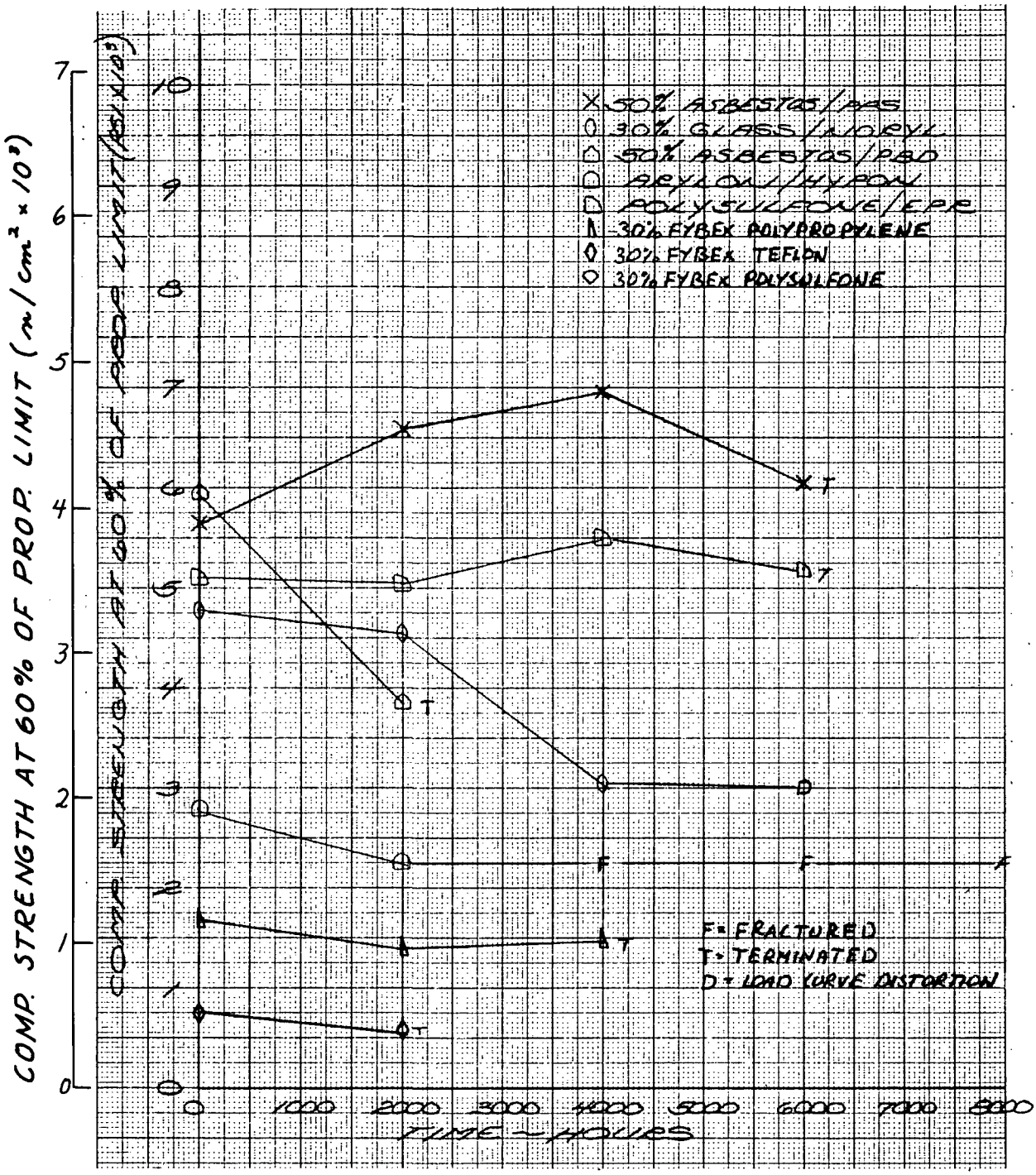

Figure 23 - Steam Environment Test Results

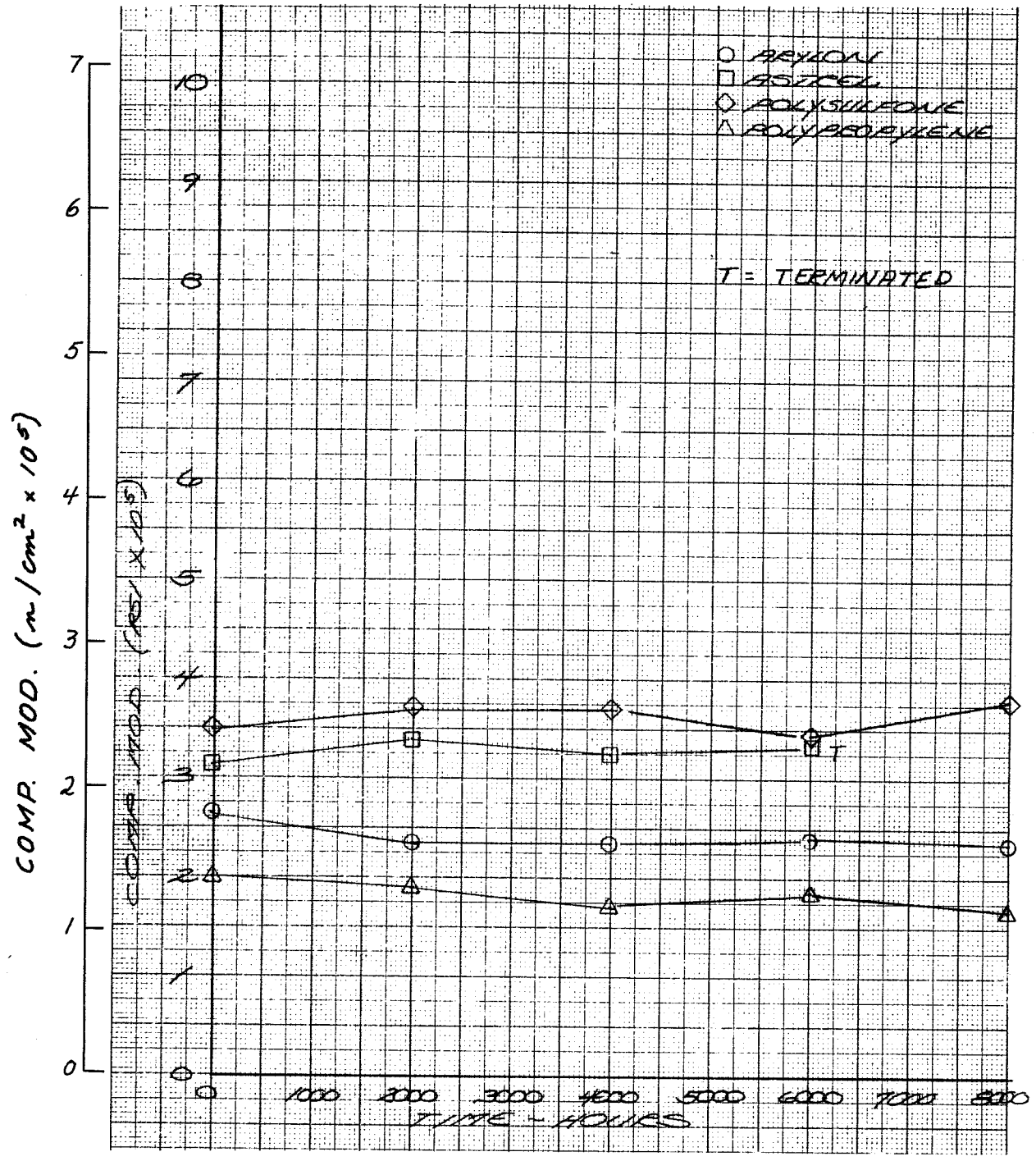

Figure 24 - Steam Environment Test Results

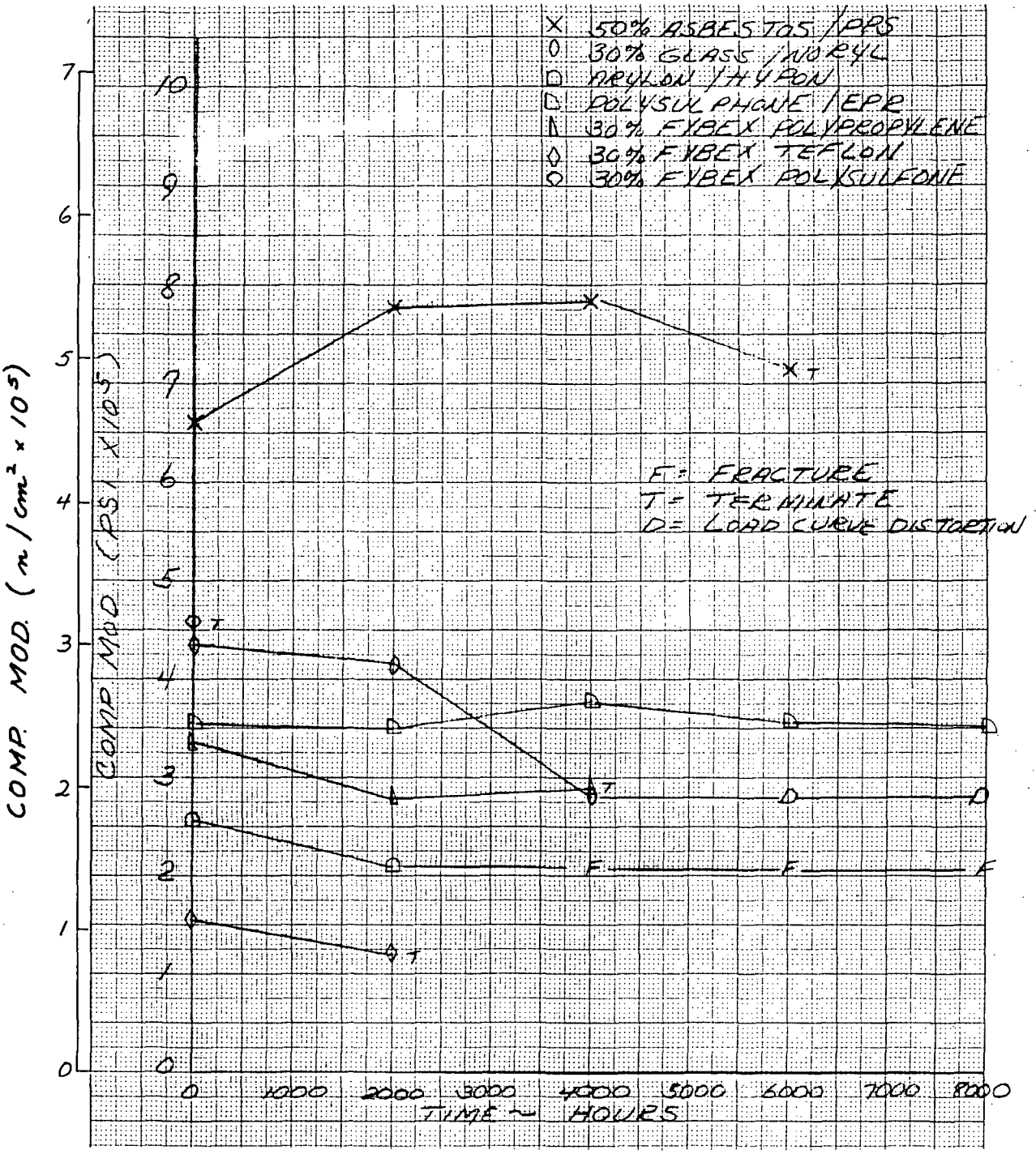

Figure 25 - Steam Environment Test Results

Electrolyte Carbonation Test Results

The results of the electrolyte carbonation tests are shown in Figures 26 through 28. Four materials; 50 percent asbestos-filled polybutadiene 30 percent glass-filled Noryl, ethylene propylene, and polyaryl ether exhibited electrolyte carbonating rates of greater than 0.5 grams K_2CO_3/cm^2 specimen/cm^3 electrolyte within 8000 hours of testing and were considered unacceptable. The remaining candidate materials exhibited rates of less than 0.5 grams K_2CO_3/cm^2 specimen/cm^3 electrolyte and were not considered unacceptable.

Oxygen Compatibility Test Results

The relative oxidation resistance of the candidate materials, obtained using gas chromatograph techniques, is shown in Figure 29. The figures illustrate the relative tendencies of the materials to produce gaseous oxidation products which could carbonate the electrolyte. These results show that all materials produced a measurable level of carbon dioxide and in some cases measurable amounts of carbon monoxide and methane. The three materials which produced the greatest amount of carbon dioxide, polyaryl ether, 30 percent glass-filled Noryl and 50 percent asbestos-filled polybutadiene also produced high levels of carbonates in the electrolyte carbonation tests. This correlation indicates that the simpler and faster oxidation test could be used to determine the relative tendencies of candidate materials to carbonate the electrolyte.

The five additional materials which were evaluated during the late portion of the program did not accumulate sufficient test time to be compared with the original candidate materials, but several significant trends were apparent. The electrolyte carbonation tests involving the Hypon-impregnated asbestos samples showed that after 3000 hours of testing, the high-cure (220°F (104.4°C), 3.5 hours) material produced approximately one-half the electrolyte carbonate rate of the low-cure (165°F (73.9°C), 1 hour) material. The 30 percent Fybex-filled polypropylene, polysulfone and tetrafluoroethylene samples all showed tendencies to gain weight and to change in compressive yield strength when exposed to the electrolyte.

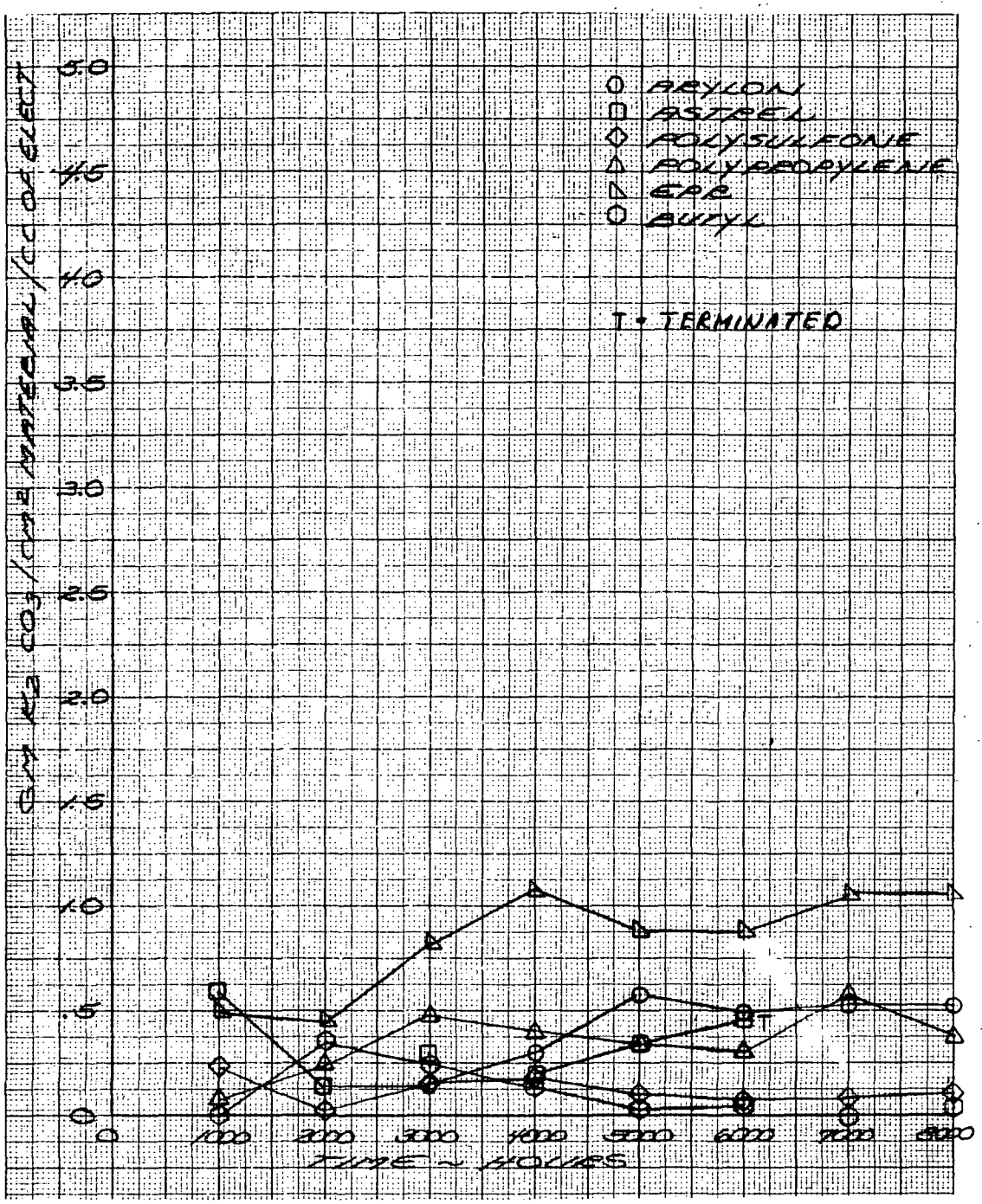

Figure 26 - Electrolyte Carbonation Test Results

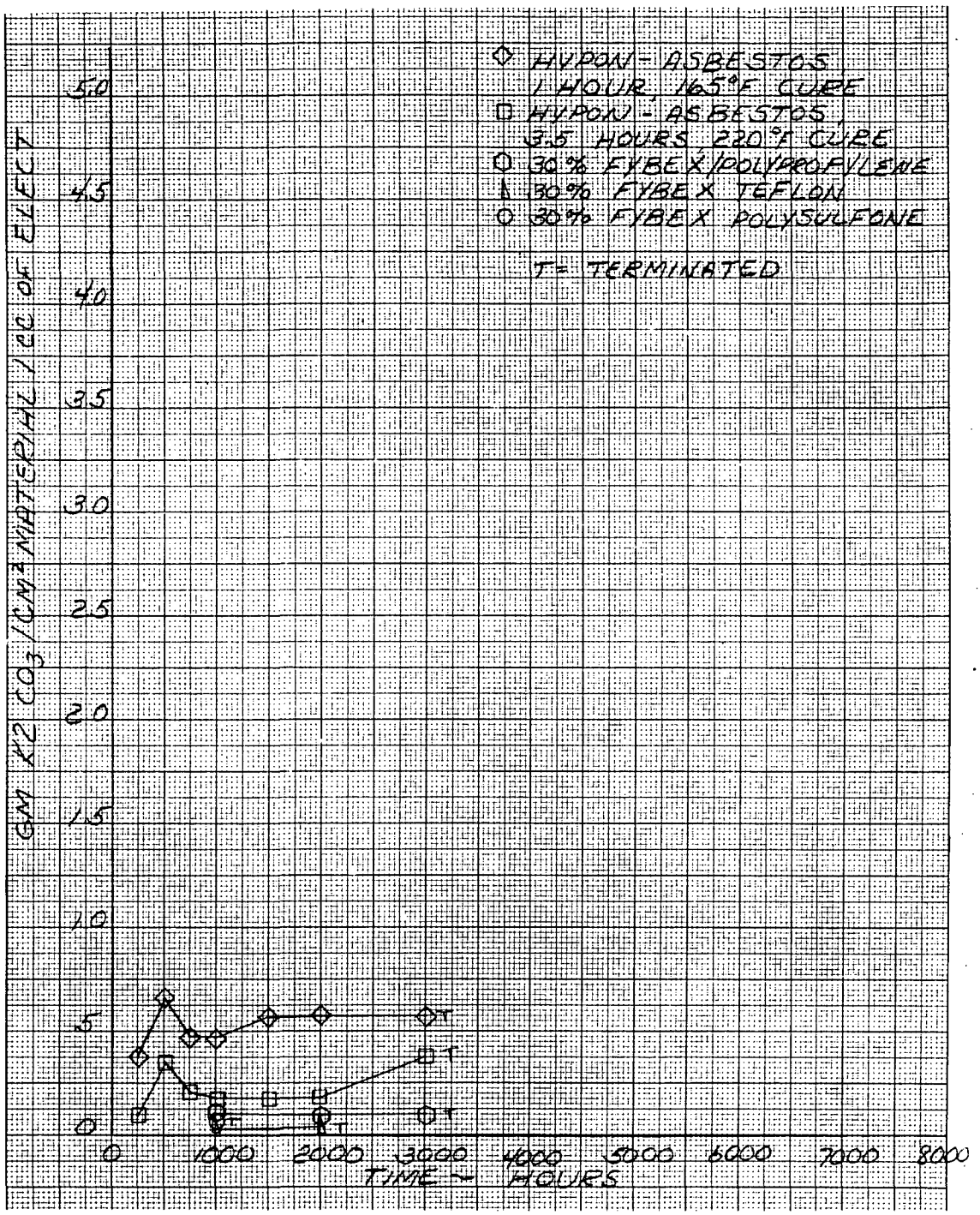

Figure 27 - Electrolyte Carbonation Test Results

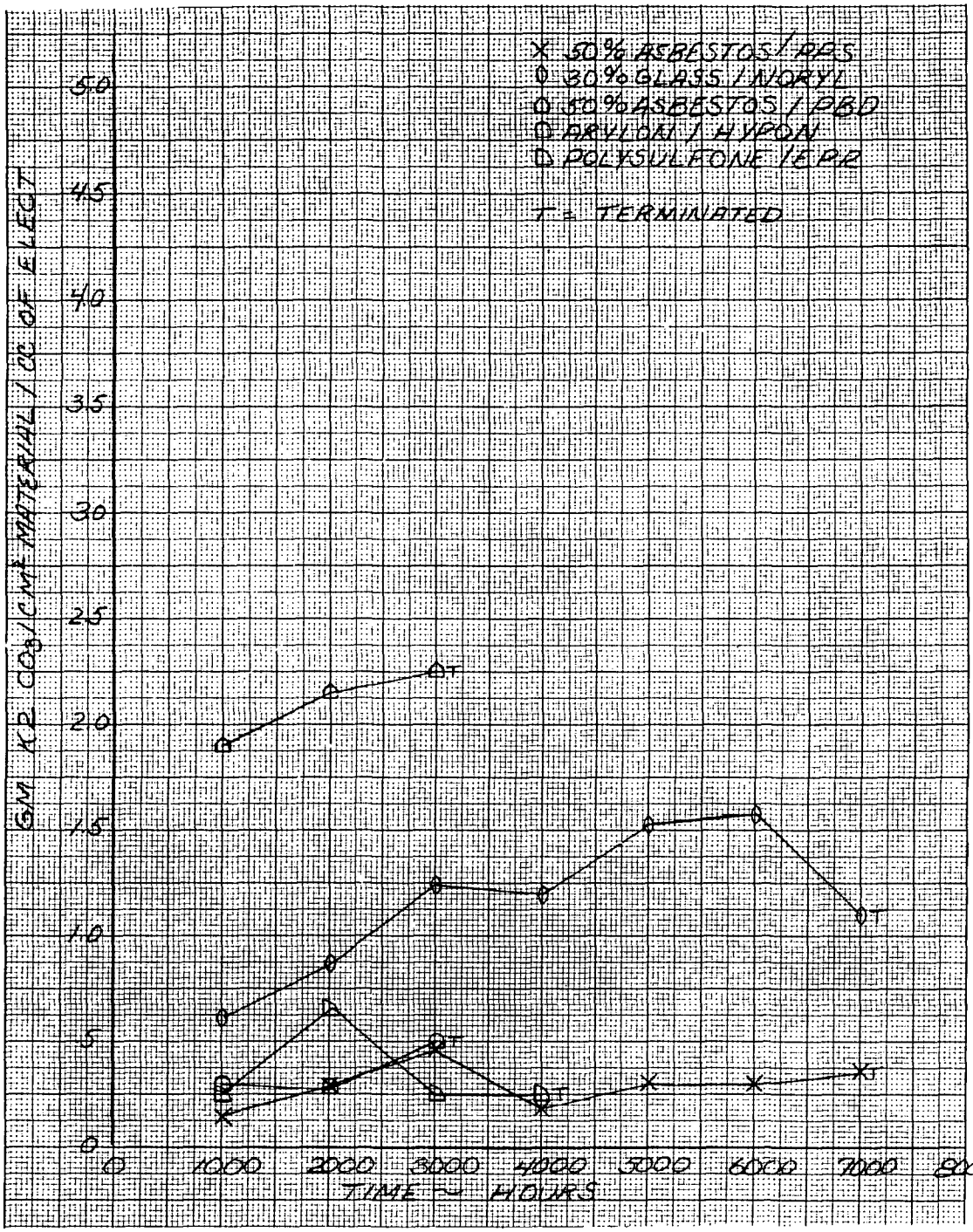

Figure 28 - Electrolyte Carbonation Test Results

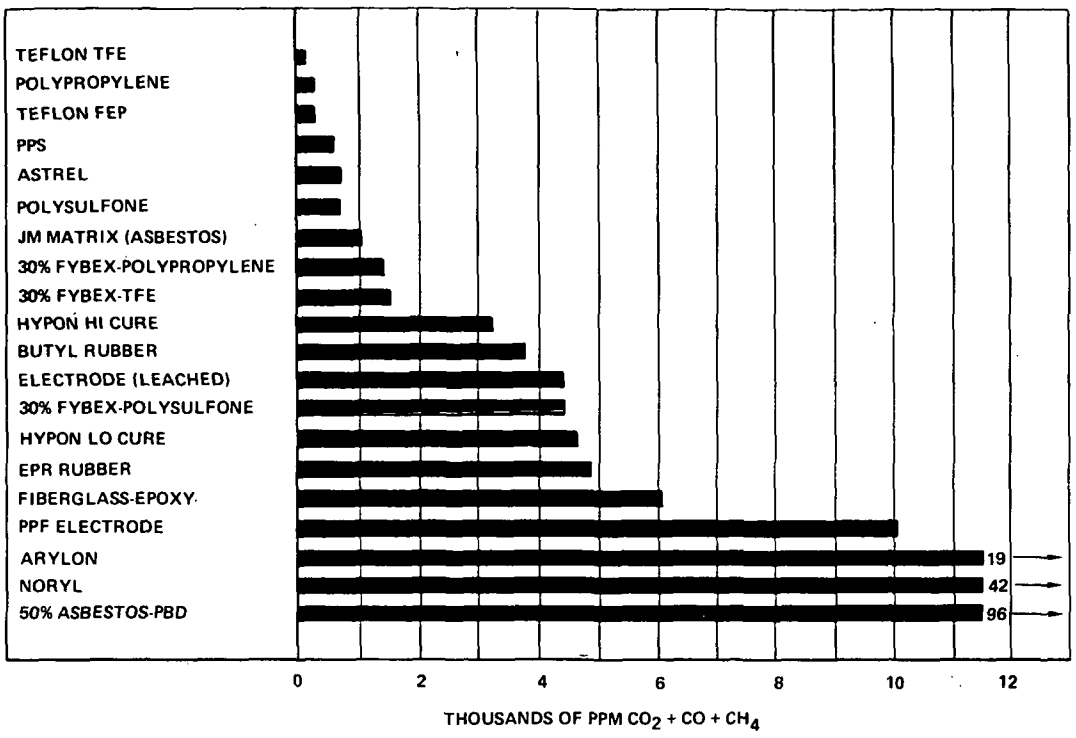

Figure 29 - Results of Gas Chromatograph Test for Products of Oxidation

C. Lightweight Electrolyte Reservoir Plate

Introduction

The heaviest single component in present state-of-the-art alkaline electrolyte fuel cell power sections is the electrolyte reservoir plate. Present electrolyte reservoir plates (ERP's) are made of porous nickel. Nickel is used because of the availability of nickel powder in sizes needed to prepare sinters of the desired pore size, sintering fabrication techniques are well developed, and nickel is highly compatible in the cell environment. Nickel's high density (specific gravity = 8.9), however, is a disadvantage. The concept of using porous polymers (specific gravity 0.9 to 1.3) in place of the nickel sinters would offer substantial weight savings. Certain polymers have been shown to have good compatibility in a cell environment. However, fabrication methods to prepare compatible, porous polymer structures with desired pore spectra and electrolyte wetting characteristics did not exist prior to this program. A research effort was therefore undertaken to develop fabrication techniques for lightweight electrolyte reservoir plates. This (Phase One) work aimed

at identifying candidate materials and processes to develop laboratory-scale ERP's. The resources of the United Aircraft Research Laboratories (UARL) and Pratt & Whitney Aircraft's South Windsor Engineering Facility were used for this task.

A schematic drawing of an electrolyte reservoir plate, its relationship to the cell and its functions are shown in Figure 30. The ERP contains electrolyte within its pores and serves to assure that the maximum amount of electrolyte communicates with the cell. It is also the media through which the product water is removed. In addition to lightweight, high pore volume and KOH compatibility, the ERP material must be easily wet and contain a narrow pore size distribution to facilitate delivery of electrolyte from its structure to the cell matrix on demand. More definitive requirements are listed in Table 6.

A review of the literature and information relating to cost, availability, water wettability and chemical resistance to KOH at 200°F (93.3°C) were used to select possible candidate materials.

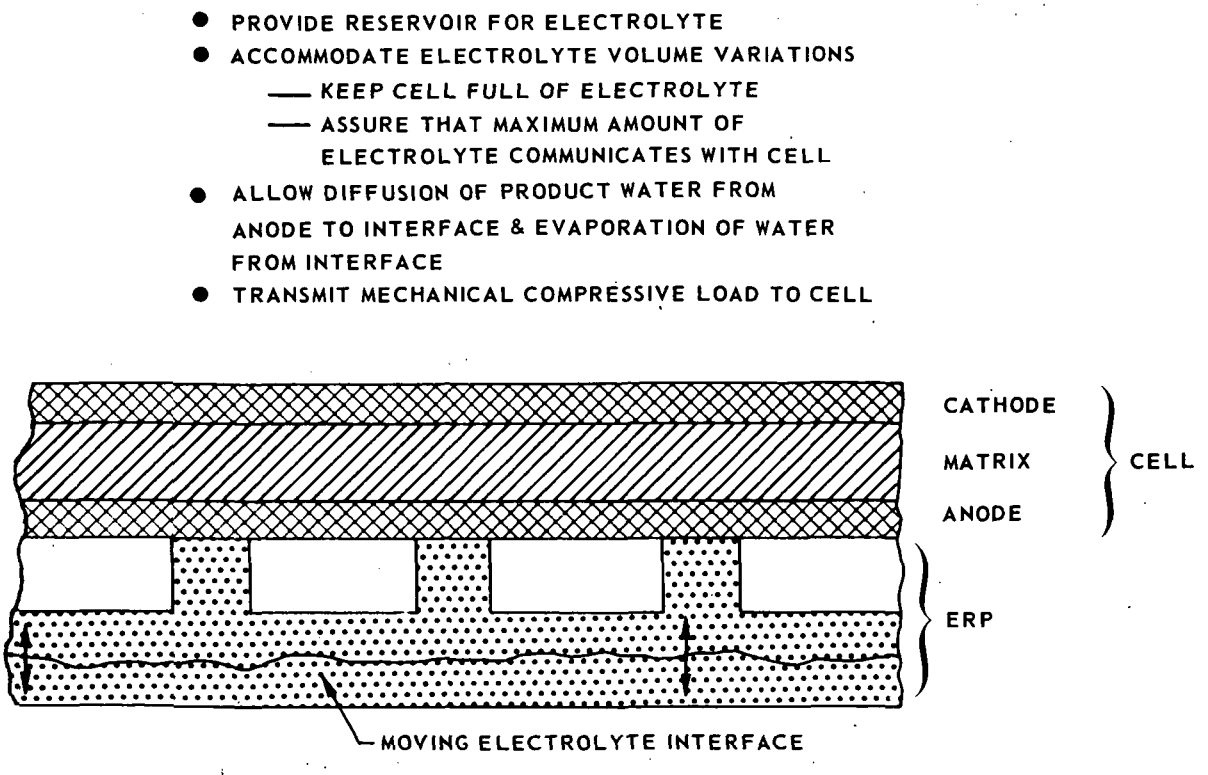

Figure 30 - Electrolyte Reservoir Plate Functions

TABLE 6

Lightweight ERP Requirements

Pore size	3 to 8 microns
Porosity	As high as practical
Electrolyte flow	Readily wet by electrolyte - minimum hysteresis - ΔP vs ΔV
Compressive strength	200 psi (138 n/cm^2) minimum
Environment	200°F(93.3°C)/10,000 hrs in 25 to 45 weight percent aqueous KOH and hydrogen
Configuration	Flat plate, 10 to 30 mil(0.25 to 0.76 mm) thick, reactant flow passages in one face

Two primary candidates were selected for study to demonstrate the feasibility of lightweight ERP systems based on UARL experience in carbon fiber production and organic resin fields and P&WA fuel cell and materials compatibility background. These were, 1) self-bonded fibrillar carbon and 2) sintered polysulfone resin.

Fabrication of High Porosity Electrolyte Reservoir Plates

Fibrillar Carbon - Acrylic filaments are used as the precursor in the manufacture of several different types of carbon and graphite fibers. In processing acrylic fibers to produce carbon yarn, an oxidation treatment is usually employed prior to pyrolysis. The oxidation treatment alters the polymer chemistry so as to render the fibers nonmelting. Shapes made by consolidating the oxidized acrylic can then be pyrolyzed into a variety of carbon articles. Carbon disks of controlled porosity can easily be made by consolidating randomly oriented oxidized fiber chopped into short lengths. Disks have been made by this method with porosities ranging from about 70 percent to less than 1 percent.

Carbon shapes were processed from Monsanto acrylic 13 μ fibers, similar to commercial Acrylan®, which is reduced to about 7 μ during pyrolysis. The cost of this precursor is approximately $1.00/lb ($2.20/Kg). This was oxidized in a continuous process. The oxidized yarn was then passed into a laboratory pulverizing mill.

Weighed samples of the fiber agglomerates were uniformly distributed into graphite molds and then placed between the platens of a preheated press. The mold was then pressurized at a pressing temperature of about 510°F (265.6°C). Pressed disks were then pyrolyzed by heating in an argon atmosphere to 1830°F (998.9°C). To insure uniform heating of the samples so as to preclude warpage during the firing, samples were placed in graphite molds inside the pyrolysis furnace. Samples undergo approximately 20 percent shrinkage in the pressing direction and 7 percent shrinkage in the transverse direction during pyrolysis. Under these processing conditions, the porosity, bulk density, and to a lesser degree specific gravity are functions of the applied pressure during hot pressing.

Micrographs of longitudinal and transverse polished sections of a disk of approximately 50 percent porosity, infiltrated with a resin for metallographic purposes, are shown in Figure 31.

Sintered Polysulfone - Polysulfone is a family of tough, rigid, high strength thermoplastic resins which maintain their properties over a temperature range from -150°F (-101°C) to above 300°F (148.9°C). The resin is available in both injection molding and extrusion grades. The former type has been used throughout this program and is designated as Bakelite® polysulfone P-1700 from Union Carbide. In large quantities the resin sells for $1.00/lb ($2.20/Kg).

Because of the pore size range (3-8 μ) required for the ERP, it was necessary to use the polysulfone in powdered form which could not be obtained commercially. Therefore, methods were developed for making small particle size resin. Two techniques were investigated; (1) solvent precipitation and (2) atomization. The two methods provide a means of obtaining powders of differing particle size and degree of agglomeration.

A solution of polysulfone resin pellets in methylene chloride (dichloromethane) was injected into a blender containing n-heptane solvent. The high speed stirring together with the insolubility of the polysulfone in the n-heptane produces a fine precipitated polysulfone powder which on separation and drying was found to be agglomerated. The spherical particles range in size from 800-1200 Å.

LONGITUDINAL

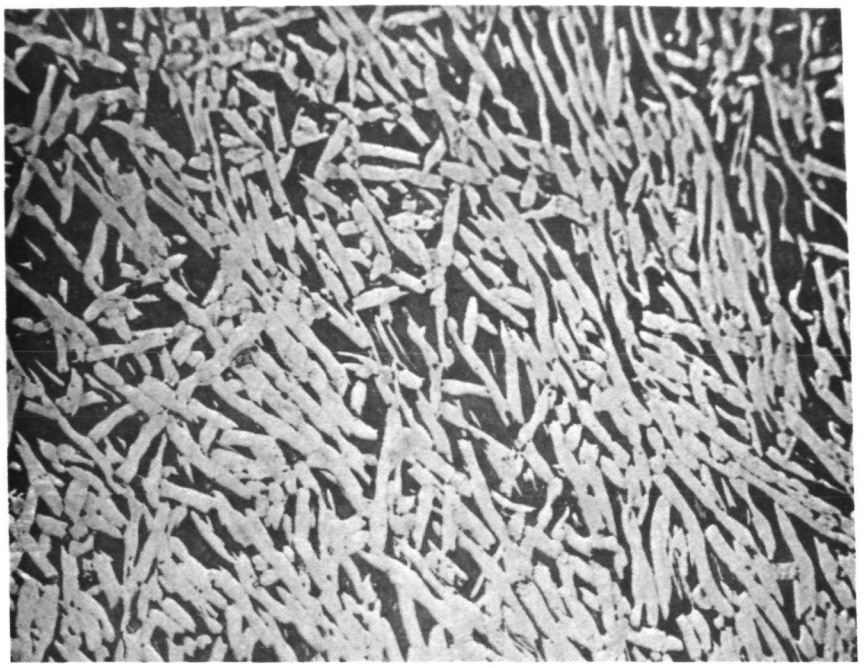

50 μ

TRANSVERSE

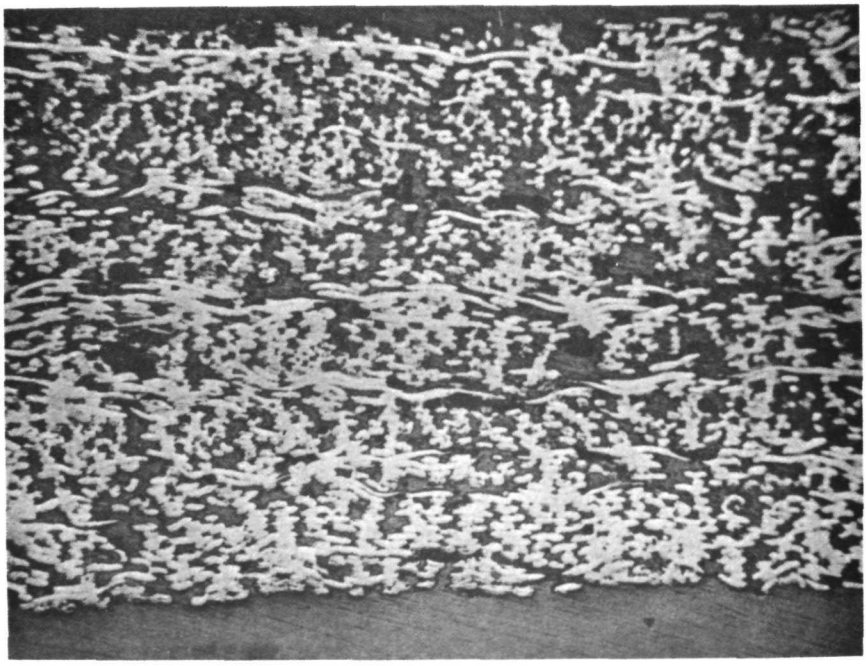

50 μ

Figure 31 - Felted Fibrillar Carbon - 55% Porous Plate

A solution similar to the one used in the previously described process was sprayed at room temperature into a large volume container containing a small volume of slowly stirred n-heptane sufficient to cover the bottom of the pan to prevent film formation. The resulting powder was separated by decantation and air dried. The spherical particles ranged in size from 25-75 μ and appear to be porous. No evidence of agglomeration similar to that found in the solvent precipitation method was noted in the powder which was sieved through a 48 mesh (297μ) screen.

Of the two methods, the atomization process is preferred because of ease of handling, use of considerably less solvent and because it should be more readily scaled up to provide sufficient quantities of powder.

In order to achieve the goal of 70 percent porosity and narrow pore range (3-8 μ) in molded polysulfone disks, it was found that the sintering of the compacted powder must be carried out at the softening point of the resin (380°F) (193.3°C) under 10 (6.9) to 15 psi (10.35 n/cm^2) pressure. Excessively high pressures and temperatures reduce porosity and increase resin flow; lower pressures and temperatures result in weak structure and shrinkage.

Two methods have been employed to obtain high porosity disks using the powders made by the above methods; (a) hot-pressed used both with nickel coated and uncoated powder and (b) cold-pressed used only with uncoated powder. The average physical properties obtained on disks molded by these methods are listed in Table 7.

Based on results to date the hot pressed method is preferred because of shorter processing times. A number of disks were made in order to determine the effect of porosity on pore size and to optimize the structure.

In order to achieve the desired degree of wettability, since polysulfone is not readily wet by water, electroless nickel plating of the disks was investigated. It was found necessary to add a nonionic surfactant, Union Carbide NP-27, to lower the surface tension of the aqueous solutions used in order to achieve uniform plating. The procedure used for plating both sintered disks and powder was to immerse in a sensitizing bath followed by immersion in the activating solution, water wash and oven drying. The material was then immersed in electroless nickel plating bath for a period dependent on the degree of coating desired. This was followed by a water wash and oven drying.

TABLE 7

Average Physical Properties of Sintered Polysulfone Disks

Property	Hot Pressed	Cold Pressed	Hot Pressed Nickel Coated Powder
Geometric porosity, %[a]	75	67.6	77.8
Pore spectral porosity, %[a]	72.4	74.7	76.1
Mean pore size, μ[a]	7.7	5.4	6.5
Pore range, μ[a]	2-16	1.5-9.5	0.3-10.3
Bulk density, g/cc[b]	0.300	0.400	0.27
Specific gravity, g/cc[b]	1.17	1.175	1.17

[a]Determined by mercury intrusion
[b]Determined by ASTM water displacement method

Plating of sintered disks by the above method resulted in only surface deposited coating. This was illustrated both by the degree of water absorption and an atomic probe analysis of a cross section of a plated disk. Incomplete penetration is undesirable since the water pick up rate is slow and long periods of time would be required to completely saturate the porous disk. It was shown that nickel could be internally deposited through a sintered disk by forcing the above described sensitizing, activating and plating solutions through the disk under pressure. The water expulsion apparatus described elsewhere was used for the internal plating.

An alternate method of achieving internal plating is the use of nickel coated powder to produce the sintered disk. Disks were readily fabricated from such powder, however, it was found that the external surfaces of the disks were not wet by water. This may be due to a thin layer of polysulfone formed on the surface during molding. Plating of the surface using the above described procedure eliminated nonwetting.

A simple method was used to determine the effectiveness of the nickel coatings in converting the polysulfone surface from hydrophobic to hydrophilic. The formed disks were immersed in water and the percent

of total water capacity (measured by the ASTM water displacement procedure) absorbed as a function of time was determined by weighing the disks at periodic intervals. The curves in Figure 32 clearly demonstrate the degree of improvement in wetting obtained between unplated, surface plated and internal plated sintered polysulfone disks. The disk made from plated powder which was then surface plated achieved the highest rate of water pickup - 92 percent of total capacity in 15 minutes. The initially plated disk, once the procedure was optimized, would probably be equally as effective.

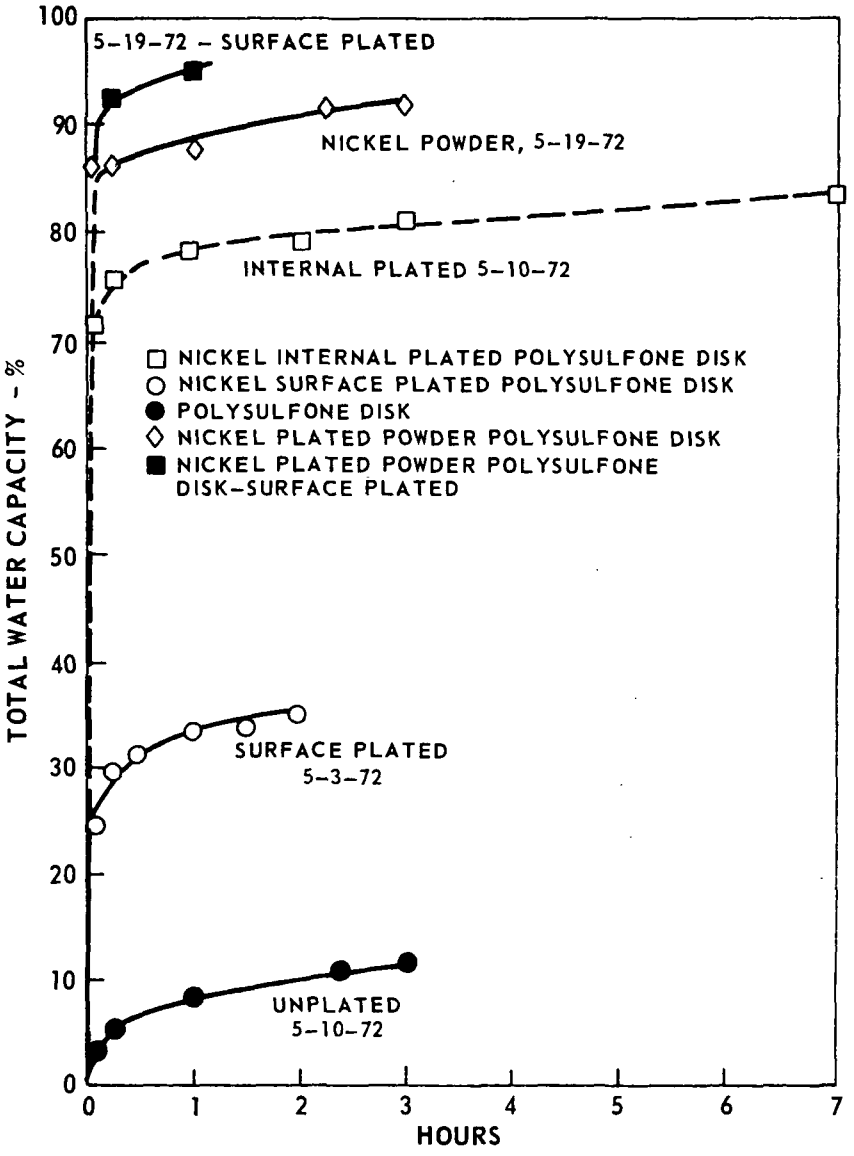

Figure 32 - Water Pick Up of Nickel Plated Polysulfone Disks

Properties of Fibrillar Carbon and Nickel Plated Polysulfone Disks

The final selection of one material for a lightweight ERP depends on many factors. Cost of materials, ease of fabrication, fuel cell performance and percentage of weight reduction, as well as physical and mechanical property characteristics must be considered. A complete characterization study to choose one material was beyond the intended scope of this program. Sufficient evidence has been obtained, however, to indicate those areas in which improvements can be made. Final selection of a single material would be simplified after having made the improvements. The following sections compare the two systems in terms of the desired physical property characteristics.

Porosity vs. Bulk Density - The relationship between porosity and bulk density for the two candidate materials is shown in Figure 33. The polysulfone has a marked advantage in terms of density at the 70 percent porosity range. In order to achieve a porosity greater than 50 to 55 percent with the carbon and still maintain the desired pore size range (3-8 μ), the use of either a smaller diameter filament or a powdered resin which could be sintered and carbonized is required. Both approaches appear highly feasible. The commercial availability of a smaller diameter fiber, however, must be assessed.

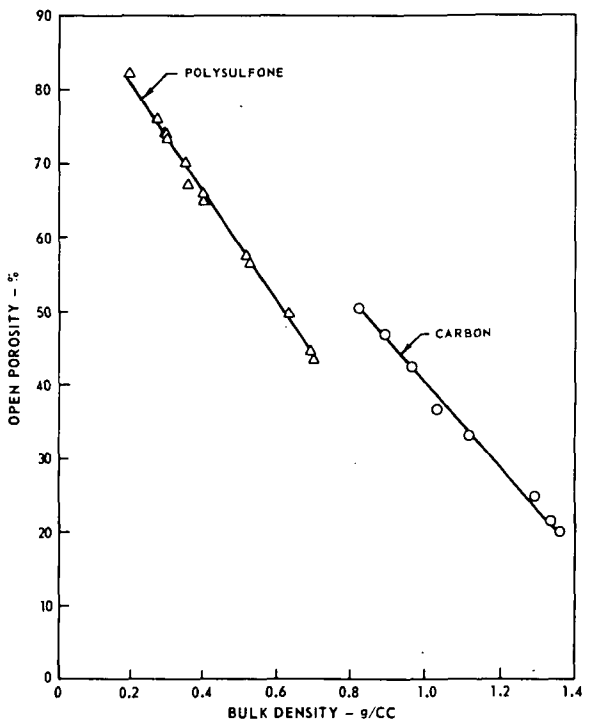

Figure 33 - Percent Porosity - Bulk Density Relationship

Porosity vs. Mean Pore Size - The comparison of the two systems in terms of porosity and pore size is shown in Figure 34. Based on these data, polysulfone plates with up to 80 percent porosity would be usable, which would have only 10 percent of the weight of the currently used nickel sinter. The carbon at 50 percent porosity is approximately 45 percent of the weight of nickel sinter. Although the mean pore size of the polysulfone disks at the high porosity level is satisfactory, the range of pore size is broad. Should a smaller range be required, modification into the powder fabrication step can be made.

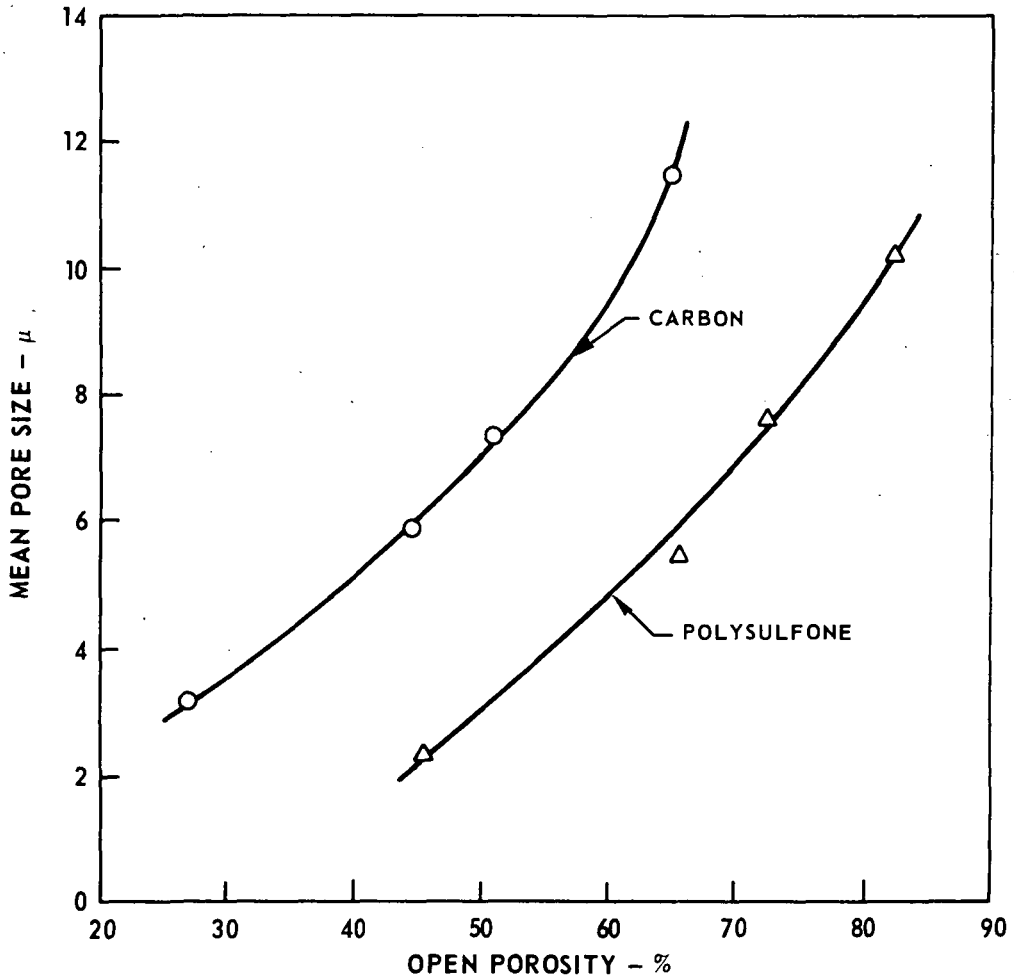

Figure 34 - Mean Pore Size vs. Porosity

Water Expulsion Characteristics - This test is employed to determine the effectiveness of a porous plate to desorb and absorb electrolyte on demand. The apparatus used is shown schmatically in Figure 35. The

porous disk saturated with water is inserted into the apparatus and pressure applied. The volume displaced from the sintered disk by a given pressure is measured with the burrette. Sufficient pressure is used to remove up to approximately 90 percent of the water. During incremental release of pressure, the uptake of water is followed until the original conditions are reached. A plot of percent water expelled vs. applied pressure provides a measure of the hysteresis which occurs during the desorption-absorption cycle. Hysteresis curves for both the porous carbon and polysulfone disks compared to the nickel sinter are shown in Figures 36 and 37.

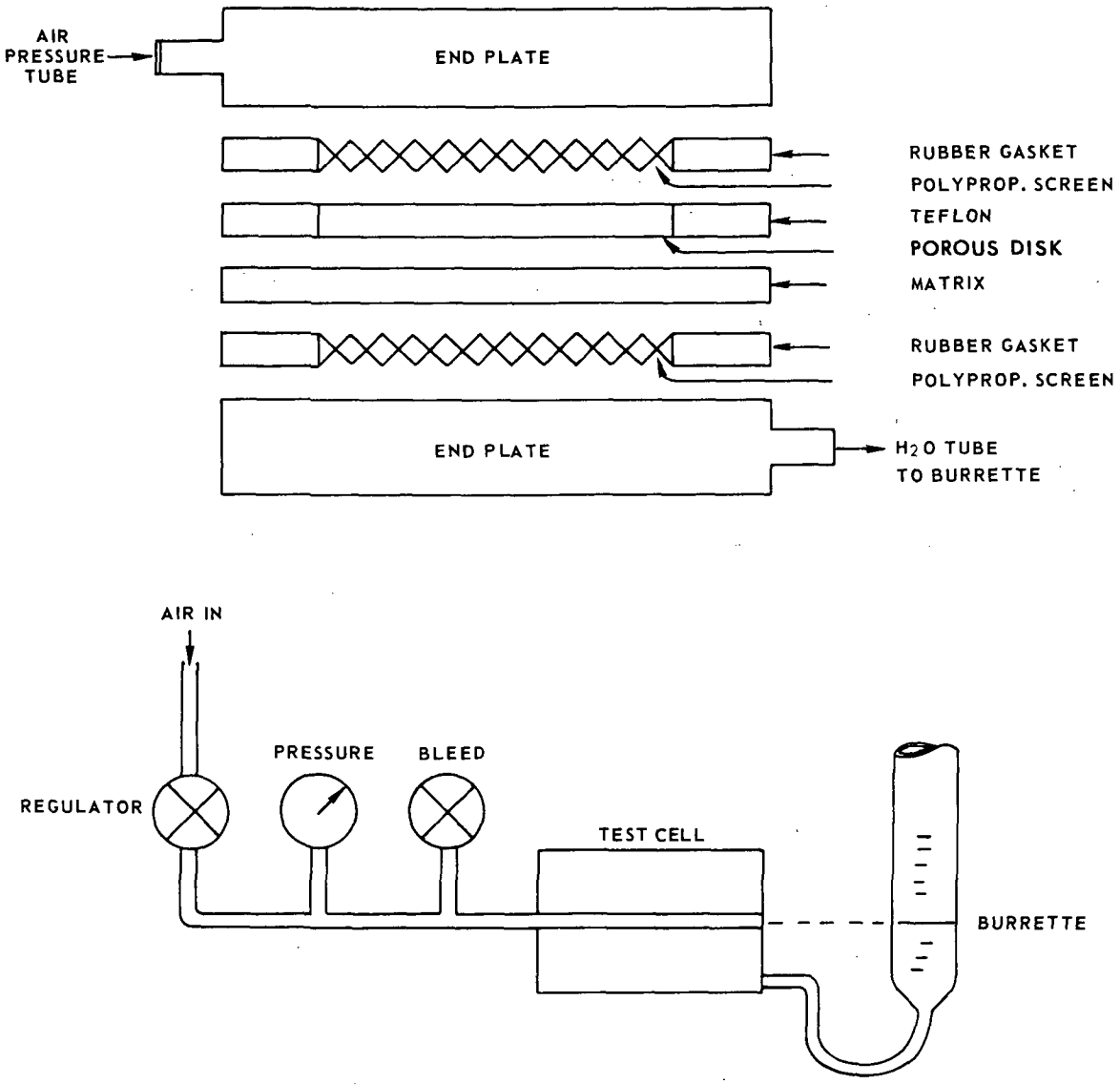

Figure 35 - Water Expulsion Test Apparatus

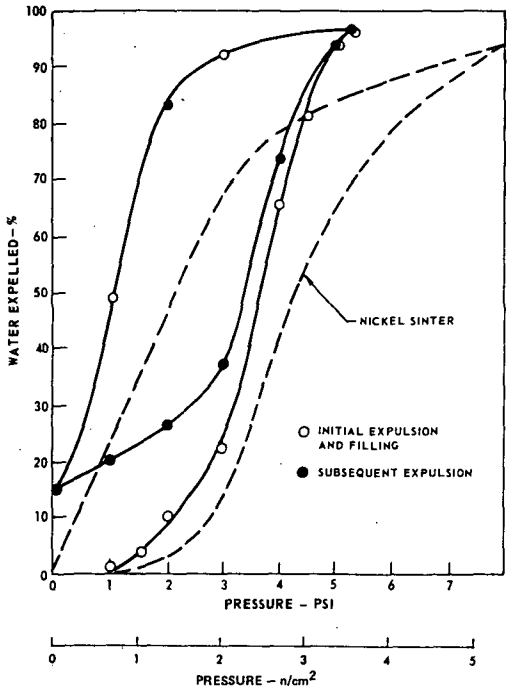

Figure 36 - Water Expulsion Characteristics of Felted Fibrillar Carbon of 52% Porosity

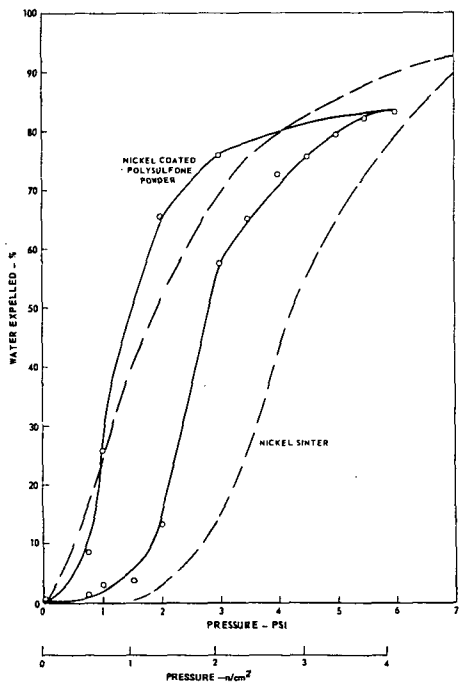

Figure 37 - Water Expulsion Characteristics of Sintered Nickel Coated Polysulfone Powder vs. Nickel Sinter

The porous carbon disk requires less pressure to reach the 90 percent water expelled point than the sintered nickel. However, on release of pressure, the carbon disk does not completely saturate with only 85 percent of the total volume being filled. Upon pressure recycle this curve is reproduced. The degree of hysteresis is similar to that of the nickel sinter. The expulsion-filling behavior of a disk made using preplated polysulfone powder is very similar to sintered nickel. In fact, as shown in Figure 37, its hysteresis is smaller than sintered nickel. Furthermore, this structure is completely resaturated upon release of pressure.

Conclusions

Two materials; sintered polysulfone and fibrillar carbon have been developed as candidate lightweight alternatives to the present sintered nickel electrolyte reservoir plate. Sintered polysulfone offers a 80 percent weight reduction where the fibrillar carbon provides 60 percent reduction over the referenced nickel sinter ERP.

Methods for producing polysulfone powder from commercial resin have been developed which when sintered provide a structure which is 70 to 75 percent open porosity and has the desired pore size range. This material, when given a light (0.5 to 1.0 weight percent) electroless nickel plate, has electrolyte wetting and expulsion characteristics equivalent to state-of-the-art nickel sinters.

A 55 percent porous carbon ERP structure has been produced by oxidizing chopped polyacrylonitrile fibers which are then hot pressed and pyrolyzed. This carbon ERP candidate has also been found to have acceptable electrolyte wetting and expulsion characteristics.

D. Matrix Materials

Introduction

During the later portion of the program, a matrix materials task was added to the program's research efforts. This was added to evaluate the suitability of developing matrices using a newly available form of potassium titanate which was being introduced by its manufacturer as a reinforcing material for polymers. During a period of approximately four months, the new potassium titanate material was characterized and matrices with satisfactory thickness, porosity and bubble pressure were prepared.

The purpose of the matrix materials task was to develop fuel cell matrices made of Fybex potassium titanate which would have mechanical properties similar to reconstituted asbestos to make use of the superior electrolyte compatability of potassium titanate. Fybex is a fiber shaped particulate material approximately 0.2 micron diameter by 5 to 8 microns long supplied by E.I. DuPont de Nemours & Company. Corrosion tests conducted at NASA LeRC have shown Fybex is compatible with 42 weight percent potassium hydroxide ay 150°C (302°F) up to 500 hours. Primary emphasis was directed toward fabrication of structures that contained the same volume of solids per unit area as a 10 mil (0.25 mm) thick reconstituted asbestos matrix (70 percent porosity). This should result in similar initial performance and internal resistance losses compared to cells containing asbestos matrices, but should permit prolonged operation at higher temperatures.

Test Results

Tests were initially conducted to characterize the Fybex material and to compare material obtained by P&WA to the material originally tested by NASA. Scanning electron photomicrographs disclosed the initial material obtained by P&WA was the same size as the NASA material. X-ray diffraction analyses disclosed the material to be octa-titanate, $K_20.8 Ti0_2$, with greater than stoichiometric titanium content. The diffraction pattern is similar to a pattern produced from a mixture of potassium tetra-($K20.4Ti02$) and hexa-($K20.6Ti02$) titanates. The following chemical results were obtained:

		Wet Chemical		Spectrographic			
Material	Ti/K	% $CO_3^=$	% C_1^-	% Ca	% Mg	% Si	% Fe
NASA	5.22	0.2	0.05	0.1	0.08	0.05	0.02
P&WA	5.62	0.2	0.04	0.1	0.08	0.05	0.01

The stoichiometric titanium to potassium ratio is 4.92 for $K_20.8Ti0_2$. The $CO_3^=$ content was analyzed as both absorbed CO_2 and chemically combined $CO_3^=$.

Matrix structures containing pure Fybex and Fybex with up to 15 weight percent crystallite fuel cell grade asbestos fibers were fabricated using P&WA developed procedures. Matrices in sizes up to 13 inches by 13 inches with characteristics approaching those desired were prepared.

The strength of the matrix structures increased significantly with asbestos contents of 10 and 15 percent. The following results were obtained.

Fybex Weight Percent	100	95	90	85
Asbestos Weight Percent	0	5	10	15
Avg. Thickness (mils)(mm)	20 (0.51)	27 (0.69)	23 (0.58)	23 (0.58)
Thickness Range (mils)(mm)	19-22 (0.48-.56)	21-32 (0.53-.81)	20-25 (0.51-.64)	17-29 (0.43-.74)
Porosity at 10 mils (0.25 mm) (%)	71	71	72	68
Bubble Pressure (psi)(n/cm^2) of 4 samples from a single sheet	33, 10 (22.77, 6.9) 20, 40 (13.8, 27.6)	19, 28 (13.11, 19.32) 20, 6 (13.8, 4.14)	30, 36 (20.7, 24.84) 30, 30 (20.7, 20.7)	43, 30 (29.67, 20.7) 42, 40 (28.98, 27.6)

Experience in handling and processing Fybex mats has been limited, but results to date indicate the mats are considerably more fragile than those made of reconstituted asbestos.

IV. CELL AND STACK DEVELOPMENT

A. Single Cell Development

1.0 Introduction

The single cell task was a major portion of the technology advancement efforts performed during Phase I of the Advanced Fuel Cell Program. This task served as the focal point integrating the results of system design analysis and the results of the materials development tasks. The NASA goals for operating life, weight and system operational features call for a significant advance in fuel cell power section state-of-the-art.

P&WA's pre-contractual study of the NASA goals led to formulation of a preliminary EMS design with the following cell requirements:

- Minimum thickness component parts and flow fields for low weight
- Plastic structural materials for low weight
- Highly compatible materials for long life
- Passive water removal
- Evaporative cooling

  } Required by the system and their use favors long life

- Edge current collection, as a consquence of the above items.

A single cell is the smallest building block for evaluation of these cell requirements. Although a single cell does not duplicate the intercell seal geometry of a plaque, and does not require evaporative cooling for temperature control, it does provide the most cost effective approach for investigation of all the other EMS cell features.

Specifically, a single cell evaluation program was needed to:

- Test different cell component configurations and materials
- Define performance characteristics
- Evaluate methods for extending life

At the start of the program, complete data on materials compatibility and mechanical properties were not available. The structural materials task of the program was set-up to provide these data as the program progressed. Similarly, data on the availability and properties of cell components such as hydrophobic membranes, flow field spacers etc. was incomplete. A multi-phase, evolutionary single cell development program was therefore planned. This would allow results from the single cell tasks to feedback into the development process. The evolutionary nature of the single cell program is depicted in Figure 38 which shows how the key development findings were fed back to improve performance and life characteristics.

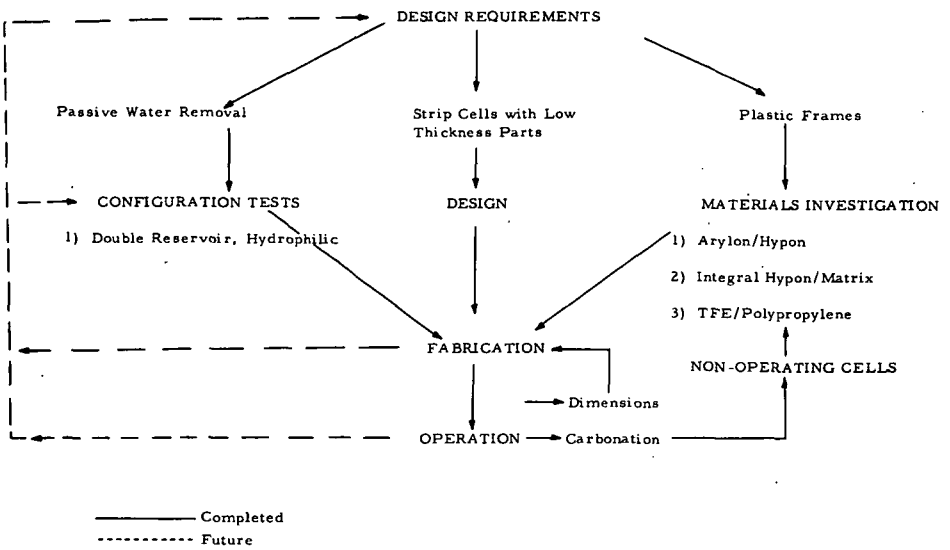

Figure 38 - Single Cell Development

The first subtask under the single cell program was an investigation of passive water removal for long operation especially as regards methods for eliminating electrolyte loss. A detailed electrolyte loss mechanism theory was formulated. The several options for different types of passive water removal were evaluated. Concurrent with this analysis, existing hardware was adapted for testing several configurations of passive water removal fuel cells. Recommendations for the passive water removal configuration used throughout the remainder of the program were based on successful demonstrations of a practical configuration demonstrated with the aid of the theoretical model.

The second subtask under the single cell program was unitization research. The term unitization defines the fabrication process whereby

electrodes and matrix are bonded to a frame to create a leak-free, dimensionally accurate assembly. The long life goal of the EMS power section demanded that the most compatible materials be used for cell frame unitization. The knowledge of which materials have the best resistance to degradation in the cell enviroment is only the starting point for this type of work. Unless the materials can be successfully processed with the other cell components to create a high quality, reproducible assembly, their attractive compatibility characteristics are of academic interest. A program was therefore started to extend P&WA's compatible frame unitization experience into edge current collection cells and to develop the techniques needed for fabricating reliable intercell seals in plaques. This program was expanded as the results from early cell test provided evidence that materials with significantly better oxidation and electrolyte resistance were required for the weight and life goals to be met. The unitization research efforts continued throughout the program. At the end of Phase 1, two promising techniques had been developed. One, the impregnated matrix method, was successfully tested in single cells; it affords excellent diminsional control and has reasonable compatibility. The second, using laminations of polymer films, offers the ultimate in compatibility, but has as yet unresolved fabrication problems.

The third subtask under the single cell program was the development of a single cell test vehicle incorporating the passive water removal investigation and unitization research. Such a cell and test fixture were designed and used successfully for all full size single cell tests, and for the delivery hardware. Four different cell configurations were tested in this manner: a prototype configuration for experimental tests, and three designs approved by NASA for verification testing. These designs are described in the following sections.

In summary, the single cell program can be divided into the five interrelated reporting topics which follow:

1) Passive Water Removal Investigation

2) Unitization Research & Cell Fabrication

3) Single Cell Designs

4) Electrolyte Carbonation Investigation

5) Performance and Endurance Test Results

2.0 Passive Water Removal Investigation

The system concept selected to meet Engineering Model System objectives resulted in the use of the passive water removal method for rejecting product water from the cells. The concept of passive water removal was well known. However, this water removal method had never been demonstrated using the thin, light-weight hardware required to meet the weight goals of this program. Nor had the question of small electrolyte losses, especially during transient operation, appear to have been fully resolved. Solving the potential electrolyte loss problem was considered important in view of the 10,000 hour life goal of the program, which had to be obtained with minimum cell electrolyte reservoir size in order to minimize weight. Several alternate passive water removal configurations had been prepared to solve these problems. A separate subtask was therefore outlined within the single cell program to determine the feasibility of these light-weight configurations to properly remove product water under all operating conditions without loss of electrolyte.

The approach used was twofold:

- To develop a theory to assist in understanding passive water removal operation for the several optional configurations that were candidates.

- To use existing hardware to allow low cost evaluation of the feasibility of different configurations.

The operation of a passive water removal fuel cell can be best envisioned by the concept of separate fuel cell and water transport plate assemblies as shown in Figure 39. The water transport plate has two functions: to transport product water from the cell to the water vapor cavity is the obvious and defining function of the water transport plate; equally essential, however, is the need to seal the reactant from the water vapor cavity, thus assuring the balance of water (partial) pressure required to maintain cell operating conditions.

There are two methods of effecting this gas seal, as illustrated in Figures 40 and 41. Both use electrolyte-filled porous plates to retain reactants in the cell while permitting water to diffuse through the plates and evaporate into the water vapor cavity. The fundamental difference in the two design approaches is the way electrolyte is retained in the water transport plate. In the hydrophobic configuration, a non-wetting porous layer prevents electrolyte from entering the water vapor cavity. In the hydrophilic configuration, a wetted porous plate retains the electrolyte without allowing reactant gas to pass through.

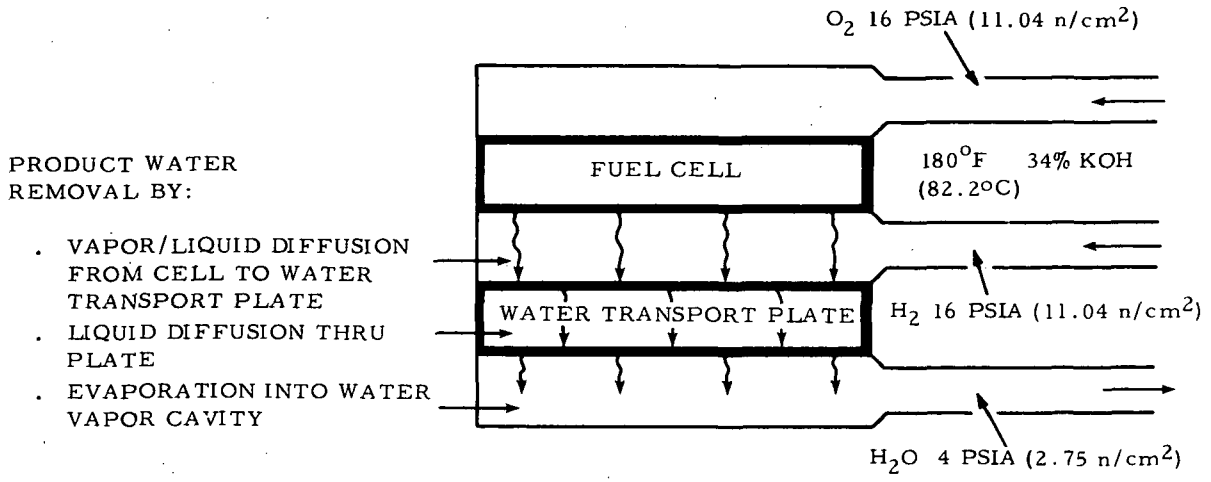

BASIC FUNCTIONS OF WATER TRANSPORT PLATE

- TRANSPORT WATER FROM CELL TO WATER VAPOR CAVITY
- SEAL REACTANT FROM WATER VAPOR

Figure 39 - Passive Water Removal

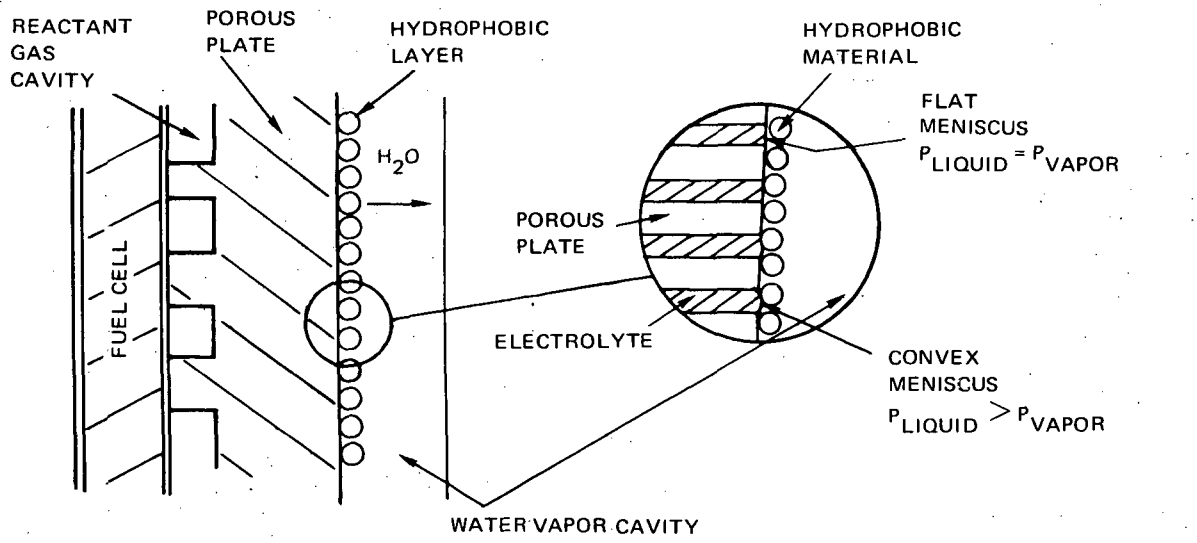

Figure 40 - Hydrophobic Passive Water Removal

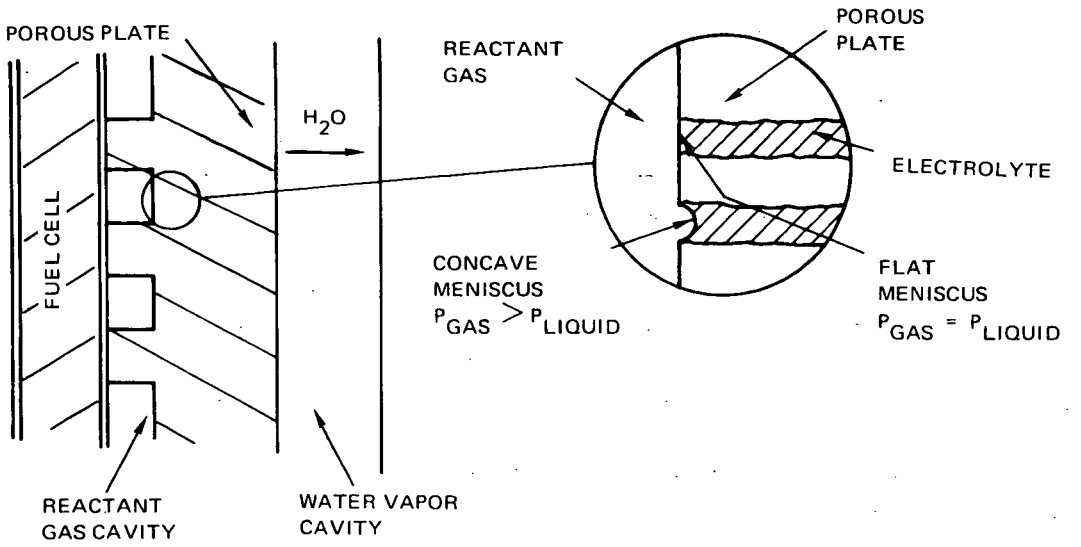

Figure 41 - Hydrophilic Passive Water Removal

The hydrophobic passive water removal concept, illustrated in Figure 40, relies on a wetproofed porous layer on the water vapor side of the water transport plate to control the position of the electrolyte-water vapor interface. The plate can be a hydrophilic porous plate with a porous layer of hydrophobic particles or a hydrophobic coating in the pores. The expanded view in Figure 40 shows a model consisting of spherical particles of hydrophobic material. In the absence of differential pressures, liquid fills the plate until a flat meniscus forms at the end of each pore as shown in the upper part of the figure. As shown in the lower part of the figure, when a differential gas to water vapor pressure is applied to the reactant gas side, the liquid is contained by the hydrophobic layer as the meniscus becomes convex. The maximum pressure difference (ΔP) across this convex meniscus is related to the surface tension (σ), maximum contact angle between the liquid and solid (θ) and the pore radius (R), in the ideal, by the equation $\Delta P = \frac{2 \sigma \cos \theta}{R}$.

Calculations based on this model using surface tension and contact angle for 30 percent KOH on PTFE at room temperature show that a pore diameter of 0.3 micron will sustain the required 12 psi (8.3 n/cm^2) pressure differential.

The hydrophilic passive water removal concept, Figure 41, uses a porous plate which is easily wet by electrolyte to control the location of the reactant gas-electrolyte interface in the water transport plate. When this plate is filled without pressure differential, the flat meniscus occurs as before. However, as shown in the expanded view in Figure 41,

an increase in reactant pressure or decrease in water vapor cavity pressure results in a concave meniscus in the pores on the reactant gas side of the plate. The resulting surface tension forces retain the liquid in the wetted porous plate. Analysis indicates a pore diameter of 4 microns is necessary to achieve the required pressure differential of 12 psi (8.3 n/cm^2) for 30 percent KOH on nickel.

In addition to the transport and sealing functions, the water transport plate needs an electrolyte reservoir, as does the fuel cell. This assures that the pores of the water transport plate gas seal remain filled when electrolyte volume varies during changing operating conditions.

The fuel cell and water transport plate reservoir can be combined or separate. In the case of separate reservoirs, the cell reservoir can be placed on either the anode or cathode side of the cell. The nature of the hydrophobic and hydrophilic sealing methods require that the water transport plate reservoirs be placed on the reactant and product water sides, respectively. Thus, there are a variety of configurations possible.

The following describes the hydrophilic configurations considered, since they were chosen for evaluation. Figures 42 and 43 illustrate separate and combined versions of this sealing method, respectively. The combined reservoir was initially considered lighter and simpler; the separate reservoir was considered easier for development since the problems of fuel cell and water transport plate could be separated. Further analysis showed that the separate reservoir concept had a potential for low weight at least as good, and possibly better than the combined reservoir approach. This can be shown by a consideration of the porous structure of the reservoirs in Figures 42 and 43. In the separate reservoir, the porous pins can be considered reservoir volume, while in the combined reservoir, the pins must form an electrolyte bridge. To do this, they must be of a smaller pore size than the electrolyte reservoir. The electrolyte bridge does not contribute "reservoir" but rather "demand" volume, which increases the required capacity of the single reservoir. These effects are shown graphically in Figure 44. The longer electrolyte transport path between the reservoir and the fuel cell also contributes to poorer tolerance response in the combined reservoir scheme. Finally, the separate reservoir scheme eliminates any danger of electrolyte boiling in the fuel cell in those cases (discussed below) where it can occur in the water transport plate. Since the size/weight characteristics were approximately equal, and the tolerance and development advantages compelling, the separate reservoir arrangement was recommended for all hydrophilic configurations.

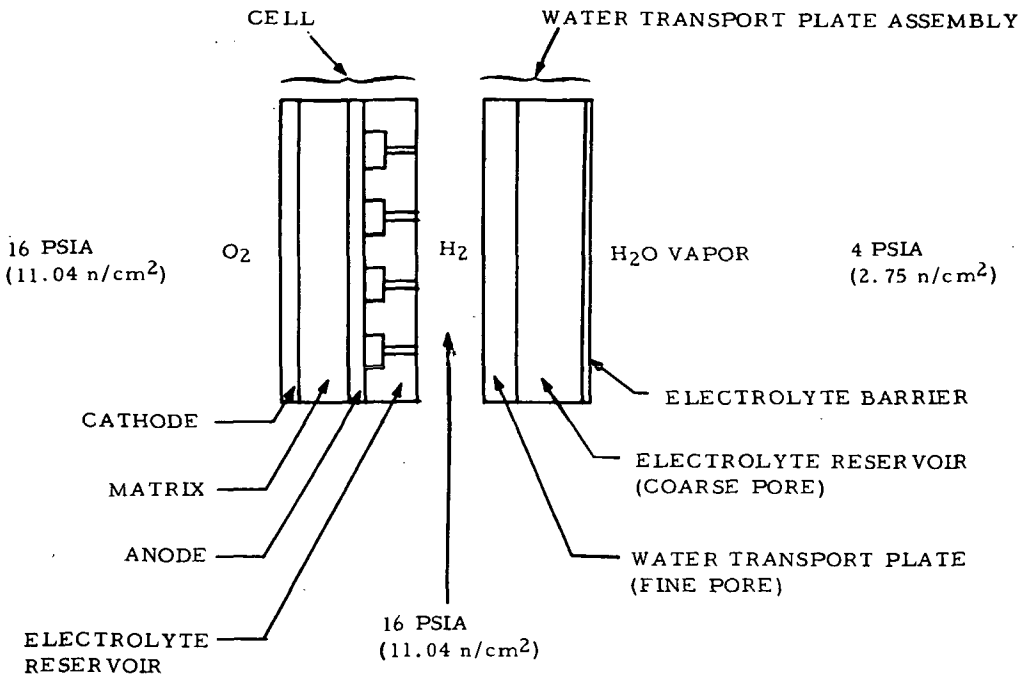

Figure 42 - Hydrophilic Passive Water Removal Separate Electrolyte Reservoir

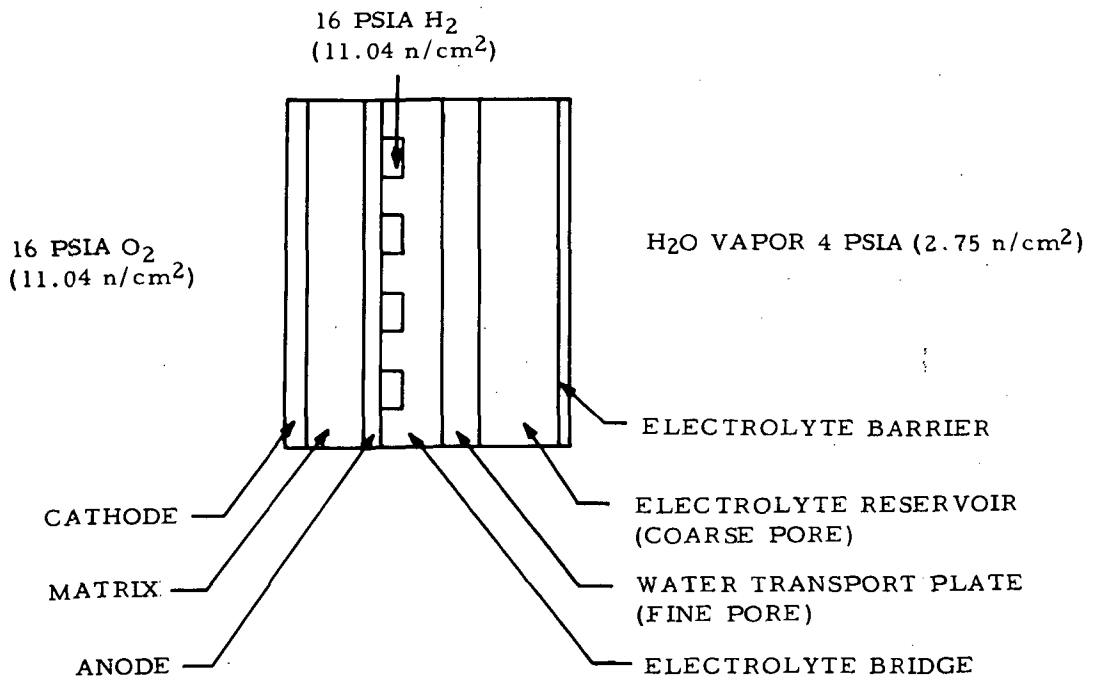

Figure 43 - Hydrophilic Passive Water Removal Combined Electrolyte Reservoir

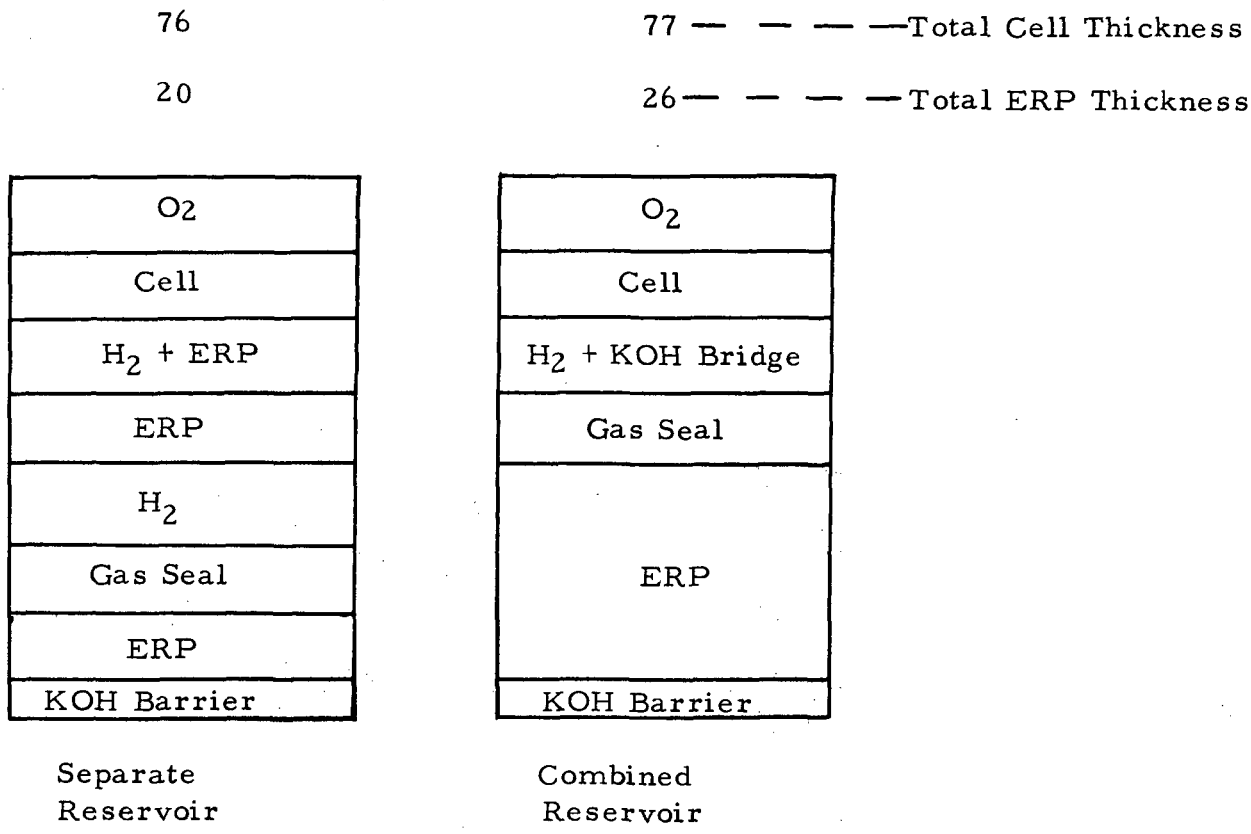

Figure 44 - Relative Sizes of Separate and Combined Reservoir Hydrophilic Cells

The location of the separate cell reservoir is another option in the design. The anode side was recommended. This location is used in other cells and extensive experience was therefore available. The eventual desire to replace the porous nickel sinter reservoir plates with a light weight, non-metallic structure also strongly favors the anode side reservoir location. A wider choice of materials are possible in this reducing environment, with less problems of carbonate conversion. The use of non-metallic reservoirs on the cathode side could also introduce undesirably high temperature gradients in rejecting heat to the evaporative cooler.

The above advantages were confirmed by early feasibility tests using available cell hardware adapted for passive water removal. Details of the test program are discussed below.

Early testing of passive water removal fuel cells demonstrated significant electrolyte loss. Analysis of this problem led to incorporation of an

electrolyte barrier. This electrolyte loss and its prevention by an electrolyte barrier can be explained by considering the capillary structure of the water transport plate. This explanation is confirmed by the fact that all cells of the combined reservoir, hydrophilic configuration tested without electrolyte barriers failed by gas leakage, which was caused by depletion of electrolyte, within periods of 300 hours.

An explanation of the electrolyte loss mechanism is shown in Figure 45. Examples are given in terms of the normal design operating conditions of 180°F (82.2°C) and 4 psia (2.75 n/cm^2) water vapor pressure, defining a nominal electrolyte concentration of 34 percent KOH. For example, during operation at lower electrolyte concentrations at temperatures lower than 180°F (82.2°C) (or at water vapor pressures greater than 4 psia), the reservoir tends to be full, and the electrolyte pressure approximates that of the water vapor chamber. During high electrolyte concentration operation at temperatures lower than 180°F (82.2°C) (or at water vapor pressures less than 4 psia (2.75 n/cm^2)), the reservoir is nearly empty, with the electrolyte pressure equal to or somewhat less than that of the water vapor chamber. During a transient from high to low electrolyte concentration, as shown in Figure 45, a situation can develop where the saturation pressure of water over the electrolyte is greater than the electrolyte pressure.

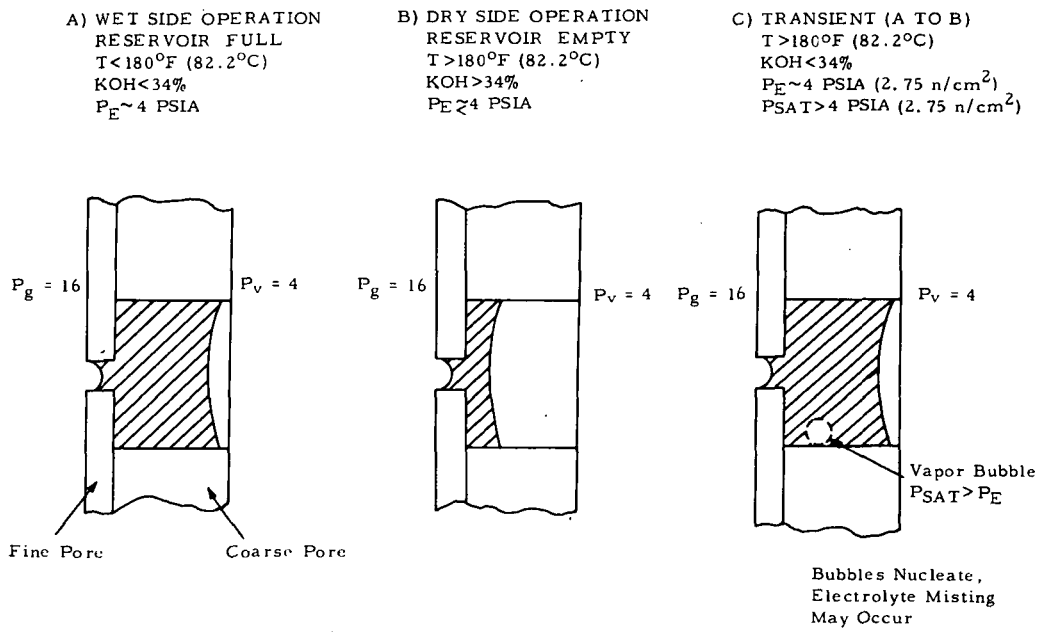

Figure 45 - Hydrophilic Water Transport Plate Possible Electrolyte Loss Mechanism

Under these circumstances (and to a lesser degree in condition B), steam bubbles can form and electrolyte may be ejected from the reservoir surface. This explanation would account for the electrolyte loss failure mode of early passive water removal cells. Misting of the electrolyte is a strong possibility, since it was found that electrolyte was lost even from cells oriented vertically with water vapor exit ports on top.

Figure 46 illustrates a method for preventing electrolyte loss by use of a non-wetting electrolyte barrier membrane. Since porous Teflon films were commercially available, they were the logical choice for such a barrier. Bench tests were run to evaluate the permeability and intrusion pressure of several Teflon films. Those with the best combination of properties were incorporated into passive water removal fuel cells and were effective in eliminating electrolyte loss. Details of these test results are presented below. Theoretically, another way to reduce the danger of electrolyte loss would be to utilize larger mean pore size reservoirs. As the electrolyte volume shrinks, this would lead to a smaller gas-to-electrolyte pressure differential for the same volume change, and therefore reduce the driving force causing electrolyte expulsion. Several tests were run with larger mean pore size electrolyte reservoirs, but the results were inconclusive, as described in the following pages.

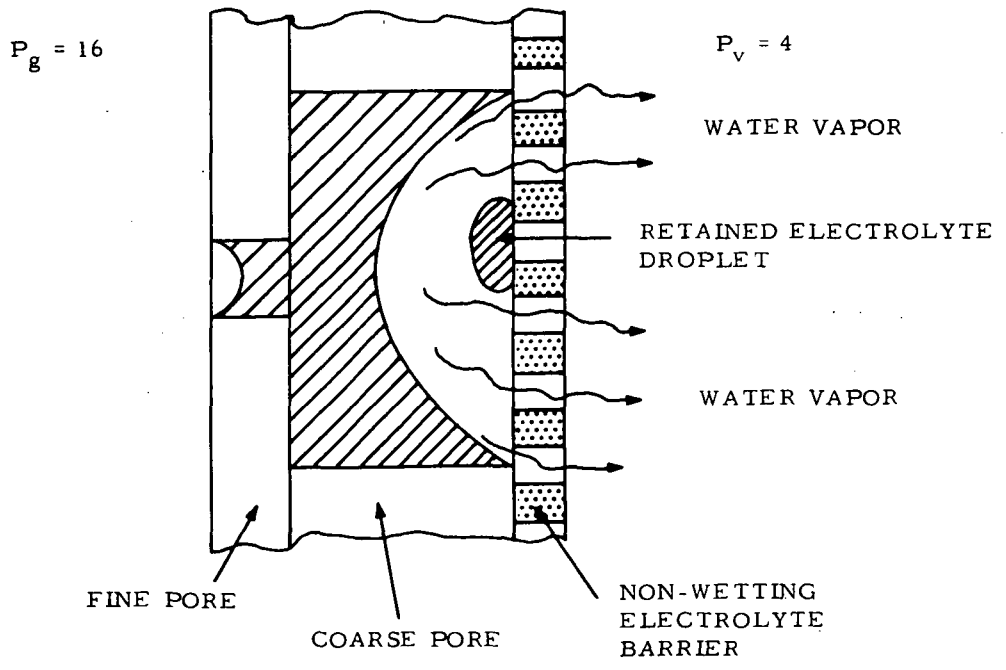

Figure 46 - Prevention of Electrolyte Loss Water Transport Plate Assembly

The previous discussions concerned the "hydrophilic" configuration for effecting the gas to water vapor seal required for passive water removal fuel cells. The other method providing a gas seal is the "hydrophobic" configuration, a schematic diagram of which is shown in Figure 40. This figure shows the relative placement of the electrolyte reservoir in all hydrophobic configurations. The major advantages of the hydrohobic configuration is that any danger of electrolyte boiling is eliminated, since the electrolyte is at a pressure level near the reactant gas pressure rather than the lower water vapor pressure. A secondary advantage of this concept could be a size and weight savings due to use of a combined reservoir. Since the water transport plate reservoir is inboard of the gas seal, a single reservoir could service both fuel cell and the water transport plate without the transport problems of a combined hydrophilic configuration.

However, the major disadvantage of the hydrophobic configuration is that the hydrophobic barrier must have a minimum intrusion pressure of 12 psi. The barrier membrane must be a perfectly uniform, pin-hole free, non-degrading barrier. Unlike the electrolyte barrier in the hydrophilic method, which can tolerate small leaks, the hydrophobic barrier must be a perfect electrolyte dam. Any breaching of it would result in complete electrolyte loss and hence cell failure.

Tests were made on porous Teflon membranes (Gore-tex® #28-25A) which demonstrated a more than adequate intrusion pressure of 24 psid (16.6 n/cm^2), plus adequate permeability to serve in a hydrophobic cell. However, the long term hydrophobicity of the membrane would have to be demonstrated. Since this would require extensive and statistical tests, the passive water removal cell test effort was first directed toward the hydrophilic method.

Test Program

The passive water removal feasibility test program was conducted in parallel with the theoretical analysis described above. Objectives of the test program were to:

a) Evaluate operation of high power density cell with passive water removal

Performance	- voltage vs. current density
Tolerance	- voltage vs. electrolyte concentration
Stability	- voltage vs. operating time

b) Determine methods of preventing electrolyte loss
c) Establish configuration(s) for single cell development

Statistics for this test program can be summarized:

Size of Cells	4.5 in. x 4.5 in. (11.4 cm x 11.4 cm)
Number of Cells	8
Total Load Time	5050 Hours
Longest Cell Test	1231 Hours
Number of Configurations	2
Number of Electrolyte Barriers Tested	3
Number of Electrolyte Reservoirs Tested	3

Available hardware was adapted for passive water removal operation to enable the feasibility tests to be started before the strip cell design was completed. Figure 47 shows this hardware, in a combined reservoir, hydrophilic configuration. The cell area measures 4.5 x 4.5 inches (11.4 x 11.4 cm) for an active area of 20.25 in^2 (130.7 cm^2). This hardware was originally developed under U.S. Army Contract No. DA-28-043AMC-00320 (E). The nickel plated magnesium cooling plates are similar to those used on other P&WA cells except for the use of gaskets rather than O-rings for sealing. Several of the cells used hardware of similar size developed under Air Force Contract No. F33615-70-C-1134 which provided for O-ring sealing. The cell shown in Figure 47 utilized a dual porosity nickel sinter for a combined electrolyte reservoir and water transport plate. The pin pattern necessary for reactant flow was machined in the fine pore layer. Although cells such as this were tested successfully prior to contract efforts, the machined dual porosity sinter was difficult to machine, expensive, and not always effective in maintaining the reactant to water vapor seal.

Figure 48 shows a modification of this hardware, incorporating both a porous Teflon electrolyte barrier and a simplified construction method for the combined reservoir configuration. Asbestos matrix material is used for the water transport plate and also as an electrolyte bridge between the passive water removal assembly and the unitized electrode assembly. This construction provided a lower cost, more reliable, gas to vapor seal and allowed faster turnaround of experimental hardware. Cells of this configuration were the first to demonstrate steady-state operation without electrolyte loss. The electrolyte barrier was formed by bonding a Zitex® E606-126 membrane to the nickel sinter reservoir with FEP Teflon.

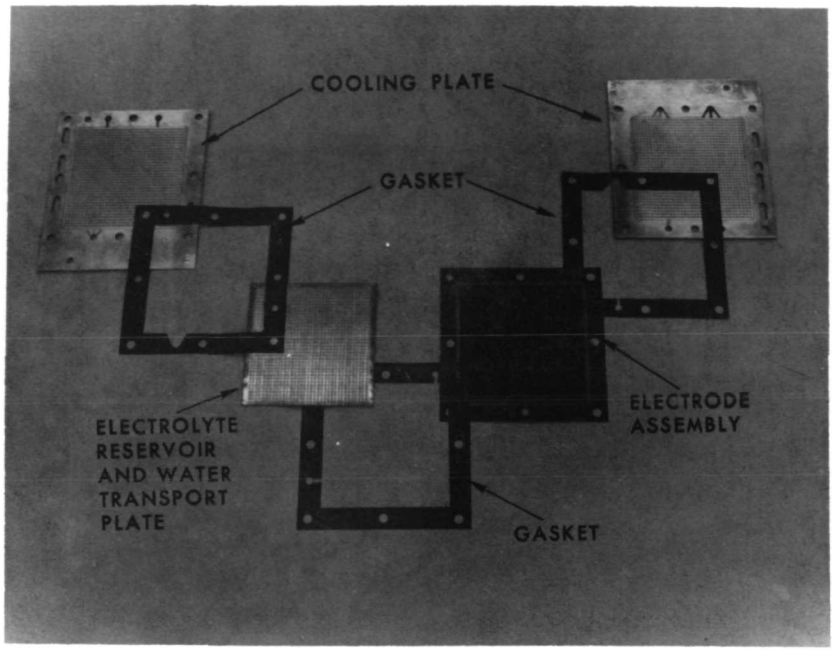

Figure 47 - Combined Reservoir Hydrophilic Passive Water Removal Cell

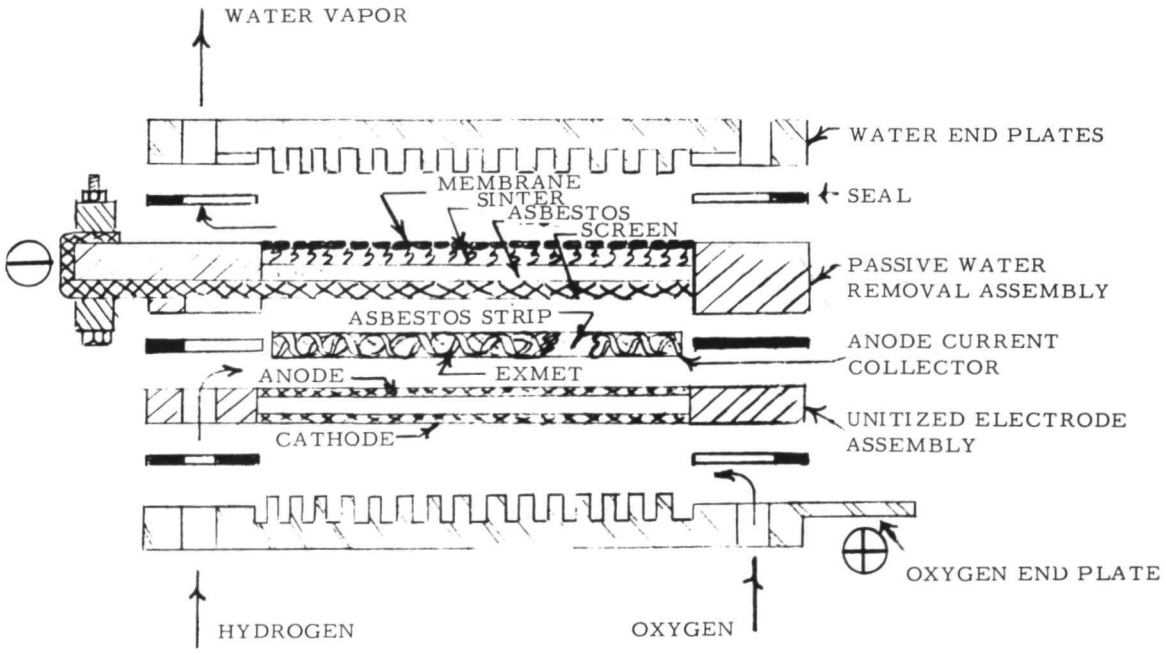

Figure 48 - Experimental Passive Water Removal Cell Combined Electrolyte Reservoir

Although effective in demonstrating electrolyte retention by means of an electrolyte barrier, this cell displayed poor response to varying electrolyte concentration. Since this particular combined reservoir configuration had questionable electrolyte transfer capability through the electrolyte bridge, and other methods for constructing a combined reservoir configuration required long lead times, it was decided to concentrate on the separate reservoir approach. This simplified cell construction and also facilitated rapid development, since such cells could more easily isolate problems specific to passive water removal.

Figure 49 shows how the cell hardware described above and readily available components were modified to form a separate reservoir, hydrophilic configuration. The most successful research cell, in terms of performance and stability, was of this configuration. Data from this cell is presented in Figures 50 and 51. The performance level was slightly higher than predicted at the sustained power point (100 ASF) (107.6 ma/cm^2), and slightly lower at the (extrapolated) peak power point (430 ASF) (462.7 ma/cm^2). Stability of this cell was good to about 800 hours when decay typical of carbonated electrolyte began. This mechanism was confirmed by post-test analysis, which revealed 36 and 16 percent conversion of the electrolyte to carbonate in the unitized electrode and water transport assemblies, respectively. These high values were due primarily to the obsolete gasket material which was used in this cell for test convenience. The product water pH data shown in Figure 51 illustrates the effectiveness of the Zitex membrane in retaining electrolyte. Product water vapor pressure excursions were run periodically to see if electrolyte loss would occur during these transients, which theory predicts would occur, if unchecked by the electrolyte barrier. Figure 50 shows that this cell tolerated such excursions which were imposed almost instaneously by changing the water vapor vacuum setting to the equivalent of a 30 to 40 percent KOH concentration change. The curve is typical of cells with integral Teflon membrane electrolyte barriers. Initially high pH values are believed due to entrained KOH left over from the flush fill procedures used to fill the cell with electrolyte. The occasional spike increase in pH is not completely explained, but may be related to the same cause or may represent severe transients beyond the liquid retention capability of the membrane, at least in locally stressed areas. It was observed that the post-test intrusion pressure of a passive water removal assembly, incorporating the Zitex E606-122 membrane that passed electrolyte, was reduced to 0.5 psi (0.35 n/cm^2) from a pre-test value of 2 psi (1.38 n/cm^2). Also, readings shown in Figure 51 do not represent a quantitatively significant loss of electrolyte. As shown in Figure 52, even with the very thin water transport plate reservoir design of 11 mils, a pH of 9.5 would represent less than 1 percent electrolyte loss in 10,000 hours of operation. Other cells of the

configuration shown in Figure 49 were subjected to the same rapid electrolyte concentration excursions while operating at a current density of 400 ASF (430.4 ma/cm^2). Electrolyte retention was satisfactory at this more severe condition as indicated by no change in the pH of the product water from a value of 7.

These research cells demonstrated that passive water removal cells with a porous Teflon electrolyte barrier could effectively eliminate electrolyte loss. The particular membrane and reservoir combination used in these cells was not optimized. Based on the analytical model of the electrolyte loss mechanism, attempts were made to run cells with theoretically better components, namely higher intrusion pressure membranes and larger mean pore size reservoirs.

Bench tests were set up to measure intrusion pressure and permeability of the membranes; standard porosimeter techniques were used to measure reservoir pore size. Of the commercially available Zitex (Chemplast, Inc.) membranes, E606-126 had the best combination of properties. Two experimental Gore-tex (Gore Associates) samples with 3 and 5 psi intrusion pressure, and higher permeability, were also tested.

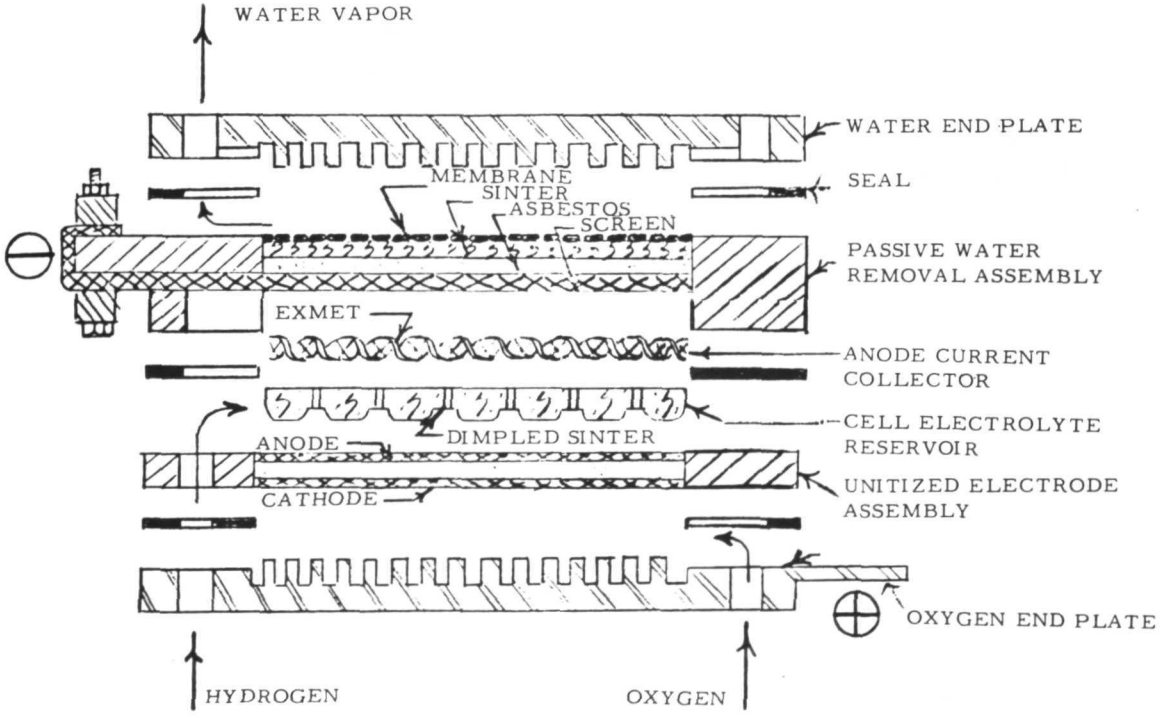

Figure 49 - Experimental Passive Water Removal Cell Separate Electrolyte Reservoir

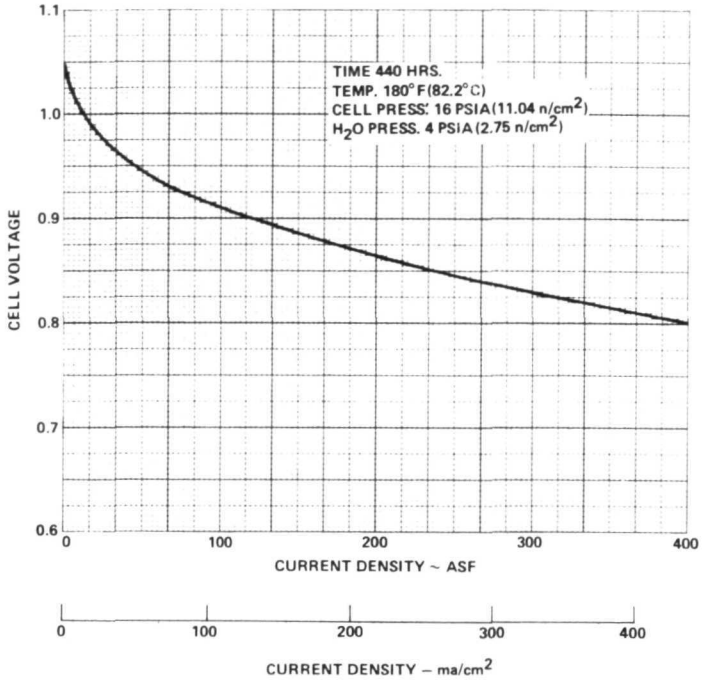

Figure 50 - Research Cell No. 2 Performance Data

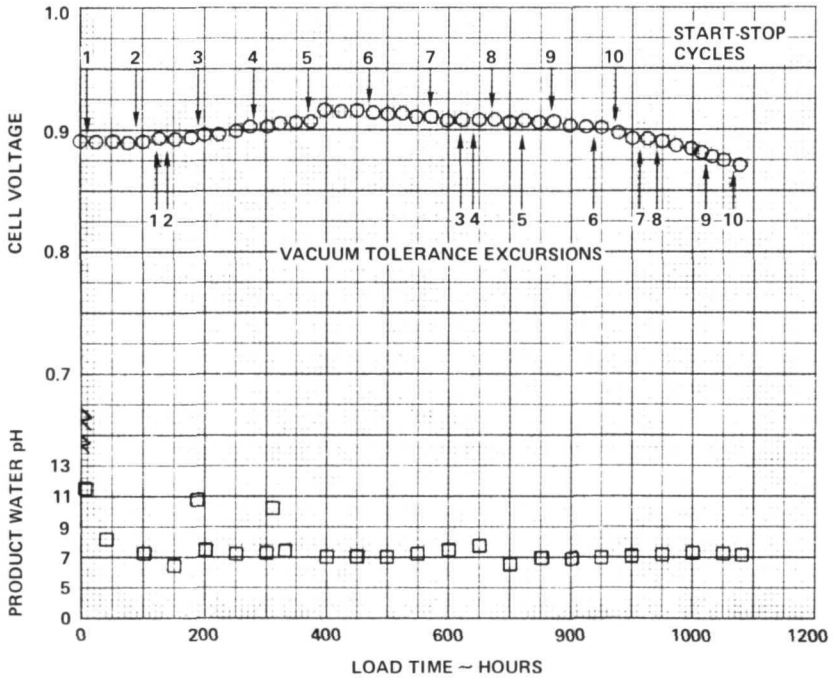

Figure 51 - Research Cell No. 2 Performance Data

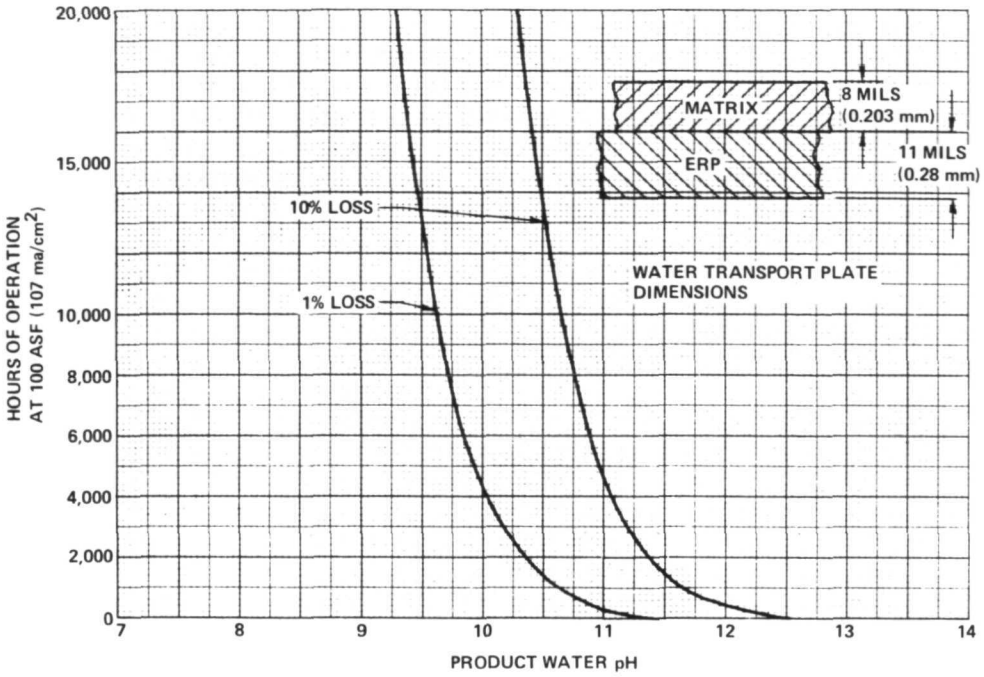

Figure 52 - Electrolyte Loss from Water Transport Plate is Negligible for pH Values Below 10.

In addition to the standard 5 micron mean pore size nickel sinter, electrolyte reservoirs were constructed from a 15 micron nickel sinter, and from a Huyck Feltmetal FM-415, of approximately 60 microns pore size.

A planned matrix of tests using these components was not successful because of membrane bonding problems. Significantly better results were not obtained on any of the theoretically better combinations tested. In the case of membranes, this was caused by tearing due to improper optimization of the membrane-sinter bond, which was developed for the Zitex E606-126 membrane. This bonding process also altered the properties of the larger pore size reservoirs. (Later tests in the full size single cell program were to prove that this bonding step was unnecessary.)

Although the optimization of the water transport plate components was not completed, the Zitex (and later Gore-tex) membranes in conjunction with the conventional nickel sinters were successful. It was therefore decided to proceed to full size single cell development using these components.

The above tests were conducted on the basis of nominal overall equilibrium conditions. An analysis was made to determine how product water diffusion through the passive water components would modify cell concentration gradients. Figure 53 shows that these conditions are not seriously affected by this simplifying assumption, even at the peak power condition. This figure shows that even with the relatively thick component parts used in the research passive water removal cells, the concentration gradient from the cell to the water vapor cavity was low.

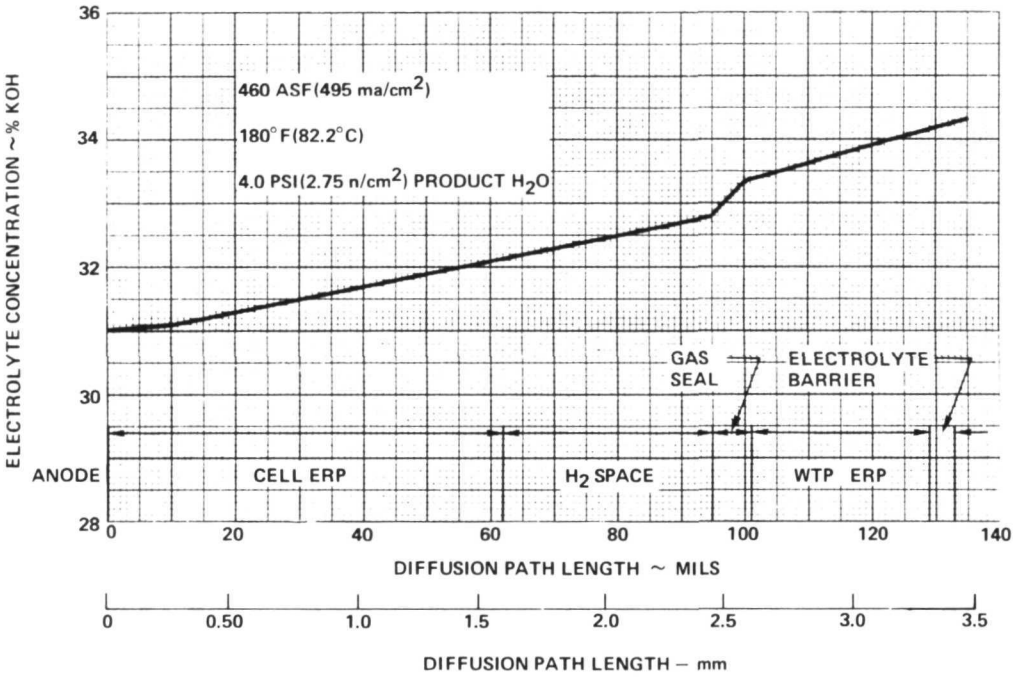

Figure 53 - Concentration Gradient in Research Water Removal Cell

The passive water removal research performed prior to and during the early portion of the contract showed:

- Performance and stability of conventional matrix-type fuel cells with passive water removal is satisfactory over the full current density range.

- An electrolyte barrier membrane prevents electrolyte loss under normal and severe transient operating conditions.

- The separate reservoir, hydrophilic configuration had the potential to meet the low weight goals of the program and should be used for full size single cell development.

3.0 Single Cell Design

This section describes the design of the single cell hardware and the successive single cell design configurations evaluated during the program. A single cell test vehicle was required to incorporate the results of the passive water removal investigation (Section 2) and unitization development (Section 4) for performance and endurance testing to prepare cell designs for the formal NASA Verification and Endurance category of testing.

In designing this vehicle, the novel features of the EMS design had to be incorporated, namely:

- Strip cell - 12.0 in. x 1.37 in. (30.5 cm x 3.48 cm) cell area
- Edge current collection.
- Improved compatibility frame unitization
- Passive water removal
- Minimum thickness flow fields and component parts.

Certain compromises were required in incorporating the ultimate materials and thickness dimensions which design studies and compatibility testing indicated to be desirable. Such compromises were recognized by NASA and P&WA as necessary for improving the reliability of the strip cell hardware constructed with new materials before minimizing dimensions in later designs.

Figure 54 shows that the cell designs tested represent a significant improvement compared to the existing state-of-the-art as represented by the cell design used in P&WA's DSV powerplant. The direct comparison between the DSV and the EMS cell is not completely "fair" since the EMS requirement to remove product water by the passive method requires that an additional subassembly, the water transport plate, be added to the EMS cell. None-the-less, the passive water removal cells tested during this program were only 60 percent as thick as DSV cells.

The only significant relaxation from the baseline EMS dimensions was in the hydrogen spacer, where for purposes of porting and gasketing in early cells some 15-20 mils (.38-.51mm) were added. Several of the early designs also had slightly larger frame or oxygen field dimensions because of material availability problems. Baseline design values were bettered for all the ERP thicknesses. A typical ERP used in nearly all cell designs is shown in Figure 55. It is 22 mils (.56mm) in total thickness. The baseline design value was 25 mils (.64 mm). This figure shows the pin field pattern for support of the anode and the groove and hole pattern for distribution of hydrogen.

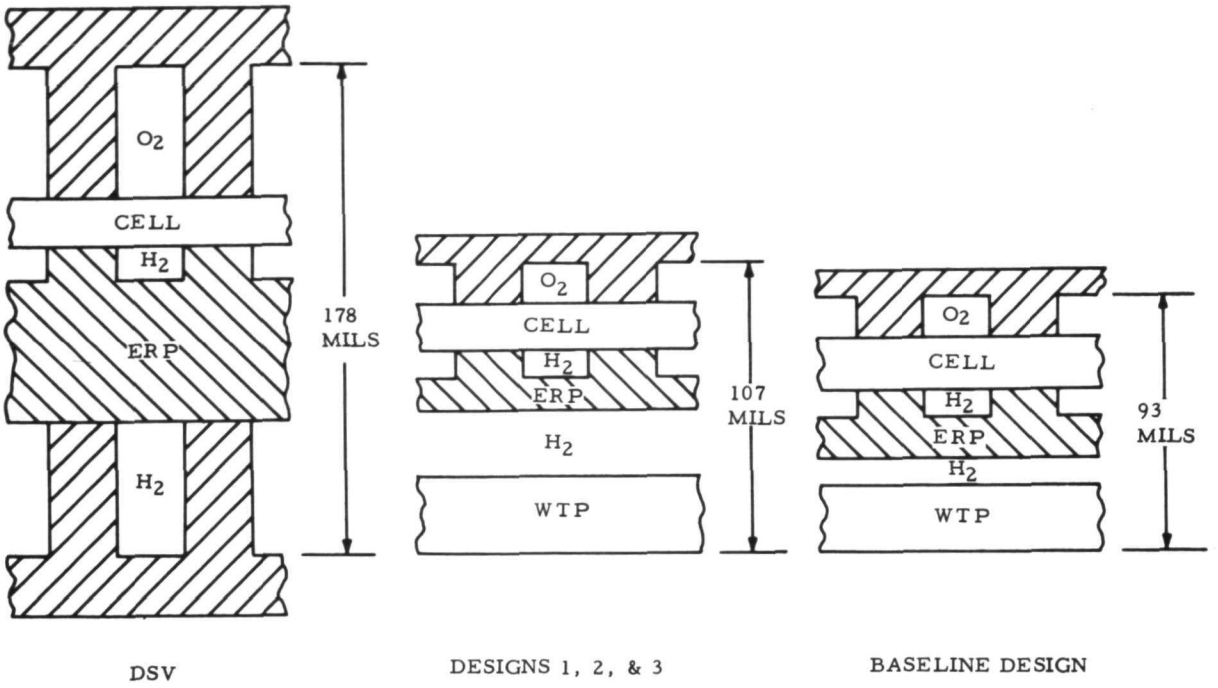

Figure 54 - Size Comparison of Cell Designs Tested

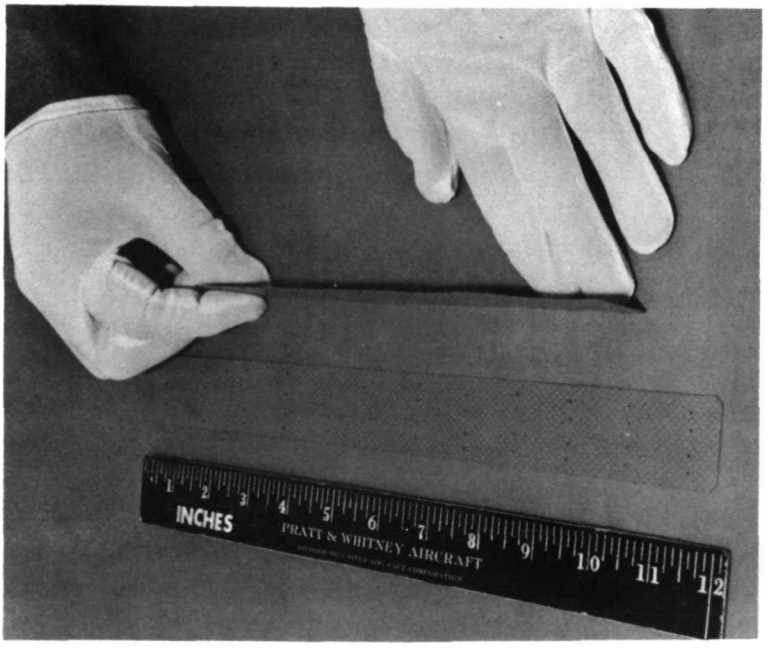

Figure 55 - Electrolyte Reservoir Plate

The cell test fixtures were deliberately overdesigned for development purposes. The resulting end plates are rigid with provision for simple sealing and fluid connections. Some of the features of these test fixtures shown in Figure 56 are:

- Flow field inserts for interchange of field patterns
- O-ring sealing for easy assembly of unitized parts
- Isothermal operation to duplicate EMS Design
- Passive heat rejection for test simplicity
- Stainless steel end plates 1/2 in. (1.25 cm) thick to provide uniform cell compression
- Nickel plating to avoid corrosion

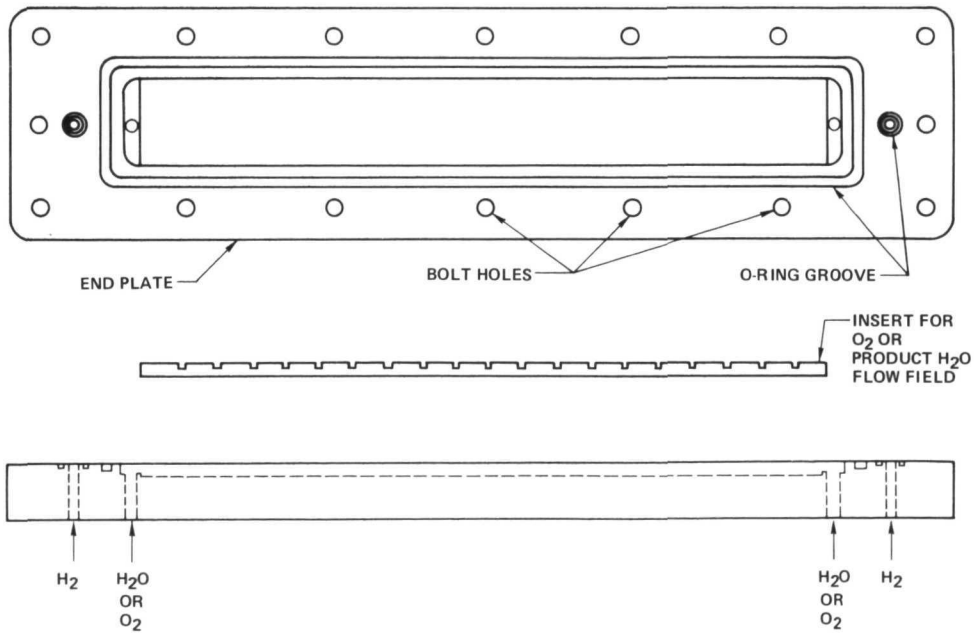

Figure 56 - Single Cell Development Test Fixture

Following the choice of the separate reservoir, hydrophilic configuration for passive water removal, separate unitized assemblies were used for early development. Thus, the plastic frame cells were unitized in two sections - a unitized electrode assembly (UEA) and a unitized water

transport plate (WTP) - joined by a gasket or glue bond as shown in Figure 57. This was convenient for early development and necessary because of the early fabrication difficulties. However it did result in a more complicated assembly.

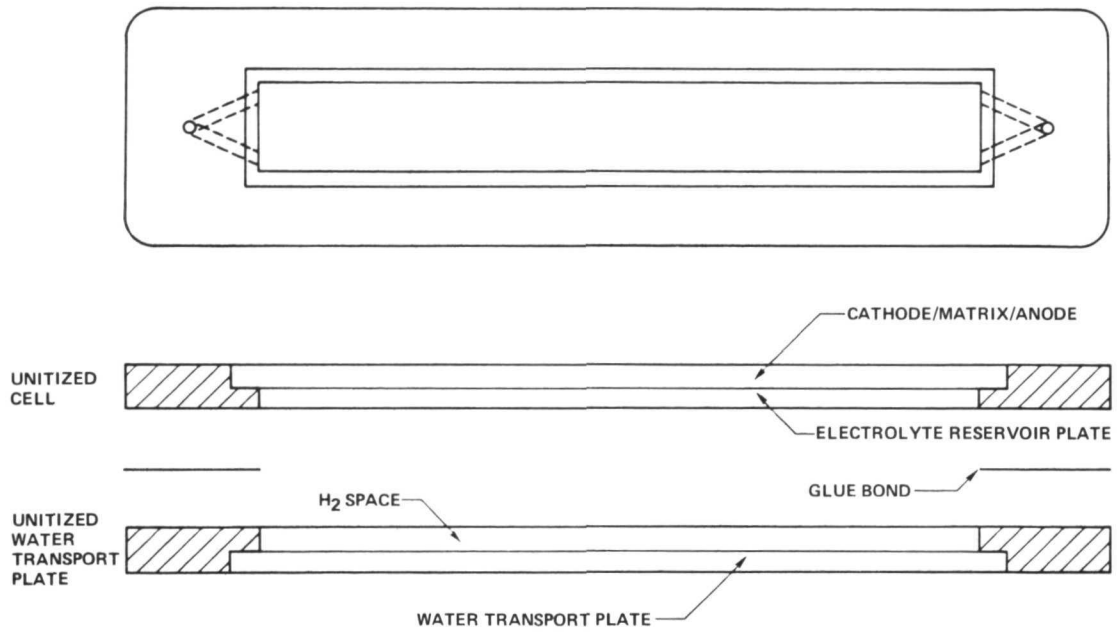

Figure 57 - Single Cell Development Plastic Frame

Three thermocouples were installed in each end plate. Temperature readings indicated uniform temperature distribution. Internal thermocouples were placed on electrodes of several cells and the temperature differed from the end plate readings by only 2 or 4° F (1.1 or 2.2° C) at the normal endurance operating conditions of 100 (107.6) and 200 (215.2 ma/cm^2) ASF.

Various unitized cell assemblies were tested in the fixtures described above. Three single cell designs were submitted for Verification approval during the program and five cells of these designs were tested on Verification and /or Endurance test schedules as described in Section 6.0 (Single Cell Test Results). In addition, eleven earlier cells were tested in the exploratory Research and Technology Test Program. All of these cells represented evolutionary stages in the development of Verification Design No. 1.

The design of the working elements of all three cell designs was the same; they differed in the construction materials used to unitize the elements and

to form the cell structure. The listing below identifies the type of unitization used in the three designs. A cross sectional view of a cell showing the relative locations and dimensions of the cell elements, and the fluid flow passages appears in Section 6.0, Single Cell Test Results.

Design No.	Type of Unitization	Cell Nos.
1	Arylon/Hypon	12-13 (1-11 similar)
2	FEP Teflon	14
3	Impregnated Matrix	15-17

As discussed earlier, the deliberate choice to use separate unitized assemblies for the cell and water transport plate did present some assembly difficulties, especially in earlier cells where fabrication difficulties resulted in poor dimensional control. Some measure of this difficulty is shown in Figure 58. This shows all of the individual parts assembled into Design No. 3.

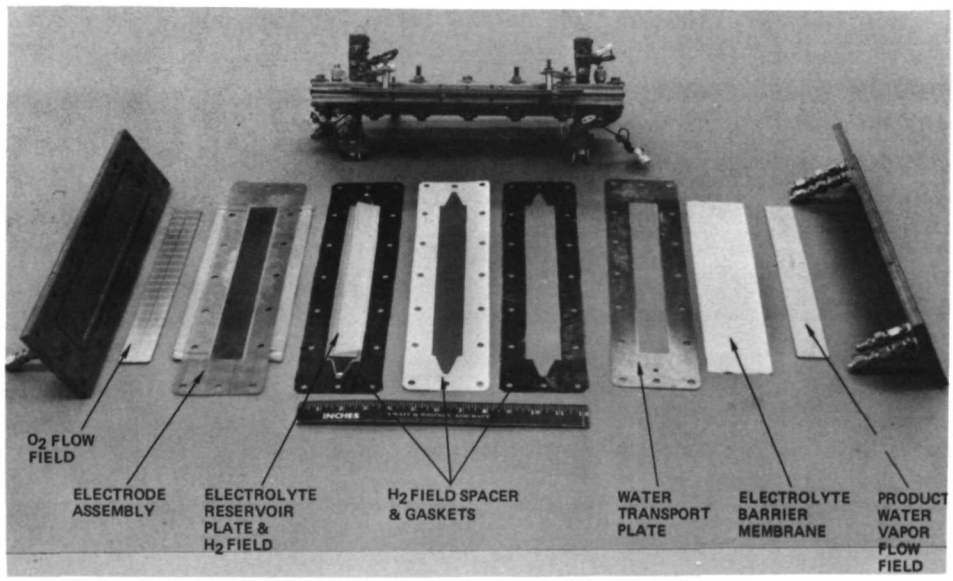

Figure 58 - Unitized Cell Assembly

As fabrication processes improved, resulting in improved dimensional tolerances, it was possible to eliminate some of the assembly problems by fabricating a one piece assembly combining both cell and water transport assemblies. Figure 59 shows such an assembly (tested in Cell No. 20) which is functionally and dimensionally similar to Design No. 3. The gaskets are eliminated and a epoxy-impregnated matrix frame

substituted for the Teflon frame. The assembly advantages are obvious; only 6, rather than 15 parts needed to be handled in the final assembly.

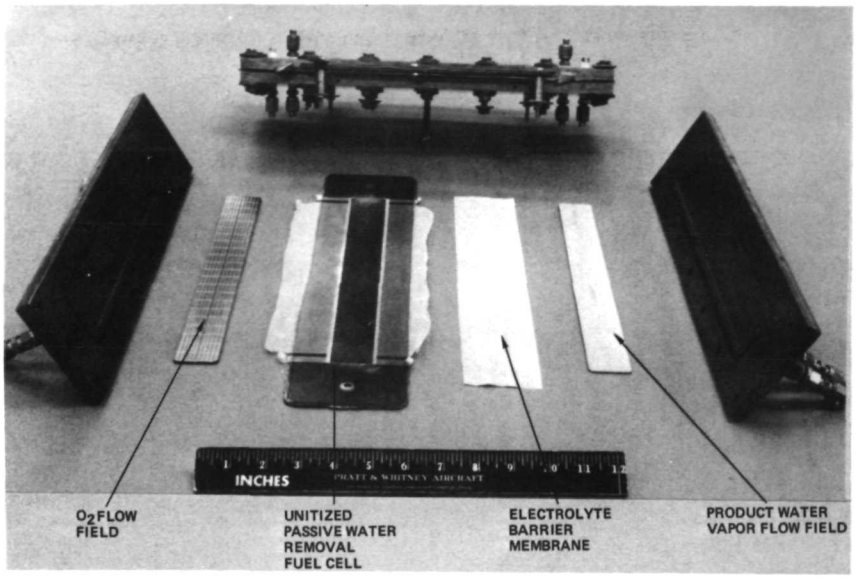

Figure 59 - Improved Unitized Cell Assembly

In summary, a satisfactory test article was designed for performance and endurance test evaluation of various single cell designs. Three such designs were approved for Verification, and successfully tested. An improved variation of the third design, which integrated all cell components into one assembly, was also successfully tested.

4.0 Cell Fabrication and Unitization Research

The EMS weight and life goals imposed stringent requirements on cell fabrication technology. The thin cells required to minimize weight must be fabricated to close tolerances. A cell frame thickness variation of a few thousandths of an inch which would be acceptable in conventional thicker cells would represent a significant percentage of total cell dimension for lightweight cells. This could result in degraded cell performance because of poor contact between cell components and sealing of adjacent subassemblies could be unreliable. The reactant differential pressure (bubble pressure) capability of the matrix-to-frame joint in the water transport plate and the fuel cell subassemblies must be reliable. The materials used to make this joint and to form the cell frame must be highly resistant to attack by reactants, water and electrolyte. Finally, assembly and bonding processes used must be compatible with normal manufacturing equipment and result in reasonable costs.

Initial efforts in the cell fabrication area used available materials which previous testing had shown to be the most compatible. As a result of investigations performed under NASA-LeRC contract NAS3-13229, it was found that a cause of cell performance degradation with time was conversion of electrolyte to potassium carbonate. A major cause of this carbonate formation was the corrosion of epoxy glass fiber cell frame material. Subsequently, an in-house program was undertaken to develop alternate materials. As a result of corrosion screening tests, polyaryl ether (Arylon) was chosen for the frame material and an ethylene propylene rubber (EPR) formulation was selected for the matrix-frame bond. Over 5000 hours of operation were accumulated on 0.5 ft^2 (464.5 cm^2) cells using this unitization method. Performance data and post-test analyses showed that carbonate formation was significantly lower-between 1/2 and 1/5 - that in the glass fiber-epoxy cells.

Development of EMS cells using these materials was hindered by the high curing temperature requirement of EPR which caused unacceptable distortion of the thin cell frames. It was also found difficult to consistently achieve satisfactory bubble pressure at the matrix to frame joint in the cell and water transport plate subassemblies.

To overcome bubble pressure limitations and frame distortion, a method was evolved whereby the edges of the matrix were impregnated with a modified epoxy (Hypon) which was then bonded to the plastic frame under pressure using a thin film of the epoxy as the adhesive (Figure 60). Because of the low temperatures required for bonding this epoxy, frame distortion was minimized. By rigorous attention to shelf-life and proper bonding pressures, strong, non-porous joints were obtained repeatedly. This construction technique was used for Cell Nos. 1 through 13.

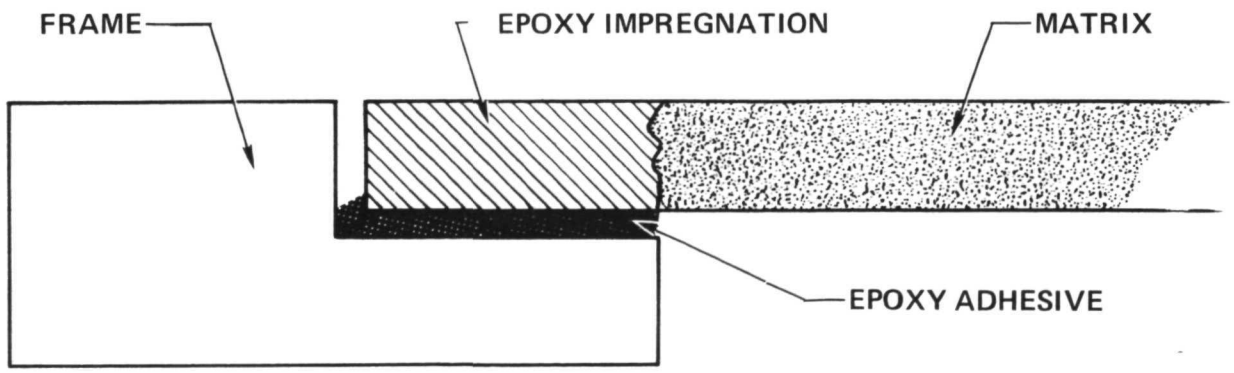

Figure 60 - Matrix Edge Impregnation Method and Bonding to Plastic Frame

Development of fabrication methods to provide for edge current collection was also required. To provide for edge current collection, it is necessary to extend the electrode screens through and beyond the plastic frame while maintaining a flat, uniform thickness frame which permits no reactant leakage outboard of the cell. Initial efforts to solve this problem involved attempts to heat seal the electrode screen into the plastic frame surface. A smooth surface resulted from this method; however, the differential thermal expansion between the electrode screens and the plastic frame produced severe warping of the frame and wrinkling of the electrodes and matrix. Variations in the time, temperature and pressing parameters resulted in improvement; however, the basic problem could not be overcome. Other attempts were made to bring the screens out through a notch in the frame and then impregnate the screens with EPR or Hypon. These methods were not successful in preventing external leakage, since they resulted in a non-homogeneous frame surface. A satisfactory method was developed which used a lamination consisting of the plastic frame and an epoxy impregnated matrix laid over the screens on the top of the cell frame and press cured in place. This method, although more cumbersome, had the advantage of separating the current carrying and reactant sealing functions. This technique produced cells with no external leakage and improved dimensional control, suitable for testing to evaluate performance and endurance characteristics.

The analyses of the first single cell tests indicated carbonation levels in excess of that predicted using the materials compatibility data which was available at the beginning of the program. The results of this was a re-orientation of the single cell program toward additional materials research including a search for improved epoxy formulations and other materials which had potential for use in cell unitization. Early fabrication attempts had indicated the necessity for low epoxy curing temperatures to minimize frame distortion during bonding of the impregnated matrix to the frame. The single cell carbonation results, however, indicated that higher curing temperatures would be necessary to improve the compatibility of the epoxy. Accordingly, a study was instituted to determine the effect of epoxy curing cycles.

This study showed that higher curing temperatures were indeed needed for complete curing of the Hypon. Accordingly, fabrication procedures were investigated to allow use of the higher cure temperature. However, the higher temperature curing cycle, while lowering corrosion, again led to unacceptable warping of the cell.

These conflicting temperature requirements of the epoxy and the plastic frame continued to inhibit the development of a dimensionally uniform cell and thus led to the elimination of the plastic frame and the evolution of the integral epoxy impregnated matrix frame concept.

In this concept, a single piece of matrix material serves as the reinforcing material in the frame and also as the matrix. This is accomplished by impregnating the desired frame area of a sheet of material with epoxy. The impregnated area when cured becomes the frame of the cell. Since the matrix and frame are integral and in the same plane, a very thin, simple assembly is achieved. The strength of the matrix reinforced epoxy together with the minimum differential thermal expansion between electrode screens and frame precludes any warpage of the part. The fabrication of the cell is a simple three step process (Figure 61). First, a trimmed matrix is impregnated in the frame area and allowed to air dry. Next the electrodes are laid in place with the screens extended outboard of the frame and the part is partially cured in a press. Final curing takes place in an oven with the part restrained. The passive water removal unit is made in the same manner except there are no electrodes.

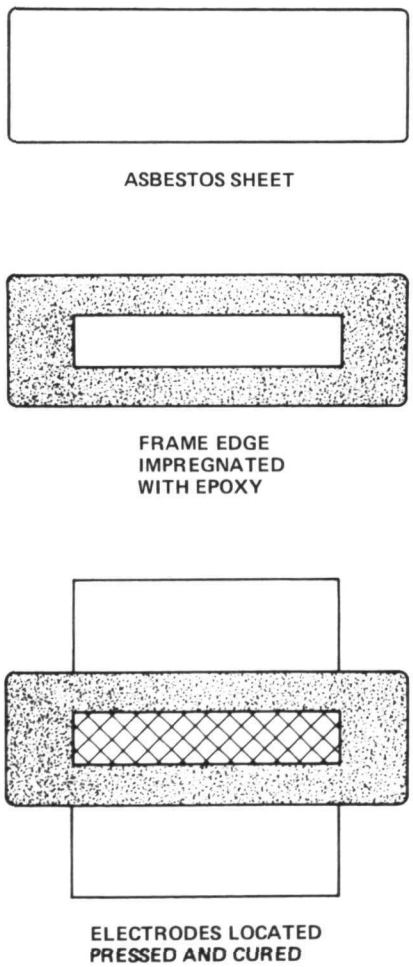

Figure 61 - Impregnated Matrix Unitization Method

Cells fabricated with this process exhibited no distortion or leakage, and had excellent dimensional accuracy (Figure 62). In addition, substantial cost savings were realized due to the elimination of the machined plastic parts and the shorter fabrication times involved. Cell Nos. 15 through 19 were built in this manner.

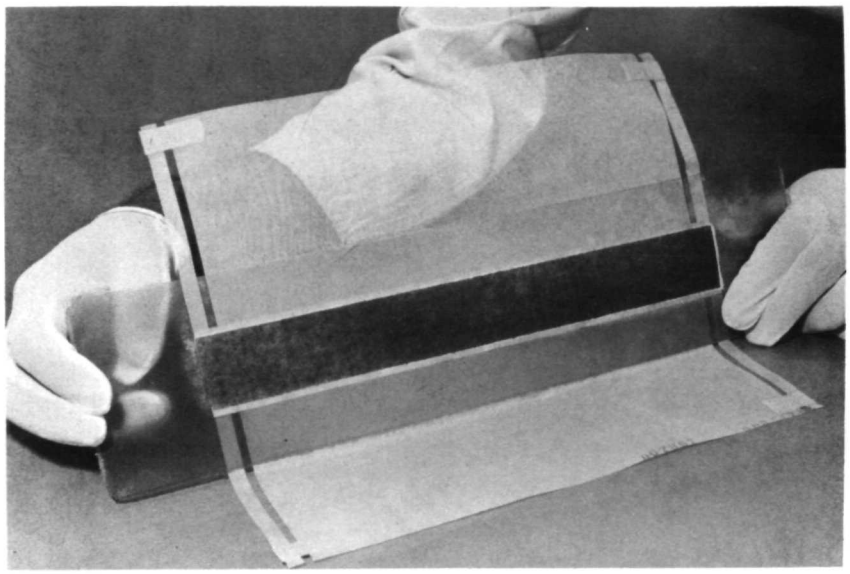

Figure 62 - Electrode Unitization Procedure

In an attempt to further improve the dimensional characteristics of the entire strip cell assembly, trials were made to combine the cell and water transport plate assemblies into one integral unit using the impregnated matrix concept. The design called for laminating the two assemblies together using several layers of impregnated matrix cut to the shape of frames. The combined thickness of these spacers would equal the total thickness of the parts separating the cell and the water transport plate. This would result in eliminating plastic spacers and elastomer seals used in the assembly thereby improving the overall dimensional tolerances and greatly simplifying the cell assembly. After initial problems of hydrogen port blockage were overcome, Cell No. 20 was built to this design, see Figure 59 in Section 3.0.

Laminating Films Unitization Development - Materials compatibility test data generated during this program coupled with the results of other investigations identified several materials which possess excellent compatibility with electrolyte and oxygen. Several of these materials are available in forms suitable for use in unitizing cell components into assemblies. These materials are TFE and FEP Teflon and polypropylene.

The special material oxidation tests developed during the program emphasized the superior cleanliness of these materials compared with the epoxies normally used for unitizing cell components. It would be an obvious benefit for very long life, lightweight fuel cell systems to be able to use these highly compatible materials for a cell frame. However, there was no experience in using these materials in the difficult application of unitizing the fuel cell sandwich into a reliable assembly capable of providing high differential pressure sealing of reactant gases and maintaining the dimensional accuracy required. A research effort was therefore undertaken with a goal of developing a cell frame design and the associated fabrication techniques to allow one or more of these highly compatible materials to be used.

There existed a background of fabrication experience for bonding polymer films to various substrates. The electronics industry, for example, had developed techniques for bonding films of polyethelene, polyproplene, FEP and others to metals. Protective coatings for printed circuit boards, flexible electrical cables, etc., are made by bonding polymer films to the metal substrates under pressure and temperature. NASA-LeRC programs were responsible for developing protective cover plates for solar cells made by bonding FEP films to the solar cell. The approach taken in the laminating films unitization effort was therefore to investigate the use of these techniques to see if they could be adapted to bonding several fuel cell elements into the desired unitized assembly.

The basic design concept of a laminated film cell frame is shown in Figure 63. The function of the laminating film is the same as the epoxy-asbestos or epoxy-glass fiber type of unitization - to bond the several cell components together to create a unitized assembly with the required gas sealing and dimensional accuracy. The several cell components together with the film are laid-up and placed between heated platens in a press. The platen temperature is set at a level where the film material softens and flows into the cell components bounding the assembly together.

The film materials selected were those which were commercially available in film form and which were known to have excellent compatibility in the cell environment. The principal candidates were FEP Teflon and polypropylene. Polyethelene was also investigated to determine if it could be used as a intermediate bonding agent. Several combinations of film and core frame materials were evaluated to determine whether a good bond could be achieved and if so, what the process temperature would be to effect a good bond. The results of these investigations are shown in Table 8.

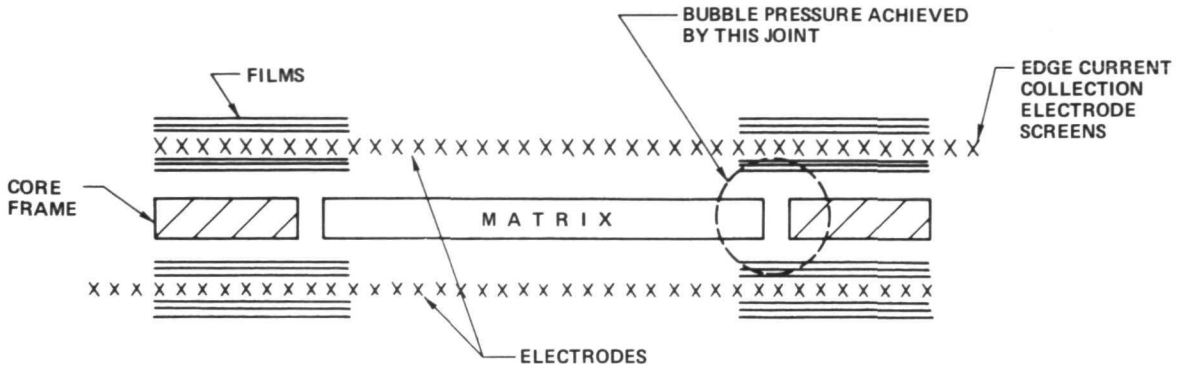

Figure 63 - Laminating Film Unitization

TABLE 8

FILM BONDING INVESTIGATION

COMBINATIONS INVESTIGATED	BONDING TEMPERATURE
TFE TO TFE	620°F (326.7°C)
TFE TO TFE WITH FEP	520°F (271.1°C)
TFE TO TFE WITH ETCHED FEP	520°F (271.1°C)
TFE TO TFE WITH POLYPROPYLENE	NO BOND
TFE TO TFE WITH POLYETHYLENE	NO BOND
FEP TO FEP	520°F (271.1°C)
FEP TO ETCHED FEP	520°F (271.1°C)
FEP TO FEP WITH POLYPROPYLENE	NO BOND
FEP TO FEP WITH POLYETHYLENE	NO BOND
FILLED TFE TO FILLED TFE WITH ETCHED FEP	350°F (176.7°C)
FILLED TFE TO FILLED TFE WITH POLYPROPYLENE	350°F (176.7°C)
FILLED TFE TO FILLED TFE WITH POLYETHYLENE	250°F (121.1°C)

Unitization trials using both materials were then performed on subscale and strip cell size (1.37 x 12 inch) (3.48 x 30.5 cm) cells. Three factors were used to evaluate the adequacy of the cell design; 1) adequate matrix to frame sealing, 2) a smooth frame surface with good control of frame thickness, and 3) the flatness of the electrode screens - whether the screens lie smoothly on the matrix.

Encouraging results were achieved in subscale samples which respect to all three evaluation criteria. The strip cell size trials provided good bonding of the components and frame flatness and surface finishes were acceptable. However, all strip cells which use the FEP frame construction displayed excessive electrode screen wrinkling. The

wrinkling was the result of the stresses introduced into the assembly by the differences in the coefficients of thermal expansion between the polymer frame and the metallic electrode screen. The FEP and the electrode screens are locked together during the 520°F (271.1°C) bonding process. In cooling to room temperature, the polymer contracts more than the screens resulting in the wrinkling. In spite of the wrinking, an all FEP cell was fabricated for test, and operated for 660 hours. The cell showed substandard performance due to the nonuniformity of the electrode-to-matrix contact caused by the electrode wrinkling. The distortion also resulted in a marginal matrix to frame seal as evidenced by the crossover failure mode of the cell. Nonetheless, this cell demonstrated the value of FEP of frame material by the very low electrolyte carbonation data obtained from the test (see Section 5.0).

Strip cells unitized with polypropylene films which use polypropylene as the core frame material were evaluated to see if the significantly lower bonding temperature (350° F) (176.7° C) could reduce electrode screen wrinkling to acceptable levels. However, the wrinkling was not significantly reduced because of the differential thermal expansion and the inherent shrinkage of the polypropylene when processed at temperatures above its glass transition temperature.

The excessive contraction of the cell frame compared to the electrode screen can be alleviated by two factors; 1) the frame core can be made of a filled polymer whose coefficient of expansion more closely matches that of the electrode, 2) the amount of laminating film material used can be minimized so that the strength of the electrode - frame combination dominates that of the film. However, the number of available filled frame materials which could be used as the frame core is severely limited. The most widely available filler material - glass fiber-can not be used because of its poor compatibility with electrolyte. Asbestos filled materials in the very low thickness required, approximately 10 mils (0.25 mm), are not readily available. A potentially attractive filler material being developed by DuPont, the Fybex grade of potassium titanate, was not available because of its newness. However, this material should be a superior reinforcing material for polymers used in alkaline electrolyte fuel cells. KOH compatibility tests of Fybex performed at NASA-LeRC showed it to be essentially unattacked by the electrolyte. Subsequently, orders were placed with several vendors who were willing to fabricate Fybex filled sheets of polypropylene, polysulfone, and TFE. The procurement lead times for obtaining these materials and vendor problems in fabricating sheets delayed their receipt to near or after the Phase 1 portion of the program.

To permit the laminating film unitization research to continue pending receipt of the Fybex filled sheets, a process for fabricating asbestos filled TFE was developed in-house. A method similar to that used in preparing asbestos matrices was used to prepare sheets of 30 weight percent asbestos filled TFE. This material was used with polypropylene films to develop strip cell and six cell plaque unitizing procedures. The cells and plaques made with this design were significantly improved in electrode flatness compared to all FEP or polypropylene frame designs. Success in fabricating single cells of this design lead to recommending the design for verification testing. A trial 6-cell plaque was fabricated using the polypropylene film - asbestos-filled frame design. This plaque incorporated 3/8 inch (9.5 mm) wide intercell seals and showed excellent dimensional control and electrode flatness. One problem not fully solved during Phase 1 was marginal gas sealing capability. The matrix to frame joint developed a bubble pressure of approximately 8 psi (5.52 n/cm^2). The polypropylene film to matrix interface was not equivalent to that of the epoxy cells. Further work is required to improve the sealing capability.

5.0 Electrolyte Carbonation

The performance of potassium hydroxide electrolyte fuel cells can be degraded if a significant portion of the electrolyte is converted to potassium carbonate. The amount of performance loss is a function of the percentage of the electrolyte converted to carbonate and the current density. For electrolyte conversion up to approximately 25 percent, the effect is minimal at low current densities. The increasing performance losses at high current density however have an adverse effect on the voltage regulation capability of a fuel cell system. A fuel cell system whose cells contained a high percentage of carbonate would continue to operate satisfactorily but its capability to meet voltage regulation requirements would be impaired.

Two sources of contamination can cause electrolyte carbonation: 1) impurities in the reactant gases and 2) the cell components. This is illustrated in Table 9. Carbon dioxide contained in either reactant reacts with the electrolyte to form potassium carbonate. Investigations at NASA-LeRC have shown that methane contained in the oxygen is oxidized and results in electrolyte carbonation. The amount of methane converted is a function of cell design, operating conditions and purge frequency.

The second potential source of electrolyte carbonation is the cell itself. The materials used in the cell can react with the fluids present creating products which react with the electrolyte. The amount of carbonate

producing substances is a function of the materials used, the surface area and mass of materials present in the cell which are exposed to electrolyte and oxygen, and the cell operating conditions.

TABLE 9

CARBONATION IN ALKALINE ELECTROLYTE CELLS

Contamination Sources	Amount of K_2CO_3 Formation
Hydrogen - CO_2	CO_2 - . PPM Contained in Reactants
Oxygen - CO_2, CH_4	. Cell Reactant Consumption (amp-hours)
Cell Structural Materials	CH_4 . PPM Contained in O_2
	. Stay-Time in Cell (Purge Frequency)
	. Operating Conditions
	Structures . Compatibility with KOH and O_2
	. Cure Time/Temperature of Adhesives
	. Surface Area and/or Mass of Material in Cell
	. Operating Conditions

The effect of the electrolyte carbonation on cell performance is related to the fraction of the electrolyte converted to carbonate. The cell designer has flexibility in selecting the amount of electrolyte capacity the cell will contain. By increasing the thickness of the electrolyte reservoir plate, a larger inventory of electrolyte is made available for absorbing any carbonate producing substances, thus keeping the percentage conversion low. This however, means a heavier cell due to the increased weight of the reservoir plate and the electrolyte it contains. The designer can also reduce the sensitivity of the cell to any contaminants produced by the structural materials used to package the active elements of the cell. Cell configurations which minimize the amount of edge frame around the electrode area would be selected.

The 10,000-hour life and the tight voltage regulation goals of this program requires that performance decay due to electrolyte carbonation be extremely low. The goal for minimum cell weight dictates that large amounts of electrolyte contained in thick reservoir plates can not be used. The system design concept requires cells with high perimeter to area ratios connoting stringent requirements for the compatibility of the materials used in the cell frames. These factors were the basis for planning several interrelated research tasks to develop the technology of lightweight cells capable of operating for long durations with minimum

performance loss because of electrolyte carbonation. These tasks were; 1) the search for more compatible materials coupled with several types of testing to measure the carbonation characteristics of candidate materials, 2) lightweight electrolyte reservoir plate development to achieve a low weight, porous reservoir to allow a greater cell electrolyte inventory with a minimum weight penalty, 3) development of cell fabrication techniques which would allow the most compatible materials to be used, and 4) testing of cells to assess the carbonation characteristics of different cell designs under actual operating conditions.

Early Operating Cell Results

The cell structural materials available at the beginning of the program and the reasons for their selection are discussed in Section III B. Testing of early strip cells of the Hypon/Arylon frame design showed the materials used had good compatibility compared to the glass fiber - epoxy materials previously used. This is illustrated in Figure 64 which shows the amount of carbonate produced per unit of cell frame perimeter for 0.5 ft^2 glass fiber-epoxy and plastic frame cells and the amount produced by the early strip cells tested under this program. The electrolyte carbonation characteristics of these strip cell designs were comparable to the best of the previous tested 0.5 ft^2(464.5 cm^2) cell designs.

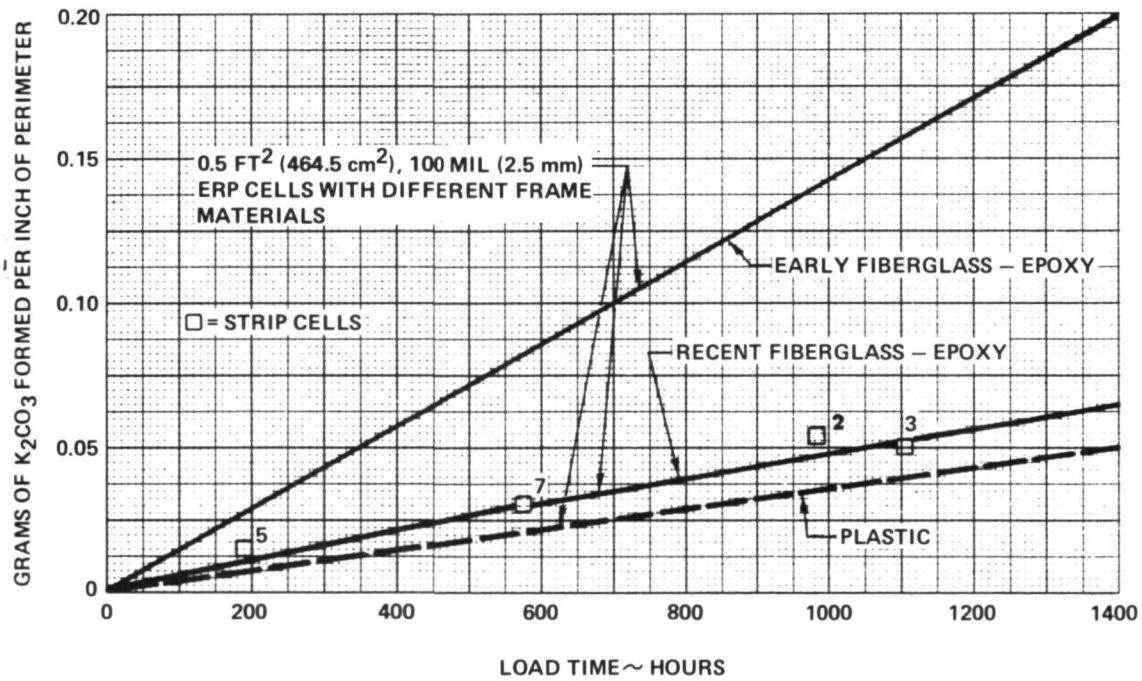

Figure 64 - Hypon/Arylon Frame vs. Glass Fiber-Epoxy Frame Data

These materials, however, were found to be unsuitable for meeting the stringent goals of this program. This is illustrated by the data shown in Figure 65, which plots the amounts of electrolyte conversion to carbonate as a function of operating time. The amount of conversion is seen to be clearly unacceptable. The low value shown for the best 0.5 ft^2 (464.5 cm^2) glass fiber-epoxy and plastic frame cells is due to: 1) a much larger amount of electrolyte inventory, and 2) a smaller cell frame perimeter to active cell area ratio. The electrolyte reservoir plate thickness in these 0.5 ft^2 (464.5 cm^2) cells was 100 mils (2.5 mm) resulting in a weight of this component alone of 1.4 lb per ft^2 (0,683 gm per cm^2). This weight in itself is greater than the weight goal of the entire cell, water removal and cooler assembly for this program.

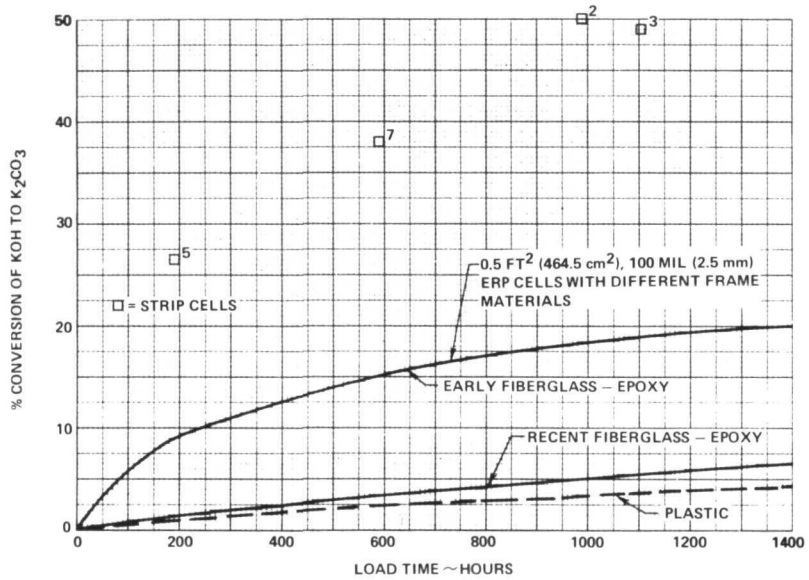

Figure 65 - Carbonate Conversion Data

The effect of cell electrolyte capacity and cell configuration on the relative sensitivity to cell produced carbonation is shown in Table 10. This table compares a 0.5 ft^2 (464.4 cm^2) cell incorporating a 100 mil (2.5 mm) thick electrolyte reservoir plate to the baseline EMS cell. To minimize weight, the EMS cell has a thin electrolyte reservoir plate resulting in an electrolyte inventory per unit cell area one-fifth that of the 0.5 ft^2 (464.5 cm^2) cell. The difference in cell geometries results in the EMS having a cell frame perimeter per unit area 3.5 times that of the larger cell. Because of these two factors, it is seen that the lightweight EMS cell is approximately 16 times more sensitive to frame-produced carbonation than the heavier cells. The EMS cell's peri-

meter to area ratio can be considerably improved from that shown here by using lower aspect ratio cell configurations (see Section V). The goal of achieving minimum weight, however, means that the amount of electrolyte in the cell should be minimum; therefore, the compatibility of the cell components must be the highest achievable.

TABLE 10

Influence of Cell Design on Structure Produced Carbonation

		NASA-MSC DM-1	Strip Cell
Active Area	In^2 (cm^2)	73.0 (471)	16.4 (105.8)
Frame Perimeter	In (cm)	34.2 (86.9)	26.7 (67.8)
Electrolyte Reservoir Plate Web Thickness	Mils (mm)	90 (2.29)	12 (0.305)
Amount of 100% KOH In Cell	Grams	26.3	1.22
Amount of 100% KOH per Inch of Perimeter	Grams/In (Grams/cm)	0.76 (0.30)	0.046 (0.018)
Relative Geometric Effect	--	1.0	16.5

The carbonation results from early strip cells indicated a need to develop more sensitive compatibility testing techniques to allow rapid screening of candidate materials and cell unitization designs. One result was the addition of the oxidation tests using gas chromotograph techniques (Section II B). Another technique developed was the use of non-operating cells to evaluate the relative carbonation characteristics of promising unitization designs. The non-operating cells provide an accelerated measurement of carbonation rates of realistic cell configurations. A cell frame represents a combination of materials not possible to simulate in simple, single fluid compatibility tests.

A non-operating cell consists of a strip cell (1.37 x 12 inches (3.48 x 30.5 cm) cell area) without an electrolyte reservoir plate, mounted between single cell end plates. A schematic drawing of this test fixture is shown in Figure 66. The cell is tested with oxygen in both reactant compartments to expose a maximum area to the oxidizing atmosphere. The cell is mounted in a 180° F (82.2° C) oven and the reactant passages pressurized with 16 psia (11.04 n/cm^2) oxygen. The cell is

exposed to this environment for approximately 200 hours. After the conclusion of the exposure period, the electrolyte is analyzed to determine the amount of carbonation present. By minimizing the amount of electrolyte in the cell - only the matrix and electrodes are filled with electrolyte - the non-operating cell is a sensitive indicator of carbonation produced by the cell components and structural materials.

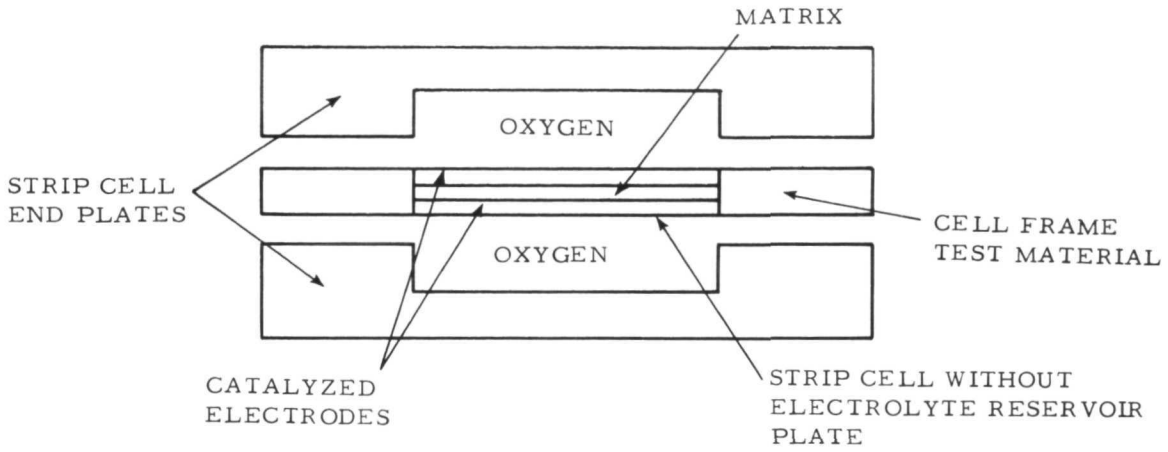

- 1.37 inches x 12.0 inches (3.48 cm x 30.5 cm) active area
- No electrolyte reservoir
- Oxygen on both electrodes - 180°F (82.2°C), 16 PSIA (11.0 n/cm^2)

Figure 66 - Carbonation Test Rig

Non-Operating Cell Test Results

Results from the non-operating cell compatibility tests are shown in Figure 67. Three categories of cell designs were evaluated; 1) epoxy based cell frames, 2) laminated film cell frames, and 3) cell components and background level tests. The test data in Figure 67 is expressed in terms of the amount of carbonation formed per hour per unit of cell perimeter.

1) Epoxy Based Cell - The cell frame design which in operating cell tests produced the high carbonation values shown previously in Figure 65 was the first cell tested in the period. The effect of modifying the cure cycles to higher temperatures and longer durations were evaluated in Cell Nos. 2 and 4. It was seen that the high cure temperature Hypon used in Cell No. 4 reduces carbonation to 30% of Cell No. 1. The use of Epon to impregnate the matrix and bond

it to the Arylon frame reduced carbonation levels further (Cell No. 6). The Hypon impregnated matrix cell design used in all later single cells and plaques was tested in Cell No. 10 of this series. It is seen to have a carbonation characteristic slightly better than the Hypon-Arylon frame design. Because of the very low carbonation levels associated with cells of the FEP and polypropylene films design (see below), a test was made to determine if applying an FEP film to the frames which were normally exposed to oxygen would protect the epoxy from oxidation. Cell No. 12 was of this construction; the results indicate only a marginal improvement.

2) Laminating Films - The superior compatibility of unitization designs based on the use of laminating films is shown by the data from Cell Nos. 3, 5, and 8. Cell No. 3 was tested prior to the start of the film unitization research. Its components were laid in place and held together by compression to maintain the proper geometry. When preliminary bonding procedures had been developed, Cell No. 5 was unitized using the same materials. The test results essentially duplicated that of Cell No. 3. After 200 hours of testing to obtain the carbonation value for Cell No. 5, this cell was refurbished and put back on test for 800 additional hours as Cell No. 7. The rate of carbonation formation was significantly lower for the refurbished cell. The relative compatibility of polypropylene films was measured by Cell No. 8. Its carbonation level was slightly higher than those of the FEP construction; none-the-less it still places it in the same class of very compatible designs.

3) Component and Background Carbonation Levels - This series of tests was run to investigate any non-frame sources of carbonation. In these tests, metal screens were used to compress the matrix between its two electrodes; no frames were used. Cell No. 9 was the first of this test type. It showed that the cell components could be responsible for a large fraction of the carbonate levels found in the cells of the laminating film design. The possibility existed that the procedures used to fill the cell with electrolyte plus handling before and after testing could be responsible for carbonation. This was investigated by Cell No. 11 of a configuration similar to that of Cell No. 9. Its testing consisted of only the normal electrolyte fill procedure, mounting in the test stand followed by removal from test without exposure into oxygen or temperature. The post-test examination showed only a small amount of carbonate was formed by these procedures-clearly not sufficient to explain the levels found in Cell No. 9.

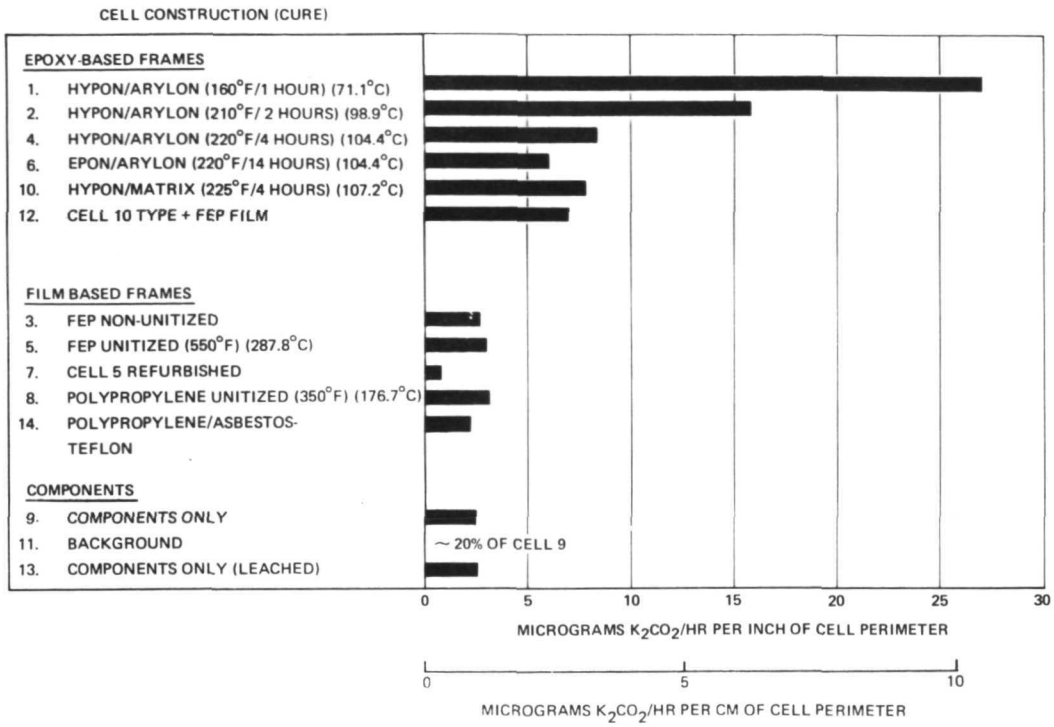

Figure 67 - Results from Non-operating Cell Compatibility Tests

Conclusions drawn from the results of non-operating cell test performed to date are:

- The laminating film unitization materials - FEP Teflon and polypropylene - show excellent compatibility. This type of unitization has the potential for making possible 10,000 hour life cells which have minimum electrolyte inventory and the high frame perimeter to cell area ratio associated with strip cells.

- The epoxies represent an intermediate class of low carbonate forming materials. Further reductions in carbonation rate should be possible with alternate epoxies and anti-oxidant formulations.

- The basic cell components contribute a small but measurable amount of carbonates to the cell assembly. Pre-treatment of these components should eliminate carbonates from this source.

- Electrolyte filling and cell handling procedures do not contribute appreciable amounts of carbonation.

Operating Cell Improvements

The results of post-test carbonation analysis of operating cells is shown in Figure 68. The percentage of the electrolyte contained in these cells which was converted to potassium carbonate is plotted as a function of test duration. The curves indicate the reduction in electrolyte carbonation is due to improved materials and the effect of refurbishment techniques. Cell Nos. 2, 3, 5 and 7 were constructed of the Hypon-Arylon materials using the 160° F (71.1° C), one hour Hypon cure cycle. The shape of the curve indicates the carbonate formation rate is rapid at the start of operation and decreases with time. The decrease in carbonation formation rate with time is also indicated by the data from refurbished cells. Refurbishment is a process whereby a cell is flushed with water to remove all electrolyte and carbonates and then refilled with fresh electrolyte. Cell No. 5 was refurbished after 190 hours of operation and redesignated as Cell No. 9 because a different water transport plate was installed. After 890 hours of operation, the carbonation level was as shown - a significantly lower rate of carbonate formation than that during initial operation. The cell was refurbished again and operated for an additional 660 hours as Cell No. 9-A. Again the carbonation rate was lower.

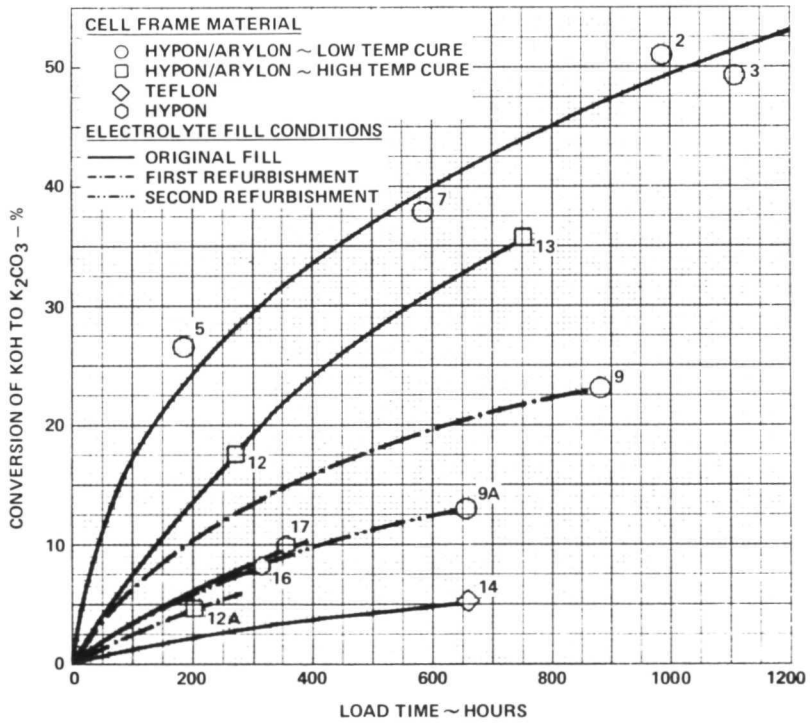

Figure 68 - Results of Post-Test Carbonation Analysis

Cells of the Hypon-Arylon construction which used the 220°F (104.4°C), four hour Hypon cure are shown as squares in Figure 68. The data from the initial running of cell Nos. 12 and 13 indicate a lower carbonate production rate than the cells made with lower temperature cure cycle. Improvement is not as much as would be predicted from the non-operating cell test. The gas chromatograph oxidation test results may provide an explanation for this. These tests showed that the Arylon has a much higher oxidation rate than does Hypon. Even with a significant improvement in the oxidation rate of Hypon, as a result of the higher cure temperature, the high rate from the Arylon could mask the total result. Cell No. 12 was refurbished (Cell No. 12-A) and shows the same type of significant reduction in carbonation rate discussed above.

Cell Nos. 16 and 17 were refurbished after their two-week duration verification tests to obtain carbonation data. These cells provided the first carbonation data on the Hypon impregnated matrix type of cell frame construction. The values shown in Figure 68 indicate the superior compatibility of this frame compared to the Hypon/Arylon design.

One operating cell of the FEP laminating film construction was tested during the program (Cell No. 14). Its very low carbonation value confirms the non-operating cell test results that these construction materials represent a superior class of materials for long life, lightweight cells. The carbonation data for Cell No. 14 was corrected to remove the amount of carbonation due to non-frame sources. These were: 1) the amount due to the cell components as determined by the non-operating cell test results, and 2) that due to oxidation of methane contained in the oxygen supplied to cell. These two sources were found to be sufficient to account for all of the conversion of electrolyte to carbonate. This tends to confirm the judgement that FEP Teflon, at the EMS operating conditions, is essentially inert.

6.0 Single Cell Test Results

6.1 Introduction - The overall goals of the single cell test program were to:

- Develop a single cell test vehicle to evaluate different lightweight, long life cell configurations;
- Perform short term performance tests, with suitable diagnostics, to determine the following performance characteristics:
  - Voltage vs. current density (performance calibration)

- Response to different operating conditions (off-design tolerance)
- Electrolyte retention
- Define endurance limiting phenomenon and develop methods for extending cell life.

This section describes the significant test results from the single cell program. In summary, over 14,600 hours of fuel cell load time were accumulated on 18 different cells. Predicted performance, off-design tolerance and electrolyte retention were demonstrated. Various cell performance deficiencies were identified by cell diagnostics and corrected. Cell endurance capability was improved markedly as a result of the unitization research program. At the conclusion of the Phase 1 portion of the program, cell tests were in progress at operating current densities of 100 (107.6) and 200 amp/ft^2 (215.2 ma/cm^2) for periods up to 2000 hours with acceptable stability.

The following sections discuss these performance and endurance results. The test facilities and procedures are first described. Next, an overview of the several cell configurations and a summary of each cell tested is presented. Then typical cell results, both good and bad, are described in sufficient depth to document the above observations. Finally, conclusions and recommendations for the Phase 2 program are presented.

6.2 Test Facilities and Test Procedures - The test facilities used for full size, single cell testing are shown in Figures 69 and 70. These stands were originally used for work performed under contract NAS3-13229 and were adapted for passive water removal cell testing during this contract. A schematic of the test stands is shown in Figure 71.

Fuel cell grade reactants are supplied to the test stands. To eliminate test variables associated with reactant impurities, the hydrogen is further purified in a palladium-silver separator bank which reduces any contamination below detectable limits. During this program, a Mine Safety Appliance catalytic oxidizer was added to the oxygen supply system. This system is shown in Figure 72. Any hydrocarbons in the oxygen stream are oxidized to carbon dioxide and are removed by the sodium-hydroxide scrubber columns. The carbon dioxide level downstream of the scrubber is continuously monitored by a LIRA gas analyzer. These readings indicate that the oxidizer is removing 8 to 12 ppm (equivalent) methane from the oxygen stream and that the carbon dioxide level entering the fuel cells is less than 0.5 ppm.

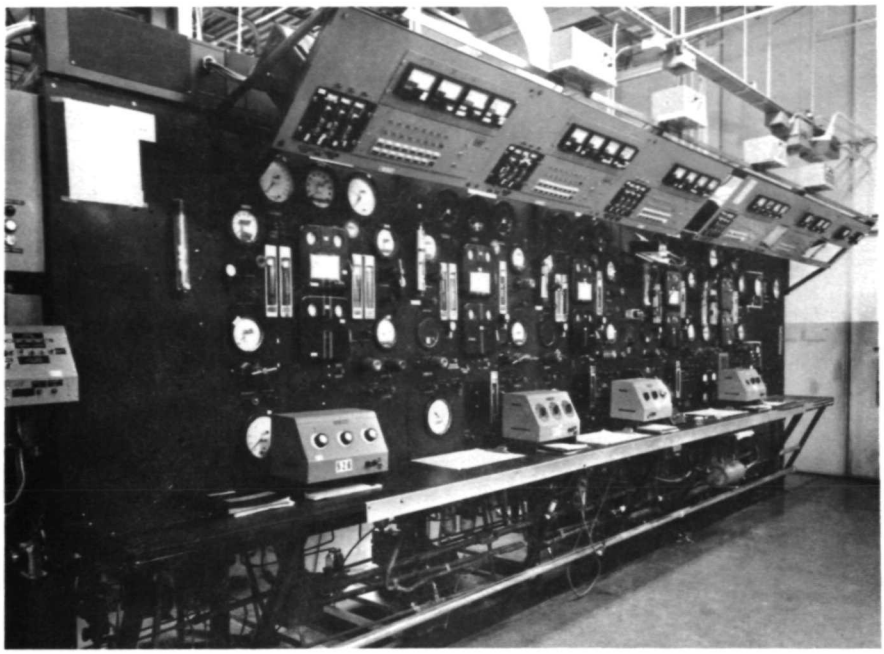

Figure 69 - Single Cell Test Facility (Front)

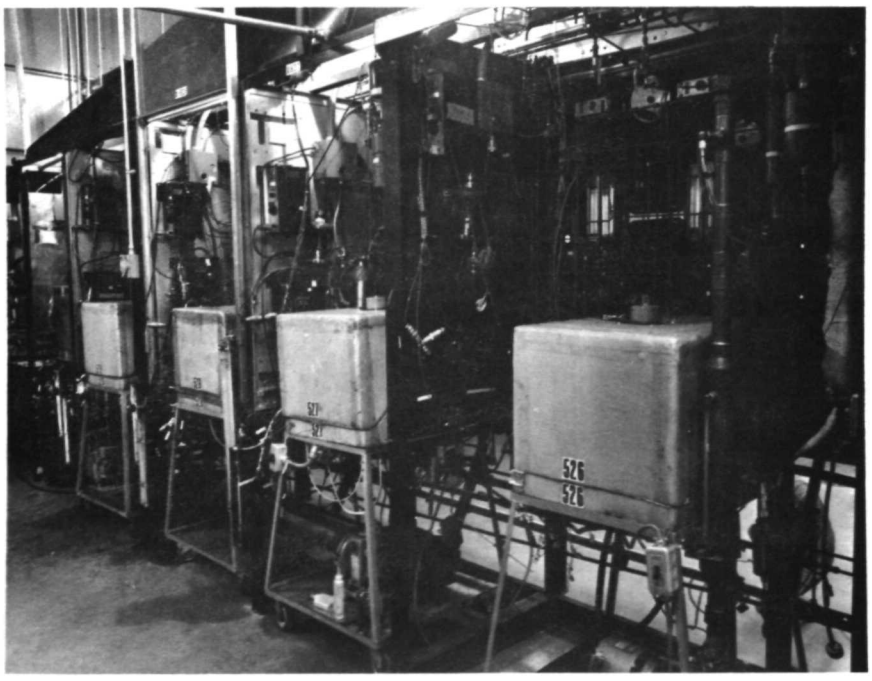

Figure 70 - Single Cell Test Facility (Rear)

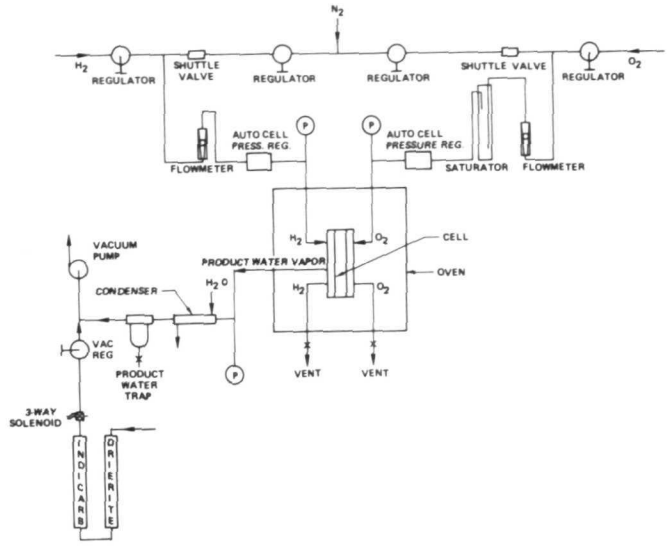

Figure 71 - Single Cell Test Stand Schematic

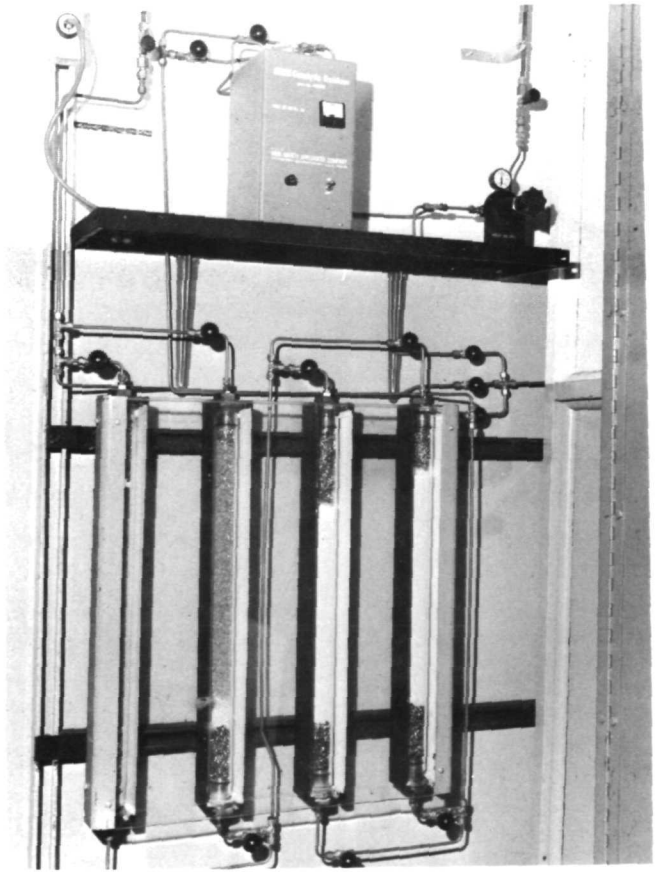

Figure 72 - Catalytic Oxidizer and Scrubber System

Temperature control of the cells is provided by an insulated oven which is maintained within 2°F (1.1°C) by a Thermoelectric solid-state temperature controller. The relatively massive single cell end plates, in combination with the isothermal oven, maintain a uniform cell temperature. Since metallic inserts are used to form the cell's oxygen flow field, and plastic inserts for the product water field as shown in Section IV, 3.0, cell waste heat is rejected primarily on the cathode side. Thus, the test rig approach realistically simulates system conditions. Cell temperature instrumentation showed that the simple oven temperature control method is effective in maintaining cell temperatures uniform within ± 1.5°F (.83°C) over a range of current densities to 300 ASF (322.8 ma/cm^2).

The product water removal system also duplicates the system design. A conventional Duo Seal® vacuum pump is used to provide the sub-atmospheric pressure sink for product water vapor. Initial problems with vacuum pressure control and contamination of the system on shutdown were solved by the regulator bleed and scrubber system shown in Figure 71. Because one of the major cell design considerations was the prevention of electrolyte loss from the passive water removal assembly by the use of an electrolyte barrier (described in Section IV, 2.0), the pH of the product water is regularily monitored. Trap water samples are checked 3 times a day, using a Beckman Zeromatic® pH Meter.

Single cell performance data is measured on P&WA's Automatic Data Aquisition and Recording (ADAR) System. The following parameters are recorded once every hour:

Parameter	Accuracy
Cell Voltage, volts	± 0.05
Cell current, amps	± 0.05
Oven Temperature	± 0.5°F (± 0.3°C)
Oxygen End Plate Temperature	± 0.5°F (± 0.3°C)
Water End Plate Temperature	± 0.5°F (± 0.3°C)

The ADAR system was designed to minimize experimental error and to reduce the amount of manual data handling. In addition to providing periodic scanning of the above parameters and transcribing them to engineering units, the ADAR system keeps an accurate log of total load hours. A sample ADAR print out for the NASA-LeRC Advanced Development Fuel Cells is shown in Figure 73. .

```
S/C STANDS X-527 THRU X-533:

   RIG 37970-16 ST X-527  DATE  6/24/72 TIME 18 0 R HRS  1135
AMPS 11.5  VOLTS  .850  02 SAT.=130.  OVEN=172.
02 PLATE: 1=177  2=177  3=177  4=177   H2 PLATE: 1=175  2=176  3=177

   RIG 37970-15 ST X-528  DATE  6/24/72 TIME 18 0 R HRS  1913
AMPS 11.6  VOLTS  .867  02 SAT.=130.  OVEN=171.
02 PLATE: 1=177  2=179  3=179  4=178   H2 PLATE: 1=176  2=177  3=175

   RIG 37970-17 ST X-529  DATE  6/24/72 TIME 18 0 R HRS  1087
AMPS 23.2  VOLTS  .883  02 SAT.=129.  OVEN=170.
02 PLATE: 1=176  2=174  3=176  4=175   H2 PLATE: 1=175  2=171  3=176

   RIG 37970-20 ST X-533  DATE  6/24/72 TIME 18 0 R HRS   240
AMPS 11.9  VOLTS  .884  02 SAT.=128.  OVEN=174.
02 PLATE: 1=180  2=181  3=180  4=179   H2 PLATE: 1=176  2=179  3=  .
```

Figure 73 - ADAR Printout

The heart of the ADAR system is a Hewlett-Packard Model 2114A digital computer. Other major components in the system are also from Hewlett-Packard; a Model 2911 Guarded Crossbar Scanner and Model 2402 Digital Voltmeter to scan and measure the test signals, and a Model 2752 Teleprinter to printout the data.

All of the above data can also be read out directly at each station on conventional stand instrumentation. Pressure and flows are controlled and monitored by appropriate regulator, gages, flowmeters and valves as shown in Figure 69.

The ADAR system has been used only for automatic data acquisition. Automatic control is provided by appropriate test stand instrumentation, with provisions for automatic shutdown of any cell when certain pre-established conditions are encountered. For the NASA-LeRC single cells, these protective controls are:

Parameter	Limit
Voltage	Low adjustable
Current	High or Low Adjustable
Temperature	High or Low Adjustable
Vacuum Pressure	High or Low

These automated control and protective features have resulted in very reliable single cell operation. Over 14,600 hours of fuel cell load were attained on 18 different fuel cells with only one stand related failure.

This was on Cell No. 10, which was flooded because of an oxygen saturator overtemperature. Some automatic shutdowns occurred because cell conditions exceeded the protective limits described above. In all of these cases, the cells were not damaged and normal testing could continue.

Single cell testing was primarily devoted to endurance testing. However, various diagnostic procedures were performed on all of the cells to document any decay mechanisms and to determine design and off-design performance characteristics of the various cell configurations.

Typical test conditions for the programs were:

Cell Current Density	100 or 200 ASF(107.6 or 215.2 ma/cm^2)
Cell Temperature	180° F(82.2° C)
Product Water Vacuum	22 in. Hg(7.33 n/cm^2)
Hydrogen Pressure	1.3 psig(11.04 n/cm^2)
Hydrogen Flow	Consumption, plus 2 minute purge every 8 hours.
Hydrogen Inlet Dewpoint	Dry
Oxygen Pressure	1.3 psig(11.04 n/cm^2)
Oxygen Flow	2 x consumption
Oxygen Inlet Dewpoint	130° F(54.4° C)
Average Electrolyte Concentration	34 percent

Diagnostic techniques which were regularly employed included the following:

Performance Calibrations: Voltage-current characteristics were generated to 500 ASF (538 ma/cm^2), which is somewhat above the EMS peak power operating conditions. Taken periodically, the performance calibration changes with time are valuable tools in determining the type and extent of any decay mechanisms. This is especially true of the semi-log representation of the performance data on an IR free basis which are commonly described as Tafel plots.

Tafel Plots: The Tafel region refers to the low current density portion of a performance calibration. In this region, anode and ohmic polarizations are minimal or correctable so the cell voltage is essentially cathode activation limited performance. The Tafel region extends from approximately 1 ASF (1ma/cm^2) to a level where diffusion losses become significant (10 to 100 ASF (10 to 100 ma/cm^2)), which is a function of operating temperature and pressure. In this region, the semi-log voltage-current curve should be a straight line, with a slope characteristic of the catalyst/reactant combination and a level proportional to the activation capability of the cathode.

Departures from this slope are an indication of parasitic loads, either internal cell shorting or gas crossover. Thus, the Tafel slope is a useful diagnostic tool in assessing the life expectancy of a operating cell. Changes in the levels of Tafel data are also a useful tool, since they indicate changes in the activity of the catalyst, either through changes in the number of active catalytic sites or structural modifications (e.g., recrystallization), changing the effective catalyst active area.

The so-called Tafel plot is also a useful diagnostic tool at current densities above the Tafel region. At these current densities, typical of operating cells, internal resistance (IR) corrections are required. When the cell performance is thus corrected, changes in the shape of the curves can be interpreted as changes in the diffusion characteristics of the electrodes. In this region, transport limitations are encountered if the electrode structure is not adequate for delivery of reactants or removal of product water. For example, diffusion problems can be related to microscopic flooding of the Teflon pores in a wet proofed electrode, or to increased concentration gradients in a heavily carbonated cell. While the semi-log performance plots alone do not distinguish such possible causes or even anode from cathode losses, they are valuable tools, in conjunction with previous experience and post-test analysis, in evaluating any performance decay trends.

Internal Resistance (IR): Internal resistance, or ohmic polarization, losses are unavoidable in any cell. However, they can be minimized by matrices with high porosity and correct assembly to insure proper cell compression. In the strip cell (edge current collection), there are also resistance losses in the electrode substrates and edge frames which are measured together with the conventional ohmic loss. IR measurements are taken periodically to insure that the initial assembly is correct and that the correct cell compression is being maintained.

IR measurements are taken by the current interruption technique. Typically, a 100 ASF (107.6 ma/cm^2) load is interrupted and the resulting step change in voltage is measured on a Tektronic Type 545 oscilloscope. Since other polarizations have a long response time, the step change is a direct measure of internal cell resistance.

Off-Design Tolerance: The function of the Electrolyte Reservoir Plate (ERP) is to provide sufficient electrolyte to the working cell components (anode, matrix, cathode) to maintain performance during electrolyte volume changes caused by concentration differences imposed by changing operating conditions. The ERP is sized for the maximum expected ranges of off-design conditions. Within this range, the ERP empties or fills

with electrolyte, but the cell always remains properly filled. Performance is thus unaffected, except for a small concentration effect (1 to 2 mV/ percent KOH). If the cell is improperly filled, or if the contact between the ERP and cell is inadequate, the off-design tolerance characteristics of the cell will depart from this theoretical value. Off-design tolerance data can be generated in various ways. In the passive water removal cells, the most convenient and most severe method is to vary product water vacuum. Since the vacuum is changed almost instantaneously, the cell is subjected to a very rapid transient, taxing the transport properties of the ERP much more severely than off-design tolerance conditions imposed by slowly changing dew points on saturated gases.

Post-test Analysis: All cells are subjected to post-test analysis. This includes visual (and microscopic) examination of components for observable changes in physical properties, structural defects or peculiar deposits. Because of the importance of low corrosion rates, all of the single cells in this program were carefully analyzed for carbonate conversion. Selected cells were also sectioned for laboratory tests, including floating half-cell tests of individual electrodes and measurement of catalyst activity and platinum migration.

6.3 Summary of Single Cells Tested - Two types of testing were performed in the Single Cell Program. Research and Technology (R&T) tests were one type, comprising the first level of testing. This test is performed on any items which are beyond the present state-of-the-art. This is a relatively informal level of testing in order to maximize the flow of technical information. Reviews of the progress of this testing are held regularly with the NASA Project Manager. When any item, in his judgment, is sufficiently demonstrated, the next level of testing is begun.

Verification and Endurance (V&E) tests were the second type, comprising the second and third levels of testing. The Verification test is a short duration test, consisting of two weekly test cycles, interrupted by a shutdown. The objective of a Verification test is to demonstrate the ability of the article under test to perform at the conditions in question. The Endurance test is of longer duration; the weekly duty cycle is used for some tests, continuous operation for others. Both Verification and Endurance tests are of more formal nature. They require written notification to the NASA Project Manager with pertinent description of the test article. Three designs were submitted for NASA approval and were tested in Phase 1 of the program. In carrying out this type of test, the NASA Project Manager reviews the results of the Verification Test and decides which items shall undergo Endurance testing.

The load profile used for V&E testing was designed to be a working approximation of the proposed duty cycle with times chosen to maximize diagnostic data with minimal operator coverage. Major features are steady-state operation at the nominal system design point (100 to 200 ASF) (107.6 or 215.2 ma/cm^2), weekly calibrations to the peak power point 460 ASF (495 ma/cm^2), periodic IR and off-design tolerance excursions as needed, and a weekly shutdown on inert gases simulating a holding period of indefinite duration.

A statistical summary of the single cell testing during Phase I of the program is given in Table 11.

TABLE 11

Full Size Single Cell Operation

Number of cells tested	18
Number of configurations tested	4
Total cell test time	14,600 hours
Longest cell run (100 ASF)	2,060 hours*
Longest cell run (200 ASF)	1,228 hours*
Reasons for shutdown:	
Stand Failure	1
Cell Failure	1
Investigation of Decay	12
Continuing on Test	4

*Continuing on 7/1/72

A summary breakdown of the cells into design configuration and types of tests is presented in Table 12.

TABLE 12

Full Size Single Cell Test Categories

Description of Unitization	Design No.	Research and Technology Test Cells	Verification and Endurance Test Cells
Arylon-Hypon	1	1 to 11	12, 13
FEP Teflon	2	14	--
Impregnated Matrix	3	15	16-19*
Integrated version of Design No. 3	--	20	--

*Cells 18 and 19 are NASA delivery cells

Details for each cell are given in Table 13. These include the small differences in construction of the unitized electrode assemblies, passive water removal assemblies and flow fields; and initial, peak and final voltages, initial IR, load level, operating times and comments.

6.4 Typical Cell Test Results - This section reviews the typical results of the several cell tests. The results discussed are from tests where performance was not as predicted and from those where the cell performed satisfactorily. The emphasis in this section is on the significance of each type of result and the methodology used to correct deficiences uncovered by the testing. Historical development of each cell is not discussed; Table 13 gives the significant details for all of the cells tested. The section which follows presents a complete report of Cell No. 17 operation which represents the level of single cell development status at the close of Phase 1. Also discussed are performance levels, IR, off-design tolerance, electrolyte retention, and performance stability of the other cells tested during Phase 1. Performance levels ranged from satisfactory to excellent. The following table gives an overview of the 18 single cells tested:

TABLE 13
Cell Test History

Cell #	UEA Description	PWR Description	O_2 Field	H_2 Field	Load Time (Hrs)	Performance Volts at 100 ASF Initial	Peak	Final	IR at 100 ASF	Comments
1	Arylon/Hypon 30 Mil ERP Std PPF Electrodes Hypon cured at 160°F	Arylon/Hypon 20 Mil Sinter Zitex Membrane	Field Machined in End Plate 0.030"	Polypropylene Screen 0.020"	1147	.882	.882	.842	13	
2	Same as 1	Same as 1	Same as 1	Same as 1	987	.890	.890	.822	13	
3	Same as 1	Same as 1	Machined Arylon Insert 0.030"	Same as 1	1106	.860	.860	.803	20	IR from load carrying screen
4	Arylon/Hypon Arylon Picture Frame Bonded w/Hypon Matrix 22 Mil ERP Cured at 160°F	Arylon/Hypon 11 Mil Sinter Zitex Membrane	Machined Arylon Insert 0.030"	Polypropylene Screen 0.025"	70	.845	.845	.841	32	TC Assembly Misalignment
5	Same as 4	Same as 4	Ni ExMet .024"	Same as 4.	188	.882	.882	.860	15	
6	Same as 4	Same as 4	Same as 5	Same as 4	1290	.865	.865	<.800	28	IR from load carrying screens UEA from cell #4
7	Same as 4	Same as 4	Same as 5	Polypropylene Screen 0.028"	586	.880	.880	.862	13	
8	Same as 4 Au plated screen electrodes PPF	Same as 4	Same as 5	Polypropylene Screen 0.028"	88	.909	.909	.885	10	
9	Same as 4	Same as 4	Same as 5	Polypropylene Screen 0.024"	1539	.875	.882	.862	18	IR measured on load carrying screens. UEA from Cell #5. Refurbished twice
10	Same as 8	Same as 4	Same as 5	Polypropylene Screen 0.028"	83	.910	.910	.898	10	
11	Arylon/Hypon Arylon Picture Frame Bonded w/Hypon Matrix Cured at 220°F Au Screen Electrodes 22 Mil Sinter	Same as 4	Same as 5	Polypropylene Screen 0.024"	404	.904	.904	.875	10	

TABLE 13 (CONT'D)

Cell #	UEA Description	PWR Description	O_2 Field	H_2 Field	Load Time (Hrs.)	Performance Volts at 100 ASF Initial	Peak	Final	IR at 100 ASF	Comments
12	Same as 11	Same as 4 but Goretex membrane	Same as 5	Polypropylene Screen 0.028"	665	.885	.885	.870	12	Cell refurbished at 305 hours
13	Same as 11	Same as 12	Same as 5	Polypropylene Screen 0.028"	750	.887	.887	.840	12	No refurbishment
14	FEP Teflon Laminated Frame PPF electrodes 22 Mil Sinter	FEP Teflon Laminated Frame 11 mil sinter Goretex Membrane	Same as 5	Polypropylene Screen 0.028"	660	.864	.868	.853	16	IR from load carrying screens.
15	Hypon Matrix Unit Construction PPF Electrodes 22 Mil Sinter	Hypon Matrix 11 Mil Sinter Goretex Membrane	Field Machined in End Plate 0.030"	Polypropylene Screen 0.024"		.890	.892		13	Refilled at 60 hours. Refurbished at 3010 hours
16	Same as 15	Same as 15	Machined insert 0.015"	Polypropylene Screen 0.024"		.895	.895		9	Refurbished at 310 hours.
17	Same as 15	Same as 15	Machined insert 0.015	Polypropylene Screen 0.024"		.875	.892		6	Performance quoted at 200 ASF Refurbished at 352 hours.
18	Same as 15	Same as 15	Machined insert 0.015"	Polypropylene Screen 0.023"						Delivered to NASA
19	Same as 15	Same as 15	Machined insert 0.015"	Polypropylene Screen 0.023"						To be delivered to NASA
20	Hypon Matrix Integral UEA/PWR		Machined insert 0.015"	Polypropylene Screen 0.022"		.880	.890		11	Cell shorted in assembly - Internal TC

	Number of Cells	Performance - mV at 100 ASF (107.6 ma/cm^2)
EMS Performance Model	--	890
Typical Cells	10	880-900
Best Cells	4	$>$900
Worst Cells	4	$<$ 880

In general, maximizing performance level was not the major emphasis during Phase I. In the early stages of single cell testing, the major emphasis was on fabrication development. As explained in Section IV, 4.0, a number of problems were encountered in the areas of bubble pressures and edge current collection. Dimensional control was less than desirable for the first cells that overcome these difficulties. Such substandard cells were accepted for test purposes in order to evaluate construction variables. This accounts for the relatively poor performance of Cell Nos. 3, 4 and 6. A similar argument applies to Cell No. 14, the only cell tested with the FEP laminated frame method of construction.

Some variation in the electrode manufacturing was also encountered in translating the standard electrode formulation into the strip cell size. The strip cell electrodes were made in small lots with interim tooling. Some lots had better performance than average (e.g., Cell Nos. 8, 10, 11). Figure 74 shows this effect of lot variation on electrode performance of Cell Nos. 7 and 8 from an average and superior lot respectively. In this plot, the difference between the cells is clearly shown to be an activation one, with about 20 mV difference in the Tafel region, which extends to the operating current densities. Lot-to-lot performance variations such as this are not representative of electrodes made with tooling and procedures optimized for a given electrode configuration. The increased number of cells required in subsequent phases of the program will allow the development of improved electrode manufacturing techniques for standardized strip cell electrodes.

Initial internal resistance (IR) values are given for the cells in Table 13. The strip cell has IR losses associated with edge current flow, but does not have the contact losses associated with series type cells (current flow perpendicular to the cell area). Typical strip cell IR values measured are around 10 mV per 100 ASF (107.6 ma/cm^2). This compares favorably with conventional (series current flow) cells. The poorest IR values

are found on the Cell Nos. 3, 4 and 6 where dimensional problems were most serious. The best IR values (e.g., Cell No. 17) compare favorably with the very best cells run in the Air Force High Power Density program where special efforts were taken to insure the best possible dimensional control and cell compression. In summary, the IR values of the strip cells were reasonable, and improved as dimensional problems were resolved.

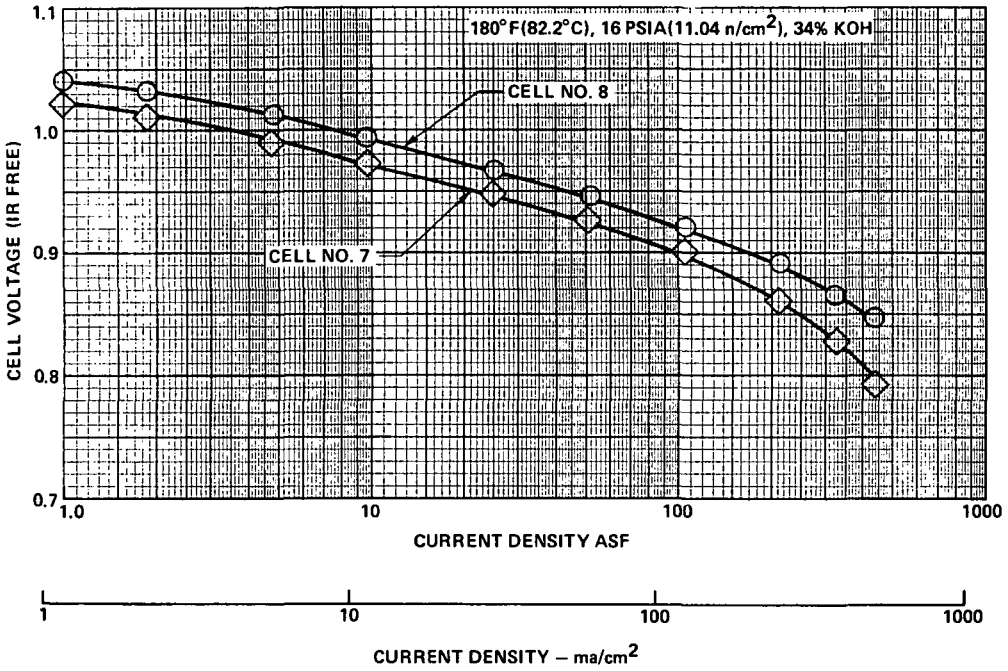

Figure 74 - Electrode Performance

Off-design electrolyte tolerance excursions were performed on the cells between average concentration levels of 30 and 40 percent. As described above, these excursions can be performed rapidly, subjecting the cell to conditions more severe than it would see in steady-state operation. Off-design tolerances have generally been good. Two problems were encountered, identified and remedied. Poor contact between the ERP and the anode is the most likely cause of poor off-design tolerance. When the ERP is not in intimate contact with the anode, electrolyte transfer is impeded. An example of this phenomenon occurred on an early passive water removal research cell. Figure 75 illustrates how a cell with insufficient compression responded to a tolerance excursion from low to high electrolyte concentration. Although the 40 percent electrolyte concentration value gradually rose to a low but possibly tolerable level,

the initial response was very poor. When the cell's undercompression was corrected, the tolerance response was normal, with good performance over the entire range. Insufficient electrolyte is another potential cause of poor off-design tolerance. This occurred on Cell No. 15 where the initial fill was inadequate. After refill, performance and off-design tolerance improvement was satisfactory.

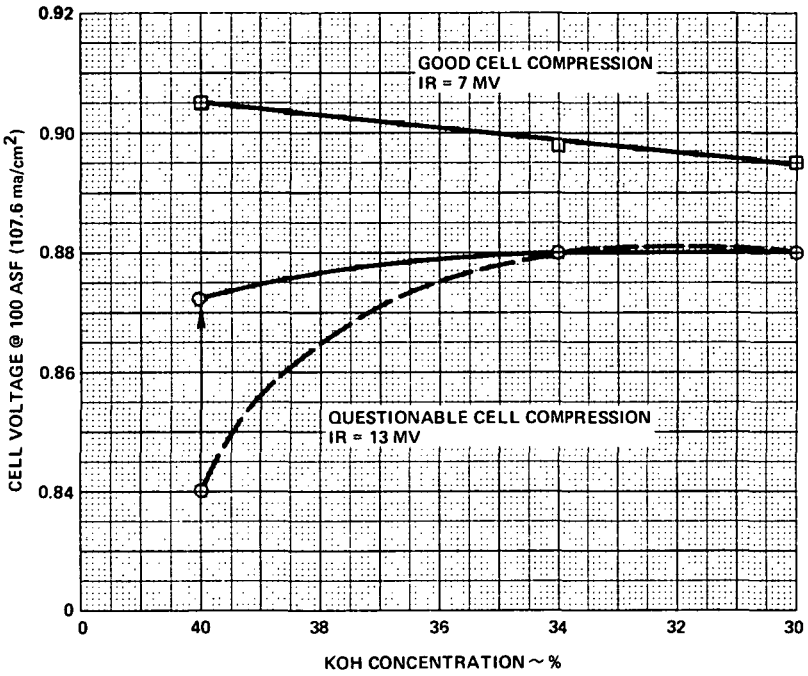

Figure 75 - Tolerance Excursion Data

Retention of electrolyte from the water transport plate as measured by the pH of the product water was generally not as good on the earlier strip cells as on the 4.5 x 4.5 inch research cells used to develop lightweight passive water removal methods. This was due to the puncturing of the thin porous Teflon membranes used for electrolyte barriers by the machined flow passage inserts used for the product water vapor field. This was more prevalent on the early cells with the poorer dimensional control. Use of the tougher Goretex membranes in later cells also helped to alleviate this problem. The performance histories of Cell 15 presented below and Cell 17 presented in section 6.5, which follows, show the generally satisfactory product water pH. The initial and post-refurbishment high pH values are attributable to residual electrolyte left in the product water passages during flush filling. The smaller occasional jumps in pH that occur are not fully explained. Some, but not all, have been related

to excessive off-design tolerance excursions, either planned or accidental. The rest are felt to be due to minute droplets of electrolyte held up in passages of the product water system.

As illustrated in Figure 52 of Section IV, 2.0, a pH of 9.5 would permit operation for much longer than the 10,000-hour program goal with the EMS sized ERP. Although some procedures may have to be modified for plaque PWR construction, there does not seem to be any inherent problems in preventing electrolyte loss in passive water removal strip cells.

The original EMS design system called for operation on dry oxygen. Analyses conducted at NASA-LeRC indicated that potentially large concentration gradients could result from such operation. Teardown of Cell Nos. 1 and 2 indicated evidence of drying at the oxygen inlet. The system was therefore changed to incorporate an oxygen recycle loop. This was simulated on the test stand with an oxygen saturator, providing 130° F (54.4° C) dew point oxygen at 2 times stoichometric flows. All cells after Cell No. 7 incorporated this change.

Performance decay was the most serious deficiency of the early strip cells. This can be seen from a review of the performance changes shown in Table 13. High levels of electrolyte conversion to carbonate were confirmed as the reason for the excessive decay. This led to increased emphasis on Unitization Research using materials of improved compatibility as described in Section IV, 4.0. The major thrust of unitization research was to develop fabrication techniques which would allow the use of high compatibility unitizing frame materials. An all Teflon frame cell was built and tested, since this material performed best in the non-operating cell compatibility tests. This cell showed improved stability, despite dimensional and sealing problems discussed elsewhere. Its performance change during 600 hours of operation was only .010 mv/hr. In parallel with the unitizing research, evolutionary improvements in reducing carbonation were undertaken. One of these was refurbishment. Figure 76 shows the effect of electrolyte refurbishment on Cell No. 9 at some 900 hours load time. The performance loss was essentially recovered although subsequent performance decay was equally rapid on this cell with materials of inferior corrosion resistance.

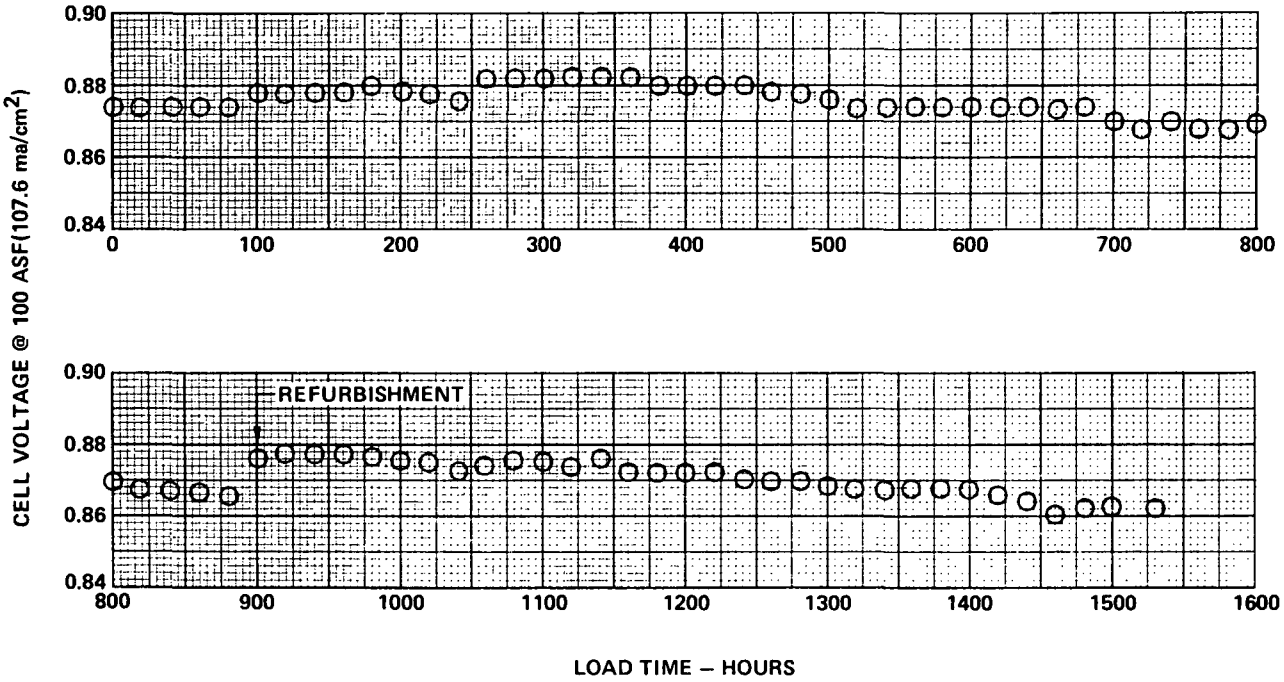

Figure 76 - Effect of Electrolyte Refurbishment on Cell No. 9

The other approach taken was to improve the stability of the epoxy based frame materials, which could be effectively used in cell construction. As described in Section IV, 4.0, the most promising method was the integral epoxy impregnated matrix approach, which was used on all cells after Cell No. 15. The performance stability of these cells has been good. Figure 77 shows the performance history of Cell No. 15, the first cell of this type. As discussed above, the cell was refurbished early because of an off-design tolerance problem. Thereafter, it demonstrated excellent stability. It was operating at the end of Phase I at 2060 hours and will be continued. Cell No. 17, a similar cell running at 200 ASF(215.2 ma/cm^2), is equally stable. Details of this cell are presented in the following section.

In summary, cell performance stability with operating time was the only serious problem encountered. The performance degradation was caused by cell structure produced electrolyte carbonation. Significant improvement in performance stability was achieved by the use of an epoxy based cell structure. Refurbishment is a valid method for restoring cell performance.

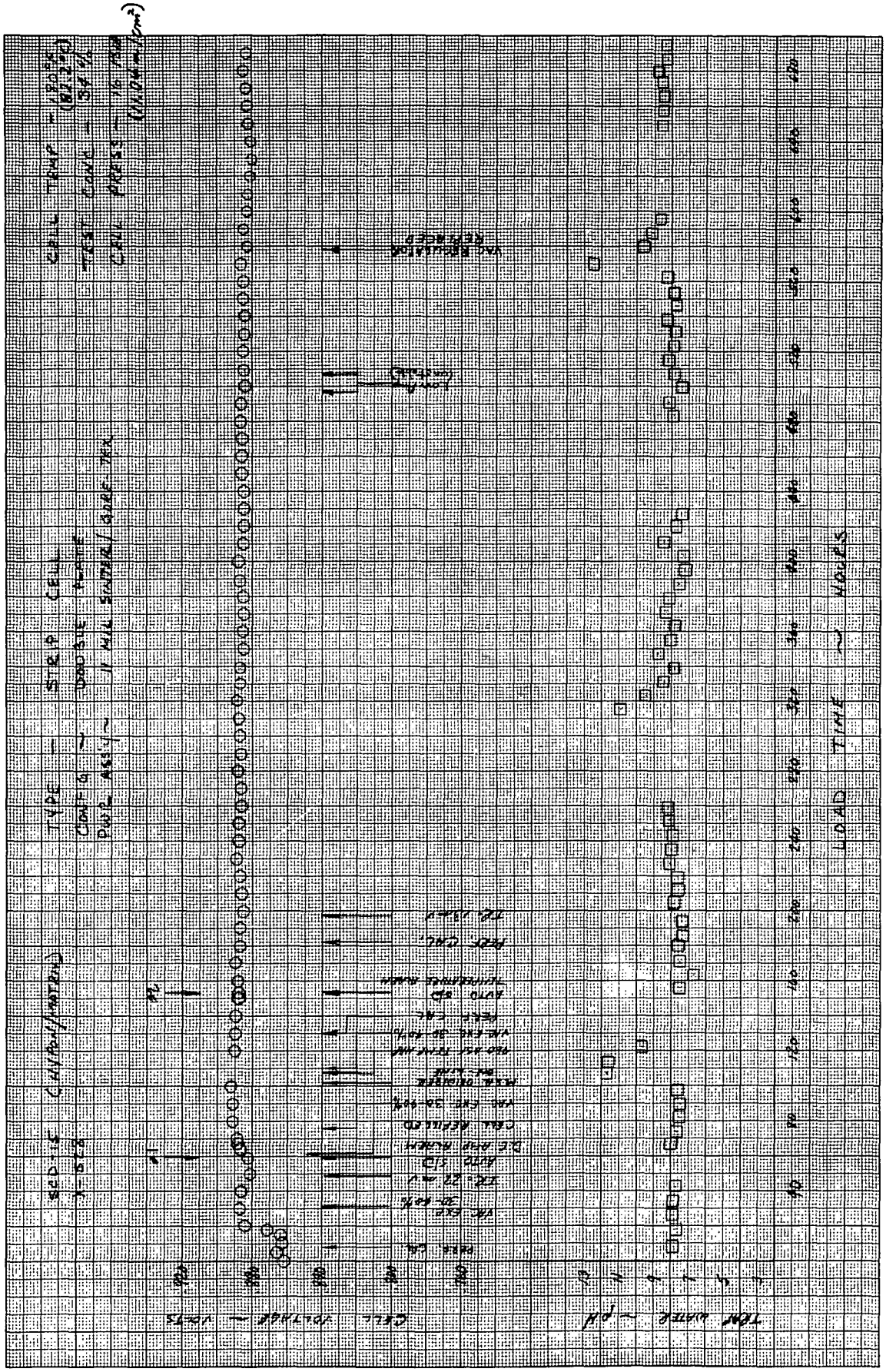

Figure 77- Performance History of Cell No. 15

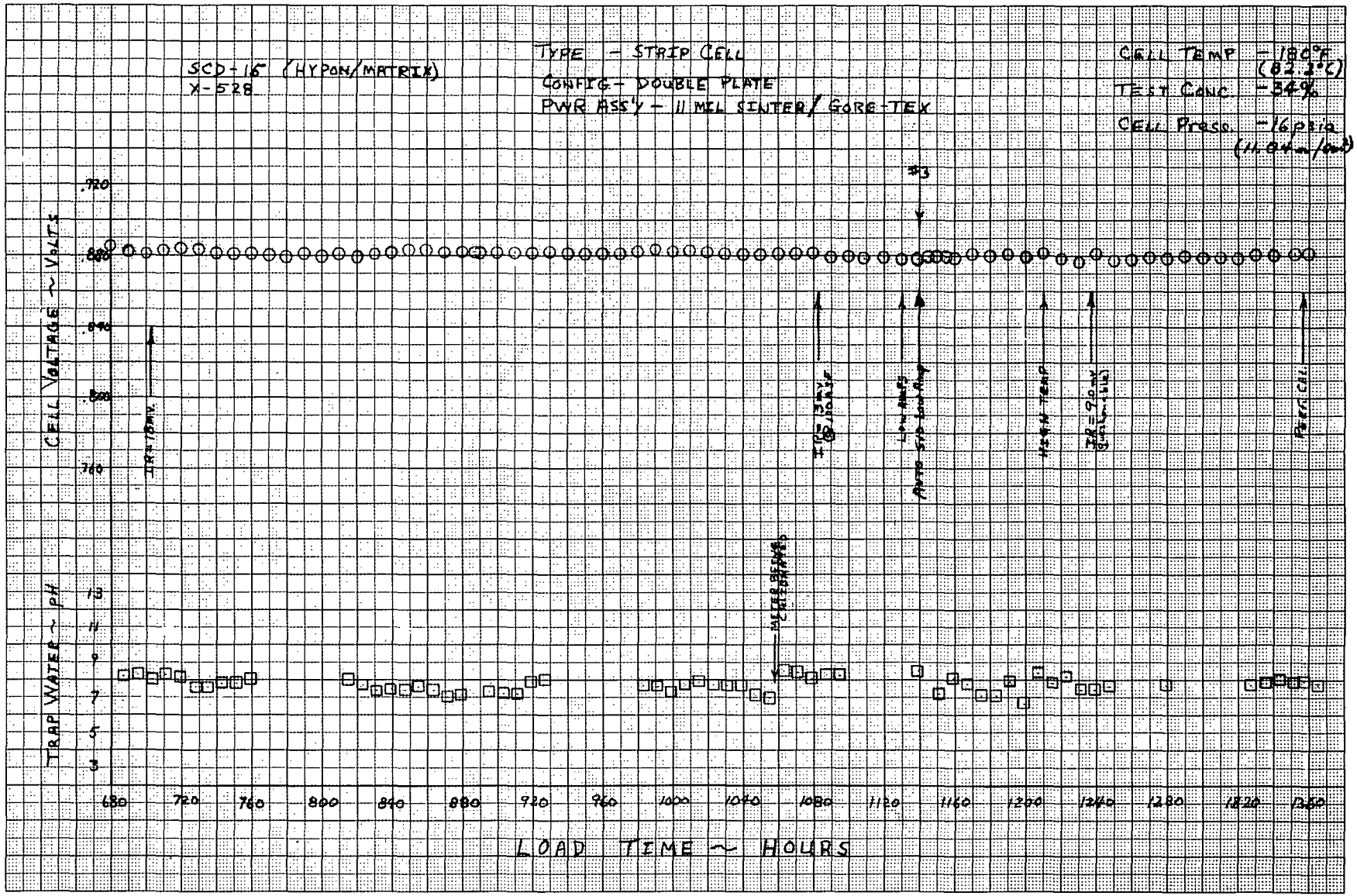

Figure 77 - Performance History of Cell No. 15

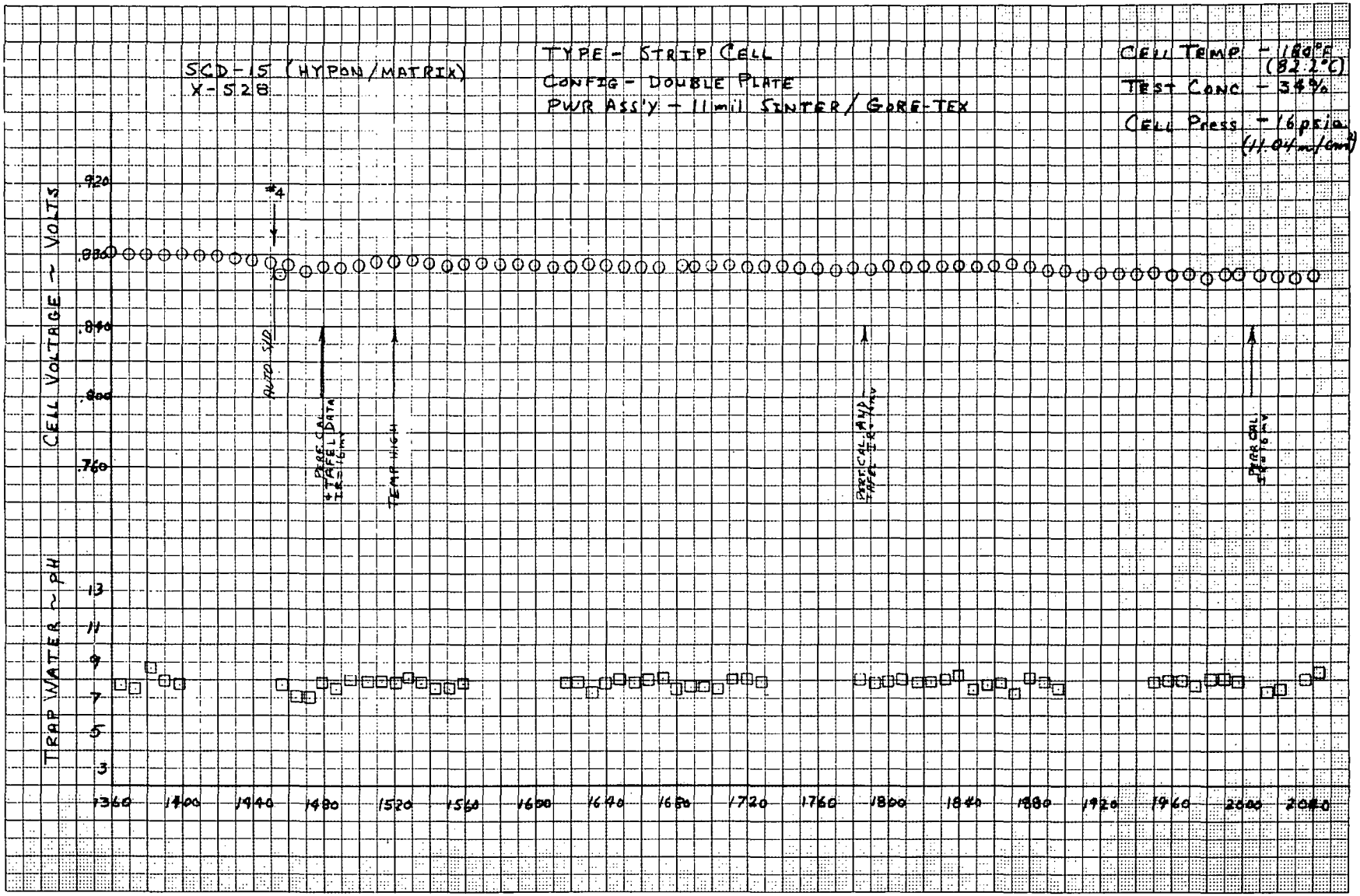

Figure 77 - Performance History of Cell No. 15

6.5 Performance History of Cell No. 17 - Cell No. 17 represents the state-of-the-art of lightweight strip cells at the end of the Phase I. For this reason, it will be described in greater detail. This cell is a verification and endurance test cell of NASA approved design No. 3. A dimensioned cross sectional view of the cell is shown in Figure 78.

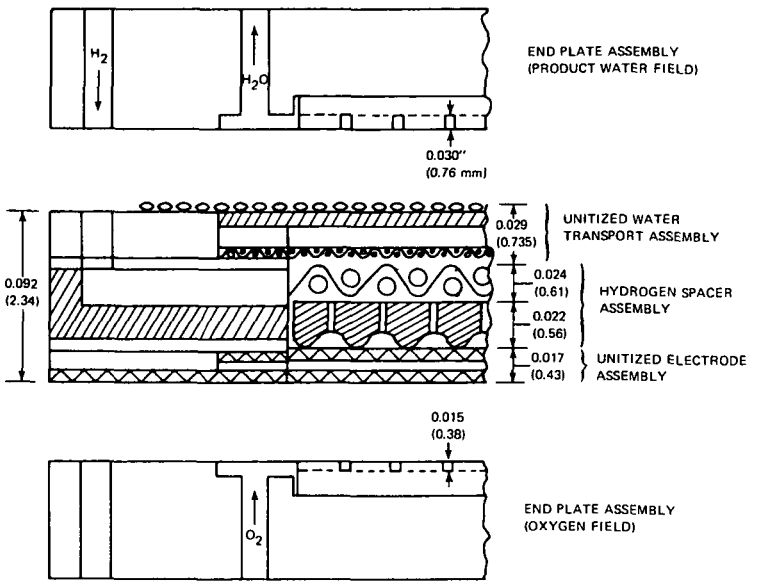

Figure 78 - Single Cell Configuration #3

The performance history is shown in Figure 79. This cell followed the load profile of the two-week Verification Test. At the request of the NASA Program Manager, it was refurbished and placed on endurance test at a steady-state 200 ASF (215.2 ma/cm^2) load. The performance level was superior at startup, but also improved significantly after refurbishment. This increase is typical for unleached electrodes. It appears to be related to refurbishment and is more of a step change than the gradual rise noted in conventional cells with unleached electrodes. Several test stand anomalies are noted on the endurance log. At about 120 hours, performance began to decrease. This dip was traced to an overfilled product water trap, which also caused an increase in product water pH. Small performance variations and to a lesser extent, product water pH variations, were also noted to coincide with unattended weekend periods. They were attributable to small fluctuations in temperature and product water vapor vacuum control and now appear to be under control. These anomalies are minor compared to the excellent stability of this cell especially considering that it is operating at 200 ASF (215.2 ma/cm^2).

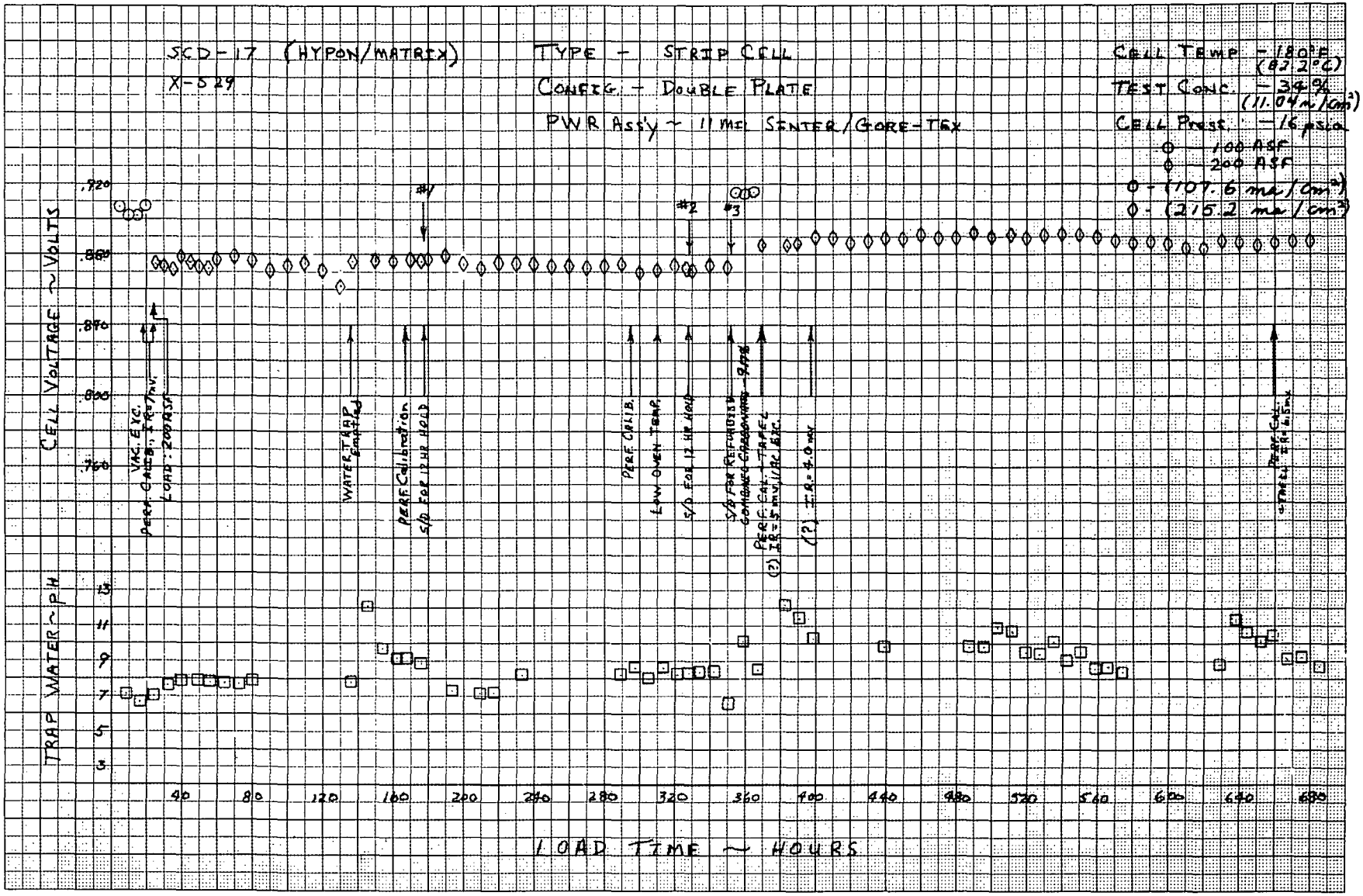

Figure 79 - Performance History of Cell No. 17

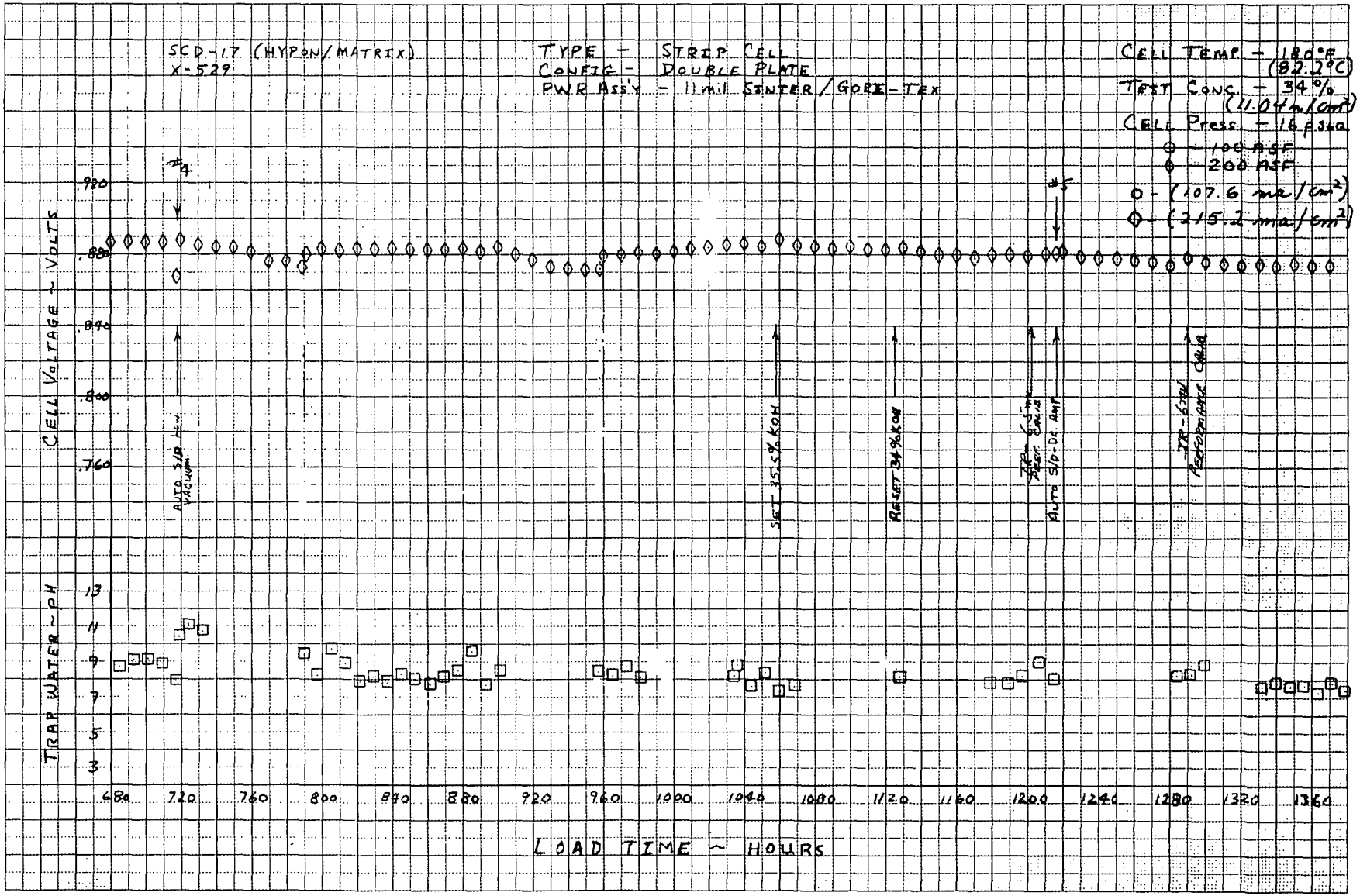

Figure 79 - Performance History of Cell No. 17

Figures 80 and 81 present the performance characteristics of Cell No. 17. In addition to the good stability, Figure 80 illustrates the other major advantage of this cell - namely, its good high current density performance. A flat voltage-current characteristic provides inherent voltage regulation over a wide range of power demands. It also provides margin for both overload power demands and margin for performance decay. These features are best seen in the Tafel type of performance plot shown in Figure 81. This plot shows the improvement after refurbishment to be in the cathode activation region. This region extends well into the normal operating ranges. In addition to this desirable feature, the diffusion losses of the electrodes are also small, and more importantly, are holding constant with time. Cell No. 17, therefore, has successfully demonstrated the performance predicted for lightweight passive water removal fuel cells. Further testing will provide data on the time to refurbishment. At the end of Phase I, Cell No. 17 had reached 1230 hours load time at 200 ASF (215.2 ma/cm^2). Endurance testing with periodic diagnostics will be continued.

6.6 Conclusions and Recommendations - Based on the single cell Research and Technology and the Verification and Endurance testing performed during Phase 1, the following conclusions and recommendations can be stated:

- Predicted cell performance has been demonstrated or exceeded - cell voltage vs. current, performance vs. electrolyte concentration variation and retention of electrolyte in passive water removal fuel cells.

- Further research in improving the compatibility of epoxy-based cell structures and/or development of fabrication techniques to allow the use of superior compatibility materials, such as FEP Teflon, is required for lightweight cells to be capable of 10,000- hour operating duration.

- The single cell and test fixture design and the automated test facilities have proven satisfactory for cell configuration development, performance characterization, and endurance testing.

- Evolutionary test fixture and facility improvements are needed for electrolyte fill weight determination and cell temperature control to allow rapid change of cell load.

- Diagnostic testing techniques used have proved adequate to identify and aid in resolving the causes of substandard performance.

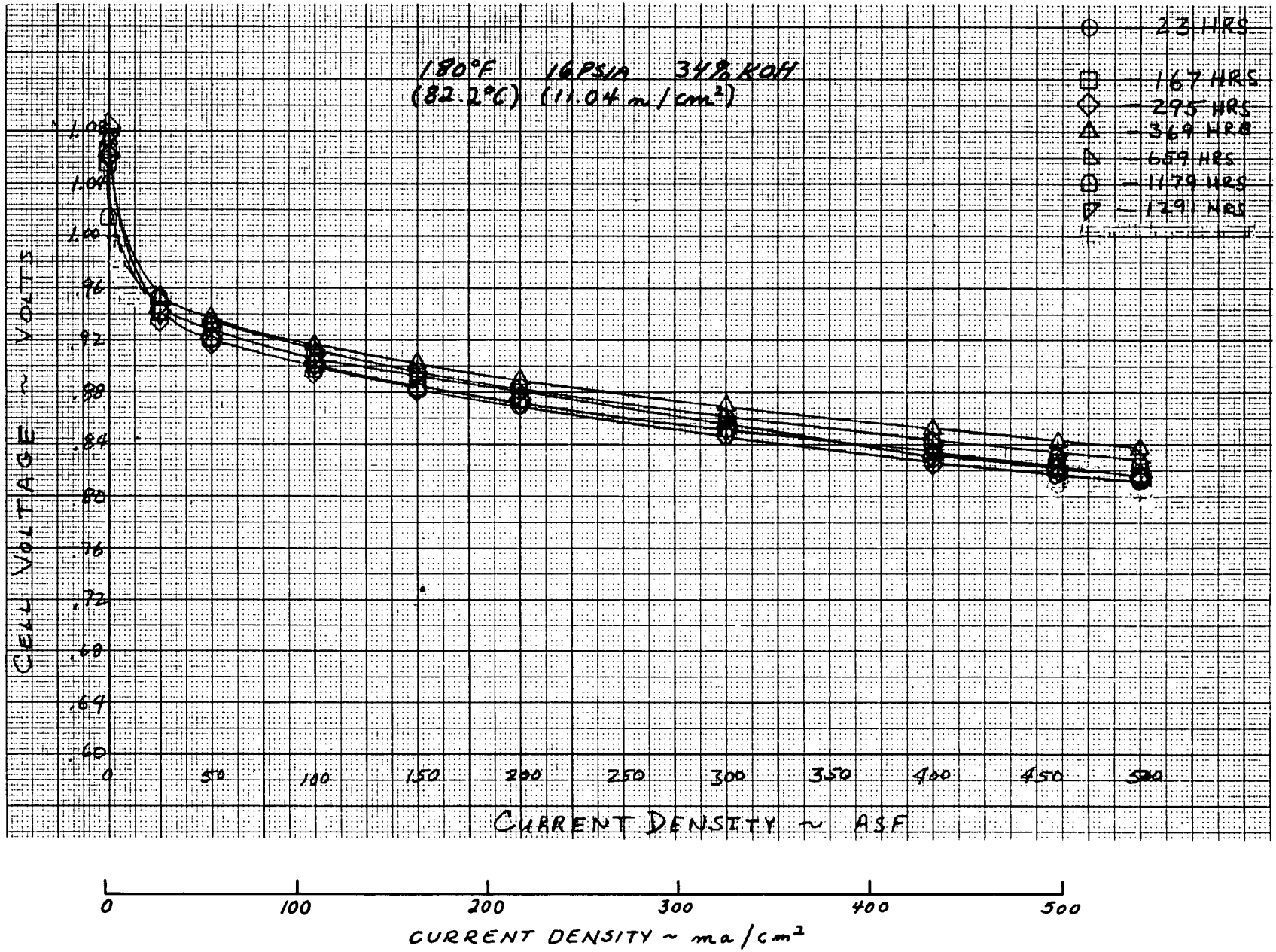

Figure 80 - Performance Calibration - Cell No. 17

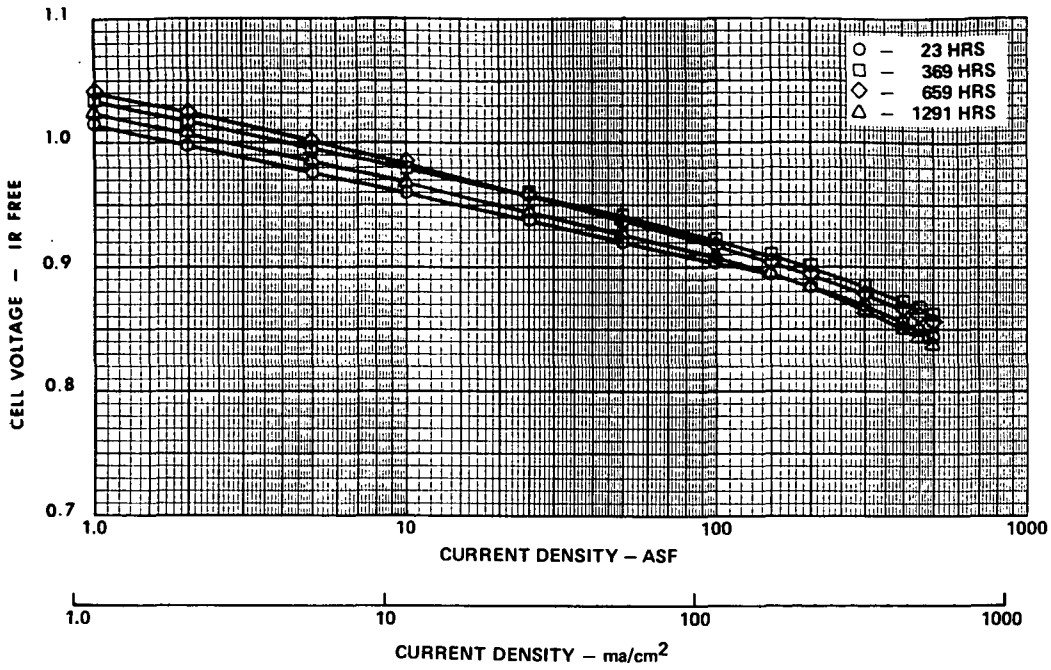

Figure 81 - Performance Characteristics of Cell No. 17

- Electrolyte carbonation was the major cause of performance degradation in early cells tested.

- Improvements in cell frame materials and refurbishment techniques resulted in greatly improved cell performance stability as evidenced by successful endurance testing of Cell Nos. 15 and 17 which continue on test.

B. Plaque Development

1.0 Introduction

A plaque is a multi-cell planar stack. The plaque concept offers weight advantages which are of particular benefit to high power, high voltage systems such as the Engineering Model System. In such systems, a large number of series connected cells is required. The plaque, by packaging a group of series connected cells into one thin plate, allows the system's power section to be assembled from fewer components. By having a number of cells share common reactant plates, coolant plates and fluid manifolds, fewer components and sealing planes are required.

There are two major development problems associated with a plaque. One is unique to the plaque, the other is common to all fuel cells:

- Intercell Seal - Series connection of cells in a common plane means the anode of one cell must be electrically connected to the cathode of an adjacent cell. Thus a current carrying member must pass from the hydrogen side to the oxygen side of the plaque without allowing any possibility of gas leakage.

- Large Total Cell Area - By grouping a number of cells into one planar sheet, the total cell area of the plaque is large. The problems associated with achieving proper reactant flow distribution and dimensional tolerances is the same as for large area cells.

The intercell seal problem was of obvious concern, but in retrospect, was the easiest to solve. The majority of plaque development efforts were associated with the "straight-forward" problems of a large area cell. These problems were deliberately made more difficult by selecting minimum flow field heights which exaggerate reactant flow distribution and thickness dimension tolerance problems. The necessity to construct the plaque from new materials and the more complex assembly associated with passive water removal also posed additional problems which had to be solved in the plaque.

The plaque fabrication and test experience sections which follow provide evidence that the plaque concept is sound. At the conclusion of Phase I of this program, a six-cell plaque, with a total active area of 0.7ft^2, (650.4 cm^2), and an oxygen flow field height of 0.015 inches (0.38 mm), operated successfully for over 500 hours.

2.0 Plaque Fabrication

Initial plaque development efforts were concentrated on the electrode assembly intercell seal. This was the only significant development problem not covered under the single cell fabrication effort. The principle requirements of the intercell seal are to: 1) transfer electric current from one cell to the adjacent cell, thus providing the desired series current flow; 2) provide a positive gas seal for the current conductor and for the cell's matrix; and 3) electrically insulate electrodes lying in a common plane. These requirements are illustrated schematically in Figure 82. .

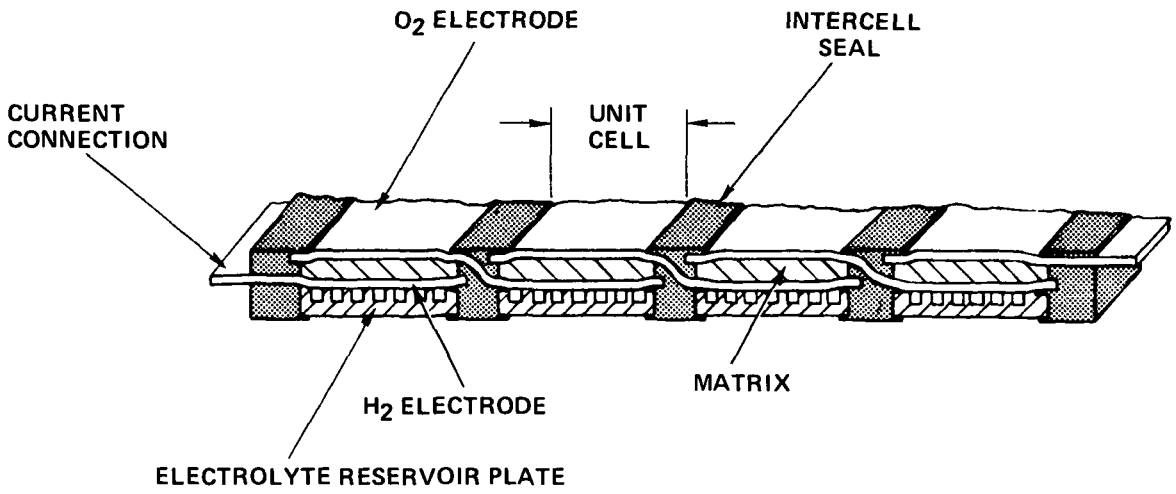

Figure 82 - Plaque Construction Showing Intercell Seal

The baseline EMS plaque design was used to guide the development efforts. To expedite fabrication and to obtain flexibility in testing, the width of the intercell seal varied between the baseline value of 0.25 inches(0.64 cm) to 0.50 inches(1.27 cm). The larger widths were used to allow development plaques to be built without special fixturing so that alternate designs could be evaluated at low cost. For flexibilty in testing plaques, and subsequently partial stacks, double-ended manifolds for the water vapor and cooling steam were added.

Since plaque development paralleled the development of the single cell, the materials and techniques used were similar. Thus, machined plastic (Arylon) frames were utilized as the backbone of the plaque structure for the first plaques built. Several intercell seal designs were investigated. As discussed in the single cell fabrication section, the elastomeric intercell seal was found to require high sealing loads and was relatively complex and not ameanable to minimum width. An intercell seal design using metal current conduction pins was rejected due to the potential for gas leakage through the pin area and because of the complex assembly required. The use of notched plastic intercell strips combined with elastromeric cemented matrices showed promise but the high curing temperature and heat sealing of metal screens to the frames caused unacceptable frame distortion.

The method chosen for the first operational plaques is shown in Figure 83. The more expensive notched frame was eliminated in favor of a simple flat frame which could be fabricated without machining. The electrode screens were heat welded in place onto the frames. The matrices were

edge impregnated with epoxy and press cured. Then the matrices were laid in place and epoxy bonded to the frame in the manner used for single cells. This type of joint provided adequate bubble pressure. The disadvantages of this method were the frame curling induced by the heat welding of the screens and the relatively tedious assembly procedure involved. The passive water removal assembly was made using one large piece of frame-bonded matrix with no internal strips. Plaques 1 and 2 were made using this procedure.

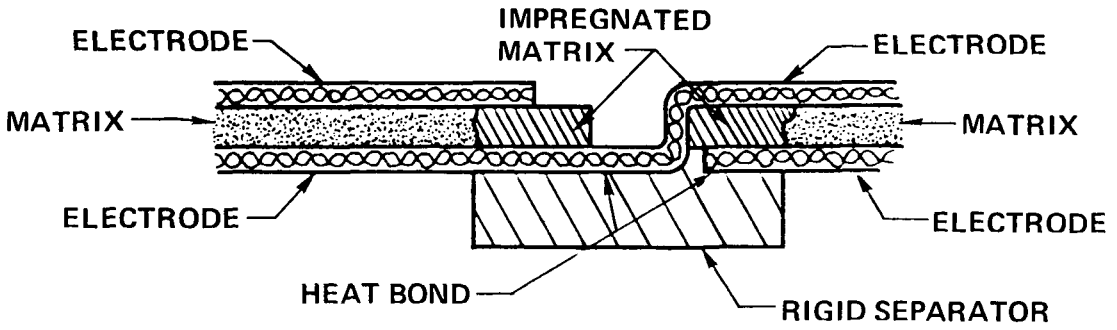

Figure 83 - Arylon-Epoxy Intercell Seal

At this time, the integral epoxy impregnated matrix frame concept was developed for the single cell design. Plaque fabrication trials were initiated to determine if this method could be applied to the plaque and especially to the intercell seal. For this method, a plaque size piece of matrix material is impregnated with epoxy in the frame and intercell seal area and allowed to semi-cure. Slots are then cut in the center of the intercell seals to the length of the active area. The electrode screens are then threaded through the slots. The layup is then press cured between machined platens with the epoxy flowing around the electrode screens to create a gas seal. A schematic view of this type of intercell seal is shown in Figure 84. In order to achieve controlled epoxy flow, it is necessary to hold close tolerances across the areas of the plaque. This was accomplished by the use of specially machined press plates. This fabrication technique resulted in plaques with good bubble pressure and dimensional control. The plaques exhibited the same flatness characteristics as the single cell and could be made at a substantial cost savings compared with the plastic frame design. In addition, this design showed the best potential of being able to obtain the 0.25 inch(0.64 cm) intercell seal width. To form the combined fuel cell-water transport plate, an Arylon spacer was used in conjunction with elastomer gaskets for sealing. This method was successful in plaques 3, 4, and 5. Figure 85 illustrates the total plaque cross section showing the electrolyte reservoir plate and hydrogen field location.

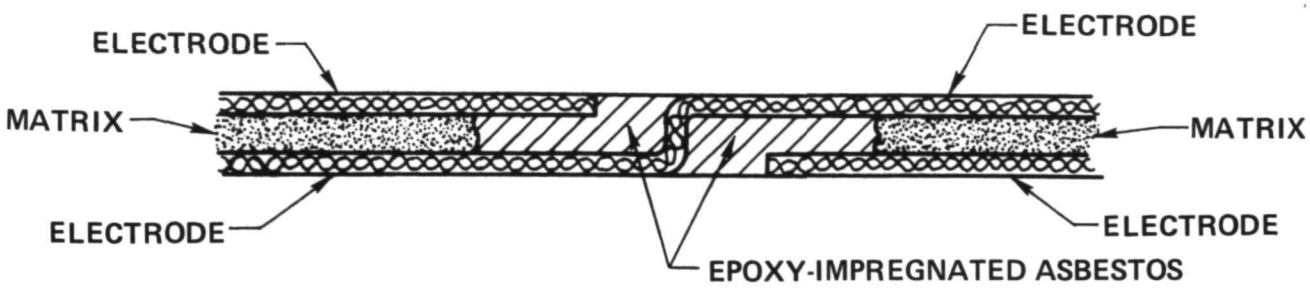

Figure 84 - Epoxy-Asbestos Intercell Seal

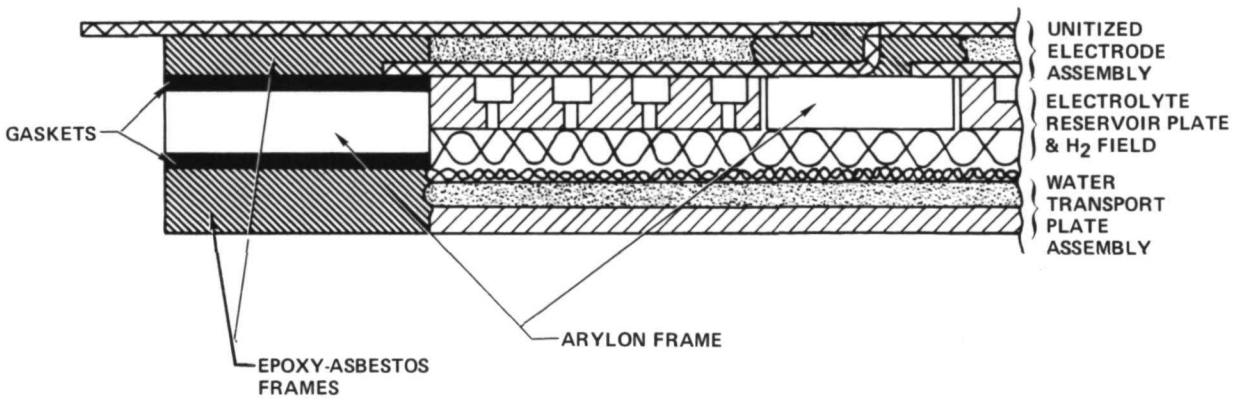

Figure 85 - Plaque Cross Section Showing Electrolyte Reservoir Plate and Hydrogen Field

The use of separate fuel cell and water transport plate subassemblies allowed passive water removal and fuel cell development problems to be solved separately. Once the adequacy of the design of these subassemblies had been demonstrated by test, it was desirable to combine them to achieve a more simple and reliable assembly. The necessity for using elastomer gaskets to seal the spacers between the fuel cell and the water transport plate in the plaque assembly created tolerance problems. The gaskets introduced a dimensional tolerance buildup into the plaque assembly despite the fact that the fuel cell and water transport plate assemblies had excellent dimensional characteristics. In addition, the final assembly process was quite lengthy. An approach similar to that used in the single cell area (Cell #20) was used to assure adequate dimensional control, simplify the assembly process and achieve a more reliable assembly. Accordingly, a one piece plaque assembly was constructed for evaluation using epoxy impregnated spacers in place of the Arylon and elastomer gaskets. Measurements of the thickness of the final assembly showed

that its dimensional accuracy was the same as each individual part and far better than the layup of separate pieces. A completely unitized plaque made of this design is shown in Figure 86.

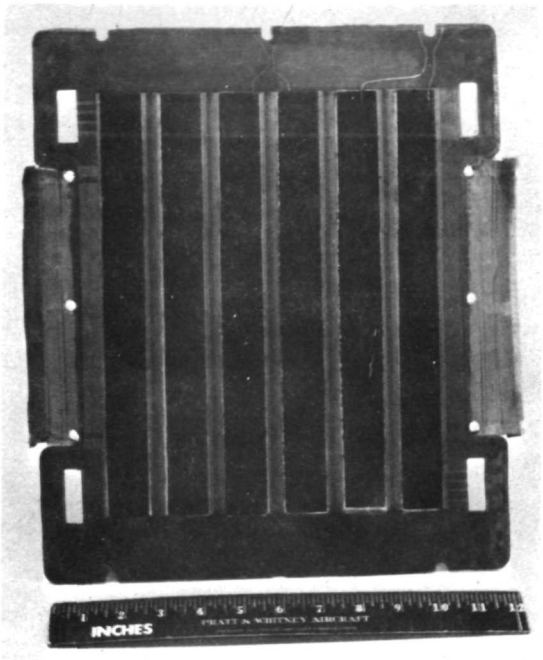

Figure 86 - Unitized Plaque

An investigation of plaque unitization processes using laminating film was carried out in parallel with the single cell unitization research. Trial plaques made with FEP and polypropylene film were constructed to determine if the smaller frame area to active area would minimize the relative thermal distortion seen on single cells and to investigate intercell seal problems. No difficulty was experienced in sealing the electrode screens where they passed through the seal; however, the differential thermal expansion between the films and other cell components results in unacceptable distortion.

The use of fiber-filled polymers to form a frame to which the films were laminated significantly improved the distortion problem in tests on subscale plaques. As discussed in Section IVA-4, unavailability of compatible filled polymer sheets in the thicknesses needed - approximately 0.01 inches(0.25 mm) - made it possible to pursue this course during Phase 1. Pending the delivery of such reinforced materials, the in-house developed asbestos reinforced TFE composite was used for the frame. Polypropylene films were used to bond plaque components to

the frame. Some wrinkling of the electrode screens was still present, but the situation was considerably improved. A complete fuel cell plaque (Figure 87) and water transport plate were made by this method. Intercell seal width was set at 0.38 inches (0.96 cm) to allow the film to overlap the matrix. This was done to provide a film-to-matrix bonding surface area to achieve the required bubble pressure gas sealing capability. The thickness dimension of this plaque's assemblies was excellent - within ±1 mil (±0.025 mm). Electrode flatness appeared acceptable. However, the matrix to frame bubble pressure capability was inadequate.

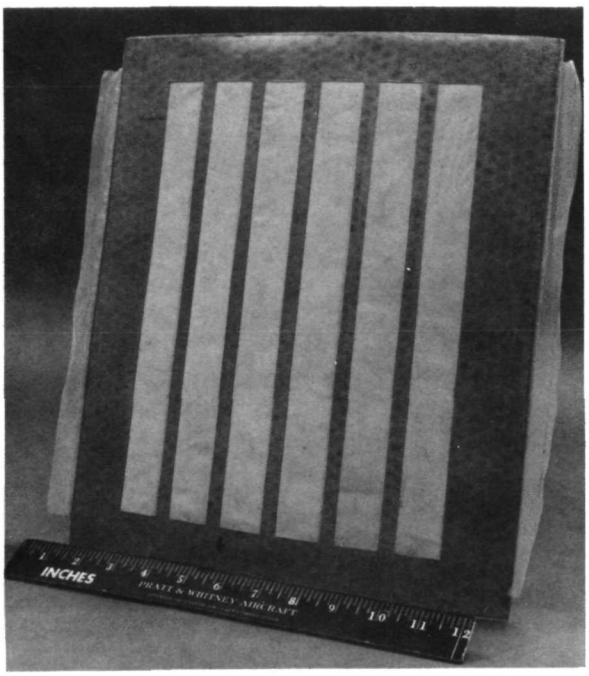

Figure 87 - Polypropylene Film Unitized Plaque

Test Fixtures and Assembly - Testing of the 6-cell plaque assembly required the use of novel test fixtures. One of the most important functions of the test fixtures is to insure uniform cell compression over the total cell area. To this end, one inch thick stainless steel end plates were designed to limit deflections. Butyl rubber gaskets were used to seal between component parts and the end plates. Internal cell compression was set by the selection of the proper combination of gasket and internal screen thicknesses.

For realistic plaque performance evaluation, it is necessary to incorporate the oxygen flow plate, which is normally an integral part of the evaporative

coolers, into the assembly. The functions of the oxygen plate are: 1) to transmit cell waste heat, 2) to provide for efficient oxygen flow distribution and 3) to transmit the cell compressive load. In plaque testing, cooling was attained by heat dissipation through the end plates to an external end plate cooler. At normal operating power densities, heat rejection was accomplished passively, to a controlled oven. Figure 88 shows the test fixtures with cooling coils installed in the oven.

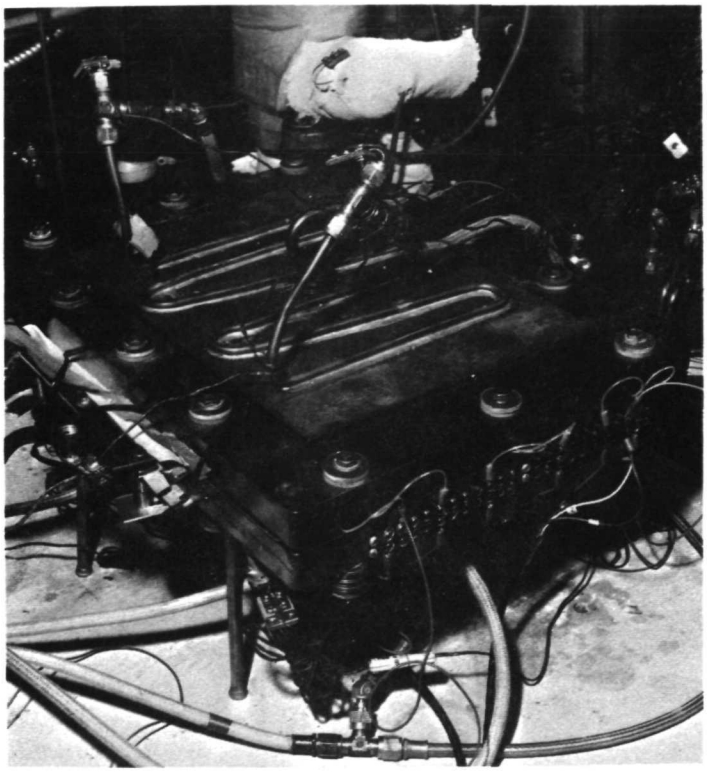

Figure 88 - Plaque Test Fixtures

The oxygen flow plate used for plaque testing incorporated the baseline EMS design flow patterns. This plate, machined from Arylon, is shown in Figure 89. A flow test of the oxygen field with dye injected into flowing water showed that the flow distribution field yielded a good filling and emptying pattern. Only small differences in emptying times were noted for the last few rows. Flow field and port pressure losses on the better plaque assemblies were 1.5 to 2.5 inches(3.81 to 6.35 cm) of water at design flows, comparable to predicted values. Higher values on one plaque were due to dimensional problems of the components, coupled with thin (15 mils) (0.38 mm) oxygen flow field.

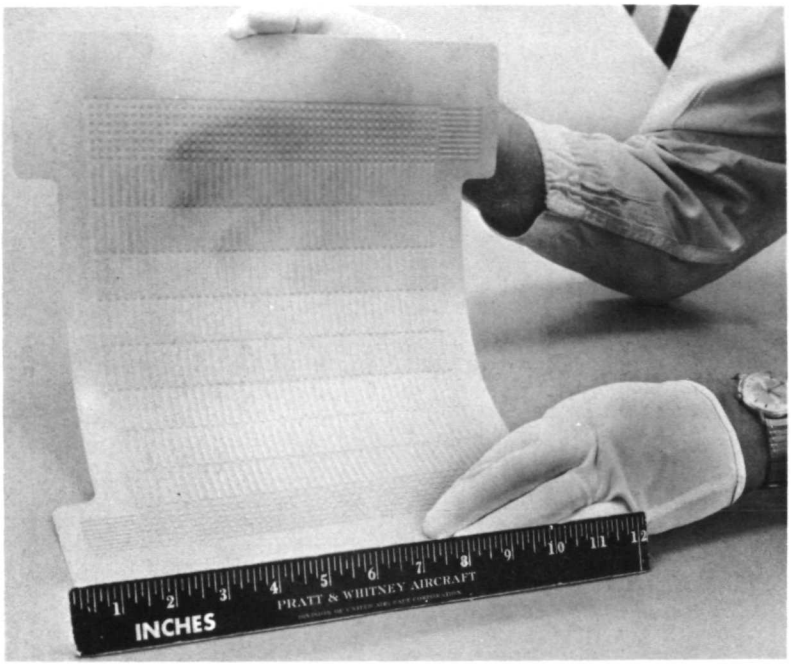

Figure 89 - Arylon Oxygen Flow Plaque

The most significant difficulty encountered in the plaque program was due to assembly tolerances. These were not unexpected, being caused by the large cell areas, internal manifolding, thin gas flow fields, and the desire to obtain flexibility and fast turnaround of experimental hardware by using a multi-gasketed assembly. With the number of components, gaskets and spacers in each assembly, the theoretical tolerance buildup could be high. Thus special care had to be taken to measure the thickness of all parts to help assure that cell compression would be proper. This problem is correctable, as in the single cell, with the use of one piece assemblies (combined unitized electrode and water transport plate assemblies). This eliminates the use of all internal gaskets and spacers. An integral unit was fabricated and successfully tested in the single cell program and an integral plaque unit has been fabricated and successfully bench tested.

3.0 Plaque Test Results

Test Program - During the contract period, five plaques were assembled and tested. Of these, the first two used the Arylon-Hypon unitization design and three used the Hypon impregnated matrix fabrication technique. Total load time accumulated was 777 hours, including 540 hours on Plaque No. 5. Four of the five plaque assemblies were performance tested. A fifth plaque was assembled but experienced leakage after being heated to operating conditions.

Performance level of the plaques was good as shown in Figure 90. In each of the plaques, the individual cell internal resistance was reasonable, ranging from 10-15 mV at 100 ASF(107.6 ma/cm^2). This indicated that despite the tolerance and assembly problems, individual cell matrix compression was reasonably good.

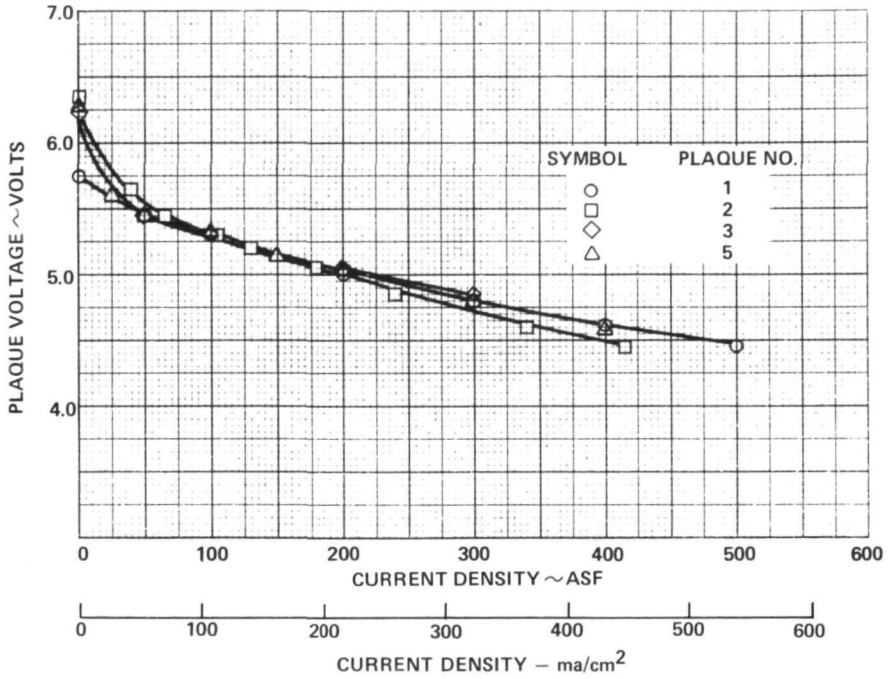

Figure 90 - Plaque Performance

The response to electrolyte concentration variation was good in the later plaques as shown in Figure 91. Early tolerance response problems were attributed to incomplete electrolyte fill.

Plaque No. 1 experienced electrolyte shunt currents due to electrolyte hang-up in the oxygen flow field. A polypropylene screen was used as the oxygen flow field in this plaque. Flush filling the plaque resulted in electrolyte hang-up in this screen which apparently was not completely removed by standard draining and purge techniques. This problem was eliminated in Plaque No. 2 by using the machined Arylon plate(Figure 89) for the oxygen flow field. The more open pattern of this flow field facilitated draining of excess electrolyte and also isolated the metal end plates from the plaque. The improvement was noted in the increase in open circuit voltage from 5.8 volts in Plaque No. 1 to 6.3 volts in Plaque No. 2.

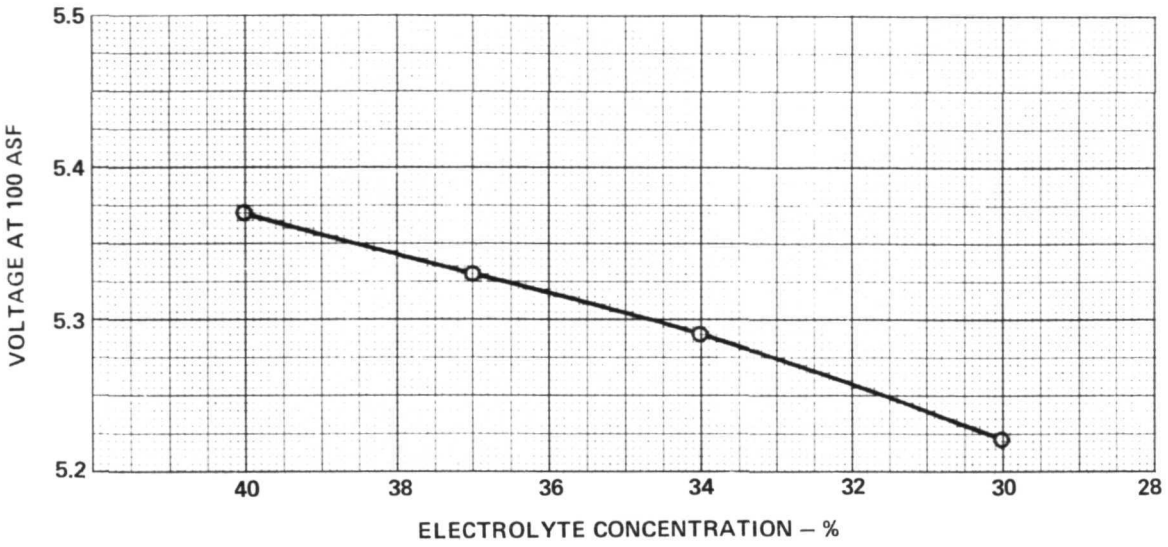

Figure 91 - Plaque Tolerance Data

Plaque No. 3 exhibited high oxygen port and field pressure losses. The reasons for this were two fold: first, an elastomer backing sheet was placed between the end plate and the oxygen plate to aid in assembly. This caused distortion of the oxygen plate web resulting in reduced oxygen flow field depths. Secondly, the shallow oxygen ports coupled with the thin frame materials resulted in tenting in the port areas and hence, partial blockage of the ports. This problem was remedied in Plaques 4 and 5 by eliminating the backing, increasing the port depths and using a stiffer bridging material in the port areas to eliminate or minimize tenting. Pressure drop data indicated these modifications were successful in achieving a low pressure oxygen flow field.

Plaque No. 5 accumulated 540 hours at a current density of 100 amps/ ft^2(107.6 ma/cm^2). Though the initial overall plaque tolerance to off-design conditions was poor, acceptable tolerance was attained by the addition of electrolyte to the oxygen cavity. Overall performance level was good, as seen in Figure 92, and stability of five of the six cells was satisfactory. No. 1 cell, however, was unstable and required a number of electrolyte additions in order to maintain a reasonable performance level.

This anomaly can be explained by consideration of the physical arrangement of the cells in the plaque and the differences between the center and the end cell electrodes. In the plaque construction, the end two cells, Cells 1 and 6, have one electrode each fabricated singly rather than as a two electrode chain. Due to a processing error during electrode fabrication, the end

electrodes, the cathode of Cell 1 and the anode of Cell 6, for this plaque were pressed at the same loading as the center pairs rather than at one-half the load. This results in a compacted electrode structure which can result in electrolyte pumping on the cathode. Analysis indicated that the oxygen flow velocity could be sufficient at high current densities to sweep away any electrolyte droplets formed on the cathode of Cell No. 1 if such were present. This particular combination of gas flow direction and No. 1 cell cathode characteristics could cause loss of electrolyte from Cell No. 1, especially at high flows.

The performance history of Plaque No. 5 is shown in Figure 92. The performance level and stability of Cells 2 through 6 are good in spite of the perturbations the plaque received as a result of Cell No. 1. The performance of Cell No. 1 varied from a level equal to that of the other cells to 80 mV lower. Selective electrolyte additions to Cell No. 1 would temporarily improve its performance. Since the basic structural problem of the Cell No. 1 cathode could not be conveniently countered by operating parameters, and since the test had demonstrated the essential soundness of this plaque design, the rig was shut down at 540 hours load time.

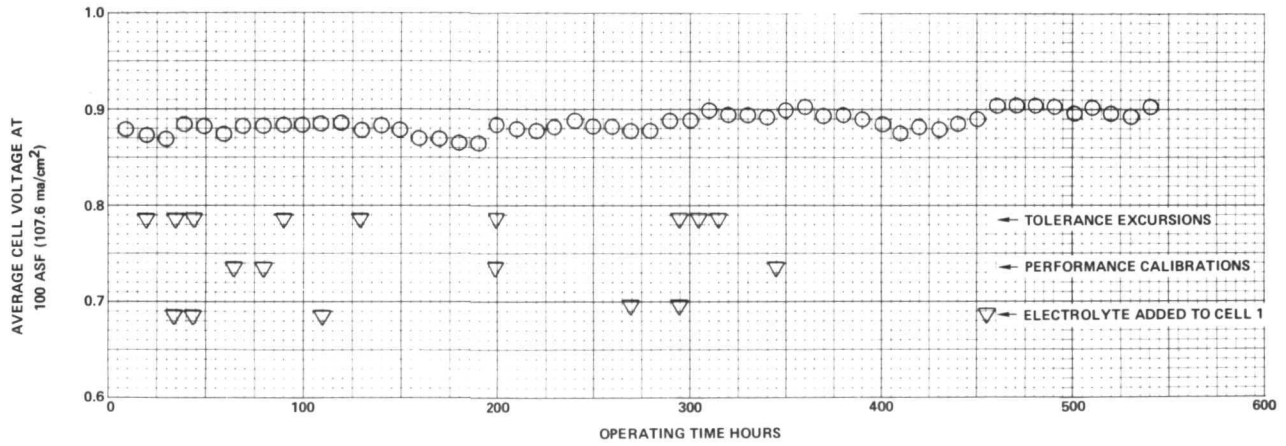

Figure 92 - Plaque No. 5 Performance History

C. Evaporative Cooler

1.0 Requirements and Operation

The EMS requirements for uniform cell temperature, over the entire cell area under all operating conditions and power levels and at a minimum in weight, can be achieved with intercell cooling by evaporation of water.

Servicing two adjacent strip cell plaques, these intercell coolers maintain cell temperature by heat conduction from the cell plaques to an internal water reservoir. Liquid water in the reservoir is vaporized and the steam passes through a hydrophobic separator into the vapor chamber. The pressure in the vapor chamber is regulated to set the desired saturation temperature which is matched to cell operating temperature.

The low weight goals of the EMS required several novel features in this cooling system. Porous polymer membranes were required for water-steam separators, the water and steam flow passages were dimensionally small and yet were required to have low pressure and temperature drops, and structural components were to be made from light-weight polymer materials.

Operation of intercell evaporative cooling assemblies had been demonstrated on single cells and partial stacks in the Air Force sponsored High Power Density Program, Contract F33615-70-C-1134. Stable and uniform temperatures, $\pm 2°F(\pm 1.1°C)$, were demonstrated at a heat flux of 7300 Btu/hr/ft^2(2300 watts/meter^2). This heat flux is equivalent to 10 times the EMS waste heat flux at peak power. The evaporative cooler assembly which evolved from the Air Force program utilized a Teflon impregnated nickel sinter to separate steam from the feedwater in each cooling assembly. The separator developed was insensitive to variations in steam-to-feedwater differential pressure, eliminating the requirement for precise control of feedwater pressure. During tests at a heat flux of 7300 Btu/hr/ft^2(2300 watts/meters^2), the water over-pressure was varied up to 5 psi(3.45 n/cm^2) with no effect on cell temperature or water separation.

The evaporative cooler assembly is schematically illustrated in Figure 93. Waste heat generated by the fuel cell is conducted through the oxygen/water plates to the water passages. The evaporation temperature at the membrane interface is controlled by the pressure maintained in the steam chamber. Water pressures higher than the steam chamber pressure assure that the water passages are always supplied with cooling water. Steam from the membranes flow parallel to the membranes in the steam field spacer which connects to a manifold for removal of steam from the stack.

The theoretical evaporative cooler operation has the following characteristics:

- No cell-to-steam temperature gradient exists
- Cell temperature is set by the pressure maintained in the steam chamber as this sets a saturation temperature at the water-membrane interface

- Cell temperature is independent of waste heat flux
- Feedwater consumption is a function only of waste heat flux
- Cell temperature and feedwater consumption is independent of water overpressure

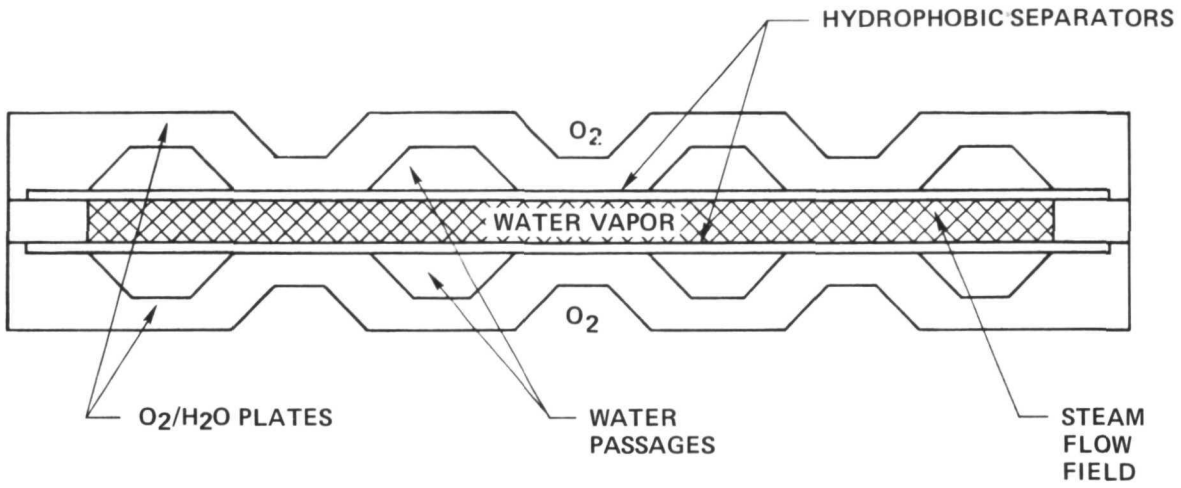

Figure 93 - Evaporative Cooler Schematic

Ideal evaporative cooler performance is illustrated in Figure 94. The curve for the ideal case shows that the steam temperature is on the saturation temperature line for water and that no steam-to-water temperature gradient exists. In an actual cooler, the pressure loss in the steam field results in an increase in the absolute pressure at the water-membrane interface with the resulting increase in the saturation temperature.

In addition, the temperature differential which exists in the water field causes a second deviation from the ideal case. Heat flow from the cell to the membrane is through the parallel conduction paths in the oxygen/water plate and the water. A high thermal conductivity oxygen/water plate minimizes the water reservoir differential temperature (ΔT). The deviation from the ideal cooler performance caused by the water field temperature rise, is also illustrated in Figure 94.

The additive effect of these two deviations from the ideal case sets a minimum cell-to-steam temperature gradient. Although this gradient can be corrected for by maintaining a lower steam pressure and, thus, maintaining the desired cell temperature, the two losses result in a minimum water overpressure constraint on the cooler. Water overpressures,

whose saturation temperatures are above the minimum cell-to-steam temperature rise, must be set to prevent boiling in the water reservoir. When boiling occurs in the cooler, temperature control is maintained by the water pressure as shown in Figure 94. Although boiling is not necessarily a failure mode, it does result in higher pressure losses in the water field and resulting increased temperature.

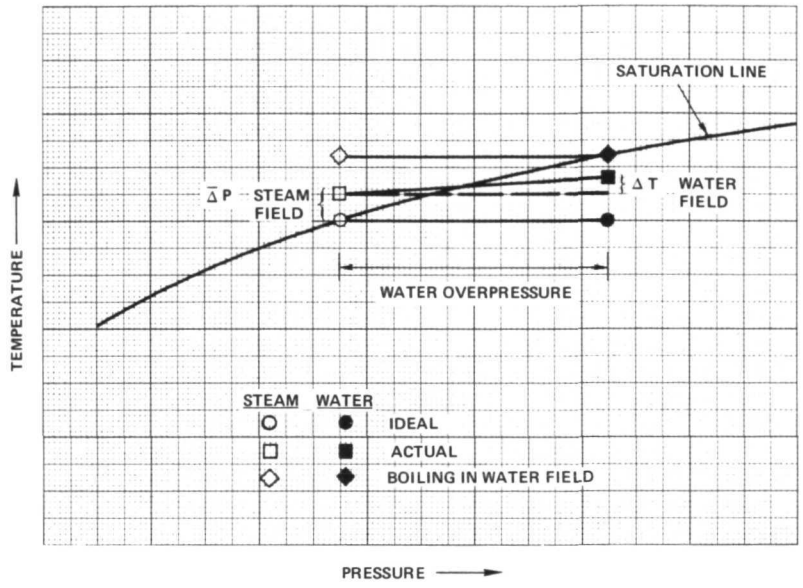

Figure 94 - Ideal Evaporative Cooler Performance

The above operational characteristics and low weight goals impose the following conflicting requirements on evaporative cooler components:

Separator Membrane:

- The water-steam separator membrane should be thin, be highly porous and have a large mean pore size to provide sufficient steam permeability, while having a sufficiently high water entry pressure which implies a thick, dense and small mean pore size structure.

Steam Field:

- The requirement for a lightweight structure which has a low in-field pressure drop suggests an open, widely-spaced structure while the requirement for sufficient membrane support dictates a closely spaced, dense structure.

Water Field:

- The requirement for a low temperature profile across the water field is best met with a small depth, metallic field. The low weight requirement calls for a small depth plastic field which has good thermal conductivity and low in-plane resistance to water flow.

2.0 Evaluation Program

The objectives and tasks established to develop an evaporative cooler meeting the EMS requirements were to:

- Determine the feasibility of porous polymer membranes to function as water-steam separators.
- Generate design data for the required thin water and steam flow fields for both available and designed materials.
- Evaluate the oxygen/coolant plate design options.

Water-Steam Separator Membranes - The water-steam separator membranes were the first evaporative cooler components investigated. Porous Teflon membranes were the logical first-choice water-steam separators because of Teflon's temperature capability and hydrophobicity properties.

The required membrane properties established for use as evaporative cooler water-steam separators were:

- Thickness - Minimum consistent with strength, water vapor permeability and water entry pressure requirements.
- Permeability - Baseline EMS evaporative cooler steam flux is 1.25 lb/hr/ft^2(6.11 kg/hr/m^2). The permeability of the separator membranes were selected to have at least twice this steam flux capability.
- Water Entry Pressure - Separators were required to have a 5 psi(3.45 n/cm^2) minimum water overpressure capability.

Two vendors, Chemplast, Inc. and Gore Associates, were contacted to determine the suitability of available porous Teflon membranes. Table 14 summarizes the physical property ranges of available membranes

from these two vendors. Gore Associates' Gore-Tex® membranes were selected because of their interest expressed in providing materials, the large range of membrane properties offered and the availability of materials. Four mil(0.10 mm) thick membranes were selected as the minimum supportable membranes. The cloth-like nature of a 4 mil(0.10 mm) membrane is shown in Figure 95. Water entry pressure and permeability capabilities are direct functions of the membranes' porosity. Membranes of 69 and 82 percent porosity were selected as most likely to meet the evaporative cooler requirements. Manufacturers' water entry pressure and permeability values for the membranes are given in Table 14.

TABLE 14

WATER/STEAM SEPARATOR MEMBRANE PROPERTIES

Membranes	Thickness mils(mm)	Porosity %(%)	Water Entry Pressure psi(n/cm^2)	Air Permeability cfm/ft^2 - psi (m/min-n/cm^2)
Available				
Zitex (Chemplast, Inc)	2.5 - 34 (0.063 - 0.86)	65 - 85	0.2 - 6.0 (0.138 - 4.14)	0.3 - 4,500 (0.132 - 1980)
Goretex (Gore Assoc.)	0.5 - 36 (0.013 - 0.91)	0 - 98	1.0 - 60.0 (0.69 - 41.4)	0 - 8,000 (0 - 3,520)
Tested				
Goretex 4SA 12.4	4 (0.102)	82	8 (5.52)	26 (est) (12.4)
Goretex 4SA 5.7	4 (0.102)	69	20 (13.8)	5 (est) (2.2)

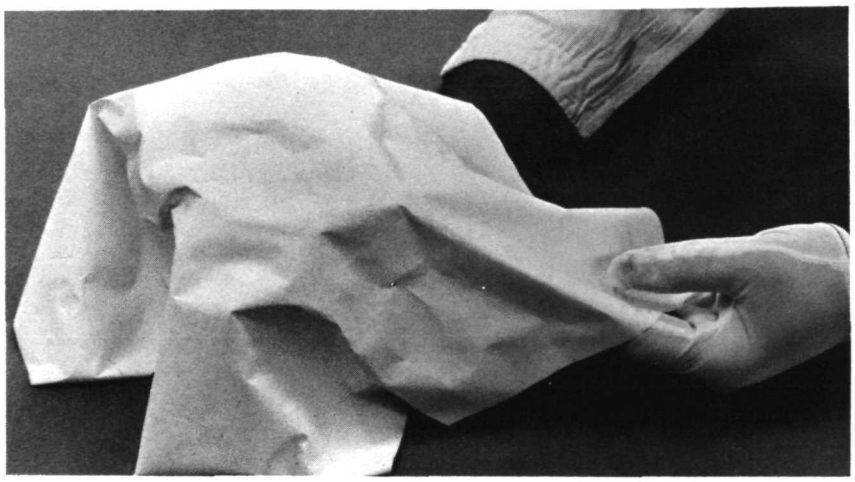

Figure 95 - Four Mil Gore-Tex Membrane

Steam Flow Field and Membrane Support - Concurrent with the water-steam separator investigations, evaluations of candidate steam flow fields were conducted. Subject to the EMS weight goals, materials which satisfied the constraints of light weight, thin dimensions, good membrane support and low in-plane pressure drop for steam flow were considered. Table 15 lists the candidate materials.

TABLE 15

Candidate Steam Passage Spacers

Woven Cloth	Teflon Polypropylene
Expanded Mesh - Exmet	Polysulfone Polypropylene Aluminum
Extruded Mesh - Vexar	Polyproylene
Heat Exchanger Core - Kintex	Aluminum
Foamed - Duocel - Skilkote	Aluminum Reinforced Polyurethane

Tests to determine the flow-pressure drop characteristics of 10 steam spacers were conducted. The flow-pressure drop characteristics are shown in Figure 96. By appropriate conversions for viscosity and density, the data on nitrogen can be expressed as laminar friction and momentum flow resistance coefficients for steam which are used in finite difference calculations to predict pressure drop in a full size cooler.

These conversions indicate that the EMS steam chamber pressure loss, ΔP (EMS), is 0.3 to 0.4 times the test rig nitrogen pressure drop, measured at the maximum equivalent steam flow which occurs where the steam flow converges toward the exit manifold. This data indicates that available screen-type spacers with heights greater than 24 mils(0.61 mm) are required if the in-field pressure drop in the steam apacer is to be less than 0.5 psi(0.35 n/cm^2).

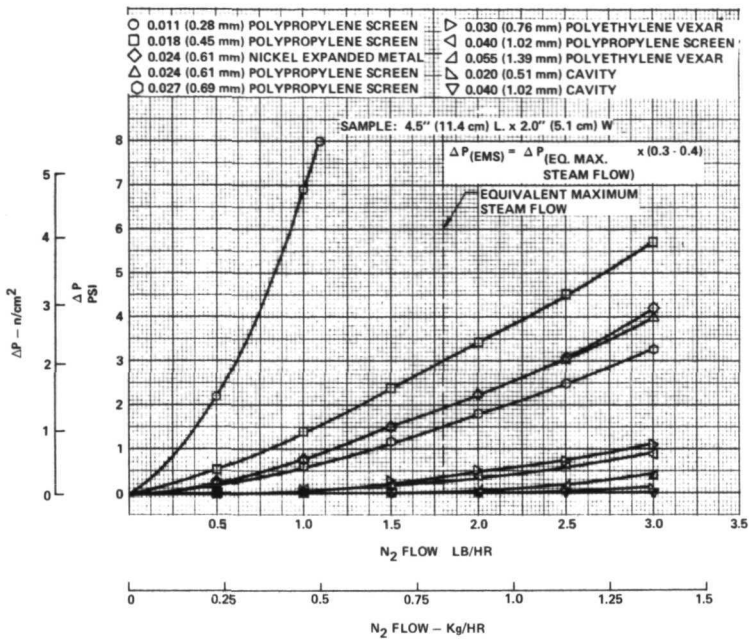

Figure 96 - Flow Pressure Drop Characteristics

Coolant Plate - Thermal analysis of several coolant plate designs were performed. These designs differ by the means used to form the oxygen and cooling water flow fields. Flow fields formed by pins or bars and those formed by screens were evaluated for temperature drop using a finite difference digital computer routine. Thermal gradients (from cathode to steam) were calculated based on:

- Heat Flux = 7300 Btu/hr/ft^2 (2300 watts/m^2) - This is the heat rejection rate at the 21 kw peak power operating point or a fuel cell current density of 460 ASF(495 ma/cm^2).

- Pin or bar coverage is 25 percent of the total heat transfer area.

- Oxygen field depth = water field depth = plate web thickness = 10 mils(0.25 mm).

- Plate material was Arylon or 30 percent graphite-filled Arylon to improve the thermal conductivity.

The results of the study indicated that designs with the oxygen flow field formed by a plastic screen are not feasible because of the high thermal resistance of the oxygen cavity. Temperature differentials were estimated to be about 45°F(20°C). Designs with pins/bars on the oxygen side were feasible. The temperature gradients of 12°F(6.7°C) and 22°F(12.2°C) were predicted for the filled and unfilled materials respectively.

The results of other program activities after these studies were performed dictated that the oxygen flow field depth increase from 10 to 15 mils(0.25 to 0.38 mm). It was decided to increase the oxygen plate pin/bar coverage from 25 to 50 percent to promote additional area for waste heat conduction. A thermal conductivity test was made of an unfilled Arylon or oxygen water plate of this design. The measured temperature differential at the 21 kw heat flux (7300 Btu/hr/ft^2) (2300 watts/m^2) was 23°F(12.8°C).

Because of the inherently low thermal conductivity of polymer materials, a coolant plate which used expanded metal for the oxygen field was designed and tested. This design and its measured temperature differential properties were compared with those of the all-plastic design described above. Its temperature difference was only 14°F(7.8°C); and its weight is 73 percent of the all-plastic plate. Thus, it is an attractive candidate for the EMS coolant plate.

Evaporative Cooler Tests - Subscale heat transfer evaluation of evaporative cooler designs were made in the test rig shown in Figure 97. Existing 0.14 ft^2 (130 cm^2) cell hardware was used to construct the evaporative cooler. The low cost advantages of the subscale hardware made extensive testing possible. A disadvantage of this hardware was that the heat loss was a significant portion of the design heat flux. Based on steam condensation collected per hour compared to Btu/hr heat input, the heat loss could not be lowered to less than 10 to 15 percent of the input. This was not a major problem since the steam condensate could be used as the measurement for applied heat loads.

In the early cooler tests, only the Gore-Tex membranes were evaluated. Bonding of the membranes to frame assemblies which formed the water and steam vapor chambers (thought to be a major problem) was readily accomplished with Hypon adhesive. The porous Teflon structure required no prior surface treatment to bond the porous Teflon to itself or to other structures.

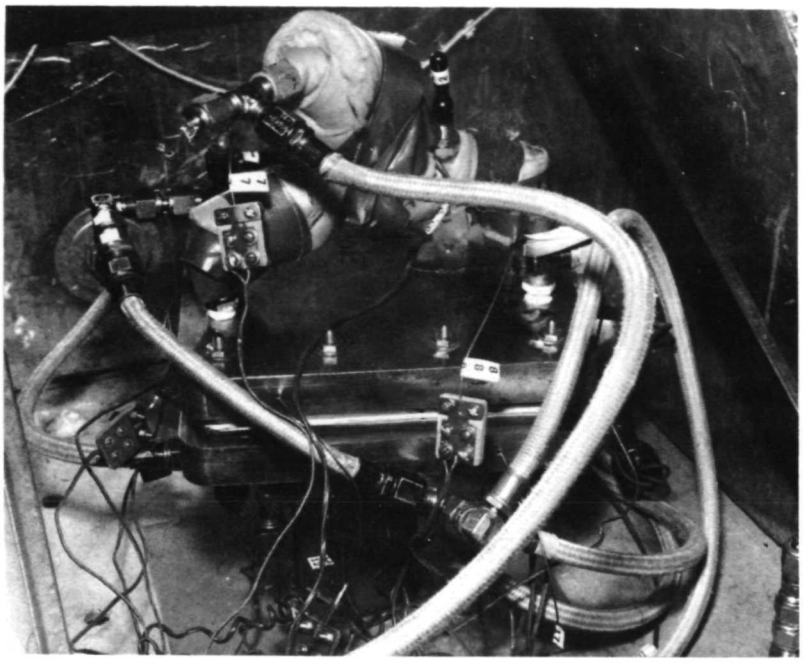

Figure 97 - Evaporative Cooler Test Rig

The results from the subscale heat transfer tests demonstrated the capability of the membranes to function as water-steam separators. Figure 98 shows the results of the water overpressure tests on the Gore-Tex 4SA12.4 membranes. Cooler No. 8 had water carry over at 3-4 psi(2.1 to 2.8 n/cm^2) water overpressure while Cooler No. 9 had no carry over up to 5 psi(3.5 n/cm^2). Manufacturers' specifications on this membrane (see Table 14) showed this membrane to have 8 psi(5.5 n/cm^2) water overpressure capability. Teardowns of these two cells showed membrane stretching occurred in both cells and in No. 8, pinholes were found. These membranes were tested with a 27 mil(0.69 mm) polypropylene screen used as the steam flow field and membrane support. Membrane support was inadequate, which contributed to the stretching. Because of the marginal results on this membrane, the more dense 4SA5.7 membrane was used in later tests with satisfactory results. Heat fluxes up to 2 times the design heat flux at 7300 Btu/hr/ft^2(2300 watts/m^2) were applied during this test. The water overpressure was varied up to 5 psi(3.5 n/cm^2) with no effect on cell temperature stability or water separation.

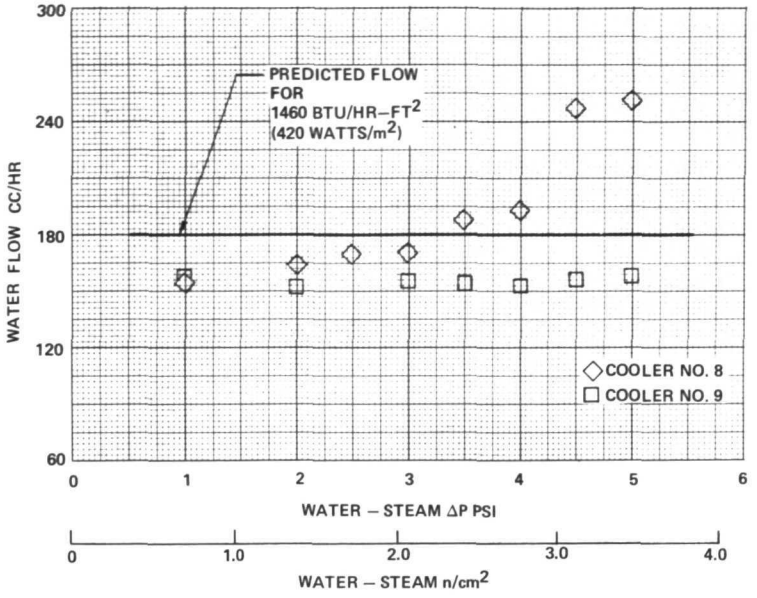

Figure 98 - Results of Water Overpressure Tests on Gore-Tex 4SA12.4

A 1000-hour endurance test was made to determine whether any long-term hydrophobicity changes would occur in the membranes. Feedwater consumption rate vs. running time is shown in Figure 99. The increase in feedwater consumption, which from the start was above the calculated rate, indicates that carryover and/or leakage occurred. Subsequent teardown and inspection of the membranes revealed membrane punctures near the water inlets, thought to be caused by overcompression in these areas. Water intrusion tests on undamaged portions of the membrane gave water entry pressures of 17 psi (11.7 n/cm^2) compared to 20 psi (13.8 n/cm^2) on new membrane samples. The membranes, however, were permanently indented 3 to 5 mils (0.08 to 0.13 mm). The endurance test showed that the effect of 1000 hours of operation did not cause any appreciable changes in the membranes' hydrophobicity, but it did again indicate that adequate membrane support was a necessity.

The subscale evaporative cooler testing also provided the membrane support data necessary to specify the configuration of the steam chamber spacer. As discussed earlier, flow-pressure drop characteristic testing indicated dicated that 24 to 27 mils (0.61m - 0.69 mm) was the samllest height plastic screen that could be used and yet meet the internal pressure drop requirement of 0.5 psi (0.35 n/cm^2). Cooler testing with a 27 mil (0.69 mm) polypropylene screen showed that this steam field provided only marginal support with even the higher density membrane (as shown during the 1000-hour endurance test). The effect of membrane indentation is to cause an additional restriction to steam flow. As discussed

earlier, any increase in the steam field pressure loss increases the minimum water overpressure required for the cooler to function properly. This condition is shown in Figure 100. A minimum of 3.0 psi (2.1 n/cm^2) water over-pressure was required to supress boiling in the water cavity. The evaporative cooler test hardware included a second steam manifold. Removing the steam through two manifolds lowered the steam field length and reduced the internal pressure loss. This advantage is illustrated in Figure 101.

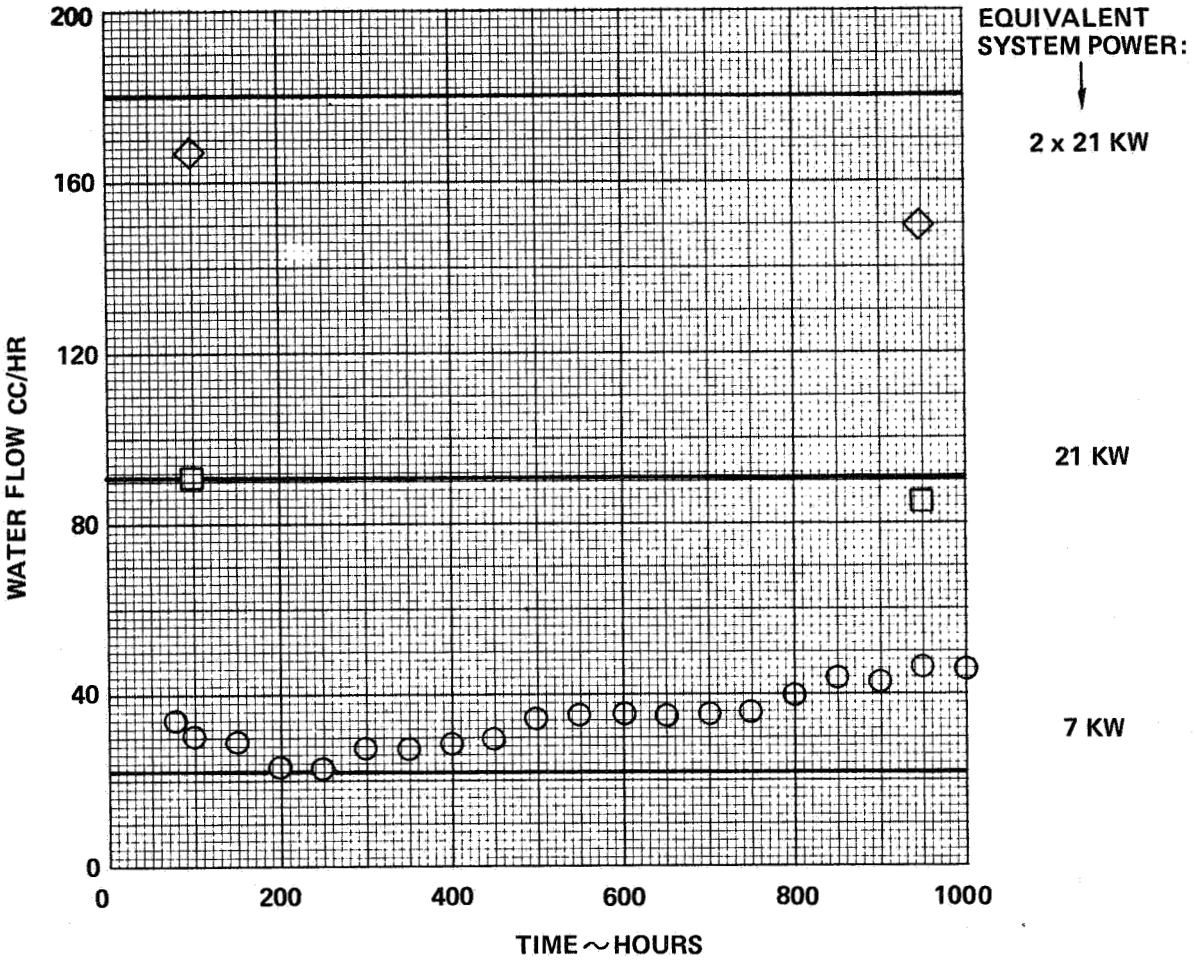

Figure 99 - Evaporative Cooler Feedwater Consumption Rate vs. Running Time

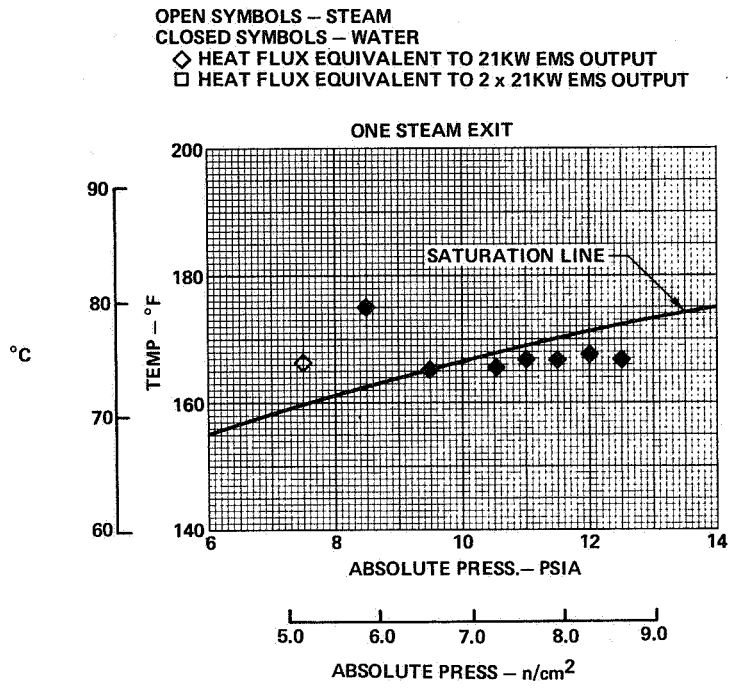

Figure 100 - Evaporative Cooler Test Data

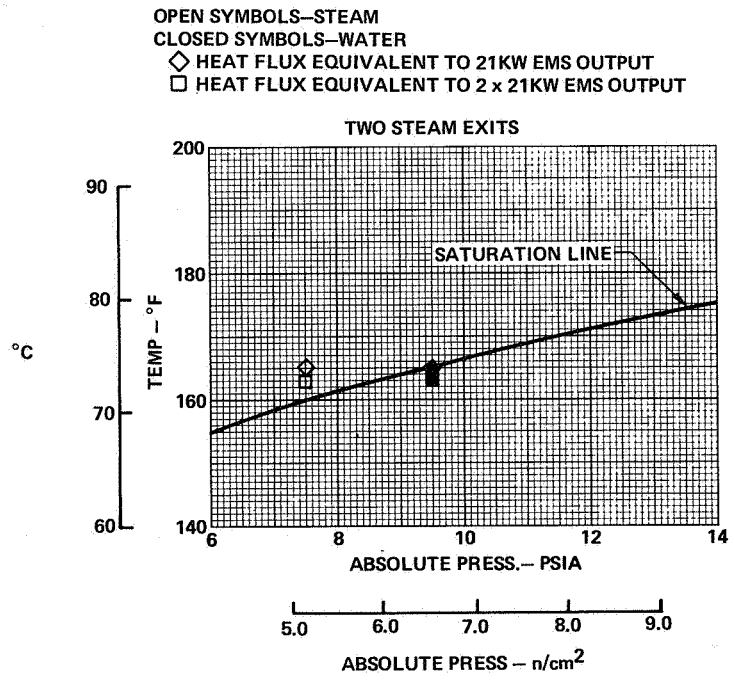

Figure 101 - Evaporative Cooler Test Data

A trilayer steam flow field spacer was constructed to prevent membrane indentation in the 27 mil (0.69 mm) polypropylene screen. This spacer and the other components making up the cooler are shown schematically in Figure 102. The trilayer spacer was constructed with the 27 mil (0.69 mm) polyproplene screen sandwiched between two layers of 3 mil (0.076 mm) thick 100 mesh nickel screen. The fine mesh nickel screen provided uniform support to prevent membrane deformation. The results of the testing are shown in Figure 103. Significant in the results is the test confirmation of the flow - ΔP data. At 1460 Btu/hr/ft^2 (460 watts/m^2) applied heat flux, 0.3 psi (0.21 n/cm^2) was measured while approximately 0.5 psi (0.35 n/cm^2) was calculated for the internal pressure loss for the steam flow through the 27 mil (0.69 mm) polyproplene screen. This test showed that the trilayer steam spacer construction is satisfactory for full size evaporative coolers.

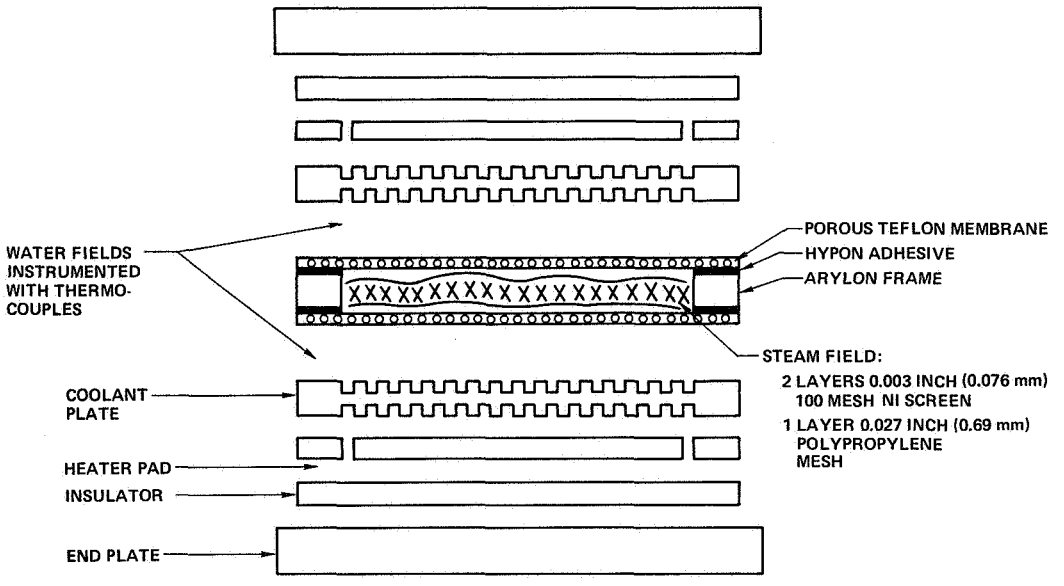

Figure 102 - Evaporative Cooler Components Showing Trilayer Steam Flow Field

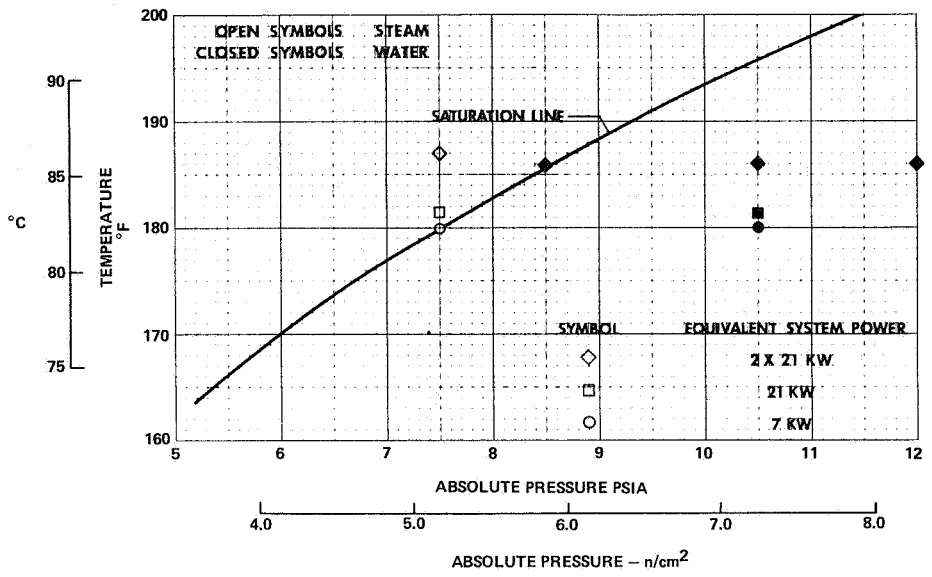

Figure 103 - Tri-layer Steam Field Cooler Test Data

3.0 Conclusions

Membranes - The porous Teflon membranes function effectively as water-steam separators. The Gore-Tex membranes evaluated meet EMS requirements. Additional endurance testing is needed to determine any long-term degradation mechanisms.

Steam field - The trilayer spacer tested provides adequate membrane support and low steam pressure drop. Trade studies, which investigate tooling costs, lead times and program requirements are required to select materials and designs for minimum weight.

Coolant Plate - Alternate designs are available for an oxygen flow field (pin/bar or metal screen) and water flow field (low height pin/bar or screens). Design trade studies similar to those of the steam field are required to select an optimum design.

V. SYSTEM DESIGN ANALYSIS

1.0 Selection of System Concept

The objectives of the system design task were to:

- Define a preliminary system design.
- Perform trade studies to help guide the technical advancement tasks.

The NASA design and performance objectives shown in Table 16 were the basis of the system design. Several of these objectives significantly influenced the selection of the system concept for the Engineering Model System; these are tabulated and discussed below.

TABLE 16

Engineering Model Fuel Cell System Design and Performance Objectives

Life	
Operating Duration	10,000 hours, or longer, with refurbishment
Structural	
Weight	20 lb/kw (9.1 Kg/kw), sustained power
Volume	0.5 ft^3/kw (14,200 cc/kw), sustained power
Reactants	
Fuel and Oxidant	Hydrogen and oxygen, nominal propulsion grade
Specific Consumption	0.7 lb/kw-hr (0.32 Kg/kw-hr)
Source Pressure	35 psia (24.2 n/cm^2) minimum; 1000 psia (690 n/cm^2) maximum
Thermal	
Nominal power heat rejection mode	Spacecraft surface radiators
Peak power heat rejection mode	Other than radiators; open cycle, steam venting water boiling, etc.
Coolant outlet to radiators	Maximum temperature consistent with life and performance goals
Electrical	
Voltage	117 volts with minimum to maximum variation over the operating power range of ± 5% from 20% to 100% of sustained power
Power	7 kw sustained. 21 kw (min.) peak, short duration (2 hrs) at a minimum of 100 volts
Ancillary Component Power	Minimized
Degradation	5 μ V/hr/Cell (Maximum), at sustained steady-state loads.
General	
Start-stop cycles	400
Components and controls	Minimum number, high reliability, no rotating parts.
Maintainability	Field maintenance and repair capability.
Check-out Validation	In place (installed) checkout capability
Start-up time	Instantaneous.
90% of Sustained Power	5 minutes
Shutdown Time	Instantaneous
By-Product Water	Discharged water shall meet potability requirements of MSC Specification C-21B. Water discharge parameters shall be conducive to transporting and storage.

Fuel Cell Power Section Weight

System Weight - 20 lbs/kw (9.1 Kg/kw) of sustained power

Power Output - 1.4 kw minimum, 7 kw sustained, 21 kw peak (2 Hours)

Voltage Band - 117 plus 5 percent, minus 14.5 percent over the full power range

These requirements call for a power system weighing less than 140 lbs (63.5 Kg). Based on the 2 hour peak power rating, the system specific weight is 6.7 lbs (2.99 Kg) per kw. To achieve the voltage regulation band requires a large total cell area in the fuel cell power system. For the EMS, approximately 60 ft^2 (5.57 m^2) of total cell area is required. Achieving the system weight goals with a full cell power section of this total cell area requires that the power section weight be reduced by a factor of 3 compared to the current state-of-the-art. This requires that the thickness of all power section components be significantly reduced and that low density, polymer-type materials be used.

Waste Heat and Product Water Removal Subsystems

Peak power heat rejection - Other than radiators: open cycle.

Components and controls - Minimum number, high reliability, no rotating parts.

The open cycle operating requirement of 21 kw for two hours led to the selection of direct evaporation cooling of the cells and the use of passive water removal for both the closed and open cycle modes of operation. Combining the product water removal and waste heat removal sybsystems into a common loop resulted in a considerable simplification of the controls required for a powerplant capable of both open and closed cycle modes of operation. The objective of no rotating components and minimizing parasite power was met by using the pressure energy of the reactants to drive the fluid circulators.

Cell Operating Conditions

Reactant pressure - 35 psia (24.2 n/cm^2) minimum

Operating life - 10,000 hours

Specific reactant consumption - 0.7 lbs/kw-hr (0.32 Kg/kw).

A low cell operating pressure was dictated by the minimum reactant, supply pressure specified. Allowing for component pressure losses, particularly the reactant driven coolant pump, resulted in the selection of a cell operating pressure of 16 psia (11.04 n/cm^2). Life considerations, balanced by the guidelines calling maximum coolant temperature to the spacecraft radiator, resulted in the selection of an operating temperature of 180°F (82.2°C). These operating conditions, particularly the low reactant pressure, result in unavoidable performance penalties. For example, a cell operating at a reactant pressure of 16 psia (11.04 n/cm^2) has a voltage output approximately 40 milli-volts less than if it were operated at 60 psia (41.4 n/cm^2) - the reactant pressure commonly used in other systems. This results in a specific reactant consumption for the 16 psia(11.0 n/cm^2) cell of 0.83 lb/kw-hr (0.376 Kg/kw-hr) vs. 0.80 lb/kw-hr (0.363 Kg/kw-hr) for the 60 psia (41.4 n/cm^2) case. Thus the low operating pressure is in conflict with the ambitious specific reactant consumption objective.

Cell Packaging

Voltage - 117 nominal

This voltage level requires that approximately 130 cells be connected in series electrically. To meet other requirements discussed above, the selected power section design includes plastic structural components and passive water removal assemblies as a part of each cell. These non-conducting components prevent cell-to-cell current transfer directly through the stack (current flow perpendicular to the cell plane) requiring the use of edge current transfer. Edge current transfer coupled with the large number of cells required to provide the output voltage level resulted in selecting a planar multi-cell stack method for packaging the cells. This cell packaging concept results in lower structural weight and offers flexibility in meeting different system voltage and power levels.

2.0 System Operation

The system selected to meet the EMS performance and operational objectives is shown in Figure 104. Reactants are supplied to the power section by demand type pressure regulator valves. These valves assure that the hydrogen and oxygen pressures in the stack are kept equal and at 16 psia (11.04 n/cm^2) over the full range of reactant flows associated with the power being supplied by the power section. Pressure energy in the hydrogen is being used to derive a positive displacement water pump.

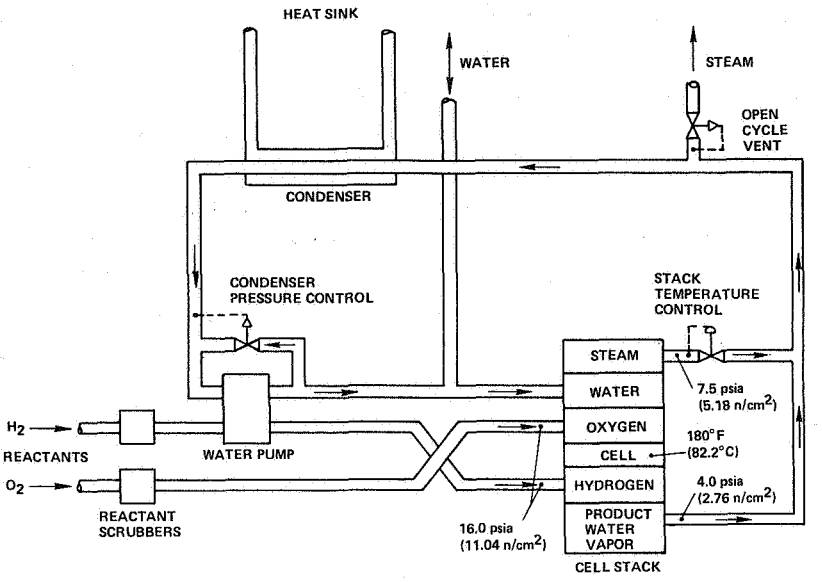

Figure 104 - Simplified EMS Schematic

Waste heat is removed from the stack by evaporative coolers located next to each cell. By controlling the cooler pressure at 7.5 psia (5.17 n/cm^2), the cell temperature is maintained at the associated water vapor temperature of 180° F (82.2° C). Product water is removed by the passive water removal method. Product water from the cell diffuses through a gas-tight water transport plate and evaporates into a 4 psia (2.76 n/cm^2) cavity. Control of this pressure maintains the proper water balance in the cells over the full EMS operating range.

The combined water vapor streams from the evaporative coolers and the product water vapor cavities flow in a common line to the condenser where the latent heat of evaporization is transferred to the spacecraft coolant. The condensate flows to the water pump. A bypass valve on this pump modulates flow to maintain the condenser pressure, and hence, the pressure in the product water vapor cavities. A portion of the pump discharge water returns to the power section for cooling. Excess water is removed from the loop and supplied to the spacecraft potable water storage system. Whenever the vapor loop heat load is greater than the spacecraft cooling loop capacity, the pressure in the vapor loop rises. This opens the vapor loop vent valve which automatically transfers the system from closed cycle to open cycle operation. During open cycle operation, water for cooling is drawn from the spacecraft water storage system.

3.0 Power Section Components Description

The basic components of the Engineering Model System Power Section are the cell, the passive water removal water transport plate, and the evaporative cooler. The schematic diagram of the evaporative cooler is shown in Figure 105. The cooling water side is located adjacent to the cell oxygen passages. The water cavity is separated from the steam cavity by a porous hydrophobic membrane. The non-wetting characteristic of this membrane prevents water flow but allows vapor and gases to flow through it. Waste heat from the cells flows through the oxygen water plate causing the water to evaporate. This water vapor passes through the membrane pores and into the vapor cavity. As shown in the system schematic, Figure 104, make-up water is automatically supplied to the water cavity by a pressure regulator which maintains a constant water to steam overpressure during all operating modes. By controlling the pressure in the steam cavity, the corresponding evaporation temperature is set, maintaining the cells at a constant operating temperature.

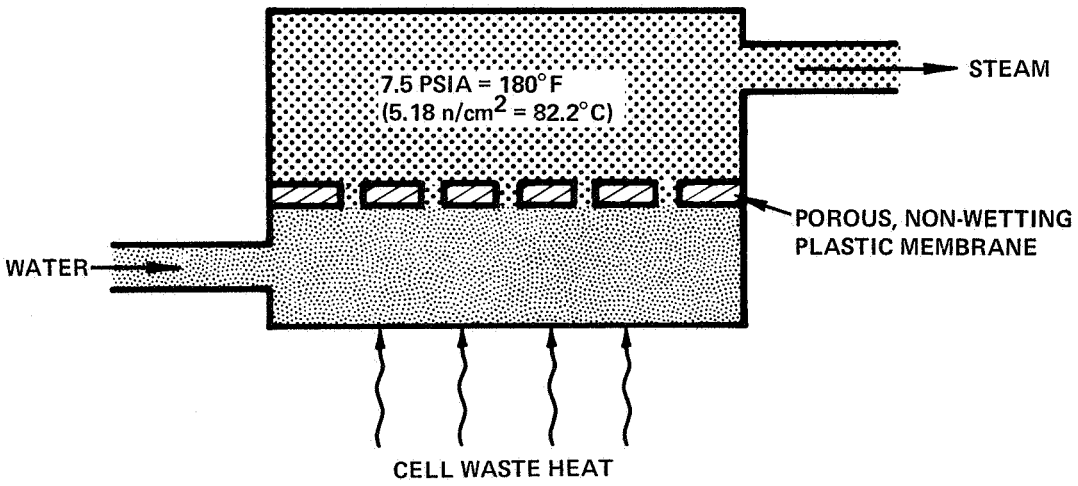

Figure 105 - Evaporative Cooler

The water transport plate is shown schematically in Figure 106. Its functions are to : 1) allow diffusion of product water from the cell to the vapor cavity, and 2) seal the 16 psia (11.04 n/cm^2) hydrogen from the 4 psia (2.76 n/cm^2) water vapor. The water transport plate consists of an electrolyte filled matrix similar to that used in the fuel cell. This fine pore structure provides a gas seal and offers a low resistance path for diffusion of the product water. The electrolyte reservoir for the matrix is provided to accomodate the electrolyte volume changes that occur during different operating conditions assuring that the matrix

is always filled with electrolyte. To prevent electrolyte loss from the water transport plate under transient conditions an electrolyte barrier is provided. This barrier consists of a fine pore hydrophobic membrane similar to that used in the evaporative cooler. It allows vapor to pass through its pores while retaining electrolyte. The 4 psia (2.76 n/cm^2) water vapor pressure combined with the 180°F (82.2 °C) cell temperature results in a nominal 34 percent electrolyte concentration in the cell.

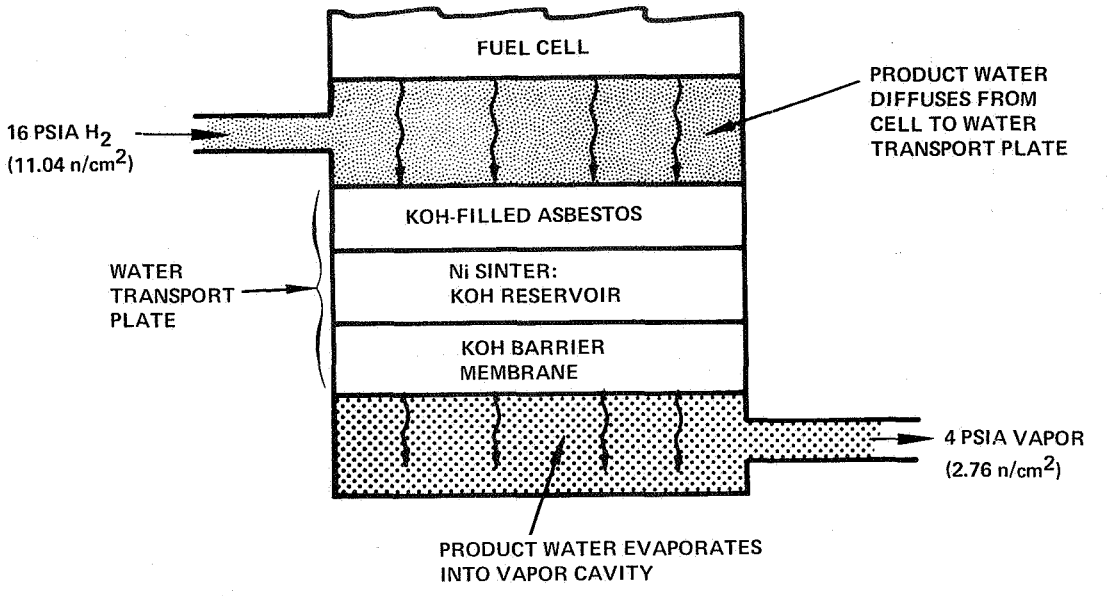

Figure 106 - Passive Water Removal

4.0 Ancillary Components Description

The components used in the reactant supply and the water vapor loop are the coupled reactant regulator, absolute and differential pressure regulators, the reactant driven water pump and the condenser. Control of the reactant supply to the stack is provided by a coupled hydrogen and oxygen pressure regulator. The coupled reactant regulator maintains the hydrogen and oxygen pressures equally and at the desired level over the full range of system supply pressure. The regulator consists of hydrogen and oxygen regulators coupled by an aneroid bellows sense assembly.

Pressure regulating valves used in the vapor loop are: 1) the evaporative cooler steam pressure regulator, 2) the cooling water to steam differential pressure regulator; 3) the open cycle vapor vent regulator, and 4) the condenser pressure control regulator. Three of these regulators are of the absolute pressure sensing type set to maintain a given pressure within

a small control band. The water supply regulator is similar except that it is referenced to the cooling steam to maintain a set differential pressure.

The reactant driven pump is a diaphragm type using spool valves to control the reactant flow, and check valves to control water flow through the pump. Reactant pressure operating on one side of the diaphragms forces the assembly in one direction; when it comes to the end of its travel a pilot valve reverses the reactant flow direction and the pump travels in the opposite direction. The pump requires no electrical power or controls. The only moving parts are the oscillating diaphragms and spool valves. Prototypes of reactant driven coolant pumps have been tested under other programs.

The condenser which converts the product water vapor and the steam from the evaporative coolers to liquid water is a plate-fin type heat exchanger cooled by the spacecraft coolant system. This component is discussed in Section VI, A.

5.0 Power Section Sizing

The basic cell voltage-current density characteristic is used to size the power section. The engineering model system cell performance model is based on high power density cell test data generated over wide ranges of pressure, temperature and current densities: pressures of 15 to 60 psia(10.3 to 42.4 n/cm^2), temperatures of 150 to 250°F(65.5 to 121.1 °C), and current densities to 3000 ASF(3228 ma/cm^2). To prepare an EMS cell performance model, these data were corrected to the 16 psia (11.04 n/cm^2), 180°F(82.2°C) EMS cell operating conditions. The estimated performance at EMS operating conditions is shown in Figure 107, along with data from the high power density cells. The figure indicates the high activity and low polarization losses of the high power density cell and shows the lower level of performance which results from the 16 psia(11.04 n/cm^2) operating pressure. The EMS performance model used in system studies is shown in Figure 108. The initial performance line is the same as the cell performance at the 16 psia (11.04 n/cm^2), 180°F(82.2°C) temperature shown in Figure 107 with allowances made for edge current conduction losses. The performance line labeled "minimum" is the result of a 21 mV allowance for performance decay over the 10,000 hour operating duration. These initial and minimum performance models were used in a series of trade studies to select the total cell stack area and the number of series connected cells for the EMS stack.

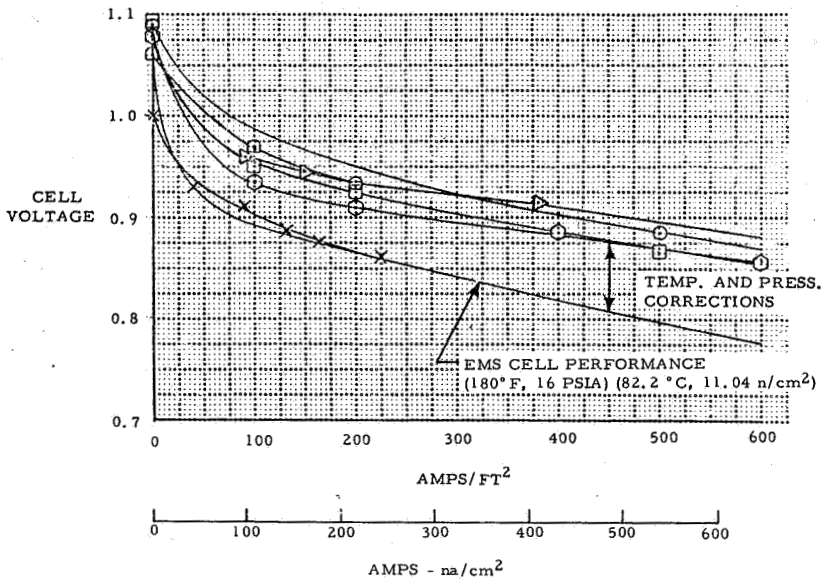

Figure 107 - High Power Density Cell Performance

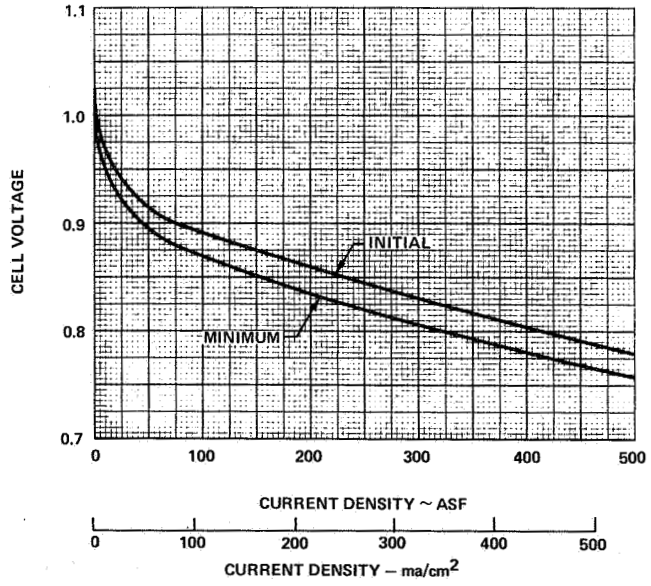

Figure 108 - EMS Cell Performance Model

The EMS power section contains 60 ft^2(5.57 m^2) of the total cell area divided into 132 equivalent series connected cells. The selection of this total cell area resulted from studies of reactant consumption, voltage regulation, and powerplant weight. Increased cell area results in lower reactant consumption and improved voltage regulation at the expense of increased powerplant weight. The mechanics of sizing a power

section involve an iterative procedure to select the total cell area and number of series connected cells that satisfies; a) minimum voltage requirement at maximum power output and maximum cell performance, and b) maximum voltage requirement at minimum power output and maximum cell performance. EMS sizing required that an additional condition be satisfied since minimum powerplant voltages are specified at two power levels (100 volts at 21 kw and 117 minus 5 percent volts at 7 kw).

The selected stack size of 60 ft^2(5.57 m^2) of total cell area with 132 equivalent cells in series was selected based on the following:

- It satisfies minimum voltage requirements at both 21 and 7 kw with margin.
- Although it does not meet the maximum voltage requirements, a voltage limiter can be used at low power. Additional studies showed this to be the most weight-effective solution to meeting this type of voltage regulation specification.
- The resulting voltage vs power characteristics are considered adequate since actual Space Shuttle voltage requirements are not fully defined and the primary purpose of the preliminary design EMS is to provide guidelines for the technology advancement tasks of this program.
- 132 equivalent cells in series provides greater flexibility in cell and plaque arrangement, i.e., the number of cells per plaque and the series-parallel electrical arrangement of plaques within the stack.

6.0 Power Section Description

Introduction

The EMS stack components are the cells, arranged in plaques, the passive water removal water transport plates and the evaporative coolers. To meet weight goals, plastic structural components were selected. The use of non-electrically conducting stack components - the water transport plate, the evaporative cooler, and the non-metallic reactant and the coolant flow distribution plates - requires the use of edge current flow to connect the cells in series electrically. Edge current transfer requires different approaches for minimizing resistance losses than those used in stacks where current flows through the stack,

perpendicular to the cell plane. Both electrical connection arrangements have resistance losses associated with transferring current from cell to cell. Losses in the through stack arrangement are due to the resistance of the metal plates used to form the reactant and coolant flow cavities and the contact resistance between adjacent plates and the cell. In the edge current transfer arrangement, the losses are due to the resistance of electrode substrate. They are minimized by selecting low-width cells i.e. - rectangular cells of high aspect ratio.

There is significant flexibility in selecting cell geometry for edge current transfer stacks. This is illustrated by the results of a parametric weight study. Figure 109 shows the trade-off which can be made between minimizing cell frame weight and the weight of the cell current conductor. The square cell geometry minimizes the amount of perimeter per unit area thus keeping the weight of the frames to a minimum. Because of the longer path for current flow, the cross sectional area of the current carrying cell member, the electrode screen, must be increased to keep resistance losses low. A high aspect ratio cell geometry reduces conductor weight at the expense of higher frame weight. Figure 110 shows how an arbritarily selected area of 0.25 ft^2(232 cm^2) - could be packaged into 4 different geometry cells varying from square (6 x 6 inches)(15.2 x 15.2 cm) to a high aspect ratio rectangle (2 x 18 inches)(5.1 x 45.6 cm). In each design, the fluid manifold area was kept the same as was the IR loss from tab to tab. The latter was accomplished by changing the wire diameter of the current transfer screens which are a part of each electrode.

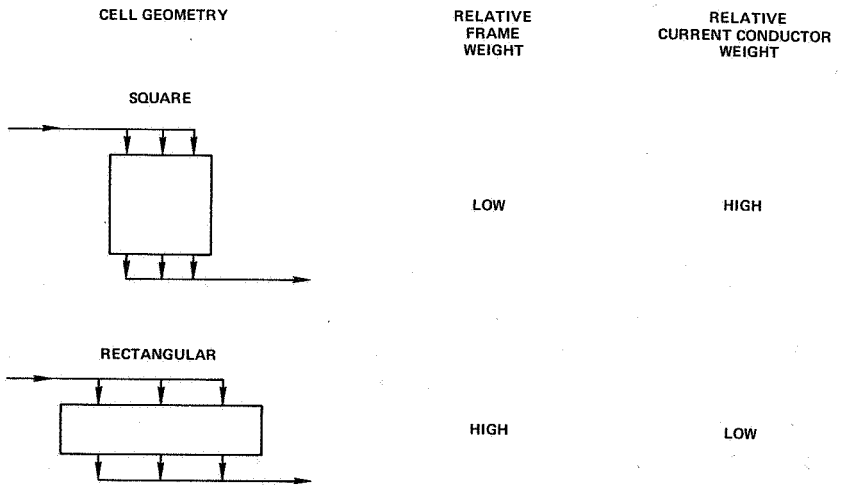

Figure 109 - Design Options for Edge Current Transfer Cells

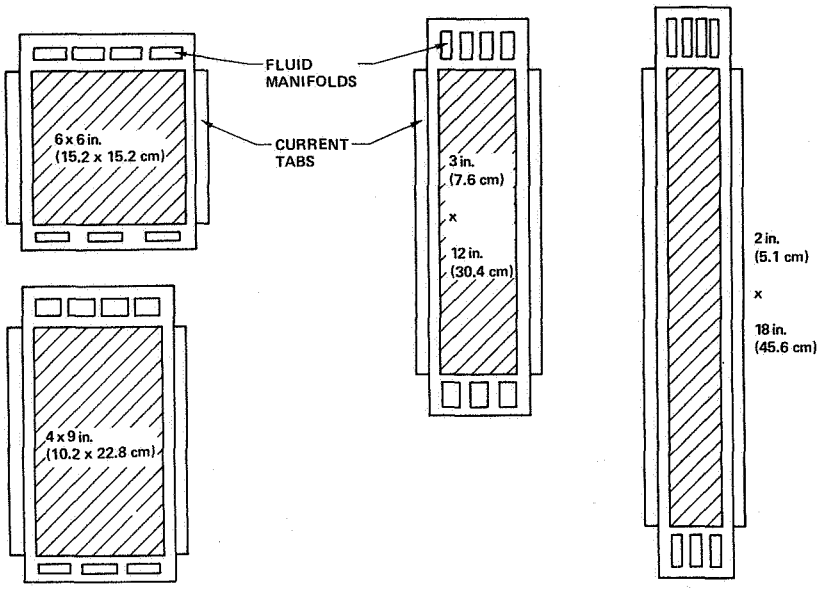

Figure 110 - Various Cell Geometries for Edge Current Transfer Cells 36 in^2(232 cm^2) Active Area

The relatively poor frame weight per unit area of the rectangular cells can be improved by grouping cells into a plaque. A plaque is defined as an edge current transfer cell assembly with the number of cells per plaque ranging from one to as many as desired. The improved packaging efficiency available with the plaque is illustrated in Figure 111. This figure shows that as additional cells are arranged in plaque form, the overall assembly approaches a square format. Economics of scale also result since the perimeter to area ratio for large total cell area is less than for small areas. Both effects result in a lower frame weight per unit of active area for plaques which contain several cells.

The results of this parametric weight study are shown in Figure 112. Plaque weight per unit cell area is shown as a function of the number of cells of a given geometry packaged into a plaque. The weight is made up of the cell elements, the edge frame and the intercell seals. The cell elements included are the electrodes with their current conducting screens, the matrices, and the non-metallic electrolyte reservoir plate. Other power section components which are a constant weight per unit area are not included. The figure shows the narrower cells result in significant weight savings. Further weight reduction results from grouping a number of cells together in a plaque. It is seen that considerable latitude is available to select cell geometry and a number of cells per plaque to achieve a balance between minimum weight and practical package size.

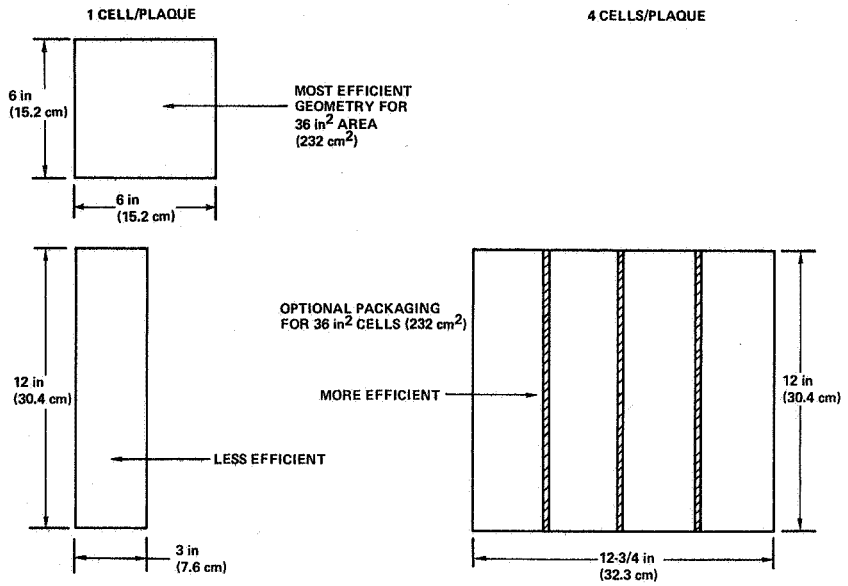

Figure 111 - Effect of Geometry on Frame Weight

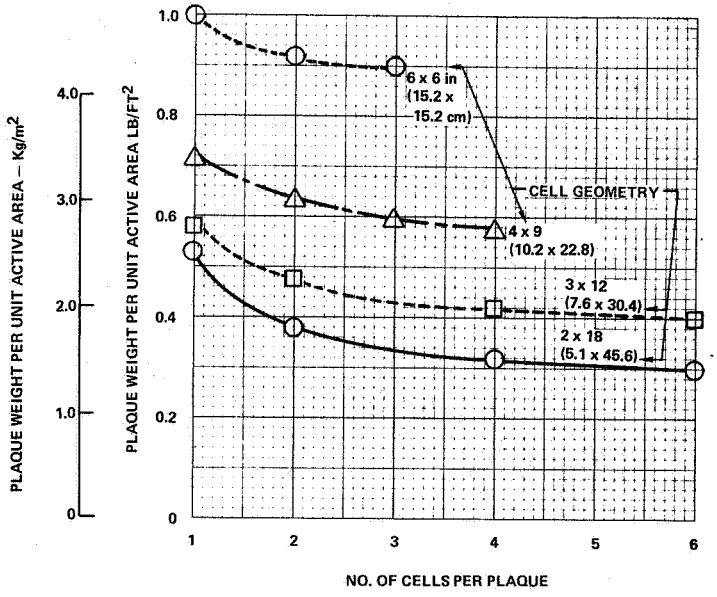

Figure 112 - Effect of Cell Geometry and No. of Cells per Plaque on Plaque Weight

With lightweight cell construction, which the plaque concept makes possible, it is feasible to use a number of smaller cells rather than a single large one. This can improve reliability of a power system by allowing arrangement of the total cell stack area into a group of electrically parallel substacks. For example, if a powerplant requires a total cell area of 30 ft^2

(2.79 m^2) and 30 series connected cells to meet system voltage-power requirements, the power section could consist of either one stack of 1.0 ft^2(929 cm^2) cells, two parallel connected stacks each using 0.5 ft^2 (464 cm^2) cells, or four parallel connected stacks containing 0.25 ft^2 (232 cm^2) cells.

EMS Cell/Plaque Arrangement

The approach described above was taken in packaging the 60 ft^2(5.57 m^2) of total cell area and the 132 series connected cells required for the EMS power section. The total cell area was arranged so the total powerplant current flows in four parallel paths. A malfunction which could cause a loss in performance in any one path would result in the cells in the other three paths picking up more of the load thus minimizing the net effect on the system.

The series - parallel electrical arrangement of the EMS power section is based on the use of six cells per plaque. Four plaques are connected in parallel to form a substack; thus each plaque carries one-fourth of the total system current. 22 substacks are connected in series to form the complete stack of 132 series connected cells.

The plaques with their water transport plates, the evaporative coolers and product water vapor spacers are grouped together as shown in Figure 113 to form the complete power section. The power section contains 88 plaques 44 evaporative coolers and 45 product water vapor spacers, housed between end plates.

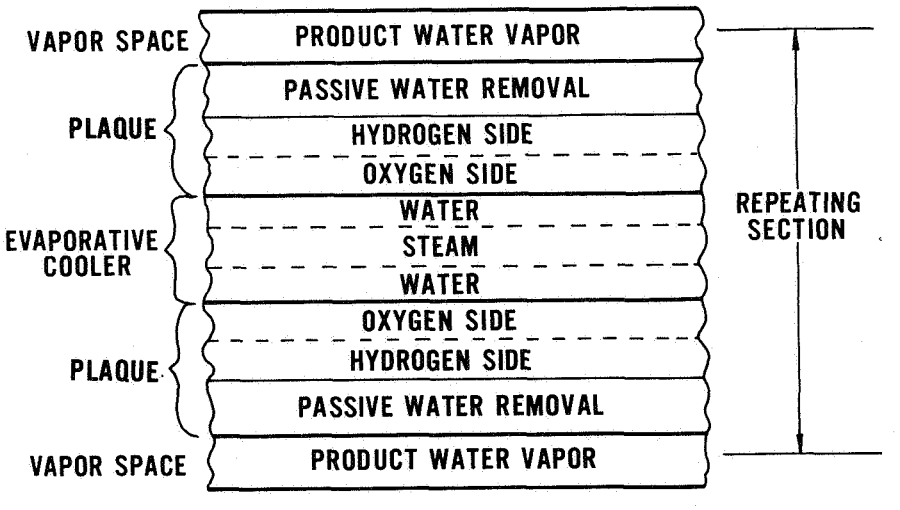

Figure 113 - EMS Stack Concept

Plaque Description

The EMS baseline plaque is an integral assembly containing six cells, intercell seals, and manifolds molded into a plastic edge frame. A plan view of the plaque is shown in Figure 114. Each cell is 12 inches (30.4 cm) long and 1.37 inches(3.48 cm) wide (16.4 in^2(106 cm^2) active area). Total active area per plaque is 0.68 ft^2(630 ft^2). The six cells are electrically connected in series by connecting the anode of one cell to the cathode of the adjacent cell through the intercell seal. These seals are 0.25 inches(0.64 cm) wide and insulate adjacent cells from each other, physically support the various cell elements, and isolate the reactant gases from each other at the cell edges. The 0.50 inch (1.27 cm) wide edge frame assembly is molded around the cells and fluid manifolds to provide a unitized plaque assembly.

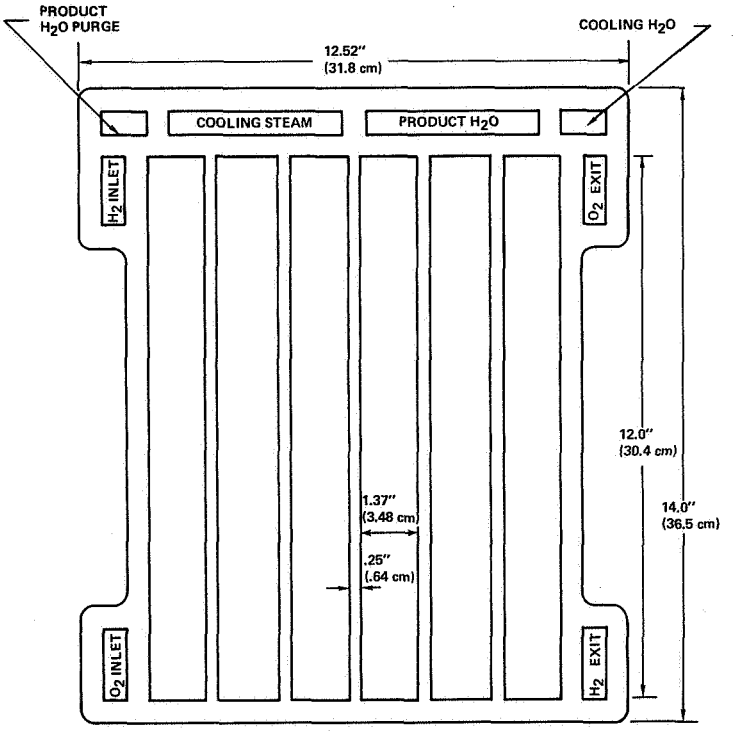

Figure 114 - EMS Baseline Plaque Plan Form

Fluid distribution is handled in two steps: manifolds and ports. Manifolds are fluid flow passages perpendicular to the plaque plane; they provide flow to or from the ports. They are formed when the openings in the edge frames of adjacent stack components are aligned during final stack assembly. As shown by the plaque plan form, there are eight manifolds within the EMS stack; two for reactant gas inlet, two for reactant gas

purge, one for cooling water inlet, one for cooling water vapor exit, one for product water vapor exit, and one for product water vapor purge.

Ports are fluid flow passages parallel to the plaque plane. They provide the flow path between the manifolds and cells. Manifolds and ports are sized to provide low pressure drops consistent with uniform plaque-to-plaque flow distribution.

The reactant purge manifolds are larger than required by flow considerations and were chosen to make the plaque plan form symmetrical. A cross-sectional view of the plaque and the associated water transport plate is shown in Figure 115. The figure shows the relationship of the component ports, their thicknesses and materials. The total thickness of the cell is 44 mils(1.12 mm) and the water transport plate 24 mils(0.61mm). A 10 mil(0.25 mm) hydrogen flow spacer is used resulting in a total passive water removal fuel cell assembly thickness of 78 mils(2.01mm).

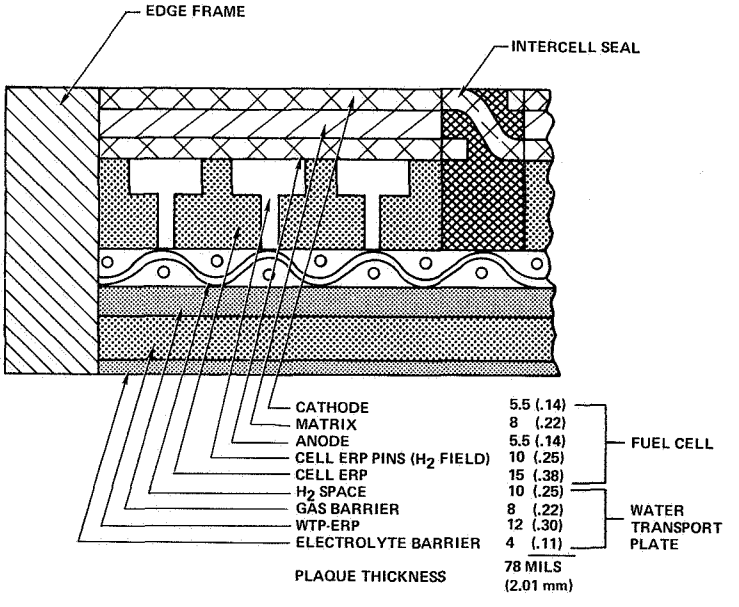

Figure 115 - Cross Sectional View of Plaque

Evaporative Cooler Description

Waste heat is removed by the evaporation of water in cooler assemblies positioned between the cathodes of adjacent plaques. Total thickness of the cooler assembly is 98 mils(2.5 mm) and the planform size is the same as the plaques. Evaporative stack cooling has two distinct advantages: 1) it maintains an isothermal plaque, which in combination

with passive product water removal maintains uniform cell electrolyte concentration; and 2) vapor is easily vented overboard for open cycle heat removal if the spacecraft radiator is inoperative or is reduced in capacity.

Figure 116 shows the cooler cross section. It contains a water vapor spacer between the supported hydrophobic separators enclosed by two coolant plates. With this design, a liquid water reservoir is maintained adjacent to the plaque on either side of the cooler assuring good thermal control of both plaques. One vapor chamber accomodates the steam emanating from both separators. The supported hydrophobic separators, the vapor spacer and the coolant plates are bonded together at their edges to form a unitized assembly. These edge frames, as with the plaque edge frames, contain the sealing surface area, manifolds and ports.

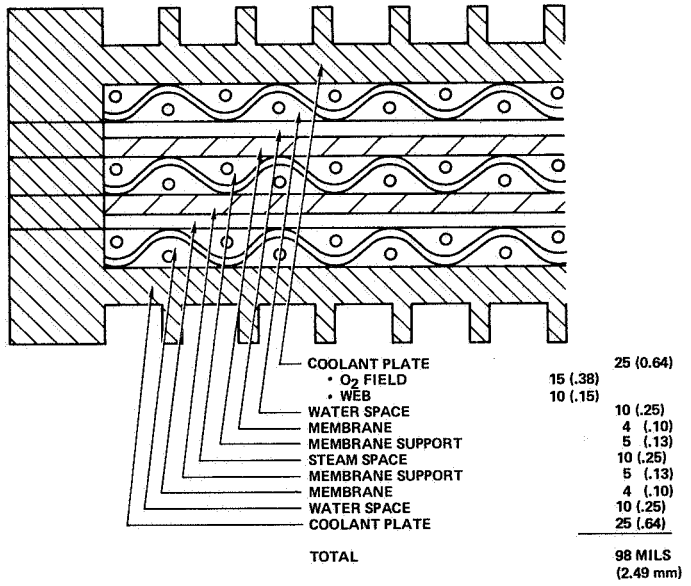

Figure 116 - Cooler Cross Section

The coolant plates are unfilled plastic and serve three basic functions: 1) they form oxygen and liquid cooling water flow fields, 2) they provide the heat conduction path from the cells to the cooling water, and 3) they provide the desired electrical insulation between adjacent back-to-back plaques. A pin and bar pattern on one side of the plate covers 50 percent of the plaque area and forms the 0.015 inch(0.38 mm) deep oxygen flow field while the other side contains space for a 0.010 inch(0.25 mm) thick plastic mesh to form the water flow field. Waste heat is conducted from the cells through the pin and bars of the oxygen flow field and the plate

web to the cooling water. Hydrophobic separators are 4 mil(0.10 mm) porous sheets of TFE with the structural integrity to withstand approximately 5 psi(3.45 n/cm^2) pressure differential. They are porous to allow the passage of steam from the liquid surface to the lower pressure vapor chamber. The hydrophobic properties of the separator also allow the passage of any non-condensable gases that might be present in the water reservoir. A plastic cloth, considerably more porous than the separator but of a finer weave than the steam and water flow field mesh, is bonded to the separator for mechanical support.

The vapor chamber spacer is a 10 mil(0.15 mm) thick plastic mesh which separates and supports the hydrophobic separators and forms the steam flow channel. It is configured to allow vapor parallel to the plane of the hydrophobic separators.

All flow passages are sized to provide proper distribution and low pressure drops as discussed in a later section. All elements within the cooler assembly are designed to transmit a lateral compressive load sufficient to ensure good thermal contact between the cooler and adjacent plaques.

Power Section Size and Weight

Envelope dimensions of the EMS baseline stack are 13.5 x 14 x 11.6 inches (34.3 x 35.5 x 29.5 cm). The estimated total weight is 60.1 lbs (27.2 Kg). Details of this total weight are shown in Table 17.

TABLE 17

EMS Power Section Weight

Assembly	Weight, lb(Kg)
Fuel Cell	30.6(13.9)
Water Transport Plate	13.8(6.2)
Evaporative Cooler	15.7(7.1)
TOTAL	60.1(27.2)

The EMS section weight estimates are based on the cell, water transport plate and evaporative cooler configuration defined above. These configurations differ from those of the passive water removal cells and plaques and evaporative coolers tested during the program in only the heights of certain flow fields. The thickness dimensions of the fuel cell, water transport plate and oxygen/water coolant plate configurations tested were equal to or less than those of the baseline design as a review of Section IV will show. Flow field spacers larger than baseline dimensions were used where procurement lead time and cost did not permit their use in the first phase of this program. Commercially available screens were used for the hydrogen, product water vapor and cooling steam flow fields. Analysis indicates that flow fields with better pressure drop-flow characteristics would allow reduced thicknesses for these ports. The cost impacts of using these "tailor-made" flow field spacers will be evaluated during the Phase 2 portion of the program.

One other difference between the hardware tested and the baseline design has an effect on the power section weight estimate. The electrolyte reservoir plates (ERP's) used in all cell and plaque tests were made of porous nickel rather than the non-metallic materials specified in the baseline EMS design. Because of the success of the lightweight electrolyte reservoir plate research efforts described in Section III, ERP's with weight characteristics used in the EMS estimates show high promise for becoming available.

7.0 Flow Studies

Plaque and stack fluid flow studies were conducted to define flow passage configurations which have proper flow distribution and pressure drop characteristics. The flow passages for hydrogen, oxygen, cooling steam and product water vapor were studied. The criteria used for design of the reactant gas flow passages were: 1) the gases cannot back-flow during purge, and 2) the system must be able to purge to atmospheric pressure.

Flow trade-off studies were conducted to define manifold, port and field configurations. The basic field flow configuration selected was that of sweep flow along the cell/plaque length with the hydrogen and oxygen flowing in opposite directions. Counterflow of reactant gas minimizes the possibility of inlet drying and the development of concentration gradients along the cell length.

A computer analysis was used to predict plaque and stack pressure drops and to predict the degree of flow maldistribution caused by manufacturing tolerances on flow passge dimensions. A plus or minus 2 mil(0.05 mm)

manufacturing variation on all critical dimensions was assumed. Table 18 presents the flow study results which show adequate purging from cell-to-cell within a plaque and from plaque-to-plaque within the stack.

TABLE 18

Flow Study Results

	Hydrogen	Oxygen
Flow through exit manifold during purge, % of consumption flow	25	50
Stack inlet flow - lb/hr (Kg/hr)	2.96(1.46)	28.2(13.9)
$\frac{\text{Minimum cell channel purge}}{\text{Average cell channel purge}}$ - %	53	34
Pressure drop of field and secondary - psi (n/cm^2) manifolds	0.15 (0.10)	0.26 (0.18)
$\frac{\text{Minimum plaque purge}}{\text{Average plaque purge}}$ - %	41	9
Stack pressure drop - psi(n/cm^2)	0.29(0.20)	0.48(0.33)

The oxygen flow study summarized here was completed before it was determined that the oxygen recycle loop would be a part of the EMS. The additional plaque exit flow and the increased oxygen flow field height, of 0.015 inches(0.38 mm), will result in improved oxygen flow distribution.

Computerized finite difference analyses were conducted to predict the pressure drops for the cooling steam and product water vapor manifolds, ports, and fields. These pressure drops are particularly important since they are factors that must be considered in determining cell electrolyte concentration. Steam and product water vapor pressure drops vary with flow (power output) and are one of the causes of cell electrolyte concentration variations. To minimize this concentration variation, cooling steam flow and product water vapor flow paths are parallel to each other. Temperature-water vapor pressure-concentration characteristics of potassium hydroxide electrolyte are such that concentration variations are minimized if water pressure variations (cell product water vapor pressure) are accompanied by corresponding temperature variations (cell cooling steam pressure).

Ports for the two flow fields are extensions of the field so that the mesh fills the area between the fields and the manifolds. The flow passage model used for the cooling steam and product water vapor is the same as that used for the reactants except for the port configuration. At the time these studies were conducted, design data for flow in the plane of meshes (as occurs in the steam and product water vapor fields) were unavailable, nor was mesh of the desired size available for design information testing. Therefore, flow through the meshes were approximated as flow in small channels through successive expansions and contractions. Future phases of this program will include design information testing of flow through meshes or other recommended flow field configurations. This information will then verify or suggest the required modifications or re-design of the EMS cooling steam and product water vapor flow fields.

8.0 Electrolyte Reservoir Plate Requirements

For effective operation, certain elements within the cell (anode, matrix, and cathode) and the water transport plate (gas barrier) must always be full of electrolyte. Electrolyte reservoir plates (ERP's) are included in the plaque assembly to accommodate changes in electrolyte volume during system operation. The actual required thickness of the ERP's is a function of; a) the range of electrolyte concentration variations, b) the useable capacity of the ERP, and c) the volume of electrolyte contained within the plaque elements that must remain full.

Electrolyte concentration variations during system operation results primarily from; a) cell temperature and water vapor pressure variations caused by droop and hystersis characteristics of the system pressure regulators, b) variations in the temperature gradient from the cell to the evaporative cooler, and c) temperature and water vapor pressure variations caused by variations in pressure drops of cooling steam and product water vapor through flow fields, manifolds, and ports. The net result is that cell temperature and water vapor pressure, therefore electrolyte concentration, varies with power output, from plaque-to-plaque within the stack, and with location in each plaque. The magnitude of cell temperature and pressure variations due to each of the above causes has been discussed above. The electrolyte concentration variation was estimated for the end and exit of the 1st and 88th plaques to establish the maximum variation. The largest electrolyte concentration variation due to all the above affects was found to be 28 to 42 weight/percent KOH. This results in a maximum-to-minimum electrolyte volume ratio of 1.7 during normal EMS operation.

Fill and expulsion data of sintered nickel plates used as ERP's in high power density cells along with a plate porosity of 70 percent were used in determining the thickness of the ERP's. Calculations based on these considerations were conducted to determine that the ERP web thicknesses required for normal EMS operation are 11.4 mils(0.29 mm) for the cell and 9.0 mils(0.23 mm) for the water transport plate.

Two other effects require consideration in the selection of ERP thickness; electrolyte carbonation and bootstrap startup. Since one of the goals of the technology advancement program is the development of highly compatible cell structures, no allowance for structure produced carbonation is provided. In addition, it is envisioned that the EMS will incorporate reactant purifiers to limit the CO_2 content of the incoming reactants to 0.25 ppm. With this CO_2 ingestion rate, the conversion of KOH to K_2CO_3 will be less than 5 percent over the 10,000 hour EMS life. This low level of carbonate formation has a negligible effect on ERP thickness.

During a bootstrap start, the water removal system remains inoperative until the cell stack has attained a temperature approaching normal operation levels. The product water formed during this interval remains in the cell as a liquid. ERP thickness, in addition to that necessary for the concentration variations during normal operation discussed above, must be provided to store the startup product water. The amount of startup product water (therefore required startup ERP thickness) depends primarily on the stack heat capacity and whether or not the EMS energy output is returned to the stack via electric heaters. Total ERP thickness for bootstrap startup was estimated to be 3 to 7 mils(0.08 to 0.18 mm) depending on the amount of EMS energy output being returned to the stack. As a result, a 5 mil(0.13 mm) bootstrap startup allowance was proportioned between the cell and WTP ERP's. The resulting total ERP web thickness for the cell is 15 mils(0.38 mm) and 12 mils(0.30 mm) for the water transport plate.

9.0 System Controls

EMS stack operating conditions are maintained by monitoring and controlling two parameters - stack temperature and product water vapor pressure. In the preliminary design EMS, each of these parameters is measured and controlled independent of the other. As explained earlier, stack temperature is indirectly controlled by a pressure regulator at the cooling steam exit. Product water vapor pressure is controlled during closed cycle operation by a pressure regulator that varies the condensate pump bypass flow rate. During open cycle operation, it is controlled by varying steam flow to space through the vent regulator.

Two alternates to this concept have been identified and can reduce the electrolyte volume variation caused by control valve tolerance and cell-to-cooler temperature gradient. These would, therefore, reduce the required ERP thicknesses as discussed earlier, resulting in reduced stack weight. The alternates are; a) direct control of stack temperature and b) coupling of the two controls. Direct stack temperature control eliminates the cell temperature variation caused by cell-cooler temperature gradients (up to 20° F(11.1° C) at peak point for the preliminary design EMS). With coupled controls, variations in one parameter (caused by control tolerance, indirect sensing, etc.) is accompanied by a corresponding change in the other parameter. In this way, cell electrolyte concentration can be maintained within a narrower range even though cell temperature and water vapor pressure change.

To study the effects of these alternate control concepts, only electrolyte volume variations caused by control tolerances and cell-to-cell temperature gradients were considered. Figure 117 summarizes the results of this study and shows that a significant reduction in electrolyte volume ratio is realized if either or both alternates are used. The figure shows the relationship between electrolyte volume ratio and temperature variation (tolerance of the cell temperature control due to droop and hysteresis) for both the independent and coupled controls. Curves are included for direct and indirect cell temperature sensing (0 and 20° F (0 and 11.1° C) cell-to-cooler temperature gradient). A ± 0.2 psia (0.14 n/cm^2) tolerance on product water vapor pressure control is included. To illustrate the effects, consider a 3° F(1.7° C) temperature variation (this is consistent with cooling steam pressure variation of about 0.5 psia (0.35 n/cm^2) as included in the preliminary design EMS). The figure shows that electrolyte volume variation can be decreased from 1.73 to 1.11 if both alternates are included. Considering the alternates individually, the reduction is to 1.52 for direct cell temperatures sensing only and to 1.27 for coupled controls only.

Based on this study it is clear that these two alternates should be considered further in future phases of the program. The benefits can be utilized in either of two ways; a) to reduce stack weight since a lower electrolyte volume ratio means ERP thickness is required, or b) to relax tolerance requirements on control components with minimum impact on stack weight.

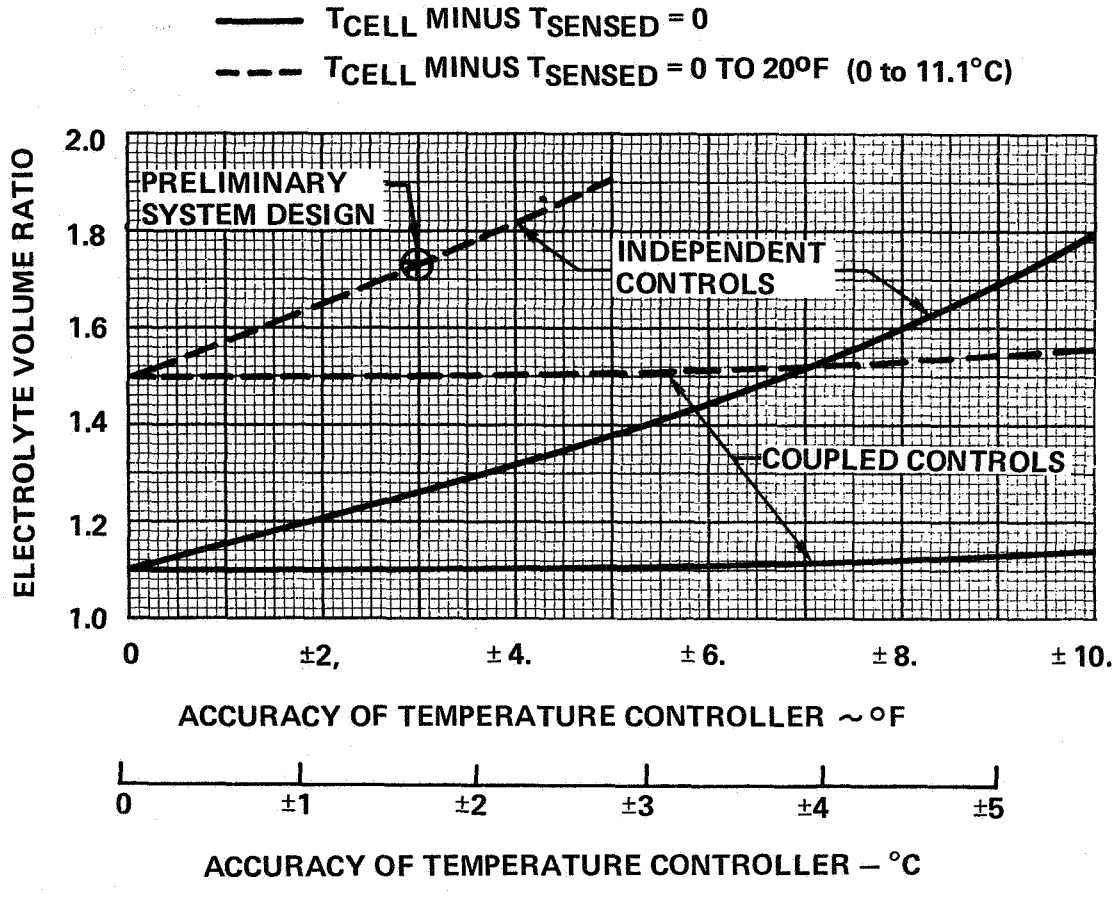

Figure 117 - Results of Alternate Control Concepts Study

10.0 System Characteristics

System Operation

A complete schematic of the EMS is shown in Figure 118. The functions of the additional components, not shown in the simplified schematic of Figure 104, are described below:

Oxygen Recycle - An ejector and recycle line are provided to accomplish:

1) Better distribution of inerts to increase time between purges and

2) Humidification of the oxygen to preclude any possibility of inlet drying.

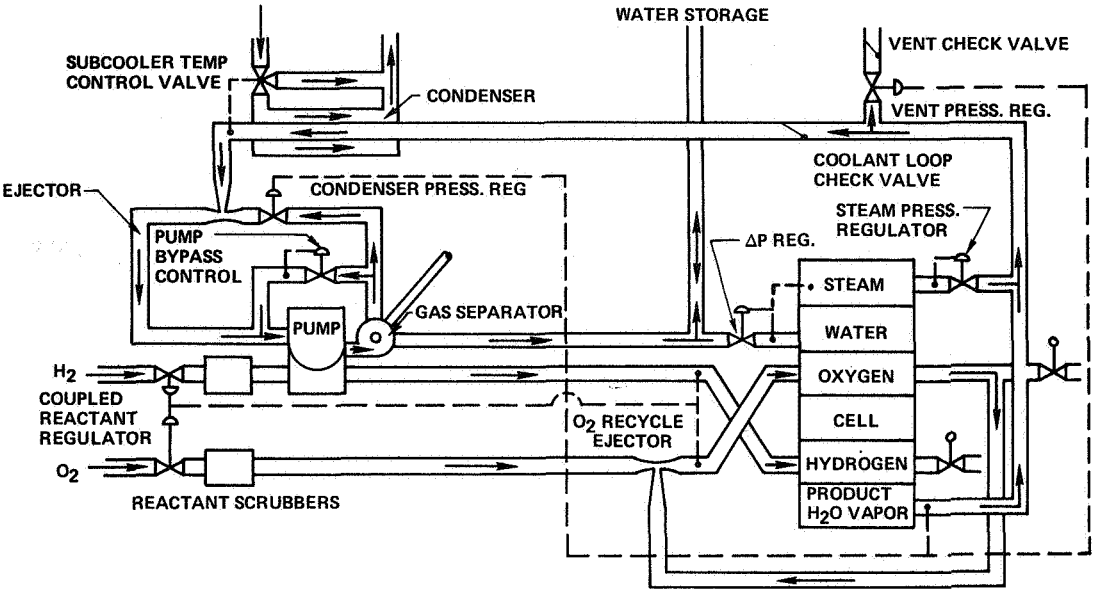

Figure 118 - EMS System Schematic

Condenser Discharge Ejector and Pressure Regulator - This loop controls the product water vapor pressure by varying the primary flow of the high pressure water to the ejector. Should the product water vapor pressure be too high, the valve opens to increase flow to the ejector lowering the pressure in the condenser. The ejector also pressurizes the condensate flow allowing the pump to handle condensate with less sub-cooling and/with a greater fraction of non-condensable gases.

Pump Bypass Control - The excess water flow not required by the ejector is bypassed by this line.

Gas Separator - The separator removes non-condensable gases from the water loop. The pump discharge pressure is approximately 15 psia (10.3 n/cm^2) allowing direct venting of non-condensables to atmosphere.

Cooling Loop Check Valve - During open cycle operation with the condenser inoperative, this valve prevents cooling water from back-flowing into the vapor line.

Purge Valves - Valves for periodic purging of inerts in the hydrogen and oxygen are provided. Additional valves are provided for purging the water cavities and vapor lines before and after storage.

The EMS is capable of operating over its full power range with or without the spacecraft heat sink in operation. The condenser is sized to condense all cooling steam and product water vapor at a power level of 7 kw. The condensed product water vapor is removed from the loop and transferred to the spacecraft potable water storage system. As power increases above 7 kw, the condenser cannot maintain the desired pressure in the product water vapor line and the open cycle vent valve opens. Since the condenser is still operating, the vent flow removes only the excess vapor which the condenser cannot handle. At power levels between 7 and approximately 10.5 kw, there is sufficient product water being condensed to provide the cooling water required, therefore, excess water continues to be transferred to the spacecraft. Above 10.5 kw additional cooling water is required and the water flow direction is from the spacecraft to the EMS.

If the spacecraft heat sink is completely inoperative, water from the spacecraft is supplied for cooling over the full power range. The water flow to and from the spacecraft as a function of output power is shown in Figure 119. The upper solid and dotted lines is the amount of product water produced in the cells. The upper solid line shows the flow of water to and from the spacecraft if the radiator remains operative. The lower solid line defines the product water flow from the spacecraft if the condenser heat sink is not available.

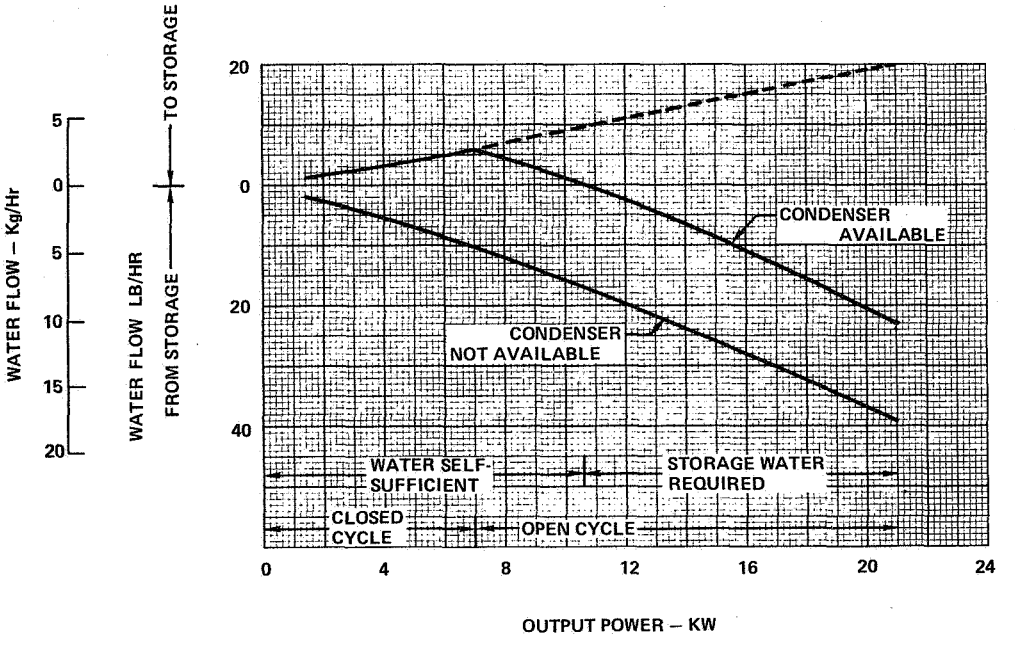

Figure 119 - Water Flow to and from Spacecraft

System Performance

The specific reactant consumption of the EMS as a function of output power is shown in Figure 120.

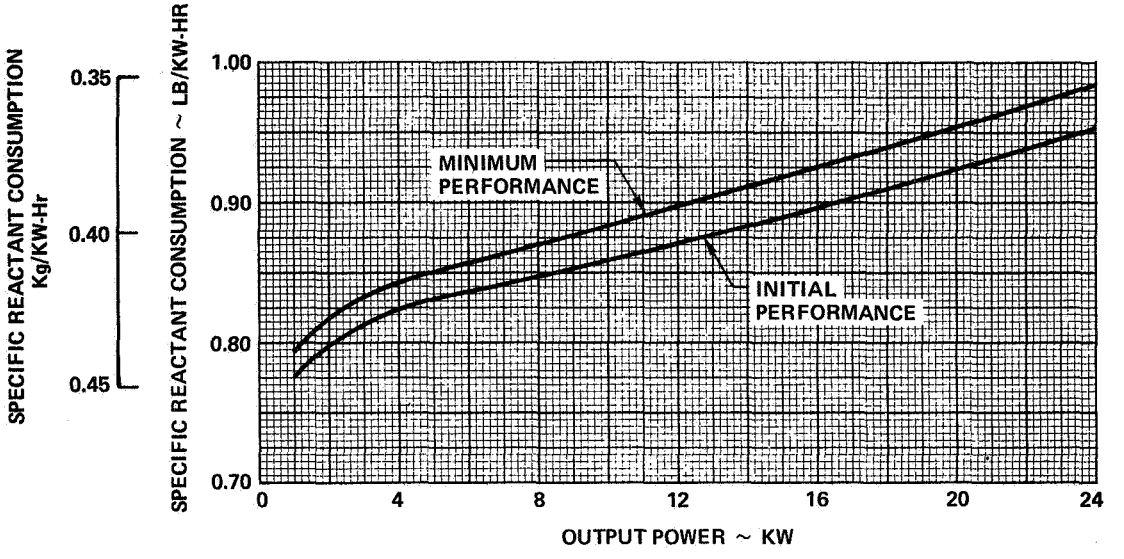

Figure 120 - EMS Specific Reactant Consumption

System voltage versus output power is shown in Figure 121. The EMS meets all system voltage regulation requirements with substantial margins at the 7 kw sustained power and 21 maximum power levels. The use of a voltage limiter to hold system voltage below the maximum allowable level at the 1.4 kw minimum power point was judged to be most weight effective. A voltage limiter allows a system to operate down to zero net power within specified voltage regulation.

The current density at 21 kw is 460 ASF(495 ma/cm^2). At the 7 kw sustained power level, the cells are operating at a current density of 136 ASF(146 ma/cm^2). Based on a NASA provided load profile, the average EMS output during a typical Space Shuttle mission would be approximately 5 kw. Thus, the average current at which the EMS would operate for a Shuttle type application would be approximately 90 ASF (97 ma/cm^2).

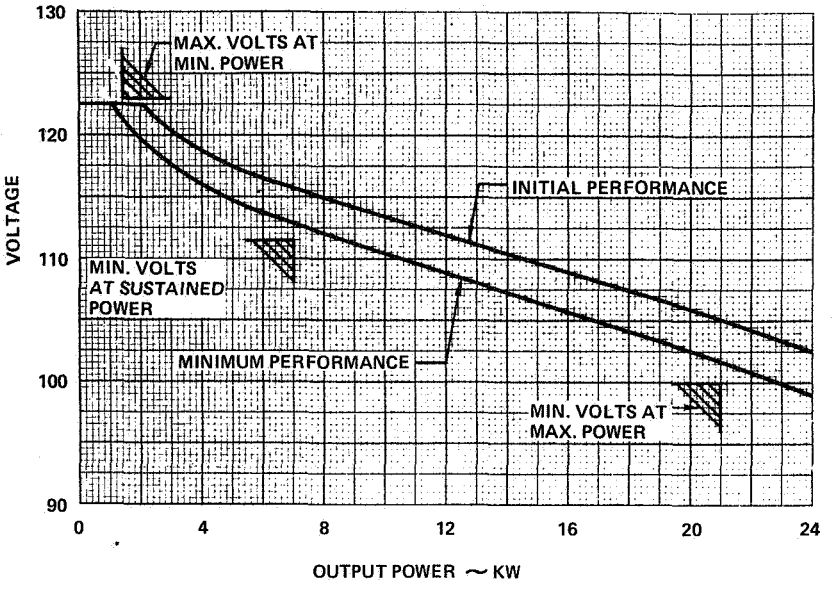

Figure 121 - System Voltage vs. Output Power

Weight and Size

The emphasis during the first phase of this program was on the fuel cell power section and its components. No resources were devoted to system packaging studies beyond those performed in the precontractual time period. Estimates of system weight and size prepared during Phase 1 were therefore based on precontractual estimates of ancillary components characteristics and the detailed studies made of the baseline EMS power section.

System weight and volume characteristics based on these results are summarized in Table 19. The estimated EMS weight of 105 lbs(47.6 Kg) is well under the objective of 140 lbs(63.5 Kg). Estimated specific weight is 14.8 lb/kw(6.7 Kg/kw) of sustained power compared to the goal of 20 lb/kw(9.1 Kg/kw). Estimated specific volume per kilowatt of sustained power is 0.33 ft^3/kw(9.4 x 10^3 cm^3/kw) also well under the objective of 0.5 ft^3/kw(14.2 x 10^3 cm^3/kw).

TABLE 19

Estimated Weight of Engineering Model System

Power Section	60.1 (27.2)
End Plates	6.0 (2.7)
Ancillary Components and Structure	38.6 (17.5)
TOTAL	104.7 lbs. (47.4 Kg)

VI ANCILLARY COMPONENT TESTING

A. Condenser

Introduction

The Engineering Model System requires a condenser to remove the heat from the water vapor produced by the power section. It must therefore condense the vapor flowing to it and sub-cool the condensate. The condenser must operate over a wide range of vapor inlet flow rates associated with EMS operation from minimum power to the maximum close cycle power of 7 kw. Stable operation in a variable gravity and zero gravity environment is required, as is the capability to handle non-condensable gases which may be contained in the vapor.

The type of condenser selected for the Engineering Model System is of the plate-fin configuration. This configuration was selected on the basis of its capability for stable operation over the wide range of flow rates in a variable gravity environment. A secondary selection factor was the efficient packaging characteristics of this type of heat exchanger, i.e. the large amount of heat transfer surface which can be packaged into a unit weight and volume of hardware. Key design consideration for this type of condenser are:

- Total steam flow area is set by allowable pressure drop at maximum steam flow rate.
- Maximum size of individual steam flow passage must be such that surface tension forces will be sufficient to insure stable operation at the minimum flow rate.

These considerations result in a selection of a number of small hydraulic diameter steam flow passages operating in parallel to handle the total required steam flow. A test program was required to measure the pressure drop and heat transfer characteristics of this type of condenser and to ascertain the minimum flow rate for stable operation.

Testing was performed using an existing plate-fin heat exchanger to obtain the data necessary for sizing a full size Engineering Model System condenser in subsequent phases of the program.

Condenser Description

The condenser used was a modified Apollo fuel cell powerplant condenser.

In the Apollo fuel cell, the condenser is used to condense product water from a hydrogen-water vapor stream. The satisfactory zero "G" operation of the condenser has been demonstrated during the several Apollo flights.

The condenser has a heat transfer surface area of 2.2 sq. ft (2044 cm^2); the core is 6 in. (15.2 cm) long and has a frontal area of 1.4 x 1.6 in. (3.55 x 4.07 cm). Both the coolant and vapor side flow passages are of similar geometry. The individual flow passages are formed by fins 77 mils (1.95 mm) high with a spacing of 18 flow passages per inch (7.1 per cm). The water vapor flow passage hydraulic diameter is 54 mils (1.37 mm). The core is made of silver brazed stainless steel. A schematic of the condenser showing its flow passage geometry is shown in Figure 122. The vapor flow passes through the distributor plate shown in the figure prior to its entry into the core. The condenser exit was reworked to install a plexiglass viewing window to allow observation of steam breakthrough and any non-condensable gases entrained in the condensate.

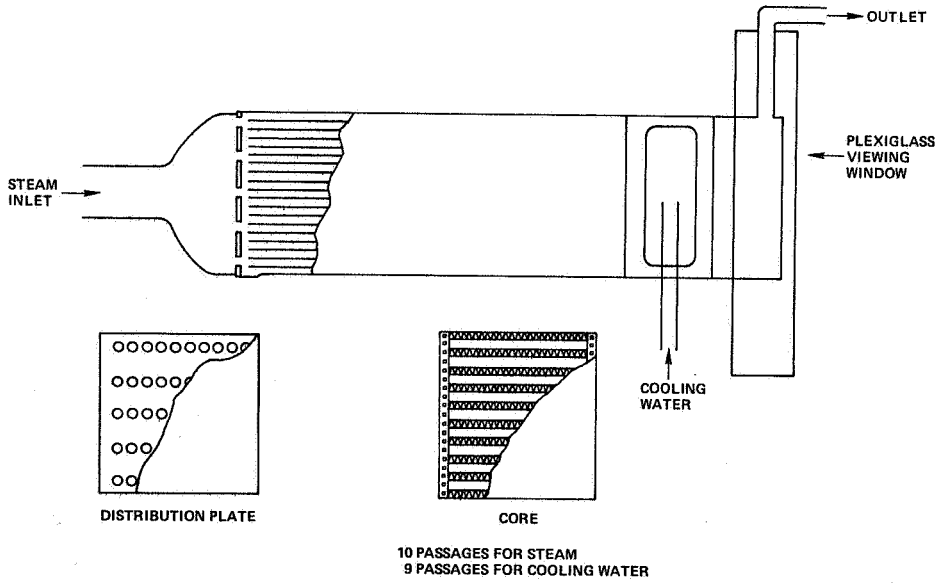

Figure 122 - Condenser Schematic Showing Flow Passage Geometry

The minimum stable steam flow rate was calculated by assuming a balanced pressure drop between any two channels of the steam side of the condenser. The pressure necessary to force condensate out of a passage can be calculated as the capillary blowout pressure:

$$\Delta P \text{ capillary blowout} = \frac{4\sigma \cos \theta}{D}$$

σ ~ Surface Tension of Water
θ ~ Contact Angle Between Water and Surface
D ~ Hydraulic Diameter

If the frictional pressure loss within a passage is not greater than this blowout pressure, there is a likelihood that the core will be partially blocked. The minimum flow rate is that at which the frictional pressure loss just equals the blowout pressure.

For the condenser core hydraulic diameter of 0.00474 ft. (1.44 mm), and assuming a contact angle θ of 0°, the blowout pressure is 0.73 in. (18.6 mm) water. At 3 to 5 lb/hr(1.36 to 2.26 Kg/hr), the core frictional pressure loss on steam at 3.5 psia (2.4 n/cm^2) is about 0.73 in. (18.6 mm) water. Therefore, a minimum stable flow rate of 3-5 lb/hr (1.36-2.26 Kg/hr) was predicted.

Test Facility Description

The condenser was tested in the facility shown schematically in Figure 123. An electrically heated boiler was used to generate the water vapor supplied by the condenser. A circulating pump-ejector system similar in concept to that of the EMS was to remove the sub-atmospheric pressure condensate and pump it to atmospheric pressure. The facility was capable of supplying vapor, however, the flow range was set by condenser capability - from 1.0 to 15 lbs (0.45 to 6.8 Kg) per hour. Condenser pressure was varied from 1 to 11 psia (0.69 to 7.6 n/cm^2).

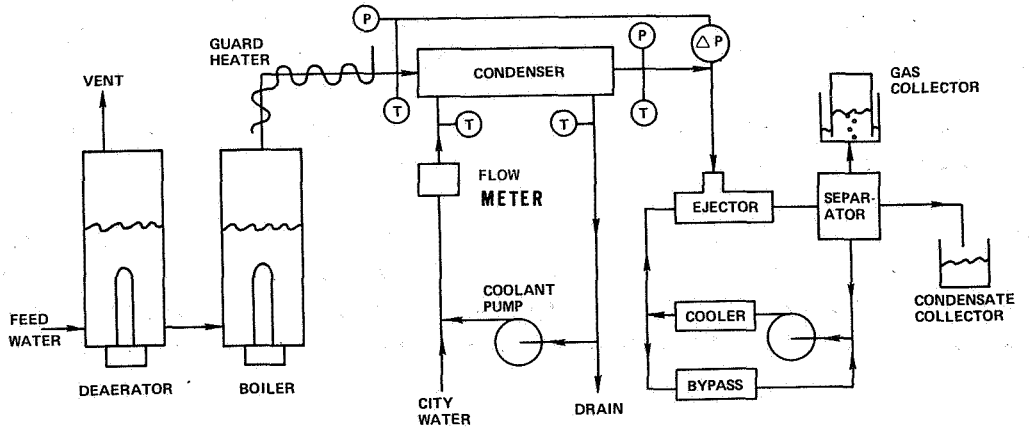

Figure 123 - Condenser Test Facility

Careful attention was given to the piping and seals in the vapor loop to prevent air from leaking into this sub-atmospheric pressure system. In addition, a separate deaerating boiler was incorporated to remove gases dissolved in the feed water. In spite of these efforts, small amounts of non-condensable gases were present during the testing. These gases generally constituted less than 0.1 percent by volume. An inverted beaker system was used to collect and measure the gases flowing from the condenser. The condensate was also collected to allow direct measurement of vapor flow rates.

The mounting of the condenser could be changed to allow testing with vapor flow in the horizontal, vertically up and vertically down directions. Guard heaters were used on the vapor inlet line to assure that saturated steam was supplied to the condenser. Cooling was provided by a circulating water loop controlled to provide a 90°F (32.2°C) coolant flow to the condenser inlet. Cooling flow rate was varied by a throttle valve. Instrumentation points were located as shown. Temperatures were measured with the thermocouples; absolute pressures were indicated with Bourdon type gages. The condenser pressure drop was measured directly by a u-tube manometer.

The test procedure consisted of the following:

1. The desired vapor flow rate was set by the amount of electric power supplied to the boiler.

2. The pump-ejector bypass loop flow was set to provide the desired condenser pressure.

3. Coolant flow rate was set at 500 lbs. (227 Kg) per hour; these operating conditions were held for approximately one hour. The condensate and non-condensable gases were collected over 10 minute periods several times during a one hour period.

4. Coolant flow rate was reset downward in steps of 100 lb/hr (45.5 Kg/hr) and data taken as above.

This sequence was repeated for different flow rates and condenser pressure levels. The entire sequence was performed to obtain data with the condenser orientated for horizontal, vertical up and vertical down flow. A typical data plot from one of the series test runs is shown in Figure 124.

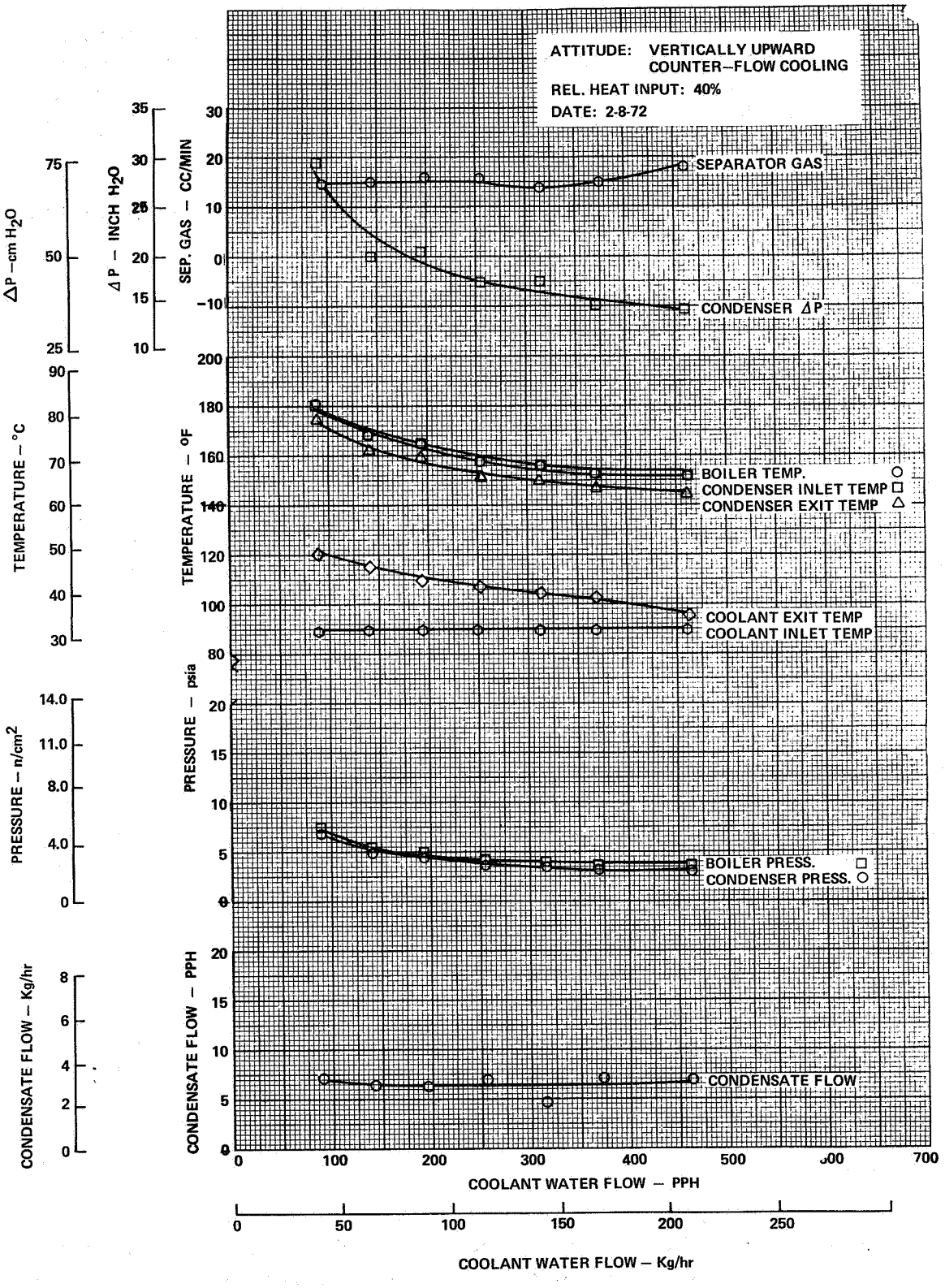

Figure 124 - Condenser Rig Test Data

Each data plot was made from the best data points recorded for given conditions. For each boiler power input level and condenser orientation, a different plot was made. Ten variables describing condenser performance were plotted versus the cooling water flow rate. Starting with the uppermost points plotted in Figure 124, the data are:

Separator Gas - This is the flow rate of non-condensible gas collected with the condensate.

Condenser Δ P - The pressure loss from upstream of the inlet manifold to the exit manifold was measured by a water manometer. When the condenser is in a vertical position, the Δ P includes the head loss due to change in height.

Boiler Temperature - The temperature of the steam generator was measured by this thermocouple.

Condenser Inlet Temperature - Steam temperature to the condenser was measured in the inlet to the condenser by this thermocouple.

Condenser Exit Temperature - Condensate temperature was measured in the exit manifold.

Coolant Exit Temperature - Coolant Inlet Temperature - The cooling water temperature was measured upstream and downstream of the condenser.

Boiler Pressure - Condenser Pressure - The absolute pressures in the boiler and at the condenser exit were calculated from the negative gage pressures recorded.

Condensate Flow - The condensate flow rate was calculated by collecting condensate over a ten-minute period.

The chronological order of data collection on the data plot is from right to left. The test was begun at high coolant flow rates and ended at the lowest coolant flow rate.

Data Analysis

The test data were analyzed to allow comparison of the measured pressure drops and condensing heat transfer coefficients with values predicted by analysis. To aid in the condensing pressure drop analysis, the condenser was tested with dry nitrogen to measure the single phase pressure drop.

For this test, the exit manifold and viewing window were removed to allow the core to exhaust to atmosphere. Figure 125 shows the computed nitrogen pressure drop broken down into several components of the condenser compared with the experimentally measured pressure drop. It is seen that there is good agreement between the experimental and predicted values. The core frictional loss is responsible for the bulk of the total pressure drop with the contribution from the distribution plate and inlet manifold increasing at higher flow rates.

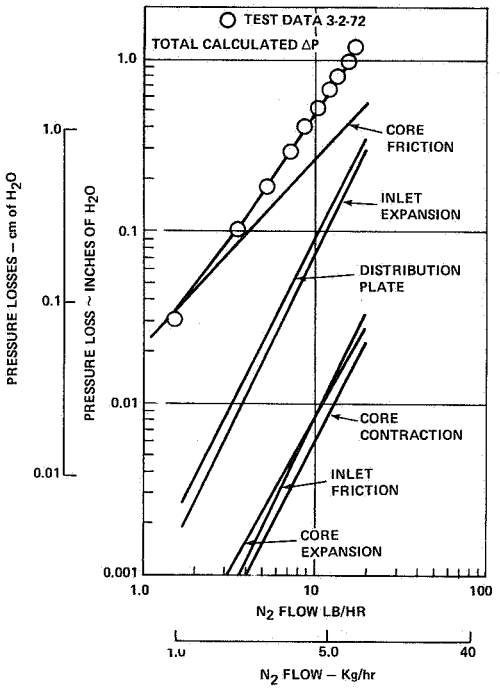

Figure 125 - Computed Nitrogen Pressure Drop

Comparison of the experimentally measured pressure drop obtained with the condenser operating with water vapor and the predicted values is shown in Figure 126. This figure also shows the predicted pressure drop for each component within the condenser. Although a two phase pressure loss correlation more sophisticated than Lockhart-Martinelli could have been used, it is apparent that additional precision in calculating these losses would not account for the factor of 3 to 8 between predicted and measured pressure losses.

When the condenser orientation (and steam flow direction) was changed from a horizontal to a vertical up position, the pressure drop (in inches (cm) of water) was expected to increase by less than the length of the

core. This increase in pressure drop would be associated with supporting the vertical column of water. But in Figure 126, the pressure drop at 9 lb/hr (4.1 Kg/hr) was 10 inches (25.4 cm) of water in the horizontal position and 20 inches (50.8 cm) of water in the vertical up position. Apparently there is also a change of two phase flow pattern that is increasing the pressure loss by more than the length of six inches(15.2 cm).

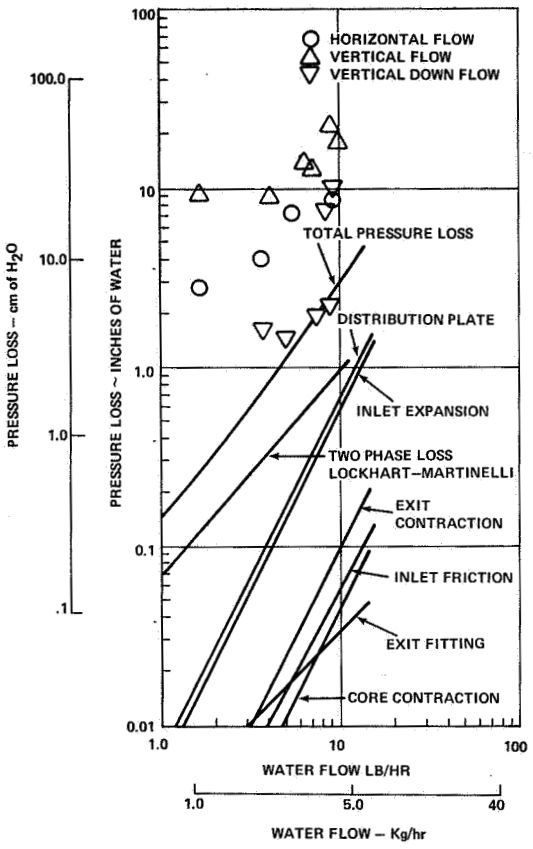

Figure 126 - Comparison of Experimentally Measured Pressure Drop with Predicted Values

Some scatter in the pressure drop data was unavoidable because of the liquid vapor mixture in the lines. Care was taken to keep instrumentation points in the same horizontal plane as the pressure taps on the condenser, but small errors were unavoidable due to routing of the connecting lines.

A condenser flow model which helps explain the condenser pressure drop characteristic measured was developed as a result of heat transfer analysis.

The condenser has three heat transfer regions: desuper heat, condensing and sub-cooling. To calculate a condensing heat transfer coefficient, the area associated with condensation must be known. If all the heat exchanger area were operating in the condensing region, the condensing area would obviously be known. Most of the test runs made were performed with a small amount of condenser area used for desuperheating. To obtain data on the heat transfer coefficients in the condensing region, the experimental data points were selected at coolant flow rates where the condenser was just able to complete condensation. Thus, the points where the cooling flow could just maintain the vapor side condition were selected for this analysis. To account for the small amount of sub-cooling nesessary to insure all the vapor was condensed, it was assumed that 2 ft^2 (1858 cm^2) of the total 2.2 ft^2 (2044 cm^2) of heat transfer area was used for condensing. Table 20 is a summary of the points selected where the condenser was operating in the condensing mode only. The three vapor flow orientations of horiziontal, vertical up, and vertical down are shown. This table compares the calculated and the experimentally determined condensing coefficients. It also shows the amount of non-condensable gases collected. The measured coefficients ranged from 75 to 100 percent of the value predicted. For a heat exchanger of this type, the cooling side film coefficient is approximately 300 Btu/hr-ft^2 -°F (1700 watts/m^2 -°C) and hence, should be controlling. Based on past data from this condenser, there can be little doubt that the value of the cooling side coefficient is correct. The film coefficient for the condensing side of this type of heat exchanger is predicted to be in the range from 800 to 2000 Btu/hr-ft^2 -°F (4536 to 11,340 watts/m^2 -°C) thus it is evident that a condensing side mechanism was operating to significantly reduce vapor side heat transfer rates.

The presense of non-condensable gases in a condenser are known to cause significant reductions in condensing coefficients. For example, Figure 127 shows the reduction in the coefficient for water vapor condensing on a flat plate at a pressure of 2.85 psia (1.97 n/cm^2). With one percent non-condensable gas in the vapor, the condensing coefficient is reduced to approximately 1/2 its value for pure steam, or for this case 400 Btu/hr-ft^2 -°F (2268 watts/m^2 -°C). An air content greater than 10 percent is required to reduce the value below 100. As shown in Table 20 the amount of air present in the test condenser was in the range of 0.001 to 0.9 percent by volume or 0.002 to 1.4 percent by weight. This air to vapor fraction would have a negligible effect on the operation of the condenser of the type shown in Figure 127.

TABLE 20

SUMMARY OF MINIMUM COOLING FLOW POINTS

	Condensate Flow lb/hr(kg/hr)	Powerstat Setting %	Coolant Flow Water lb/hr(kg/hr)	Condenser Exit Pressure psia(n/cm^2)	ΔP Calculated w/o Gravity Effect in. (cm) H_2O	ΔP Actual in. (cm) H_2O	U overall Calculated Btu/hr-ft^2-°F (watts/m^2-°C)	U overall Actual Btu/hr-ft^2-°F (watts/m^2-°C)	Air Collected cc/min	Air By Volume %
Horizontal										
Counterflow	1.7(0.78)	20	140(63.5)	4.0(2.76)	0.7(1.78)	2.5(6.35)	225(1275)	18(102)	36.	0.198
Counterflow	3.7(1.68)	30	255(115.7)	3.5(2.41)	0.51(1.29)	4.0(10.9)	270(1530)	40(227)	18.	0.016
Counterflow	5.1(2.31)	40	280(127.0)	3.5(2.41)	0.84(2.14)	7.5(19.1)	240(1360)	51(289)	Not Available	
Counterflow	9.2(4.17)	50	315(143.0)	3.5(2.41)	2.14(5.43)	9.0(22.9)	240(1360)	97(550)	Not Available	
Vertical Down										
Counterflow	2.6(1.18)	20	95(43.0)	3.5(2.41)	0.30(0.76)	1.0(2.54)		20(113)	16.	0.058
Counterflow	3.8(1.72)	30	195(88.5)	3.8(2.62)	0.53(1.34)	1.5(3.80)	206(1168)	33(187)	13.	0.032
Coflow	5.0(2.26)	30	195(88.5)	2.0(1.38)	1.50(3.80)	2.5(6.35)	181(1026)	101(573)	6.	0.011
Counterflow	9.2(4.17)	40	255(115.7)	2.6(1.79)	2.90(7.38)	3.0(7.64)	231(1310)	156(884)	1.	0.001
Coflow	7.5(3.40)	40	255(115.7)	3.5(2.41)	1.60(4.07)	2.0(5.08)	245(1389)	85(482)	15.	0.019
Counterflow	9.6(4.35)	50	370(168.0)	3.2(2.20)	2.40(6.10)	6.5(16.5)	204(1156)	130(737)	14.	0.013
Coflow	8.6(3.90)	50	370(168.0)	3.0(2.07)	2.30(5.85)	5.0(12.7)	182(1032)	120(680)	14.	0.015
Vertical Up										
Counterflow	2.0(0.92)	20	440(199.0)	3.0(2.07)	0.24(0.61)	10.0(25.4)	248(1406)	19(108)	17.	0.079
Coflow	0.11(0.05)	20	450(204.5)	3.5(2.41)	0.01(0.03)	3.5(8.9)	251(1423)	1.5(8.5)	10.	0.850
Counterflow	2.6(1.18)	30	255(115.7)	3.5(2.41)	0.30(0.76)	8.5(21.6)	233(1322)	24(136)	13.	0.047
Coflow	3.0(1.36)	30	370(168.0)	3.5(2.41)	0.37(0.94)	7.5(19.1)	240(1360)	29(164)	7.	0.016
Counterflow	7.2(3.26)	40	370(168.0)	3.0(2.07)	1.70(4.33)	15.0(38.1)	227(1288)	53(300)	1.	0.001
Coflow	6.5(2.95)	40	370(168.0)	3.5(2.41)	1.20(3.05)	14.0(35.6)	200(1130)	49(278)	6.	0.009
Counterflow	10.0(4.54)	50	470(213.0)	3.7(2.55)	2.30(5.85)	17.5(44.5)	257(1457)	104(590)	6.	0.006
Coflow	9.0(4.08)	50	470(213.0)	4.2(2.89)	1.80(4.58)	19.0(48.3)	246(1395)	75(425)	6.	0.006

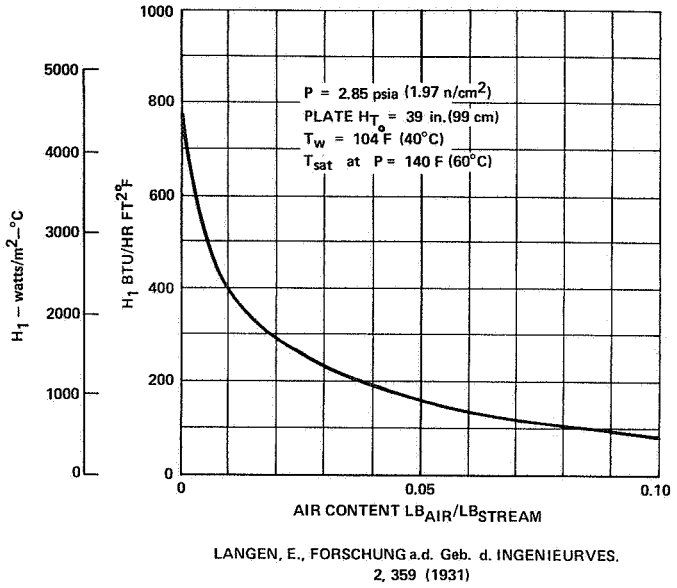

LANGEN, E., FORSCHUNG a.d. Geb. d. INGENIEURVES. 2, 359 (1931)

Figure 127 - Reduction in Water Vapor Condensing Coefficient on Flat Plate

Using the data from Figure 127 and the range of cooling side coefficients for two different coolant flow rates, the predicted overall heat transfer coefficient for the test condenser is shown in Figure 128 as a function of percent by volume air in the inlet vapor. The experimentally determined coefficients are also shown in the figure for the relative amounts of non-condensables determined to be in the condenser. While the air content in the vapor is very small compared to the vapor mass or inlet volumetric flow rates, the air does represent a substantial fraction of the condensate volume. This is illustrated in Figure 129 which shows the velocities of the vapor, liquid, and air in the condenser. For the conditions shown, approximately 1/3 of the exit volumetric flow rate is due to non-condensable gases.

This relatively large volume fraction of air in the condensate can provide a possible explanation for the high pressure losses and low heat transfer coefficients measured on the test condenser. The flow pattern within the small hydraulic diameter condenser tubes could be slugs of liquid which could trap pockets of gas. The surface tension of the capillary tubes could cause the condensate to bridge and form slugs which would then accelerate to the velocity of the vapor. An estimate was made of the pressure loss due to the friction of the liquid slugs moving at the vapor velocity. The results shown in Figure 130 indicate that this type of flow regime could be responsible for the pressure losses measured. Since the air pockets effectively reduce the amount of capillary wall area available for condensation, this flow pattern could also account for lowering the condensing heat transfer coefficient.

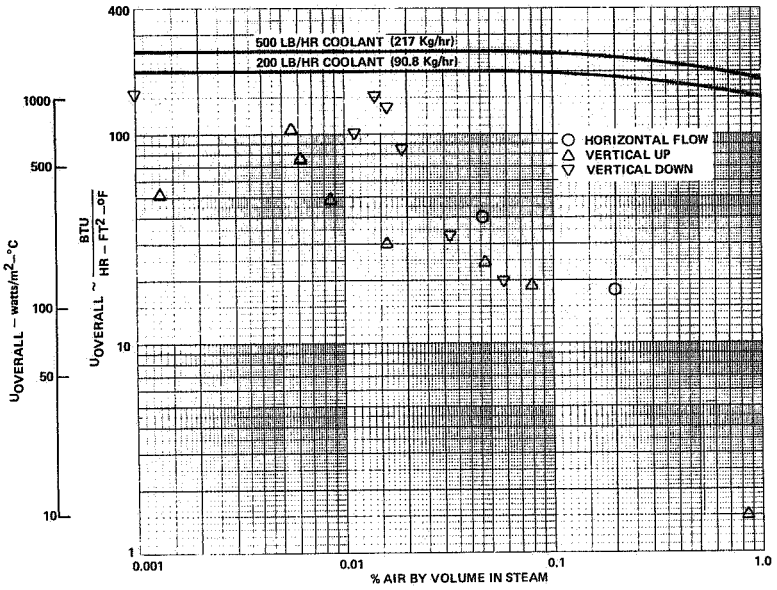

Figure 128 - Condenser Overall Heat Transfer Coefficient

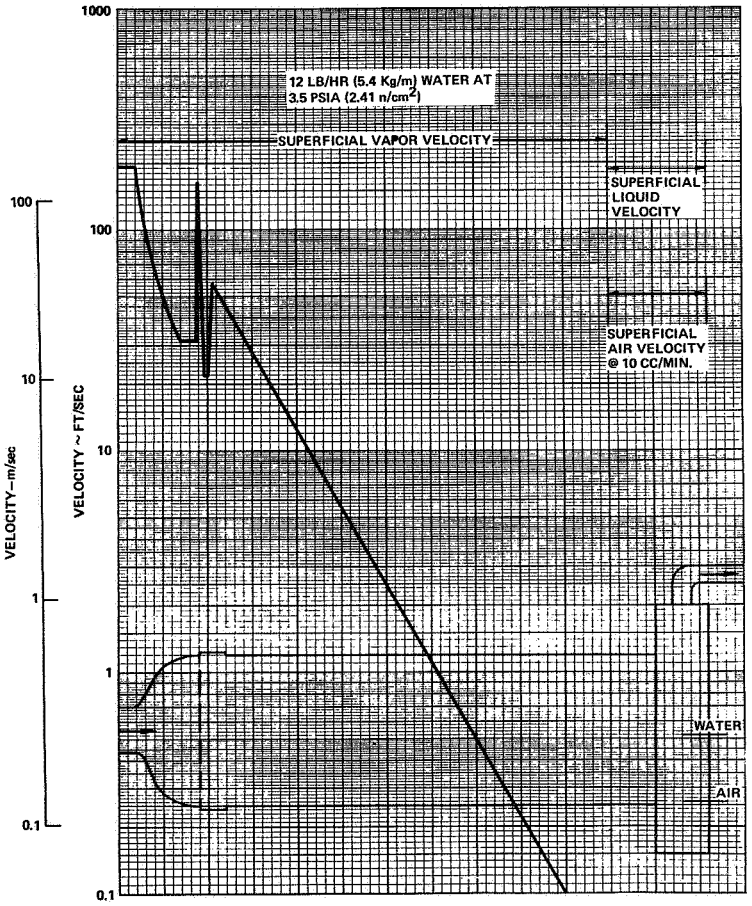

Figure 129 - Velocities of Vapor and Liquid in Condenser

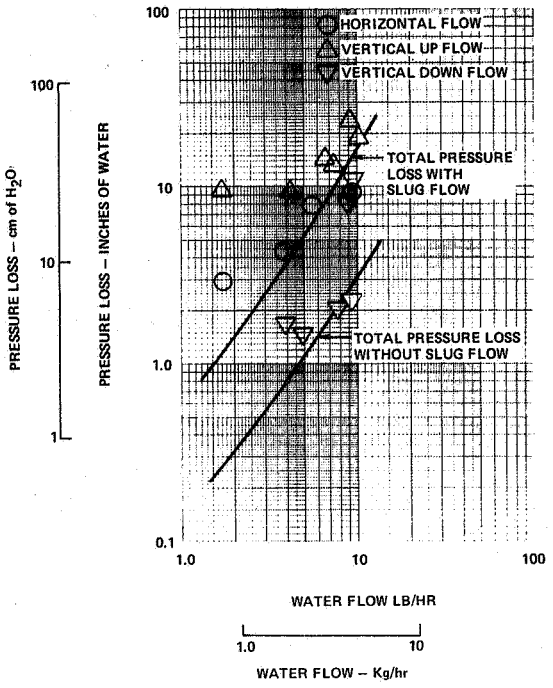

Figure 130 - Estimate of Pressure Loss due to Friction of Liquid Slugs Moving at Vapor Velocity

It is important that a condenser used in the EMS be able to handle non-condensable gases. A small amount of hydrogen will diffuse into the vapor loop from the passive water removal components in the power section. The approximate amount of hydrogen estimated to diffuse into the EMS loop compared with the amount of air measured in the test condenser is shown in Table 21. The typical value of 10 cc per minute of air measured in the test condenser is seen to be 10 times the volume of the hydrogen. This lesser amount of hydrogen would significantly reduce the effect of non-condensible gases on the condenser operation. However, even this small amount of non-condensible gas would have to be considered in the design of the condenser.

Conclusions

The concept of using small hydraulic diameter flow passages to maintain a stable vapor-liquid interface was demonstrated in the vertical upflow orientation, a minimum stable flow rate of 3-5 lb/hr (1.36-2.26 Kg/hr) was predicted; a stable flow rate of 2.5 lb/hr (1.13 Kg/hr) was demonstrated.

Additional design data should be generated with a test condenser operating with pure water vapor and with controllable amounts of non-condensable gases in the vapor.

TABLE 21

Non-Condensable Gas

Steam Flow lb/hr. (Kg/hr)	10 $\frac{cc}{min}$ Air Collected % Air at 3.5 PSIA (2.41 n/cm^2)		1.2 x 10^{-5} $\frac{lb}{hr}$ (0.55 x 10^{-5} $\frac{kg}{hr}$) H_2 % H_2	
	By Weight	By Volume	By Weight	By Volume
1 (0.45)	0.17	0.092	0.0012	0.01
2 (0.9)	0.08	0.047	0.0006	0.0049
5 (2.26)	0.033	0.019	0.00024	0.0019
10 (4.5)	0.017	0.0092	0.00012	0.001

B. Reactant Purifiers

Introduction

Carbon dioxide as an impurity in reactant gases is a contaminant to alkaline electrolyte fuel cell systems. It can be easily removed by various commercially available scrubbing materials. These materials are largely metal hydroxides, some of which are impregnated onto a support such as asbestos to increase the surface area.

Candidate commercially available scrubber materials include; soda lime (calcium hydroxide with a small amount of sodium hydroxide), barium lime (calcium hydroxide with a small amount of barium hydroxide), lithium hydroxide and sodium hydroxide. Ascarite, a trade-name for sodium hydroxide on an asbestos support was chosen because it is the only material which performs in a dry atmosphere. Sodium hydroxide removes carbon dioxide in the reaction $2NaOH + CO_2 \longrightarrow Na_2 CO_3 + H_2O$. This material is commercially available and manufactured by the Arthur H. Thomas Company. Ascarite is normally used to remove carbon dioxide from combustion products for combustion gas analysis. In this application, the manufacturer recommends that a water absorbent be used to dry the gas upstream of the scrubber. This prevents the Ascarite from becoming wet and melting or fusing into a large unuseable mass. Ascarite is very effective in removing carbon dioxide for this type of application; the conditions under which it is used are:

- The CO_2 concentration is high.

- Even when quantitative removal of CO_2 is expected for combustion analyses, it is still not necessary to lower the CO_2 to less than one part-per-million.

- The water produced in the CO_2 removal reaction causes the Ascarite to remain slightly wet. This allows the reaction to take place in an aqueous media and prevents an imprevious solid carbonate coating from covering the Ascarite pellets.

- For this application, Ascarite has a capacity of about 0.25 lbs. CO_2/lb Ascarite.

Ascarite is routinely used in fuel cell test stands to scrub CO_2 from reactant gases. Its capacity is unimportant for this application, therefore precise measurements of capacity have not been performed. For fuel cell powerplants used in space applications, achieving a minimum weight scrubber is important. Hence it is necessary to test this material under space application conditions to measure its effectiveness. These applications are quite different from the normal combustion analysis type of scrubbing for which Ascarite is normally used. The major differences are:

- The requirement of less than one part-per-million CO_2 in the product gas.

- The low CO_2 level in the inlet gas to be scrubbed (approximately 10 ppm).

- The lack of any moisture in the gas and the extremely low water production capacity from reacted CO_2.

The scrubbing capacity of Ascarite could be affected by particle size, humidity pressure and temperature. As the particle size is decreased, the external surface area per unit volume is increased. If the particles are not particularly porous, or if the CO_2 can not diffuse through the carbonate layer, then the capacity of the Ascarite becomes dependent on the external surface area available for absorption. Gas with too high a moisture content will cause the Ascarite to become wet and melt or fuse into an unuseable mass. Too low a moisture content may inhibit the reaction or allow an impervious carbonate layer to form over the particle, thus lowering the absorption capacity of the scrubber. Pressure and temperature would only affect the scrubbing capacity of Ascarite if a low humidity were definitely a problem. In this case, high pressures and low temperatures would prevent Ascarite from drying out by conserving the moisture formed in the reaction.

Ascarite was tested under space powerplant type conditions to determine its effectiveness for scrubbing CO_2.

Test Procedure

The test scrubbers consisted of tubes filled with Ascarite through which a measured flow rate of oxygen containing a known concentration of CO_2 was passed. These scrubbers were separated into discrete sections using glass fiber to separate the sections so that they can be analyzed for carbonate after the test had been completed. This allowed a carbonate concentration profile to be drawn along the length of the reactor. Because of the high CO_2 content in air, the Ascarite was handled in a nitrogen purged dry-box. Clear glass tubes were used as scrubber containers so that any color change (from the original brown color to white as the carbonate is formed) could be observed as the Ascarite became depleted. The reactant used was blended from a mixture of oxygen containing 1000 parts per million (ppm) CO_2 and oxygen containing less than 2 ppm CO_2. These two gases were mixed to the proper CO_2 level which was monitored with an infrared analyzer (LIRA, manufactured by Mine Safety Applicances Company). This instrument was capable of measuring well below one part-per-million of carbon dioxide and so was also used to detect carbon dioxide exiting from the scrubber. Three tests were run with Ascarite. The first two were run to break through at 1 ppm, while the third test was run until the exit CO_2 concentration was equal to the inlet CO_2 concentration. Details of each test are shown in Table 22. An oxygen flow rate equivalent to a power output of approximately 5 kw was used for all tests.

Table 22

Summary of CO_2 Scrubbing Test

Test No.	1	2	3
Mesh Size	8-20	20-30	20-30
Ascarite Weight - lbs(Kg)	0.285(0.129)	0.285(0.129)	1.12(0.509)
Reactant Gas	O_2	O_2	O_2
CO_2 Concentrationin - ppm	5	5	10
CO_2 Concentration out - ppm	<1.0	<1.0	<1.0
Gas Flow - pph(Kg/hr)	4(1.82)	4(1.82)	4(1.82)
Pressure - psia(n/cm^2)	90(62.1)	90(62.1)	65(62.1)
Temperature	Room	Temperature	(70°F-80°F) (21.1°C-26.7°C)
Reactor Diameter - in.(cm)	1.315(3.34)	1.315(3.34)	1.44(3.65)

Test Results

It can be seen in both Figures 131 and 132 that Ascarite is capable of lowering the carbon dioxide level to well below one part-per-million. Once break through occurs, it is rapid, indicating that the reaction front is very narrow. This can be seen in Figure 133 which shows the carbon dioxide loading versus the scrubber length for the first two tests. These tests were run to just beyond break through. The use of transparent reactors proved rather useless in these tests as the low carbon dioxide loadings and the low moisture content on the Ascarite was insufficient to cause any distinct color changes. A summary of the test results is shown in Table 23. .

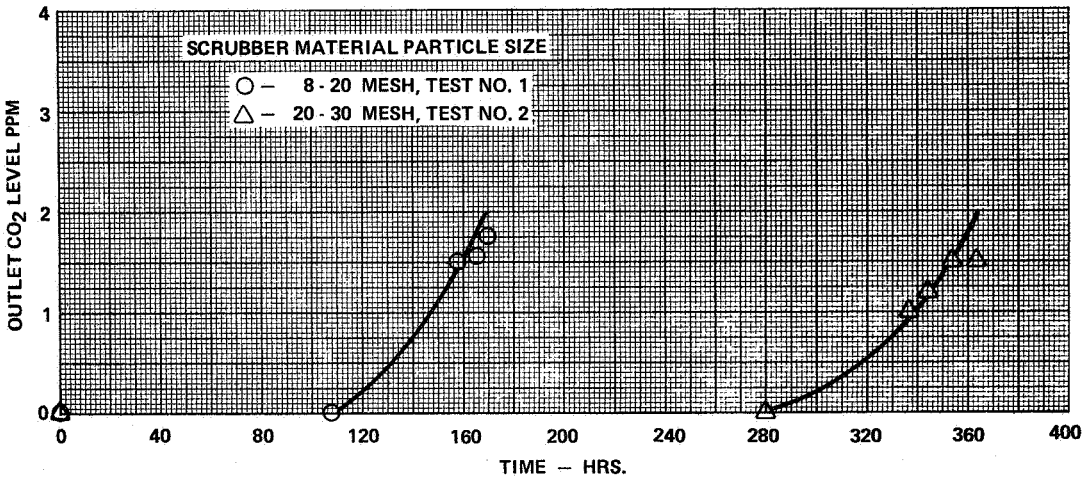

Figure 131 - Ascarite Scrubber Tests #1 and #2

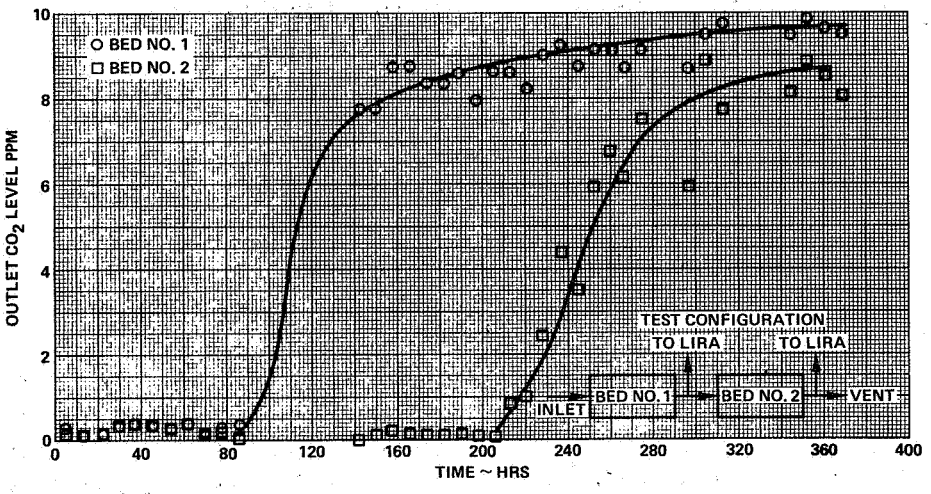

Figure 132 - Reactant Purifier Test No. 3

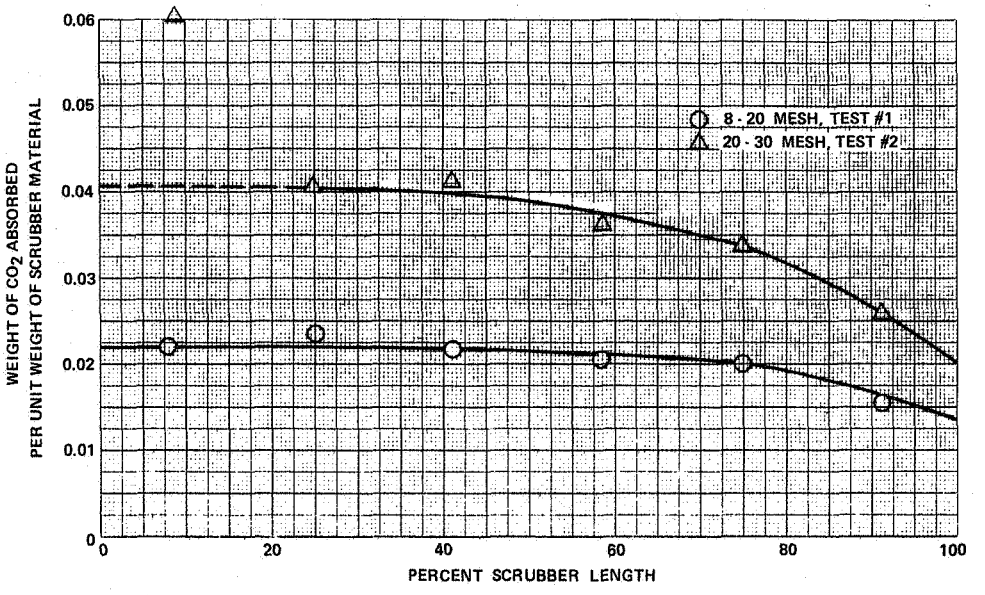

Figure 133 - Carbon Dioxide Loading vs. Scrubber Length

Table 23

Weight of CO_2 Absorbed Per Unit Weight of Scrubber Material

Test No.	1	2	3
Analyzed Loading	0.022	0.0405	0.0273
Calculated	0.0129	0.0323	0.0117

The table shows two values for the amount of CO_2 absorbed. The analyzed loading results from post-test analysis of the scrubber material; the calculated value is computed from a knowledge of the total amount of CO_2 which was removed from the inlet gas stream. That the sets of values do not agree more closely could be because of inadvertent exposure of the samples to the atmosphere. Refined dry box handling techniques are required when dealing with loadings at levels as low as these.

The first two tests were run to determine any effect of particle size on loading. As shown in Table 23, the smaller particle Ascarite had a higher capacity for carbon dioxide than did the larger particles. An analysis of this data was made assuming that all particles absorb CO_2 to the same depth, forming an impervious carbonate shell around each particle through which the CO_2 can be penetrate. This analysis indicates that the Ascarite absorbed CO_2 to a depth of about 0.0043 inches (0.109 mm); and in this shell volume the average absorption capacity is only about 0.075 pounds

of CO_2 per pound of Ascarite. Another model could consist of an external molecular layer of sodium hydroxide completely converted to sodium carbonate but with the concentration of sodium carbonate decreasing rapidly towards the center of the Ascarite particle. To determine which model is correct requires that a cross section of a particle be analyzed for carbonate distribution. Such an analysis was beyond the scope of this test project. The third test was run with the same particle size Ascarite as Test 2; however, neither the calculated loading nor the analyzed loading of Test 3 was as high as those of Test 2.

Test 3 was run at a lower pressure level than Tests 1 and 2. Temperatures were all at room temperature. If the basic scrubbing reaction ($2\ N_2OH + CO_2 \rightarrow N_aCO_3 + H_2O$) takes place only in the presence of water or when the sodium hydroxide is slightly damp, then the relative humidity as well as the temperature and pressure of the reactants could have a strong effect on the scrubbing efficiency of this material. The oxygen being scrubbed is very dry, so the only source of water is from the reaction. Since the oxygen tends to dry out the Ascarite during operation, any increase in the driving force of moisture from the Ascarite to the gas stream will dry out the absorbent and decrease its capacity. Increasing the temperature of the gas stream from 70° F to 80° F (21.1° C to 26.7° C) could increase the Ascarite drying rate by over thirty percent and decreasing the pressure from 90 psia (62.1 n/cm^2) to 65 psia (44.8 n/cm^2) could increase the drying rate of the Ascarite by over twenty five percent. This drying out could easily account for the discrepancy in CO_2 capacity between Test 2 and Test 3. Because of the hygroscopic nature of sodium hydroxide, the lack of moisture would not usually be a problem; however, when dealing with a gas containing water in only part-per-million quantities, it is necessary to examine published data more closely.

Several other materials are used commercially to remove carbon dioxide from gases. Published data has shown that most of these; soda lime (calcium hydroxide with a small amount of sodium hydroxide), barium lime (calcium hydroxide with a small amount of barium hydroxide) and lithium hydroxide must be used over fairly narrow humidity ranges. Previous experience at Pratt & Whitney Aircraft, for example, has shown that soda lime used for scrubbing CO_2 from air can be operated over a humidity range from approximately 30 to 90 percent. Maximum absorption capacity, however, was found to require operation near 75 percent humidity. Molecular sieves do not scrub carbon dioxide to the desired low levels. If potassium hydroxide is more hygroscopic than sodium hydroxide, it might prove more useful under dry space applications.

Conclusions

- Ascarite has the capability of lowering the carbon dioxide level in the reactant gas to less than one part-per-million.

- The absorption capacity of Ascarite is in the range of 0.022 to 0.04 pounds of CO_2/pound of Ascarite under the conditions tested.

- For a typical fuel cell powerplant (5 kw average output) operating a typical Space Shuttle mission (one week), all CO_2 can be removed from the oxygen supply with less than one pound (0.45 Kg) of Ascarite.

- It may be possible to modify the scrubber operating conditions so that the absorption capacity can approach the capacity obtained (0.2 pounds of CO_2/pounds of Ascarite) when this material is used in high CO_2 level gas streams. This may be accomplished by lowering the temperature, raising the pressure, or increasing the humidity of the stream.

- Other candidates for CO_2 scrubbing; soda lime, barium lime and lithium hydroxide have a narrow but high range of humidity over which they will operate efficiently. Molecular sieves will not lower the carbon dioxide to a sufficiently low level.

- System analyses should be performed to determine the pressures, temperatures and humidities which can be provided readily for the inlet gas streams. This information coupled with available knowledge of scrubber materials will allow design and testing to verify the absorption capacity of candidate scrubbers under conditions most conducive to achieving high effectiveness.

OFFICIAL DISTRIBUTION LIST FOR FUEL CELL REPORTS

NASA

National Aeronautics and Space Administration
Scientific and Technical Information Facility
P.O. Box 33
College Park, Maryland 20740

Mr. Ernst M. Cohn, Code RPP
National Aeronautics and Space Administration
Washington, D.C. 20546

Dr. A. M. Greg Andrus, Code Code SCC
National Aeronautics and Space Administration
Washington, D.C. 20546

Mr. Richard Livingston, Code MTG
National Aeronautics and Space Administration
Washington, D.C. 20546

Mr. Ronald V. Murad, Code MHE
National Aeronautics and Space Administration
Washington, D.C. 20546

Mr. Louis Wilson, Code 450
Goddard Space Flight Center
National Aeronautics and Space Administration
Greenbelt, Maryland 20771

Mr. Jack E. Zanks, MS 488
Langley Research Center
National Aeronautics and Space Administration
Hampton, Viriginia 23365

Dr. Louis Rosenblum, MS 302-1
Lewis Research Center
National Aeronautics and Space Administration
21000 Brookpark Road
Cleveland, Ohio 44135

Mr. Harvey Schwartz, MS 309-1
Lewis Research Center
National Aeronautics and Space Administration
21000 Brookpark Road
Cleveland, Ohio 44135

Dr. J. Stuart Fordyce, MS 309-1
Lewis Research Center
National Aeronautics and Space Administration
21000 Brookpark Road
Cleveland, Ohio 44135

Mr. Charles Graff, S&E-ASTR-EP
Marshall Space Flight Center
National Aeronautics and Space Administration
Huntsville, Alabama 35812

Mr. W.E. Rice, Code EP5
Manned Spacecraft Center
National Aeronautics and Space Administration
Houston, Texas 77058

Mr. Bill Dusenbury, Code EP5
Manned Spacecraft Center
National Aeronautics and Space Administration
Houston, Texas 77058

Mr. Phillip Quattrone
Ames Research Center
National Aeronautics and Space Administration
Moffett Field, California 94035

Mr. Daniel Runkle, MS 198-220
Jet Propulsion Laboratory
4800 Oak Grove Drive
Pasadena, California 91103

Mr. Aiji A. Uchiyama, MS 198-220
Jet Propulsion Laboratory
4800 Oak Grove Drive
Pasadena, California 91103

ARMY

Energy Conversion Research Laboratory
U.S. Army Engineer R&D Labs.
Fort Belvoir, Virginia 22060

U.S. Army Electronics Command
Attn: AMSEL-TL-P
Fort Monmouth, New Jersey 00703

Harry Diamond Labs.
Room 300, Building 92
Connecticut Ave. & Van Ness St.,
Washington, D.C. 20438

NAVY

Director, Power Program, Code 473
Office of Naval Research
Arlington, Virginia 22217

Mr. Harry W. Fox, Code 472
Office of Naval Research
Arlington, Virginia 22217

Mr. S. Schuldiner, Code 6160
U.S. Naval Research Laboratory
4555 Overlook Ave., S.W.
Washington, D.C. 20390

Mr. Robert E. Trumbule, STIC
4301 Suitland Road
Suitland, Maryland 20390

Mr. Bernard B. Rosenbaum, Code 03422
Naval Ship System Command
Washington, D.C. 20360

Mr. Albert Himy, Code 6157D
Naval Ship Engineering Center
Center Building, Prince George Center
Hyattsville, Maryland 20782

Mr. Phillip B. Cole, Code 232
Naval Ordnance Laboratory
Silver Spring, Maryland 20910

Mr. J.H. Harrison, Code A731
Naval Ship R&D Laboratory
Annapolis, Maryland 21402

Chemical Laboratory, Code 134.1
Mare Island Naval Shipyard
Vallejo, California 94592

AIR FORCE

AFAPL/POE-1/D. R. Warnock
Wright-Patterson AFB,
Ohio 45433

Mr. Edward Raskind, LCC Wing F
AF Cambridge Research Lab.
L.G. Hanscom Field
Bedford, Massachusetts 01731

Mr. Frank J. Mollura, TSGD
Rome Air Development Center
Griffiss AFB, New York 13440

HQ SASO (SMTAE/Lt. R. Ballard)
Los Angeles Air Force Station
Los Angeles, California 90045

OTHER GOV'T ORGANIZATIONS

Dr. Jesse C. Denton
National Science Foundation
1800 G Street, N. W.
Washington, D. C. 20550

PRIVATE ORGANIZATIONS

Aerospace Corporation
Attn: Library Acquisitions Group
P. O. Box 95085
Los Angeles, California 90045

Dr. E. A. Heintz
Technical Department
Airco Speer Carbon-Graphite
P. O. Box 828
Niagara Falls, New York 14302

Mr. R. A. Knight
Research Division
AMF Inc.
689 Hope Street
Stamford, Connecticut 06907

Dr. H. Shalit
ARCO Chemical Co.
Division of Atlantic Richfield Co.
500 South Ridgeway Avenue
Glenoiden, Pennsylvania 19036

Dr. H. L. Recht
Atomics International Division
North American Aviation Inc.
P. O. Box 309
Canoga Park, California 91304

Mr. R. F. Fogle, GF 18
Autonetics Division, NAR
P. O. Box 4181
Anaheim, California 92803

Dr. John McCallum
Battelle Memorial Institute
505 King Avenue
Columbus, Ohio 43201

Mr. D. O. Feder
Bell Telephone Laboratories, Inc.
Murray Hill, New Jersey 07974

Dr. Carl Berger
13401 Kootenay Drive
Santa Ana, California 92705

Mr. Sidney Gross
M. S. 84 79
The Boeing Company
P. O. Box 3999
Seattle, Washington 98124

Professor Ernest Yeager
Department of Chemistry
Case Western Reserve University
Cleveland, Ohio 44106

Dr. L. J. Minnick
G & W. H. Corson, Inc.
Plymouth Meeting, Penna. 19462

Mr. V. L. Best
Elpower Corporation
2117 South Anne Street
Santa Ana, California 92705

Xerox Corporation
Electro-Optical Systems, Inc.
300 North Halstead Street
Pasadena, California 91107

Dr. H.G. Oswin
Energetics Science Inc.
4461 Bronx Blvd.
New York, New York 10470

Mr. Martin Klein
Energy Research Corporation
15 Durant Avenue
Bethel, Connecticut 06801

Dr. J.G. Cohn
Engelhard Industries
497 Delancey Street
Newark, New Jersey 07105

Mr. L. Berkowitz
Government Research Laboratory
P.O. Box 8
Linden, New Jersey 07036

Dr. William B. Tarpley
Director, Materials Science
and Engineering Department
Franklin Institute Research Labs.
Philadelphia, Pennsylvania 19103

Mr. K.A. Thompson
Garrett Corporation
1625 Eye Street, N.W.
Washington, D.C. 20013

Mr. R.P. Mikkelson
Electrical Systems Dept., 967-5
General Dynamics/Convair
Aerospace
P.O. Box 1128
San Diego, California 92112

Mr. F.T. O'Brien
Direct Energy Conversion Programs
General Electric Company
930 Western Avenue
Lynn, Massachusetts 01910

Mr. L.J. Nuttall
General Electric Company
930 Western Avenue
Lynn, Massachusetts 01910

Dr. E.L. Simons
Environmental Protection Operation
Building 36
General Electric Company
Schenectady, New York 12345

Mr. Aaron Kirpich
General Electric Company
Space Systems, Room M2614
P.O. Box 8555
Philadelphia, Pennsylvania 19101

Mr. Elmer McBride
General Electric Company
777 14th Street, N.W.
Washington, D.C. 20005

General Motors Corporation
Attn: Library, Research Lab.
P.O. Box 988
Warren, Michigan 48090

Dr. Eugene Y. Weissman
Globe-Union, Inc.
P.O. Box 591
Milwaukee, Wisconsin 53201

Dr. J.E. Oxley
Gould Ionics, Inc.
P.O. Box 1377
Canoga Park, California 91304

Dr. P.L. Howard
Centreville, Maryland 21617

Mr. R. Hamilton
Institute for Defense Analyses
400 Army-Navy Drive
Arlington, Virginia 22202

Dr. R. Briceland
Institute for Defense Analyses
400 Army-Navy Drive
Arlington, Virginia 22202

Dr. R.C. Evans
Applied Physics Laboratory
John Hopkins University
8621 Georgia Avenue
Silver Spring, Maryland 20910

Dr. W.C. Schwemer
LTV Research Center
P.O. Box 6144
Dallas, Texas 75222

Dr. A. Moos
Leesona Moos Laboratories
Lake Success Park, Community Dr,
Great Neck, New York 11021

Dr. R.A. Wynveen, President
Life Systems, Inc.
23715 Mercantile Road
Cleveland, Ohio 44122

Mr. William B. Collins, MS 1620
Electronics Research Department
Martin-Marietta Corporation
P.O. Box 179
Denver, Colorado 80201

McDonnell Douglas Astronautics
Company
Headquarters-Space Systems
Center
Bldg. 11-3-12 MSV 12
5301 Bolsa Avenue
Huntington Beach, California 92647

Mr. A.D. Tonelli, ME 17 Bldg. 22
McDonnell Douglas Astronautics
Company
5301 Bolsa Avenue
Huntington Beach, Calif. 92647

Professor William L. Hughes
School of Electrical Engineering
Oklahoma State University
Stillwater, Oklahoma 74074

Dr. C. Bocciarelli
Pennsylvania Research Associates
101 North 33rd Street
Philadelphia, Pennsylvania 19104

Rocketdyne Division
Rockwell International Corp.
Attn: Library
6633 Canoga Avenue
Canoga Park, California 91304

Dr. R. Bordreaux
Rockwell International Corp.
12214 Lakewood Boulevard
Downey, California 90241

Power Information Center
University City Science Institute
3401 Market Street, Room 2210
Philadelphia, Pennsylvania 19104

Dr. Fritz R. Kalhammer
Stanford Research Institute
19722 Jamboree Blvd.
Irvine, California 92664

Dr. W.R. Scott (M 2/2154)
TRW Systems, Inc.
One Space Park
Redondo Beach, California 90278

Dr. Jose Giner
Tyco Laboratories, Inc.
Bear Hill, Hickory Drive
Waltham, Massachusetts 02154

Union Carbide Corporation
Development Laboratory Library
P.O. Box 6056
Cleveland, Ohio 44101